Testing of Models for Predicting the Behaviour of Radionuclides in Freshwater Systems and Coastal Areas

Report of the Aquatic Working Group of EMRAS Theme 1

Environmental Modelling for RAdiation Safety (EMRAS) Programme

FOREWORD

Environmental assessment models are used for evaluating the radiological impact of actual and potential releases of radionuclides to the environment. They are essential tools for use in the regulatory control of routine discharges to the environment and also in planning measures to be taken in the event of accidental releases; they are also used for predicting the impact of releases which may occur far into the future, for example, from underground radioactive waste repositories. It is important to check, to the extent possible, the reliability of the predictions of such models by comparison with measured values in the environment or by comparing with the predictions of other models.

The International Atomic Energy Agency (IAEA) has been organizing programmes of international model testing since the 1980s. The programmes have contributed to a general improvement in models, in transfer data and in the capabilities of modellers in Member States. The documents published by the IAEA on this subject in the last two decades demonstrate the comprehensive nature of the programmes and record the associated advances which have been made.

From 2002 to 2007, the IAEA organised a programme titled “Environmental Modelling for RAdiation Safety” (EMRAS). The programme comprised three themes:

Theme 1: Radioactive Release Assessment

Working Group on the revision of IAEA Handbook of parameter values for the prediction of radionuclide transfer in temperate environments (Technical Reports Series (TRS) 364).

Working Group on model testing related to countermeasures applied to the intake of iodine-131 from the Chernobyl accident.

Working Group on testing of models for the environmental behaviour of tritium and carbon-14 following routine and accidental releases.

Working Group on testing of models for predicting the behaviour of radionuclides in freshwater systems and coastal areas.

Theme 2: Remediation Assessment

Working Group on testing of models for the remediation of the urban environment.

Working Group on modelling the transfer of radionuclides from naturally occurring radioactive material (NORM).

Theme 3: Protection of the Environment

Working Group on the review of data and testing of models for predicting the transfer of radionuclides to non-human biological species.

This report describes the work of the Aquatic Working Group under Theme 1. The IAEA wishes to acknowledge the contribution of the Working Group Leader, L. Monte of Italy and J. Brittain of Norway (Editing) to the preparation of this report. The IAEA Scientific Secretary for this publication was D. Telleria of the Division of Radiation, Transport and Waste Safety.

CONTENTS

SUMMARY

During last decades a number of projects have been launched to validate models for predicting the behaviour of radioactive substances in the environment.

Such projects took advantage from the great deal of experimental data gathered, following the accidental introduction of radionuclides into the environment (the accident at the Chernobyl power plant was the most obvious example), to assess the contamination levels of components of the ecosystem and of the human food chain.

These projects stimulated intensive efforts for improving the reliability of the models aimed at predicting the migration of ^{137}Cs in lakes and of ^{137}Cs and ^{90}Sr in rivers. However, there are few examples of similar extensive model validation studies for other aquatic systems, such as coastal waters, or for other long lived radionuclides of potential radiological importance for freshwater systems.

The validation of models for predicting the behaviour of radionuclides in the freshwater environment and coastal areas was the object of the EMRAS working group on testing of models for predicting the behaviour of radionuclides in freshwater systems and coastal areas.

Five scenarios have been considered:

(1) Wash-off of ^{90}Sr and ^{137}Cs deposits from the Pripyat floodplain (Ukraine). Modellers were asked to predict the time dependent water contamination of Pripyat River following the inundation of the river floodplain heavily contaminated following the Chernobyl accident. Available input data were the deposits of radionuclides in the floodplain, the time dependent contamination of water in the river entering the floodplain, the water fluxes and several other morphological, meteorological and hydrological data. Concentrations of radionuclides in the water of the River Prypiat down-stream of the floodplain were supplied to assess the performances of the models.

(2) Radionuclide discharge from the Dnieper River (Ukraine) into its estuary in the Black Sea. Modellers were asked to predict the time dependent ^{90}Sr and ^{137}Cs contamination of water of the estuary. Input data were the atmospheric deposition of radionuclides of Chernobyl origin, the concentrations of radionuclides in the Black Sea, hydrological, morphological and environmental (temperature, salinity, pH, etc.) data. The performances of the models were assessed by comparison of model results with time dependent empirical data of radionuclide concentration in the estuary.

(3) ^{3}H migration in the Loire River (France). This scenario was aimed at assessing the dispersion of tritium releases at different points in the river, along a large domain (~ 350 km) and over a period of six months. Water discharges from tributaries, hydrological data and tritium discharges from four nuclear power plants were supplied as input data. The results were compared with empirical measurements of tritium concentration at Angers, a city along the river.

(4) Release of radionuclides into the Techa River (Russia). The objective of this scenario was to test models for radioactive contamination of river water and bottom sediments by ^{90}Sr, ^{137}Cs and ^{239,240}Pu. The scenario was based on data from the Techa River (South Urals) which was contaminated mainly in 1949–1952 as a result of discharges of liquid radioactive waste into the river.

(5) Behaviour of ^{226}Ra in the Huelva estuary (Spain). The estuary was affected by contamination from former phosphate industry. The exercise consisted of providing the time evolution of the total ^{226}Ra inventory in the bed sediments and the time evolution of the concentration in the water column.

Scenarios (1) and (3) were so-called "blind" exercises, that is the modellers were not given access to the observed data in advance of their modelling attempt.

Modellers from several international institutes participated in the exercises: AEP, Atomenergoproject (Russia); EDF, Electricité de France; ENEA, Ente per le nuove tecnologie l'Energia e l'Ambiente (Italy); IGE,Institute of General Energy (Ukraine); IMMSP, Institute of Mathematical Machine and System Problems (Ukraine); Institute of Experimental Meteorology SPA "Typhoon" (Russia); IRSN, Institut de Radioprotection et de Sûreté Nucléaire (France); ISDAE, Institute of Safety Development of Atomic Energy (Russia); UHMI, Ukrainian Institute for Hydrometeorology (Ukraine); University of Sevilla (Spain); University of Uppsala (Sweden).

Several state-of-the-art models were assessed in the frame of the project.

The performed exercises provided the opportunity to learn more about the proper usage of models for the management of complex environmental problems in view of the uncertainty and, often, of the vagueness of the input data, the uncertainty of the model parameters and the compatibility of different kinds of models applied to a specific contamination scenario.

Models showing different characteristics and levels of complexity from those based on simple box-type approach to those making use of the shallow-water and transport-diffusion equations were assessed. Although different approaches, simplifications and approximations are used by the models, there are some conceptual and structural similarities that are apparent in an overall perspective. An obvious example is the modelling of radionuclide interaction with suspended matter and bottom sediments by means of a compartmental approach.

It should be noted that, as tritium does not interact with sediments, the only processes that controls the migration of this radionuclide are diffusion and transport by the current. Therefore, exercise (3) was an important test to evaluate the reliability of the modules for the simulation of the hydrological and the diffusion transport processes in the assessed models. This "blind test" exercise showed that the behaviour of radionuclides that scarcely react with suspended matter and sediments is generally predicted within acceptable levels of accuracy by models even if based on relatively simple hydrological sub-models and on a "box-type" approach for predicting the migration of contaminant through the watercourse.

In contrast, the results of sub-models for predicting the behaviour of radionuclides strongly interacting with sediment and soil particles are affected by significant levels of uncertainty. Exercise (1) was crucial in this respect. This blind test showed that models properly predicted the remobilisation of strontium from the contaminated Pripyat River floodplain, whereas they significantly overestimated the remobilisation of radiocaesium. The modelling of the complex dynamics of extreme hydrological events, such as inundation of large flood plains, was also recognised as an important source of uncertainty for reactive radionuclides. Indeed, the concentration of re-mobilised radionuclides in water depends on the time of inundation and on the proportion of water flowing on more or less contaminated areas. In many circumstances these quantities cannot be predicted with sufficient accuracy and, therefore, have a major influence on overall model uncertainty.

It is quite obvious that different models supply different results when applied to the same contamination event. Nevertheless, in spite of the range of variability of the model predictions, the results of the different tested models were generally compatible and reproduced the time behaviour of radionuclide concentration in the components of the analysed systems ("behavioural models").

The spread of the results reflected the various methodological approaches used to model the complex processes occurring in the aquatic environment as well the different values used for the parameters in the models.

The exercises have shown the benefits of using several models for the same contamination scenario (multi-model approach). This approach is of particular value when the environmental processes are complex and when there are, therefore, difficulties in selecting appropriate site-specific values of model parameters. In such circumstances, different hypotheses and approaches may be used by modellers to represent the same situation. The exercises performed in the working group showed that a multi-model approach can be useful for the management of complex problems in environmental assessment. Through this approach, the conclusions that obtain the greatest degree of consensus among modellers are clearly evident, while the aspects that are subject to dispute and which should therefore be handled carefully also become clear.

CHAPTER 1. INTRODUCTION

1.1. Background

During the last decades, a number of projects have been launched to validate models for predicting the behaviour of radioactive substances in the environment that can be applied for the purposes of radiation protection.

Such projects took advantage from the great deal of experimental data gathered, following the accidental introduction of radionuclides into the environment (the accident at the Chernobyl power plant was the most obvious example), to assess the contamination levels of components of the ecosystem and of the human food chain. Although the aim of these projects was to improve models applicable to radioecological modelling and assessment, the progress obtained in the area of modelling can easily be applied to environmental stressors other than radionuclides.

BIOMOVS (BIOspheric Model Validation Study), an international project initiated by the Swedish National Radiation Protection Institute (NRPI), was the first example of a cooperative study aimed at validating the performances of environmental models [1]. BIOMOVS activities focused on both terrestrial and aquatic ecosystems. The success of the BIOMOVS project, in terms of new results and in relation to the benefits from the international cooperation, suggested the launch of several other validation exercises.

BIOMOVS II covered the period from 1991 to 1996 with the same main aims of BIOMOVS. It was organised by the Atomic Energy Control Board of Canada, Atomic Energy of Canada Limited, CIEMAT (Centro de Investigaciones Energéticas Medioambientales y Tecnologicas, Spain). Empresa Nacional de Residuos Radioactivos SA (Spain) and the Swedish Radiation Protection Institute.

In 1990, the VAMP project (Validation of Model Predictions), supported by IAEA, was launched. Among the different tasks of this project the validation of models for predicting the migration of radionuclides in lakes, reservoirs and rivers was carried out using empirical data from several European fresh water systems contaminated with ^{137}Cs of Chernobyl origin [2].

The BIOMASS (BIOsphere Modelling and ASSessment) project was launched in 1996 and was sponsored by IAEA. Although the programme was aimed at addressing radiological issues broader than simple model assessments, several model validations and comparisons were carried out.

Table 1.1 lists some types of exercises carried out within the frame of the above mentioned projects.

Both the BIOMOVS and VAMP projects stimulated intensive efforts for improving the reliability of the models aimed at predicting the migration of ^{137}Cs in lakes and of ^{137}Cs and ^{90}Sr in rivers. However, similar cooperative studies for model validation were not undertaken for other important fresh water systems such as coastal waters and drainage areas. Moreover, apart from radiocaesium and radiostrontium, there are few examples of equally extensive model testing exercises for other long-lived radionuclides that can be of importance for the medium and long term effects related to the contamination of the fresh water environment.

Table 1.1. A list of model testing exercises carried out in the frame of several international projects.

Aquatic ecosystem	Type-A exercise (comparison of model output with independent empirical data)		Type-B exercise (inter-comparison of the results of different models when independent empirical data were not available)	
	Radionuclide	**Project**	**Radionuclide**	**Project**
Lakes	^{137}Cs, ^{14}C	BIOMOVS,VAMP BIOMOVS II	^{226}Ra, ^{230}Th	BIOMOVS
Reservoirs	^{137}Cs, ^{90}Sr	VAMP		
Rivers	^{137}Cs, ^{90}Sr Hg	VAMP BIOMOVS		
Wash-off and groundwater (transport to water bodies)	^{137}Cs, ^{90}Sr	BIOMOVS II	^{137}Cs, ^{90}Sr. ^{237}Np, ^{239}Pu	BIOMOVS

The IAEA Programme on Environmental Modelling for RAdiation Safety (EMRAS) was initiated in 2003 and continued some of the previous work of the aforementioned projects. The work of EMRAS has focused on areas where uncertainties remain in the predictive capability of models, notably in relation to the consequences of releases of radionuclides to particular types of environment (e.g., urban and aquatic environments), the restoration of sites with radioactive residues and the impact of environmental radioactivity on non-human species.

Regarding the area of radioactive release assessment, the objectives of EMRAS were to test the accuracy of the model predictions to develop and improve model capabilities for particular environments and to provide a forum for the exchange of experience and research information.

The activities of the Working Group on testing of models for predicting the behaviour of radionuclides in freshwater systems and coastal areas of the IAEA project EMRAS have been aimed at bridging some of the above gaps, taking advantage not only from the contamination data of Chernobyl origin, but also data from other sources and types of environmental contamination.

1.2. Scenarios for model intercomparison

Several priorities were selected for the intercomparison exercises carried out in the frame of the EMRAS Aquatic WG:

- Important radionuclides other than Cs and Sr;
- Extreme events;
- Physical factors dealing with remobilisation; and
- Modelling radionuclide behaviour in coastal areas/estuaries.

Five scenarios (details and data are available in the EMRAS website: http://www-ns.iaea.org/projects/emras/emras-aquatic-wg.htm) have been considered to implement intercomparison exercises on the basis of the above priorities (Table 1.2):

(1) Wash-off of ^{90}Sr and ^{137}Cs deposits from the Pripyat floodplain (Ukraine). Modellers were asked to predict the time dependent water contamination of Pripyat River following the inundation of the river floodplain, heavily contaminated following the Chernobyl accident. Available input data were the deposits of radionuclides in the floodplain, the time dependent contamination of water in the river entering the floodplain, the water fluxes and several other morphological, meteorological and hydrological data. Concentrations of radionuclides in the water of the River Prypiat down-stream of the floodplain were supplied to assess the performances of the models [3].

(2) Radionuclide discharge from the Dnieper River (Ukraine) into its estuary in the Black Sea. Modellers were asked to predict the time dependent ^{90}Sr and ^{137}Cs contamination of water of the estuary. Input data were the atmospheric deposition of radionuclides of Chernobyl origin, the concentrations of radionuclides in the Black Sea, hydrological, morphological and environmental (temperature, salinity, pH, etc.) data. The performances of the models were assessed by comparison of model results with time dependent empirical data of radionuclide concentration in the estuary [4].

(3) ^{3}H migration in the Loire River (France). This scenario was aimed at assessing the dispersion of tritium releases at different points in the Loire River (France), along a large domain (~ 350 km) and over a period of six months. Water discharges from tributaries, hydrological data and information and tritium discharges from four nuclear power plants were supplied as input data. The results were compared with empirical measurements of tritium concentration at Angers, a city along the river [5].

(4) Release of radionuclides into the Techa River (South Urals, Russia). The objective of this scenario was to test models for radioactive contamination of river water and bottom sediments by ^{90}Sr, ^{137}Cs and $^{239,240}Pu$. The scenario was based on data from the Techa River, which was contaminated mainly in 1949–1952 as a result of discharges of liquid radioactive waste into the river.

(5) Behaviour of ^{226}Ra in the Huelva estuary (Spain). The estuary was affected by contamination from former phosphate industry. The exercise consisted of providing the time evolution of the total ^{226}Ra inventory in the bed sediments and the time evolution of the concentration in the water column.

Scenarios (1) and (3) were so called “blind” exercises, that is the modellers were not given access to the observed data in advance of their modelling attempt.

Modellers from several international institutes participated in the exercises (Table 1.3).

Table 1.2. The scenarios selected for the EMRAS Aquatic Working Group activities.

Scenario	Relevant issues	Notes
Wash-off of ^{90}Sr and ^{137}Cs deposit from the Pripyat floodplain	Extreme events. Physical factors dealing with remobilisation.	Two flood events were considered in this scenario, the events from 1991 and 1999.
Release of ^{137}Cs, ^{90}Sr and $^{239\,240}$Pu into the Techa River	Important radionuclide other than Cs and Sr. Physical factors dealing with remobilisation.	
^{3}H migration through Loire River	Important radionuclide other than Cs and Sr	Assessment of ^{3}H migration through Loire River (France) following multi-point routine discharges of radionuclide in water
Radionuclide discharge from Dnieper into its estuary	Physical factors dealing with remobilisation. Modelling radionuclide behaviour in coastal areas	
^{226}Ra behaviour in Huelva estuary	Important radionuclide other than Cs and Sr Physical factors dealing with remobilisation. Modelling radionuclide behaviour in coastal areas	Assessment of the ^{226}Ra self-cleaning process observed in an estuary formerly affected by the phosphate industry

Table 1.3. Institutes taking part in the modelling exercises.

Institute	Country	Scenario
AEP, AtomEnergoProject	Russia	Release of ^{137}Cs, ^{90}Sr and $^{239\,240}$Pu into the Techa River
EDF, Electricité de France R&D	France	^{3}H migration through the Loire River ^{226}Ra behaviour in the Huelva estuary
ENEA, Ente per le nuove tecnologie l'Energia e l'Ambiente	Italy	Wash-off of ^{90}Sr and ^{137}Cs deposits from the Pripyat floodplain Radionuclide discharge from the River Dnieper into its estuary ^{3}H migration through the Loire River ^{226}Ra behaviour in the Huelva estuary
IGE, Institute of General Energy	Ukraine	^{3}H migration through Loire River
IMMSP, Institute of Mathematical Machine and System Problems	Ukraine	Wash-off of ^{90}Sr and ^{137}Cs deposit from the Pripyat floodplain Radionuclide discharge from the River Dnieper into its estuary ^{3}H migration through the Loire River ^{226}Ra behaviour in the Huelva estuary
Institute of Experimental Meteorology SPA "Typhoon"	Russia	Release of ^{137}Cs, ^{90}Sr and $^{239\,240}$Pu into the Techa River
IRSN, Institut de Radioprotection et de Sûreté Nucléaire	France	^{3}H migration through the Loire River Release of ^{137}Cs, ^{90}Sr and $^{239\,240}$Pu into the Techa River
ISDAE, Institute of Safety Development of Atomic Energy	Russia	Release of ^{137}Cs, ^{90}Sr and $^{239\,240}$Pu into the Techa River
UHMI, Ukrainian Institute for Hydrometeorology	Ukraine	Wash-off of ^{90}Sr and ^{137}Cs deposits from the Pripyat floodplain
University of Sevilla	Spain	Wash-off of ^{90}Sr and ^{137}Cs deposits from the Pripyat floodplain Radionuclide discharge from the Dnieper River into its estuary ^{226}Ra behaviour in Huelva estuary
University of Uppsala	Sweden	Radionuclide discharge from the Dnieper River into its estuary

CHAPTER 2. WASH-OFF OF CHERNOBYL ^{90}SR AND ^{137}CS DEPOSITION FROM THE PRIPYAT FLOODPLAIN

Luigi Monte, Ente per le Nuove tecnologie l'Energia e l'Ambiente, ENEA, Rome, Italy; Raul Periañez, Departamento Fisica Aplicada, University of Sevilla, Spain; Sergey Kivva, Institute of Mathematical Machines and System Problems, IMMSP, Ukraine; Giacomo Angeli, ENEA, Italy; Haydn Barros, Departamento Fisica Aplicada, University of Sevilla, Spain; Mark Zheleznyak, IMMSP Ukraine

2.1. Introduction

A floodplain plays an important role in determining river water quality. This is enhanced by the fact that industrial facilities are often located on river banks because of technological requirements. In the case of an accident, the floodplain becomes a long-term source of potential contamination for river waters. Therefore, reliable models are required for prediction of the migration of contaminants from floodplains to rivers. Validation of such models is the main objective of the present scenario.

The scenario aimed at evaluating the features of models for predicting the migration of radionuclides from flooded areas to rivers. It deals with the complex problem of assessing the re-mobilisation of radioactive substances from heavily contaminated areas following inundation events. This modelling exercise was performed for ^{137}Cs and ^{90}Sr, two radionuclides of significant environmental importance. It supplies valuable information in view of the different behaviour of these radionuclides in the aquatic environment.

The scenario provides an opportunity for: (1) assessing the migration of contaminants from the floodplain to the river; (2) a better understanding of the contaminant transport in the soil-water system at the process level, and, (3) developing and testing methods to estimate key parameters such as contaminant resuspension rates.

Three flooding events took place, in 1991, 1994 and 1999 in the vicinity of the Chernobyl NPP (Figure 2.1). The flooded area, including a part of the Pripyat River floodplain, was highly contaminated as a result of the Chernobyl accident in 1986. In spite of being relatively small, this area can significantly contribute to the contamination of the Pripyat River.

The input data available for the model applications include the following: the topography of the Pripyat River floodplain area; ^{90}Sr and ^{137}Cs deposition densities in the Pripyat River floodplain area; ^{90}Sr and ^{137}Cs activity concentrations for the input cross section; hydrological and meteorological data; chemical composition of the Pripyat River water; soil characteristics; vertical distributions of radionuclides in soil; and particle size distributions for soil and suspended sediment.

The scenario endpoint was the evaluation of ^{90}Sr and ^{137}Cs activity concentrations in the output cross section of the flood plain. The empirical data included the measured concentrations of these quantities and were made available to modellers after the modelling exercise as described in Section 2.3.

More details of the scenario are provided in Appendix I, with a list of the types of available test data. The scenario description is followed by tables containing information to be used as input data by modellers. The test data are not included in the present report, but are available for the scientific community at the website http://www-ns.iaea.org/projects/emras/.

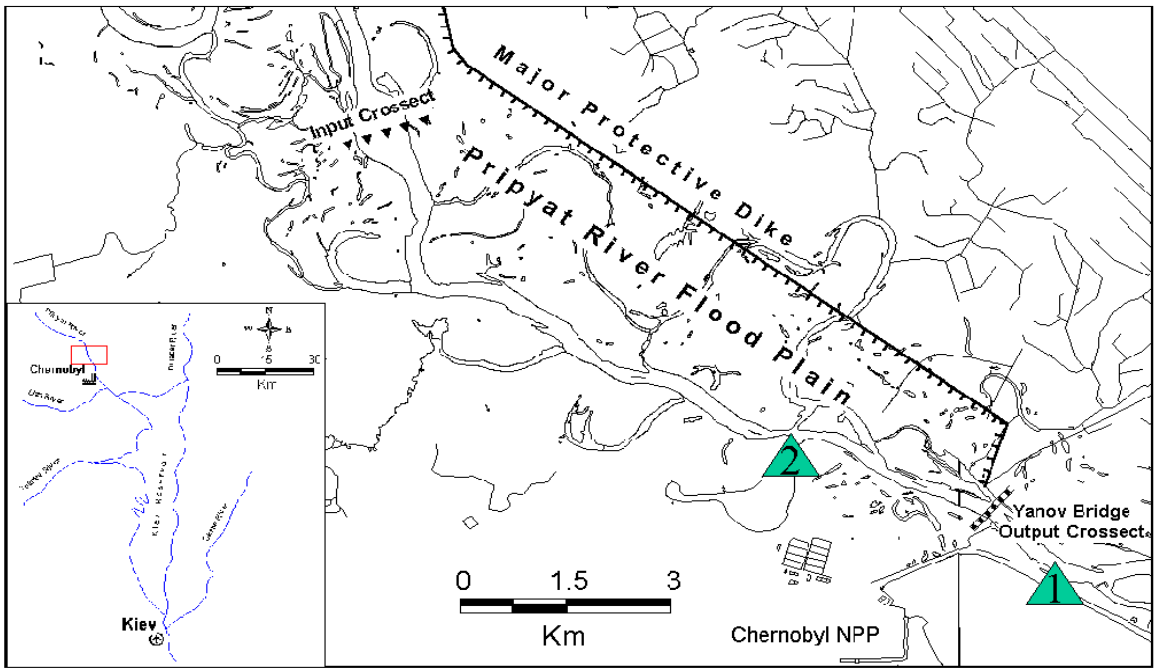

1 - Gauge Station BNS; 2 - Gauge Station D3

Fig. 2.1. Scheme of the Pripyat River floodplain in the vicinity of Chernobyl NPP (before 1992).

2.2. Main characteristics of the models

The models used in the present exercise were developed by the University of Sevilla (Spain), ENEA (Italy) and IMMSP (Ukraine) and are described in Appendix II.

The results of an application of a commercial software tool to the floodplain scenario by the Ukrainian Institute of Hydrometeorology, UHMI (Ukraine) is discussed in detail in Chapter 7. This application was performed by an "expert user" of a commercial mathematical code that is mainly designed for hydrological assessments and that was equipped, for the specific purpose of the present exercise, with a simple routine for the assessment of radionuclide resuspension from the floodplain.

The University of Sevilla, ENEA and IMMSP models are based on common methodologies and approaches. Each model comprises a hydrological module aimed at evaluating the water fluxes and, consequently the dynamics of the floodplain inundation and a radionuclide migration model. The present exercise focused on the assessment of the features of the radionuclide migration modules.

The University of Sevilla model was implemented in two different versions (-3C and -4C) as described in Appendix II.

The analysis of the mathematical features of the three models demonstrates that they show similar basic structures. Indeed, their equations can be written in the following common form:

$$\frac{\partial hC}{\partial t} = -(k_{wf} + k_{ws} + \lambda)hC + k_{fw}D_f + k_{sw}D_s + [(adv + dif)hC]$$
$$\frac{\partial D_f}{\partial t} = k_{wf}hC - (k_{fw} + k_{fs} + \lambda)D_f + k_{sf}D_s \quad (2.1)$$
$$\frac{\partial D_s}{\partial t} = k_{ws}hC + k_{fs}D_f - (k_{sf} + k_{sw} + k_s + \lambda)D_s$$

where adv and dif represent, respectively, the advection and diffusion operators. A list of symbols in Equations (2.1) is given in Table 2.1.

The mathematical form of Equations (2.1) makes quite apparent the meanings of the terms hC, D_f and D_s (radionuclide amount per square metre in each environmental component) and of the products of these terms by the rates k_{ij} (s^{-1}) (the fluxes of radionuclide per square metre exchanged among the system components). The comprehensive structure of the sub-model controlling the radionuclide interaction with sediment is shown in Figure 2.2. It should be noted that: a) in University of Sevilla-3C model D_f and D_s are defined as the "reversible" and the "slow reversible" radionuclide fractions in sediment; b) in ENEA model, D_f is the radionuclide in suspended matter and in a very thin layer of soil strongly interacting with radionuclide in water (it is assumed that the radionuclide concentration in such a layer is equal to the concentration in suspended matter), D_s is the radionuclide contamination in soil; and c) in model COASTOX, developed by the IMMSP, D_f and D_s correspond to the radionuclide in suspended matter and in the upper soil layer of the floodplain, respectively.

The University of Sevilla-4C model considers 4 compartments that correspond to the radionuclide in water (dissolved phase), the radionuclide in suspended matter and radionuclide concentrations in floodplain soil (fast and slow exchangeable forms).

The models COASTOX and University of Sevilla-3C and -4C implemented the advection and diffusion terms by well known partial differential equations.

Table 2.1. List of symbols in Equations (2.1).

Symbol	Description	Dimension
C	Radionuclide concentration in water (dissolved form)	Bq m^{-3}
D_f	Radionuclide (particulate phase) per square metre (fast component)	Bq m^{-2}
D_s	Radionuclide (particulate phase) per square metre (slow component)	Bq m^{-2}
k_{wf}	Radionuclide migration rate from water (dissolved form) to particulate phase (first exchange process)	s^{-1}
k_{ws}	Radionuclide migration rate from water (dissolved form) to particulate phase (second exchange process)	s^{-1}
k_{fw}	Radionuclide migration rate to water (dissolved form) from particulate phase (first exchange process)	s^{-1}
k_{sw}	Radionuclide migration rate to water (dissolved form) from particulate phase (second exchange process)	s^{-1}
k_{fs}	Radionuclide migration rate from the first to the second component of radionuclide particulate phase	s^{-1}
k_{sf}	Radionuclide migration rate from the second to the first component of radionuclide particulate phase	s^{-1}
k_s	Radionuclide fixation rate (irreversible process)	s^{-1}
λ	Radioactive decay constant	s^{-1}
h	Depth of the water column	m

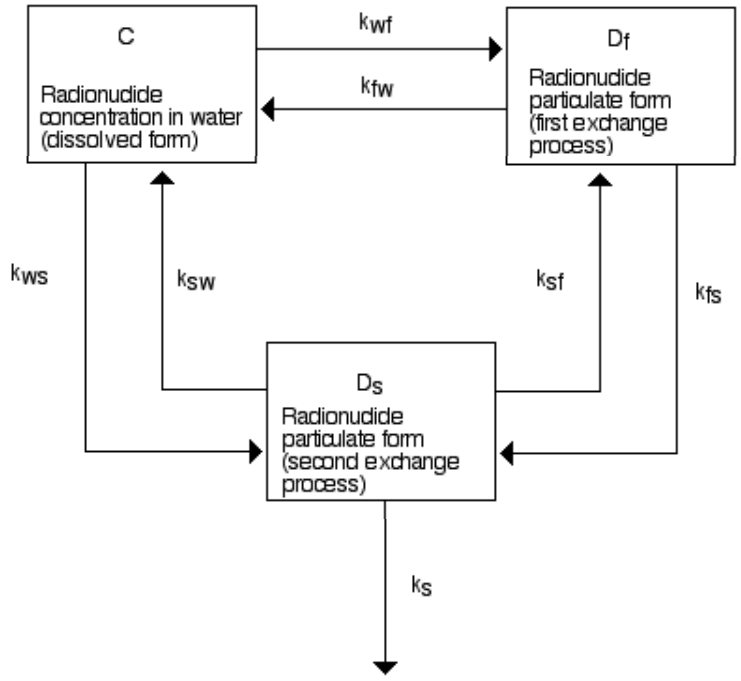

Fig. 2.2. Comprehensive structure of sub-models for predicting the behaviour of radionuclide in the water-sediment system.

The ENEA model simulated the diffusion and the advection processes by subdividing the water body into sectors covering the river and the floodplain. The radionuclide fluxes between two contiguous sectors were calculated accounting for the water fluxes exchanged between these sectors.

The COASTOX model simulated the sedimentation and resuspension of radionuclide in fuel particles and in non-exchangeable phase by equations that are structurally similar to the ones controlling the corresponding processes for the exchangeable phase although are independent of these last (uncoupled equations).

2.3. Results and discussion

The assessment of the model performances compared the model output with empirical concentrations of radionuclides in water collected at the "output" cross section of the floodplain. The empirical data covered periods of time from approximately one month before the flooding event to one month after the event. The sampling frequency was of the order of one week.

Two exercises were performed to assess the model performances: (a) a blind test of model applications to the flooding event occurred in 1991; and, (b) an application to the 1999 flooding event of models calibrated accounting for the results of the blind test.

The "blind test" (the empirical data of water contamination at the "output" section of the floodplain were not disclosed to modellers) was performed by the University of Sevilla-3C and the ENEA by model applications to the 1991 flooding event.

The COASTOX model has been applied, since the early nineties, to this floodplain modelling as a part of the studies for justification of water protection measures [6, 7]. Consequently, COASTOX did not participate in this phase of the exercise as the developers of this model had access to the empirical data.

Figures 2.3 and 2.4 show the model results obtained for the flooding event in 1991. As seen from the figures, both models predicted the increase of ^{90}Sr concentration in water following the inundation of the floodplain. In contrast (Figure 2.4), the models significantly overestimated the concentration of ^{137}Cs in water. The inundation did not cause a major increase of radionuclide concentration in the river water predicted by the models.

It should be noted that the time behaviour of the contamination is influenced by the flooding dynamics that, in view of the lack of sufficient information, were not properly accounted for at this stage of the exercise. This explains the differences in the radioactive contamination decline with time between the model output and the empirical data.

Following the first phase of the exercise based on the above described blind test, the output data were disclosed and modellers were asked to carry out further applications using the improved models (exercise phase-2).

The new results of the modelling were obtained by using parameter values that better reflected the low re-mobilisation of ^{137}Cs from soil. The application of the University of Sevilla model was done by considering a fourth compartment to simulate more accurately the interaction of the radionuclide with the suspended matter. Obviously, the results of these calibrated models are of less interest as they are much closer to the empirical data. However, the assessment of the results of the improved models to predict the effects of the flooding event occurred in 1999 in order to evaluate the performances of the models in a situation for which they were not previously calibrated is of greater interest. The results of these further applications are shown in Figures 2.5 and 2.6.

It should be noted that the most important factor influencing the contamination of water in the floodplain is the remobilisation of radionuclides from the heavily contaminated soil. The blind text exercise clearly showed the propensity of modellers to hypothesise a significant remobilisation of contaminants from the polluted floodplain. The comparison of the model results with the empirical data clearly demonstrated that such a hypothesis is valid for ^{90}Sr, but should be used with caution for ^{137}Cs.

Many studies have demonstrated that ^{137}Cs shows a lower mobility than ^{90}Sr [8–10]. These results were generally accounted for by modellers as demonstrated, for instance, by the ratios v_{ws}/k_{sw} and the values of k_{ds} for caesium and strontium used by the ENEA model for the blind test application (Table 2.2). The higher value of the ratio v_{ws}/k_{sw} for ^{137}Cs indicates a more intense migration of this radionuclide from water to sediment. Moreover the high value of k_{ds} denotes a more effective burial of the radionuclide and a consequent significant decrease of its remobilisation rate. In spite of these values, this exercise demonstrated that the remobilisation of caesium was still overestimated by the examined state-of-the-art models. Table 2.2 shows the calibrated values of the migration parameters used for a more accurate simulation of the behaviour of radiocaesium.

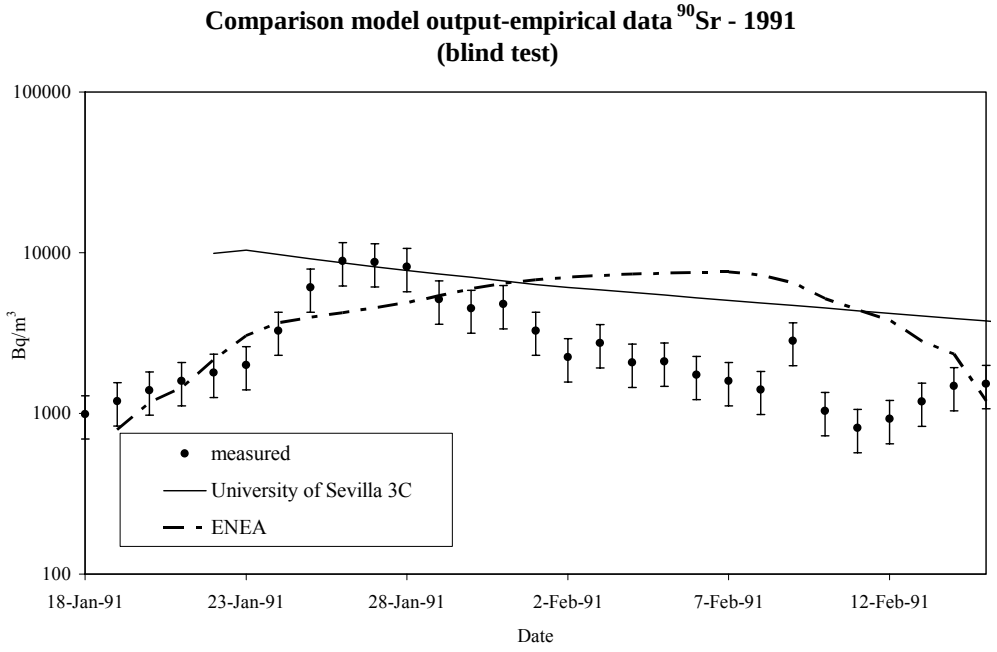

Fig. 2.3. Comparison of model predictions with empirical data (daily averages) of ^{90}Sr concentration in Prypiat River ("Output section"). Results obtained from a "blind test" of model validation.

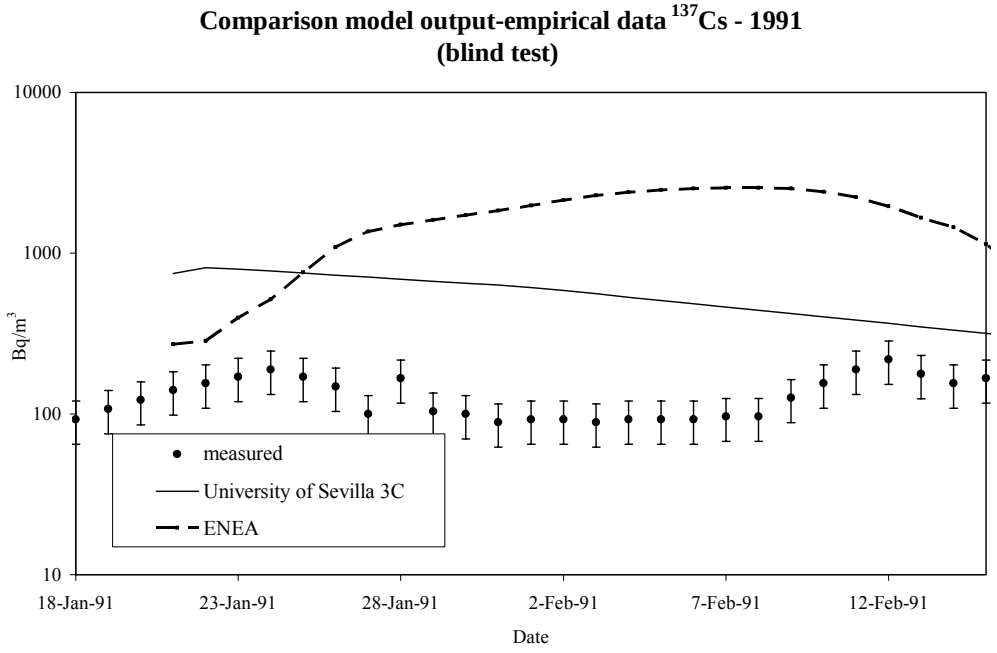

Fig. 2.4. Comparison of model predictions with empirical data (daily averages) of ^{137}Cs concentration in River Prypiat water ("Output section"). Results obtained from a "blind test" of model validation.

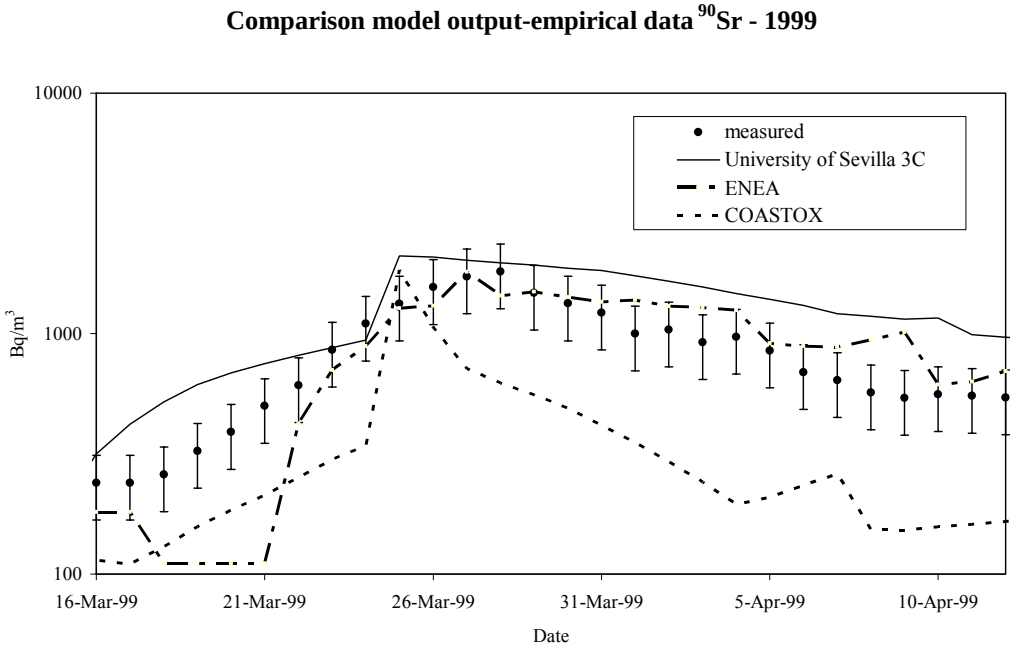

Fig. 2.5. Comparison of model output and experimental concentrations (daily averages) of ^{90}Sr in the "output section" of the flood plain in 1999.

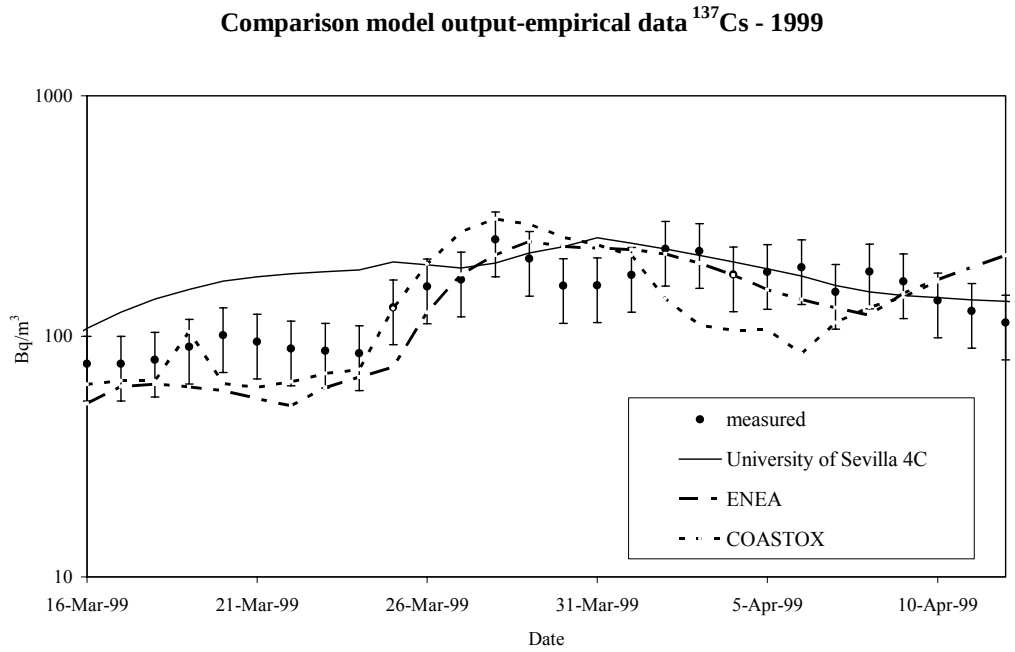

Fig. 2.6. Comparison of model output and experimental concentrations (daily averages) of ^{137}Cs in the "output section" of the flood plain in 1999.

Table 2.2. Values of the parameters in the "water-sediment" radionuclide migration of model ENEA [11].

Parameter	Description	Units	^{90}Sr (blind test)	^{137}Cs (blind test)	^{137}Cs (calibrated)
v_{ws}	Radionuclide migration velocity to sediment	m s^{-1}	1.0×10^{-7}	1.6×10^{-6}	2.8×10^{-5}
k_{sw}	Radionuclide resuspension rate from sediment to water	s^{-1}	5.6×10^{-9}	1.5×10^{-8}	5×10^{-9}
k_{ds}	Radionuclide migration rate to deep sediment	s^{-1}	8.8×10^{-10}	1.2×10^{-8}	1.2×10^{-9}

It is worthwhile noting that different sets of values of the migration parameters can be used to obtain model results matching with the empirical data, provided that high overall radionuclide fluxes from water to sediment are simulated. High overall fluxes can be obtained in several ways by selecting different sets of values of the rate of irreversible fixation of radionuclide on soil (k_s), of the re-mobilisation rates (k_{sw}, k_{fw}) and of the rates of radionuclide migration from water to soil (k_{ws}, k_{wf}). In view of the uncertainties of the empirical data (radionuclide concentrations in water and the spatial distribution of the radionuclide deposition on the floodplain), the lack of detailed information concerning the flooding dynamics, the variability in space of the floodplain characteristics (for instance, the nature of soil) and the sensitivity of the models, it is difficult to determine an unequivocal "calibrated" set of parameter values.

The time behaviour of radionuclide concentrations in water is very sensitive to the dynamics of flooding. Indeed, the concentration of radionuclides in water depends on the time of inundation of areas showing different contamination levels and on the proportion of water flowing over more or less contaminated areas. Therefore, the results of the "phase-2" exercise of University of Sevilla and ENEA models were obtained following a "calibration" of the hydrological modules of the models to assure that the predicted time behaviour of radionuclide in water was compatible with the empirical data. On the contrary, the results of model COASTOX were obtained, for the present exercise, without special tuning of the hydrological module. It should be kept in mind that the present work, as previously noted, is not aimed at evaluating the performances of the hydrological modules of the assessed models. The complexity of the inundation dynamics and the large amount of data necessary to predict the time behaviour of the flooding event prevented such an evaluation.

2.4. Conclusions

The aim of the present exercise was to ascertain if state-of-the-art models properly predicts the time dependent levels of radionuclide concentrations in the river water before and following flooding events.

Radionuclide re-suspension is the most important factor controlling the amount of radionuclide in waters inundating highly contaminated areas. The experimental evidence from the inundation events of the Chernobyl floodplain demonstrated that remobilisation of radiostrontium from contaminated soils is an important process implying a significant radioactive load of water flowing over contaminated floodplains. On the contrary, there is no empirical evidence of similar behaviour for radiocaesium.

The remobilisation of strontium was properly predicted by state-of-the-art models, whereas caesium remobilisation was significantly overestimated, as demonstrated by the blind test.

The present exercise supplied useful information to improve the models in order to obtain more realistic predictions of the contamination levels of water flowing on contaminated floodplain. The results should be accounted for the improvement of models aimed at supporting the management of the aftermath of nuclear accidents.

It was also demonstrated that the predictions of the hydrological processes should be undertaken with reasonable accuracy in order to reduce the uncertainty prediction of radionuclide transport. Flooding dynamics is clearly the main factor controlling the time behaviour of radionuclide concentrations in flood waters.

CHAPTER 3. INTERCOMPARISON OF MODELS FOR PREDICTING THE BEHAVIOUR OF ^{137}CS AND ^{90}SR OF CHERNOBYL ORIGIN IN THE DNIEPER-SOUTHERN BOUG (DNIEPER-BUG) ESTUARY

Luigi Monte, ENEA, Italy; Lars Håkanson, Uppsala University, Sweden; Raul Periañez, University of Sevilla, Spain; Gennady Laptev, Ukrainian Institute for Hydrometeorology, Ukraine; Mark Zheleznyak, Institute of Mathematical Machines and System Problems, Ukraine; Vladimir Maderich, Institute of Mathematical Machines and System Problems, Ukraine; Giacomo Angeli, ENEA, Italy; Vladimir Koshebutsky, Institute of Mathematical Machines and System Problems, Ukraine

3.1. Introduction

Due to the biological value of the coastal zone and the different demands on the utilization of coastal waters it is easy to understand why so much interest concern this zone. However, in context of aquatic radioecology, it is easy to conclude that much more efforts have been focused on lakes and rivers [2, 12, 13] rather than on coastal areas. In fact, it is very difficult to find the data necessary to test coastal models. The project EMRAS (initiated by the IAEA in September 2003) has been intended to compile available data on radionuclide contamination, radionuclide concentrations in water, sediments and biota and the necessary co-variables related to the characteristics of coastal areas, to achieve a proper scenario description needed for model tests and comparative studies. The present study is an intercomparison of different models and modeler's approaches to predict the behaviour of ^{137}Cs and ^{90}Sr in the estuarine environment of the Dnieper and Bug Rivers following the contamination due to the Chernobyl accident of Dnieper River and its catchment.

The Dnieper-Bug Estuary (DBE, Dniprovs'ko-Pivdenno Bougzhs'kyi Liman – in Ukrainian) water system (Figure 3.1) consists of the Dnieper Estuary with the adjoining Southern Boug Estuary (surface area = 1006 km^2). The average depth of the DBE is 4.4 m. The main factor affecting the regime of the system is the process of mixing fresh river waters with saline marine waters. This forms the saline wedge in the estuary, which, in the summer months, can reach Kherson city. Stratification in the estuary ranges from almost none in the eastern part at the Dnieper mouth to a defined two layer system in the western marine part of the DBE. These processes are highly season-dependent. The regime of this drowned river estuary varies from stratified to partially mixed. More details concerning the characteristics of the estuary are reported in Appendix I.

The Dnieper-Bug Estuary was contaminated by radionuclides introduced in the environment following the accident at the Chernobyl nuclear power plant. The contamination was due to the direct deposition onto the estuary and to the contaminants transported by the Dnieper and Bug Rivers. The following input data were available for modellers:

- Bathymetry of DBE and coastal area of the Black Sea (2 km grid);
- Daily discharges of Dnieper River and S. Bug River in 1984–1987;
- Daily sea level in Kinbourn Strait (Ochakov) in 1986–1987;
- Daily temperature and salinity (ppt) at water surface;
- Three hour values of wind, air temperature, relative humidity and cloudiness (0–10);
- Survey data in 1986 of water temperature and salinity measurements; and
- Survey data in 1987 of water temperature, salinity and velocity.

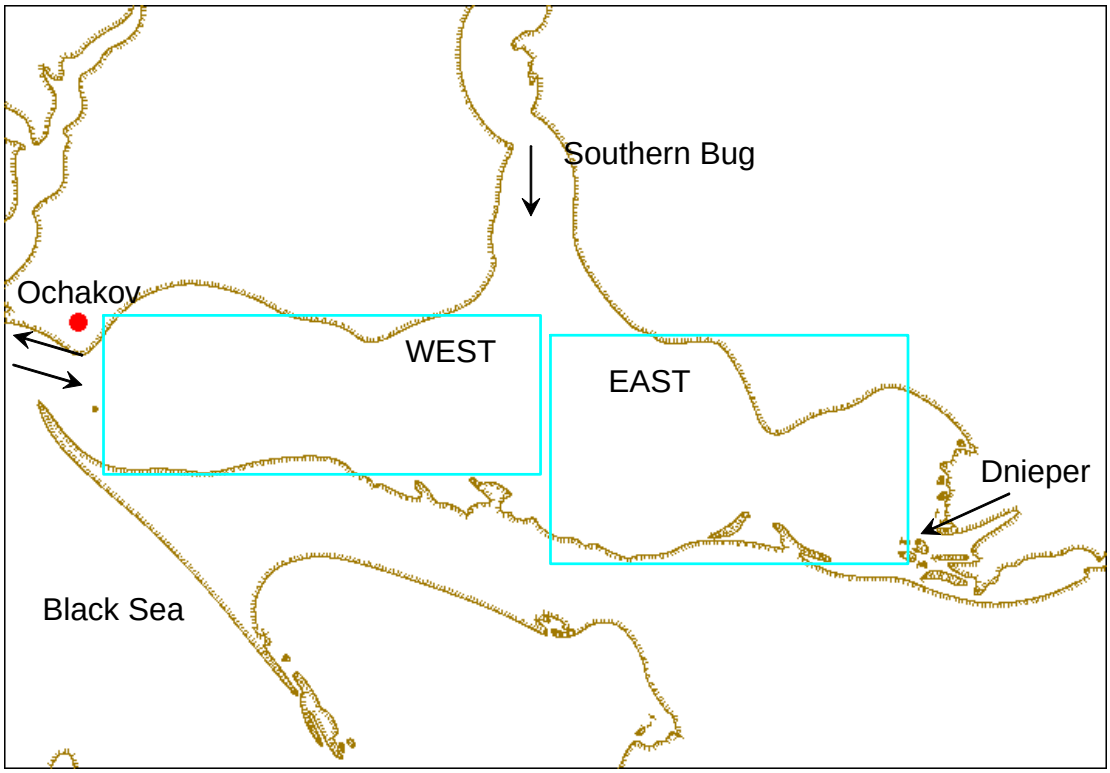

Fig. 3.1. Outline of the Dnieper-Bug Estuary. The boxes correspond to the sectors for which empirical radiological data were available for the present exercise.

Other parameters of DBE hydrology were not available: temperature in the Dnieper River and S. Bug River, temperature and salinity profiles in the Kinbourn Strait. Information was supplied on their seasonal changes.

Whereas copious data relevant to the morphometry, the hydrology and the meteorological conditions of DBE were available, radiological input data were more difficult to find. These data were gathered by two different Ukrainian Institutes (Institute of Mathematical Machines and System Problems and Ukrainian Institute for Hydrometeorology) on the basis of experimental campaigns carried out by several laboratories [14, 15]. It should be noted that a significant effort of selection and evaluation of the empirical data was performed to assure the quality of these data sets.

The input data were the time dependent radionuclide concentrations in Black sea and in the Dnieper River. An estimated value of 5000 Bq m^{-2} of ^{137}Cs initial deposition onto DBE was used by ENEA. University of Uppsala used 3000 Bq m^{-2} for Cs and 1000 Bq m^{-2} for Sr. It should be recognized that modelers derived these values by assessment from fallout maps and circumstantial information [16]. It is not surprising that a so high uncertainty affects the deposition in view of the difficulties inherent to the evaluation of such a distributed quantity and of the interpretation of the available data.

Table 3.1 shows radionuclide concentrations in the Dnieper River, the main tributary of the coastal area. Tables 3.2 and 3.3 show the concentrations of radionuclides in South Bug outlet and North west Black Sea.

Table 3.1. Fluxes of ^{137}Cs and ^{90}Sr from Dnieper to the estuary.

Date	Dnieper mouth (gathered by Institute of Mathematical Machines and System Problems)			Dnieper mouth (gathered by Ukrainian Institute for Hydrometeorology)	
	^{137}Cs (dissolved) Bq m^{-3}	^{137}Cs (suspended) Bq m^{-3}	^{90}Sr Bq m^{-3}	^{137}Cs (total) Bq m^{-3}	^{90}Sr Bq m^{-3}
Pre-Accident				3.0	23–33
May-86	27.8	20.4	18.5	76.0	
Jun-86	12.2–14.1	14.8	37	4–11 / 16 / 7	26–92
Jul-86	7.8	12.2	100	7.0	58–61
Aug-86	7.4	12.2	78		
Sep-86	6.7	4.4	56		
Oct-86	7.0	4.1	63–89		
Nov-86	7.4	3.7	59–104	10.0	37–55
Dec-86	7.8	3.7	89		
Feb-87	14.1	–	48.		
Apr-87				3–11 / 5.2	660–470
Jun-87	5.6–19.2	3.7–6.7	40–278	2 / 7.2	
Sep-87	8.1–14.8	5.2			
Dec-87					300–330

Table 3.2. Concentration of radionuclides in the Southern Bug outlet (data gathered by Ukrainian Institute for Hydrometeorology).

Date	^{137}Cs Bq m^{-3}	^{90}Sr Bq m^{-3}
Pre-Accident	3.5–7 (NOSS)	7–10.5 (NOOS)
Jun-86	16 (UCME)	
Oct-86	10 (UCME)	
Dec-87	3.5 (UCME)	

Table 3.3. Concentration of radionuclide in the North-west Black Sea (data gathered by Ukrainian Institute for Hydrometeorology).

Date	^{137}Cs Bq m^{-3}	^{90}Sr Bq m^{-3}
Pre-Accident	18 (IEM) 15 (IBSS)	22 (IEM) 18–20 (MGI)
Jun-86	55–80 (IEM) 125–185 (IBSS)	26–33 (IEM) 30–130 (IBSS)
Oct-86	110 (UCME)	
Apr -87	33–140 (IBSS)	19–63 (IBSS)
Jun- 87	52 (UCME)	

Table 3.4. Concentration of radionuclides in West DBE (validation data; data gathered by Ukrainian Institute for Hydrometeorology).

Date	^{137}Cs Bq m^{-3}	^{90}Sr Bq m^{-3}
PreAccident	3.5–7 (NOSS)	7–10.5 (NOOS) 28±5 (MGI)
Jun-86	12–34 (UCME)	26–41 (IBSS)
Oct-86	14–18 (UCME)	
Apr -87	14–30 (UCME)	220 (IBSS)
Dec-87		220 (IBSS)

Table 3.5. Concentration of radionuclides in the East DBE (validation data; data gathered by Ukrainian Institute for Hydrometeorology).

Date	^{137}Cs Bq m^{-3}	^{90}Sr Bq m^{-3}
PreAccident	3.5–7 (NOSS)	7–10.5 (NOOS) 28±5 (MGI)
Jun-86	12–19 (UCME)	26–41 (IBSS)
Oct-86	14–18 (UCME)	
Apr-87	3–10 (UCME)	400 (IBSS)
Dec-87		260 (IBSS)

Tables 3.4 and 3.5 show data of measured radionuclide concentrations in water of the West and East part of DBE (data for the assessment of the model performances). Abbreviations in parentheses indicate the Institutes that collected samples and performed the radiological measurements:

- IBSS: Institute for Biology of the Southern Seas, Sebastopol;
- IEM: Institute of Experimental Meteorology (Typhoon), Obninsk;
- MGI: Marine Hydrophysical Institute, Sebastopol;
- UCME: Ukrainian Centre for Marine Ecology, Odessa; and
- NOSS: Nikolaevskaya Oblast Sanitary Station, Nikolaev.

3.2. Main characteristics of the models

Detailed descriptions of the models object of the present study are reported in Appendix II. In this section, we will briefly outline the general, theoretical foundations of the models.

In principle, most approaches for predicting the migration of radionuclides through estuaries are similar to the ones implemented in models for lakes and rivers [13, 17]. It is, however, necessary to account for the particular environmental conditions and processes that significantly influence the behaviour of contaminants in coastal environments.

Generally speaking, the overall structure of models for predicting the behaviour of radionuclides in estuaries comprises the following sub-models:

(1) modules for predicting the physical, hydrological, hydraulic and biotic processes that occur in the estuarine system (such as water temperature and salinity profiles, water fluxes and current velocities, erosion-sedimentation processes and dynamics of suspended matter in water, growth rates of organisms, tidal cycles, etc.) and are supposed to influence the contaminant migration;

(2) modules for predicting the radionuclide transfer:
   (a) to the estuary from its catchment;
   (b) through the abiotic components of the estuary
   (c) from the abiotic components to the biota.

The main processes accounted for by the models are, basically, the diffusion of dissolved substances due to water turbulent motion (eddy diffusion), the transport due to the water current, the interaction of dissolved pollutant with suspended matter and bottom sediment, the mixing processes between different layers of water and, finally, the migration of pollutants from the water to the bottom sediments (sedimentation) and from the bottom sediment to the water (re-suspension).

The most general equations for predicting hydrodynamic processes are the full 3D hydrodynamic equations including baroclinic terms (density differences). However, "2D vertical depth-averaged" models are often used when a vertical mixing of the water column can be hypothesised [18]. These models provide predictions of the water current. Suspended sediment transport is also described by transport/diffusion equation accounting for water velocity and erosion and deposition processes [19, 20].

Not all the models are based on hydrological/hydraulic sub-models for assessing the quantitative behaviour of the environmental processes influencing the migration of pollutants through the components of an estuary ecosystem. Some models make use of empirical values of those parameters that relate the migration of pollutants to the environmental processes and that are averaged over finite regions of space and intervals of time (for instance, monthly averages of time-dependent quantities, average water fluxes among different sections of a water body, etc.).

The sub-models for predicting the interaction of radionuclide in the water column with suspended matter and bottom sediments show different degrees of complexity ranging from simple kd-based assumptions (it is supposed that a reversible equilibrium between dissolved and particulate phases of radionuclide is quickly achieved) to complex multi-stage interactions [21]. Many of these mentioned aspects were described in the previous section "Wash-off of ^{90}Sr and ^{137}Cs deposit from the Pripat floodplain".

Some particular environmental conditions and processes are typical of the estuarine ecosystem and significantly influence the migration of toxic substances. For instance, the different density between sea and fresh waters generates a vertical stratification that affects the diffusion of pollutants through the water column. Moreover, tidal cycle is a further factor that should be considered and modelled for assessing both the hydrodynamics of estuaries and the dispersion of contaminants through estuaries [22].

The main features of the models object of the present assessment are summarised in Table 3.6.

It can be useful to classify models according to their horizon and to their Time and Spatial Resolving Powers (TRP and SRP) in view of their scopes and aims.

The horizon range of information (knowledge obtained from investigation and study, instructions and requested input data) that the model is meant to process and of the outcomes that is meant to predict, defines the starting and the end points of a model. For instance, a model can use as input data the deposition of radionuclide onto the water surface and the catchment area of the estuary. The model horizon is different when the input data are the deposition onto the water surface and the empirical values of radionuclide flowing from the tributary rivers. Obviously in the first example, the model aim is more ambitious and the model is more informative as it does not require information (input of contaminant from rivers) that can be difficult or impossible to obtain for some scenarios (for instance, in case of an accident). Nevertheless, a larger horizon generally implies a higher uncertainty.

Table 3.6. Main features of the models that participated in the exercise.

Model	Developer	Main model features	Horizon
CoastMab	Uppsala University, Sweden	Generic, process-based, dynamic, high emphasis on ecological aspects. TRP= monthly averages SRP= the entire coastal system	Compartment model to predict monthly average values of radionuclide concentrations in water and fish accounting for prevailing ecological and environmental processes when radionuclide concentrations in sea and direct radionuclide deposition over the coastal area are available (for the specific applications also direct radionuclide flux from rivers are supplied as input data).
U. Sevilla	University of Sevilla, Spain	2-dimensional (depth-averaged) based on advection-diffusion equation, high emphasis on hydrodynamic processes TRP and SRP: in principle the model can supply very detailed information.	2-dimensional model. The hydrological characteristics of the system that influence the migration of pollutant (water current velocity field) are modelled from fundamental equations accounting for meteorological conditions.
ENEA	ENEA, Italy	Generic, process-based, dynamic, emphasis on radionuclide flux balance and migration to sediment TRP= monthly averages SRP= for the present application the coastal system is subdivided in three sectors	Compartment model to predict monthly average values of radionuclide concentrations in deep and surface water accounting for prevailing radionuclide fluxes when radionuclide concentrations in sea and direct radionuclide deposition over the coastal area are available. Balance of radionuclide in the system is evaluated using, as input data, a) the radionuclide fluxes from the rivers flowing into the coastal system; or b) the deposition of radionuclide over the whole Dnieper catchment (regional model for ^{90}Sr).
THREETOX	IMMSP, Ukraine	3-dimensional model based on advection-diffusion equation, high emphasis on hydrodynamic processes TRP and SRP : in principle the model can supply very detailed information	3-dimensional model for predicting concentration in water when radionuclide input into the system is known. The hydrodynamics is simulated on the base of three-dimensional, time-dependent, free surface, primitive equation model The hydrological characteristics of the system that influence the migration of pollutant (water current velocity field) are modelled from fundamental equations accounting for meteorological conditions. The model account for the processes governing the exchange of radionuclide between water and suspended/bottom sediment.

TRP= Time Resolving Power, SRP= Spatial Resolving Power.

The resolving power of a model is a measure of the level of details of its predictions. The "time resolving power" (TRP) is the ability of a model to predict differences in the system behaviour over a given interval of time. In other words, the model is supposed to describe the average behaviour of the system over a defined time interval. Example of factors affecting the TRP are the intervals of time necessary to assure the damping of some transient processes which are not intended to be modelled in a sufficient detailed time scale (for instance, the time necessary to approach a homogeneous distribution of the contaminant in the water column, a condition that, obviously, is not immediately achieved, when box models are used; the sorption and de-sorption processes of radionuclide on suspended matter when the model is based on the hypothesis of an "instantaneous" equilibrium between the dissolved and the particulate contaminant phases, etc.).

Similarly the spatial resolving power (SRP) is the ability of a model to predict differences in the system behaviour over a given spatial grid. For instance, the SRP of box models for predicting the spatial distribution of a substance in water is the size of the boxes.

3.3. Results and discussion

Comparisons of model output and empirical data of radionuclide concentration in water are reported in Figures 3.2 and 3.3. The figures show the ranges of the empirical data compared with the model predictions. Uppsala University and ENEA models supplied results for both deep and surface waters (respectively, DW and SW) whereas THREETOX and University of Sevilla models predicted the radionuclide concentrations averaged over the whole water column.

Figure 3.3 shows the results from an application of the ENEA model at a regional scale. The input data of this ”regional model” was the deposition of ^{90}Sr onto the catchment of the Dnieper system around the Chernobyl power plant. The contribution of contaminant to the estuary from the Dnieper River was evaluated by an application of model MARTE to the whole basin of the river (the other model applications made use of measured fluxes of radionuclides from the River Dnieper as input data). In spite of the larger horizon of this particular model application, the predictions of the time behaviour of radionuclide concentration in the estuary were compatible with the results obtained by the other models. This suggests that the transport of pollutants characterised by weak adsorption on bottom sediment can be predicted with a sufficient accuracy although migration occurs over large distances.

A first factor of uncertainty for model applications is the prompt availability of reliable contaminant input data, such as the radionuclide deposition, during an accident. The modellers made use of different values of radionuclide deposition onto the estuary. An estimated value of 2000–5000 Bq m^{-2} of ^{137}Cs initial deposition onto the DBE was obtained from graphical data reported by De Cort et al. [16]. The differences among the output of the models at initial time reflect the uncertainty of the assumed ^{137}Cs initial deposition. Unfortunately, empirical evaluations of ^{90}Sr deposition were not available. Although several evidences indicate negligible contamination levels of the environment due to the initial fall-out of ^{90}Sr in areas far from the Chernobyl power plant, one of the modellers used a cautionary, conservative value of 1000 Bq m^{-2}. This gives reason of the initial peak of ^{90}Sr contamination in water predicted by the Uppsala University model.

Generally speakin, the difficulty for predicting quantitatively the interaction of the dissolved pollutant with sediment (contaminant diffusion from the water column to sediment, sedimentation and resuspension) is one of the main factors of uncertainty of models for the aquatic environment. Nevertheless in the present exercise, due to the fast dynamic of water within the estuary and the low interaction of radionuclide with sediment in seawater, this difficulty has not significantly affected the model performance. Indeed, in spite of the different approaches and the different parameter values and algorithms used by the models, there are no significant differences between the model results that can be attributed to the way the contaminant removal from the water column due the mentioned processes is assessed.

From Figures 3.2 and 3.3 it is quite clear that, in spite of the above mentioned difficulties, there is an apparent consensus among modellers concerning the time behaviour of radionuclides in water. Figures make intuitive what information obtained from the models can be perceived worthy of consensus and in which measure model output should be considered illustrative of the empirical outcomes. For instance, a delay of radionuclide concentration peak in water is predicted for ^{90}Sr, whereas for ^{137}Cs the concentration in water shows a clear decline on time.

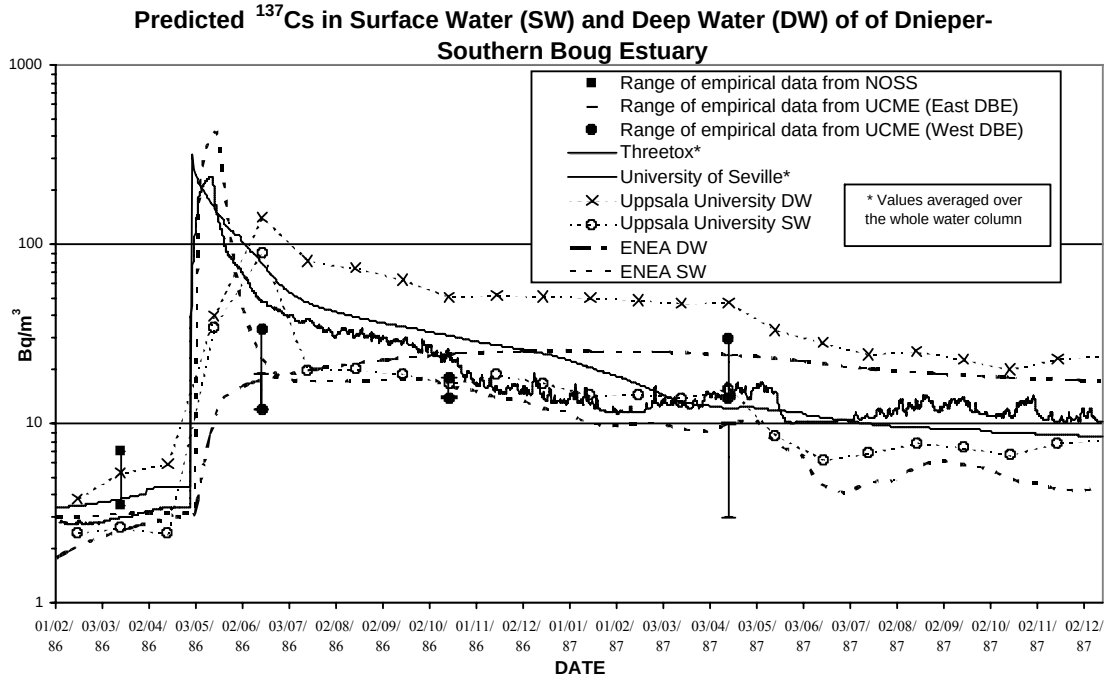

Fig. 3.2. Comparison of the results of the models with empirical data of ^{137}Cs concentration in water.

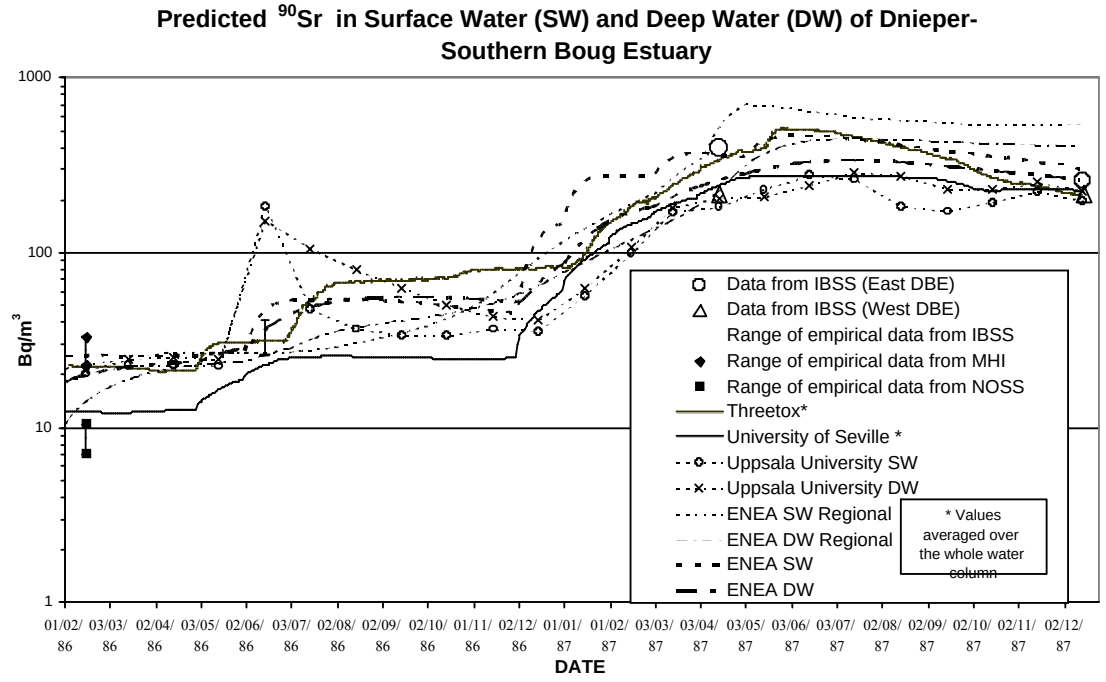

Fig. 3.3. Comparison of the results of the models with empirical data of ^{90}Sr concentration in water.

The range of variability of model output is comparable with the range of variability of the empirical concentrations. This confirms that model performances reflect the intrinsic uncertainty of knowledge concerning the quantitative behaviour of the involved environmental process, the ambiguity of interpretation and parameterisation of such processes, the inherent variability of environmental quantities, etc.

3.4. Conclusions

The different time dependent behaviour of radionuclide concentrations in the estuary water is a consequence of the various degrees of mobility of the pollutants through the environment and of the different initial spatial distribution of contaminantion in the region affected by the Chernobyl accident. Whereas ^{137}Cs deposition was significant at large distance from the site of the accident, ^{90}Sr contamination prevailingly affected areas surrounding the nuclear power plant.

It is worthwhile to note that, beyond the uncertainties of the results, the predictions of the models were compatible with the time behaviour of both ^{137}Cs and ^{90}Sr as Figures 3.2 and 3.3 show. In particular, the model application at regional level demonstrate that state-of-the-art models can properly predict these non-trivial results when the model input is the initial deposition of radionuclide over the Dnieper River and its catchment and the contamination of Black Sea is used as boundary condition.

The examined models are structurally different, make use of different set of parameters and of parameter values and are based on several different hypotheses (Appendix II). Nevertheless, they supply compatible results although spreaded over a variability range of about one order of magnitude. The present exercise shows that there are several difficulties that modellers face for the application of environmental models such as vagueness, ambiguity and incompleteness of information and input data relevant to the examined environmental scenario.

In many circumstances, input data demands from modellers do not correspond to the data offered by experimentalists. Therefore, we have considered a complex situation that includes several actors: the data/information suppliers (the “scenario developers” in this exercise) and the modellers. In this respect, the present exercise is not simply aimed at evaluating the assessed models in order to rank the quality of their performances. In this work, we are concerned with the evaluation of potential advantages of a multi-modelling approach for the management of a complex environmental problem when input data are insufficient and non-univocal. In such conditions, the so called “expert judgment” is an essential factor.

The compatibility of the results from different models showed that a multi-model approach can be useful for the management of complex problems of environmental assessment. The approach makes clear what are the conclusions that obtain a consensus from modellers and what are the ones that should be carefully handled. More details on this subject can be found in the specialised literature [4].

CHAPTER 4. MIGRATION OF TRITIUM IN THE LOIRE RIVER

Luck M., Goutal N., Siclet F. (EDF-LNHE, France), Monte L., Angeli G. (ENEA, Italy), Boyer P. (IRSN, France), Zheleznyak M., Dzyuba N., Treebushny D. (IMMSP, Ukraine), Sizonenko V.P. (IGE, Ukraine)

4.1. Introduction

The present work aims at assessing the performances of models for predicting the migration of tritium through Loire River.

Two exercises of model applications were performed (Appendix I).

The first exercise was a blind test of models aimed at assessing the dispersion of tritium releases in the Loire River:

- from Belleville to MontJean, which represents a domain length of about 350 km;
- on a period of six months, from the 1st of July to the 31st of December 1999;
- taking into account water discharges from tributaries and tritium discharges from 4 nuclear power plants (by using real hydraulic conditions of the year 1999).

Measurements of tritium concentration made in Angers (a city along the Loire River) during the year 1999 were used to assess how efficiently the models simulate the tritium migration in the Loire River.

A second exercise ("schematic case") was based on hypothetical contaminant releases from Belleville nuclear power plant, considering different realistic water flux conditions.

Both scenarios were prepared by EDF-LNHE (France). Obviously, the first exercise was a blind test for all the participants, except for EDF-LNHE.

4.2. Main characteristics of the models

The participants who have presented computations on the two scenarios (blind test and schematic exercise) and the models they tested are given in Table 4.1.

Only the participants appearing in bold in the table have participated to the blind test.

In principle, the main processes governing tritium migration are:

- advection of the pollutant by river flow, that defines the position of the pollution peak in time and space (advection is fully defined by river flow velocities);
- eddy diffusion of the pollutant due to river turbulence, that influences the magnitude of the pollution peak and its spatial spreading.

As tritium does not interact with suspended matter and bottom sediment, the considered scenario of tritium transport in Loire River, well supported by the detailed sets of measured data, is an excellent example to assess how efficiently the models simulate the advection and the diffusion in river water of pollutants that are entirely in dissolved form (non-reactive pollutants).

Table 4.1. Models that participated in the exercise.

Models used for the exercise	Organization	Country
CASTEAUR, in 2 versions: – version v0. 0 (1d steady mode), – version v0.1 (box unsteady mode). – 1d model	IRSN	France
MASCARET – module Tracer – version v5. 0 (characteristics method), – version v5.1 (finite volumes method).	EDF-LNHE	France
MOIRA – module Marte, in 3 cases: – 1: with standard monthly data, – 2: with customised monthly data, – 3: with customised hourly data. ET-model	ENEA	Italy
RIVTOX	IMMSP	Ukraine
UNDBE	IGE	Ukraine

Table 4.2. Hydraulic module (Output: flow velocity or water fluxes).

Models features	CASTEAUR	MASCARET	MOIRA	RIVTOX	UNDBE
– Full 1D St-Venant Equations – Real geometry of the river – Steady and unsteady flow		X		X	
– Continuity equation for the discharge – Manning-Strickler equations – Steady and unsteady flow	X *(with simplified geometry of the river)*				X *(with real geometry of the river)*
– Power relationships between the geometrical features of the river (width and depth) and the water fluxes – Continuity equation for the discharge – Steady flow and non-steady flow			X		

Table 4.3. Transport (advection-diffusion) module (Output: concentration of the pollutant).

Models features	CASTEAUR	MASCARET	MOIRA	ET	RIVTOX	UNDBE
Form of the transport equation: – Non conservative form – Conservative form – Simplified model (transport with a constant velocity – dilution)	X (v0.0) X (v0.1, 1d)	X (v5.0) X (v5.1)	X	X	X	X
Physical diffusion	X (v0.0, 1d)	X (v5.0, v5.1)			X	X *(equivalent volume of dilution)*
Numerical resolution: – finite volumes or box model – characteristics method	X	X (v5.1) X (v5.0)	X			X
Refined space discretisation	X	X			X	

In the model ET (Easy Tool), the velocity is considered constant all along the domain.

Taking into account that advection and diffusion are driven by the hydraulic processes, success of the modeling efforts to predict tritium concentration depends mainly on model ability to simulate crucial hydraulic parameters (discharge, cross section area and its derivatives: cross sectional averaged velocity and bottom shear stress) or to accept such basic data from some "external" hydrological calculations and/or empirical hydrological data.

The main features of the different models used are reported in Tables 4.2 and 4.3..

4.3. Results and discussion

The participants who have participated in the blind test scenario and the models they tested are listed in bold in Table 4.1.

The tested models and their applications to the Loire River are described in Appendix II.

The calculated temporal series of tritium concentrations were compared to the measured ones in Angers, located downstream of all the tritium discharges (approx. 320 km, 290 km, 190 km and 60 km downstream of the 4 discharges of the Loire NPP).

For each model, we plotted these comparisons on graphs, each of them covering 2 successive months (graph 1: July and August 1999; graph 2: September and October 1999; graph 3: November and December 1999) (Figures 4.1–4.4).

Inter-comparisons of the results provided by the different models at different points along the Loire River were also made.

We chose to reproduce these inter-comparisons at 4 points along the Loire River:

- Ouzouer (just downstream of the second nuclear power plant);
- Nouan (just downstream of the third nuclear power plant);
- La Chapelle (around 125 km downstream of the third nuclear power plant); and
- Angers (point where the measurements were made).

These inter-comparisons are reported in Figures 4.5–4.8. For the organization who presented different computations (IRSN and ENEA), only the best results were considered.

4.3.1. Analysis of the models' results (blind test)

4.3.1.1. CASTEAUR

The comparisons between the empirical data measured at Angers and the calculations of CASTEAUR v0.0 for average conditions and of CASTEAUR v0.1 are presented in Figure 4.1.

For CASTEAUR v0.0, these results traduce the limitation due to the occurrence that permanent hydraulic conditions were assumed. The calculations follow the general behaviour of the empirical data, but the precision stays in a range of a factor ten, resulting from the approximation on the water discharges. The best agreements are obtained when the real water flow is near of the average situation considered for these calculations. In these cases, the maximal values are approached (01/12/99 and 13/12/99); that confirms the application domain of the model to short terms assessments, when the regime of the river can be considered as quasi-permanent.

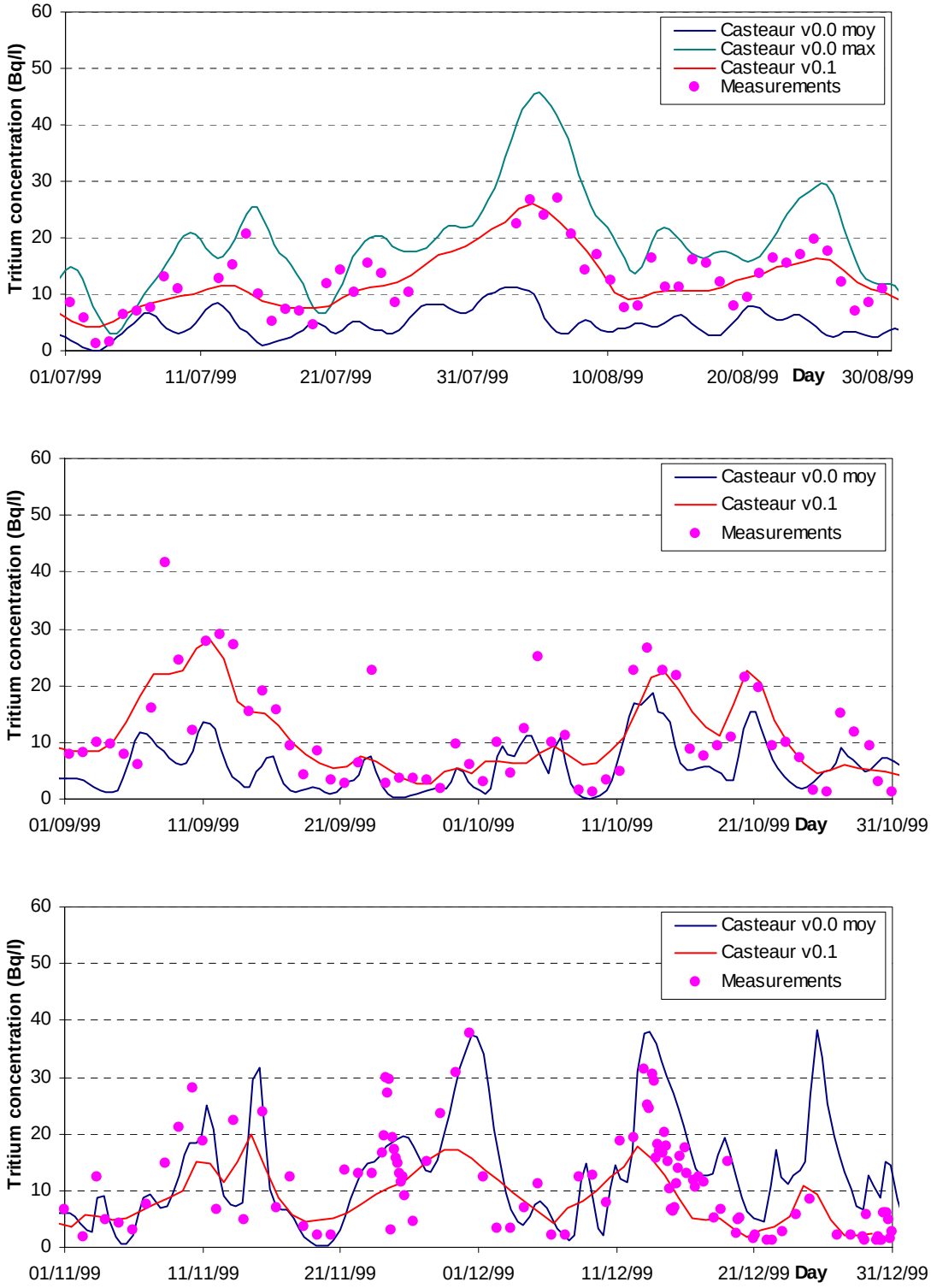

Fig. 4.1. Comparison between calculated and measured tritium concentration at Angers for CASTEAUR.

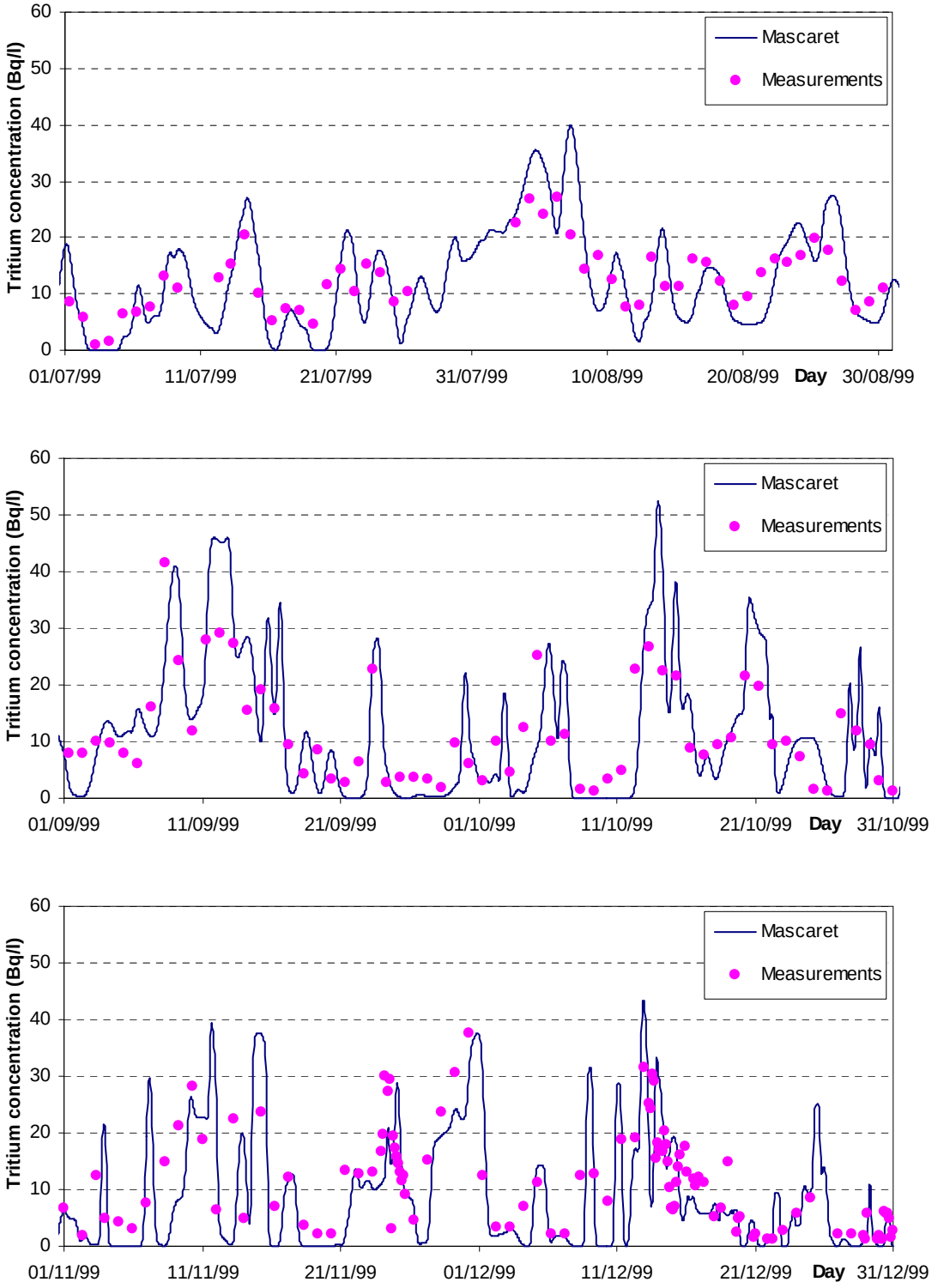

Fig. 4.2. Comparison between calculated and measured tritium concentration at Angers for MASCARET.

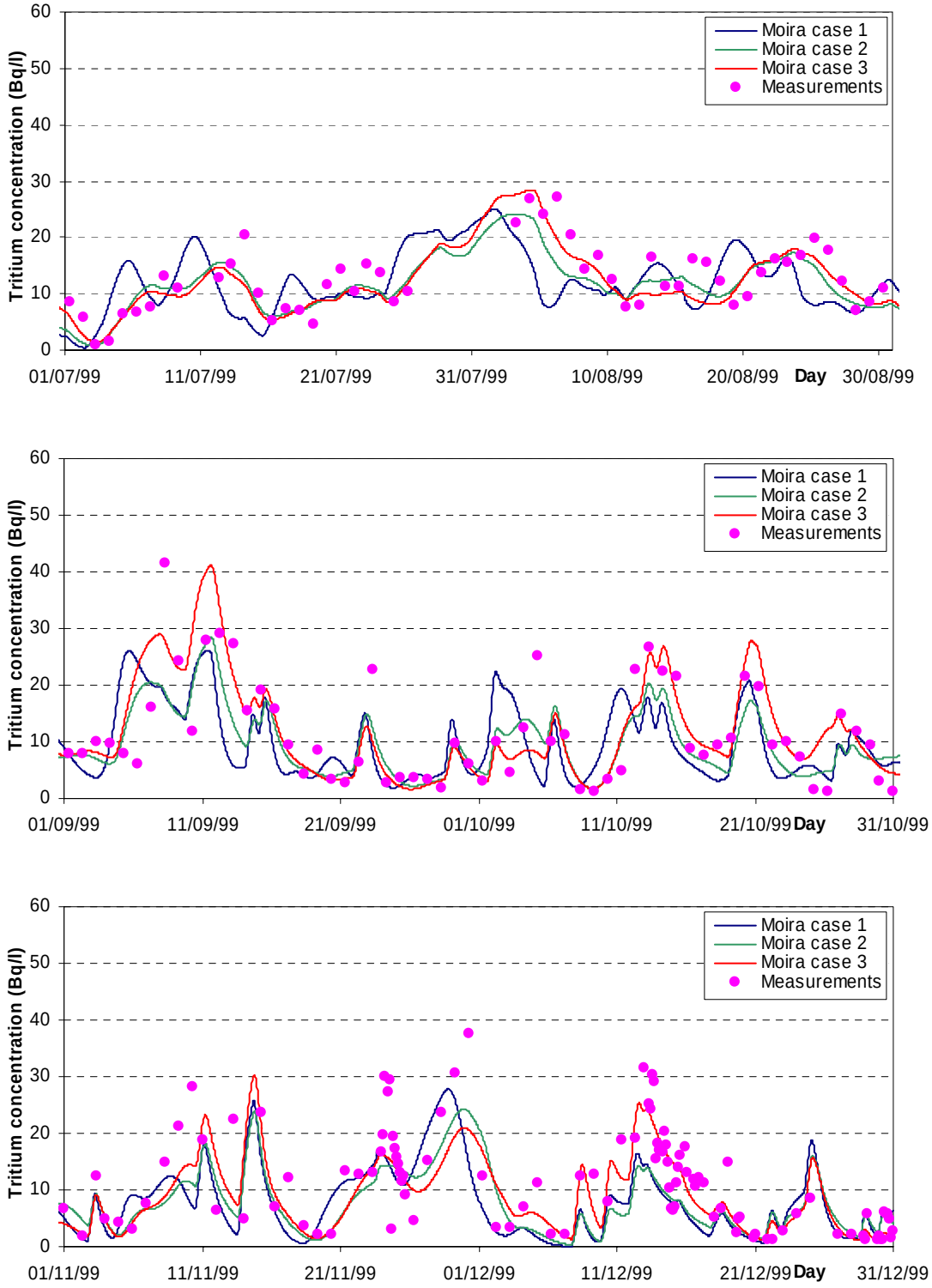

Fig. 4.3. Comparison between calculated and measured tritium concentration at Angers for MOIRA.

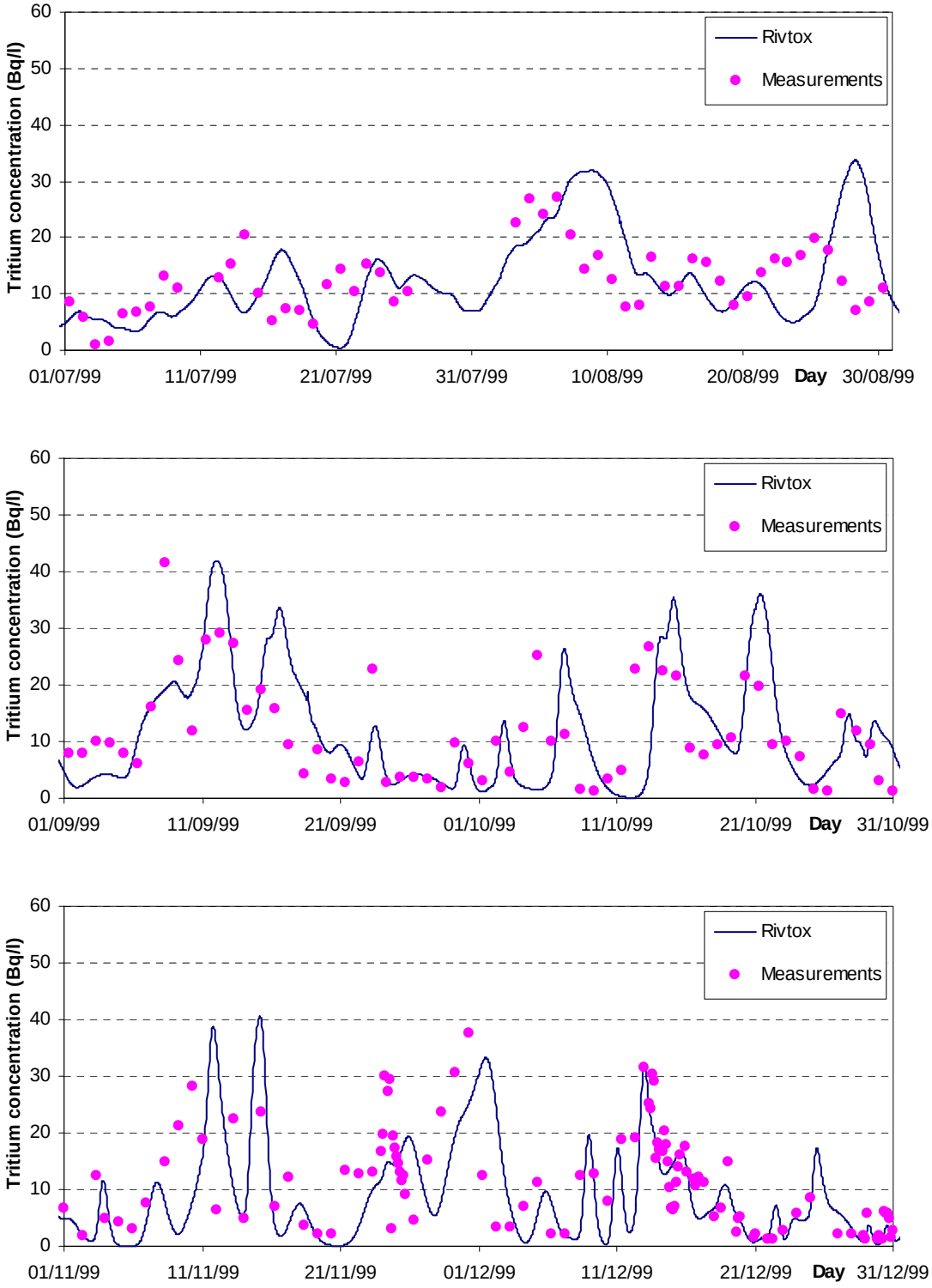

Fig. 4.4. Comparison between calculated and measured tritium concentration at Angers for RIVTOX.

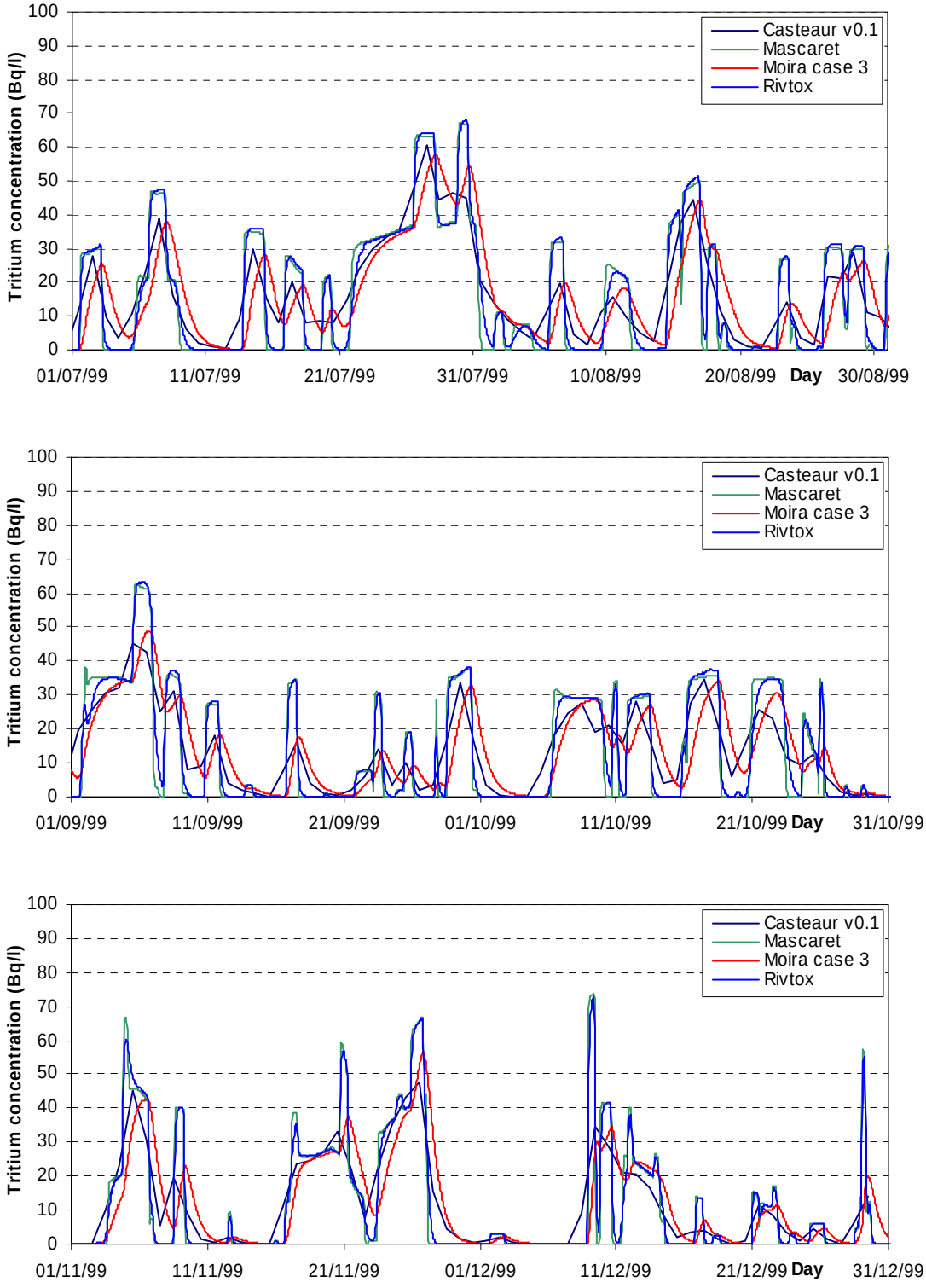

Fig. 4.5. Inter-comparison of the calculated tritium concentrations at Ouzouer.

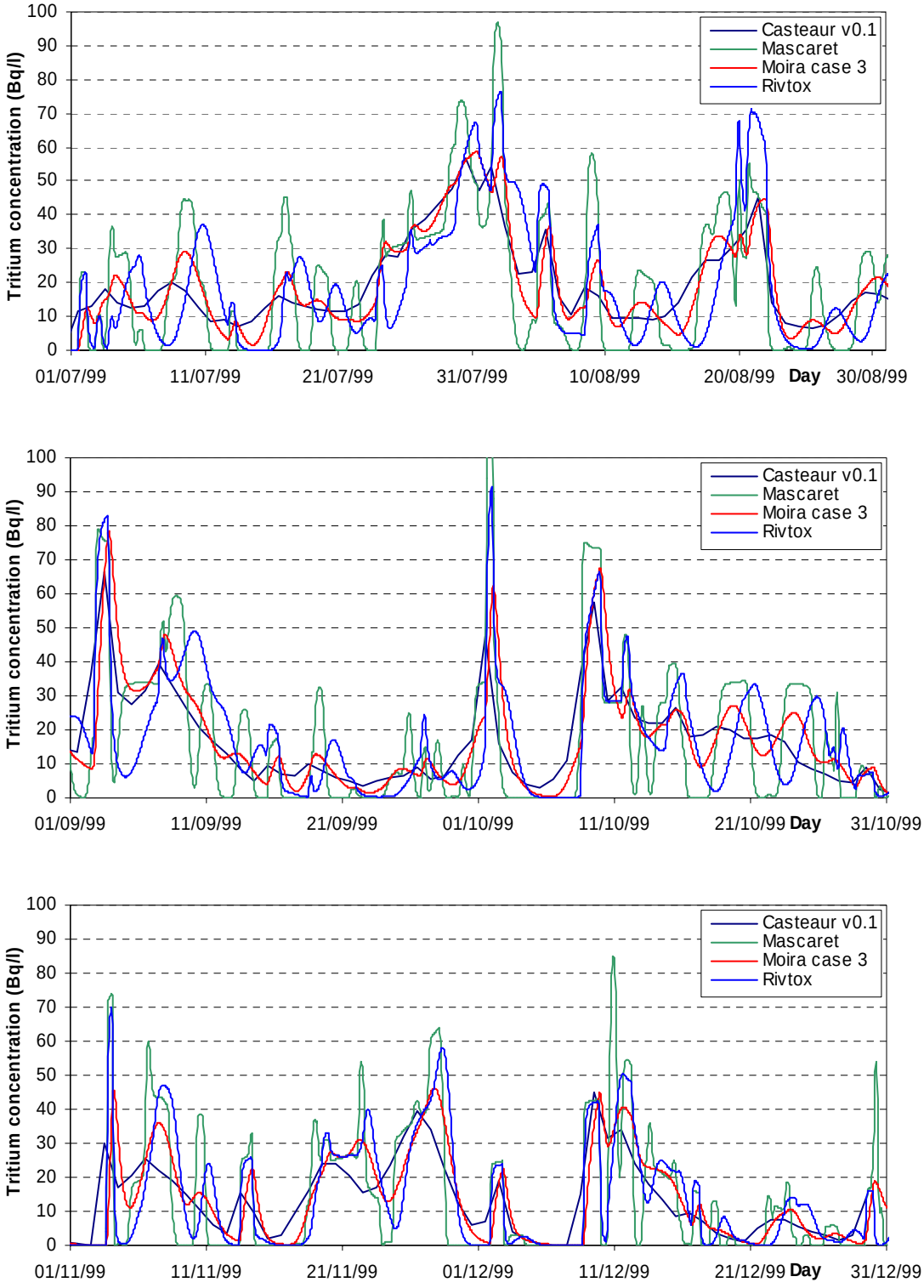

Fig. 4.6. Inter-comparison of the calculated tritium concentrations at Nouan.

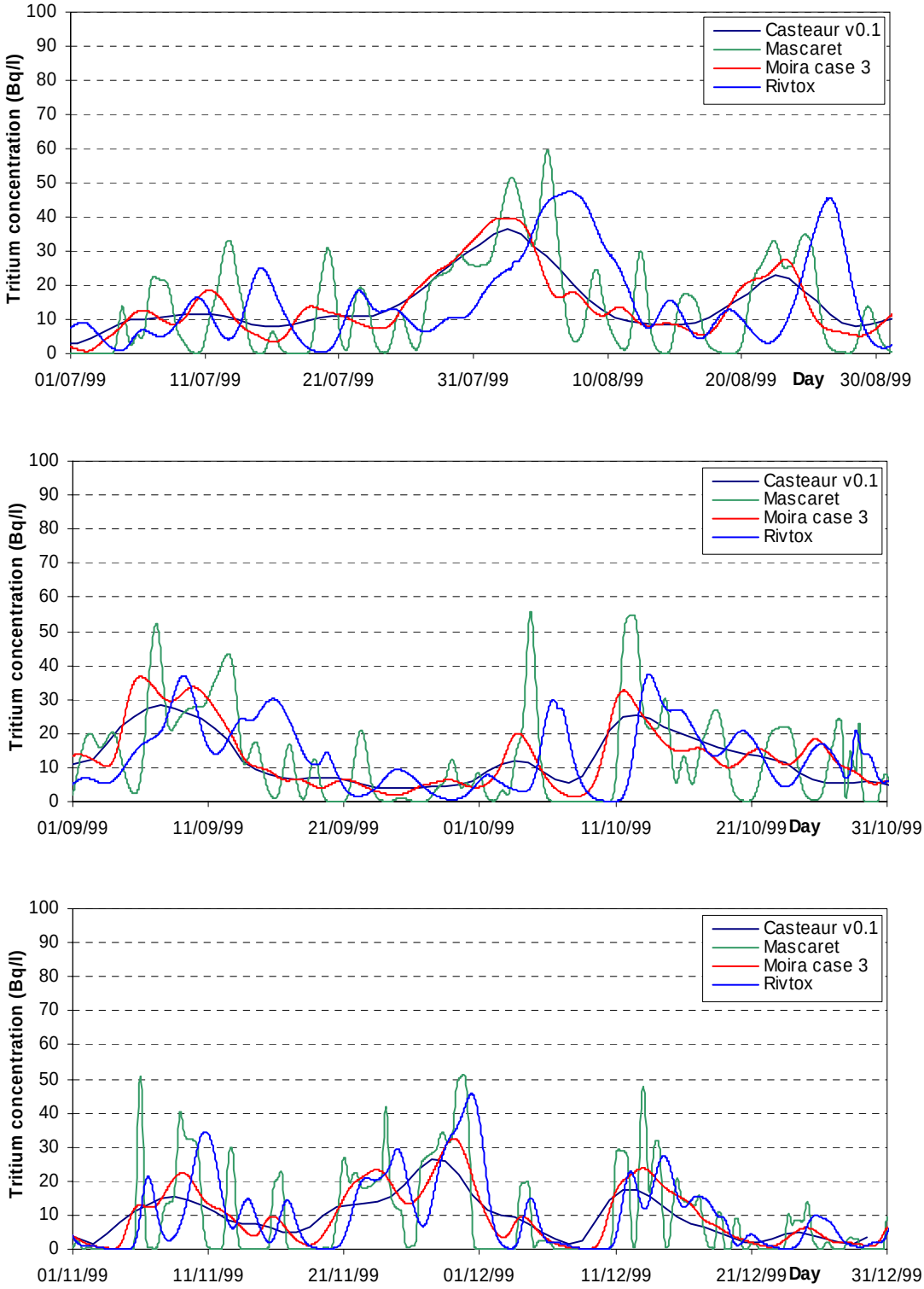

Fig. 4.7. Inter-comparison of the calculated tritium concentrations at La Chapelle.

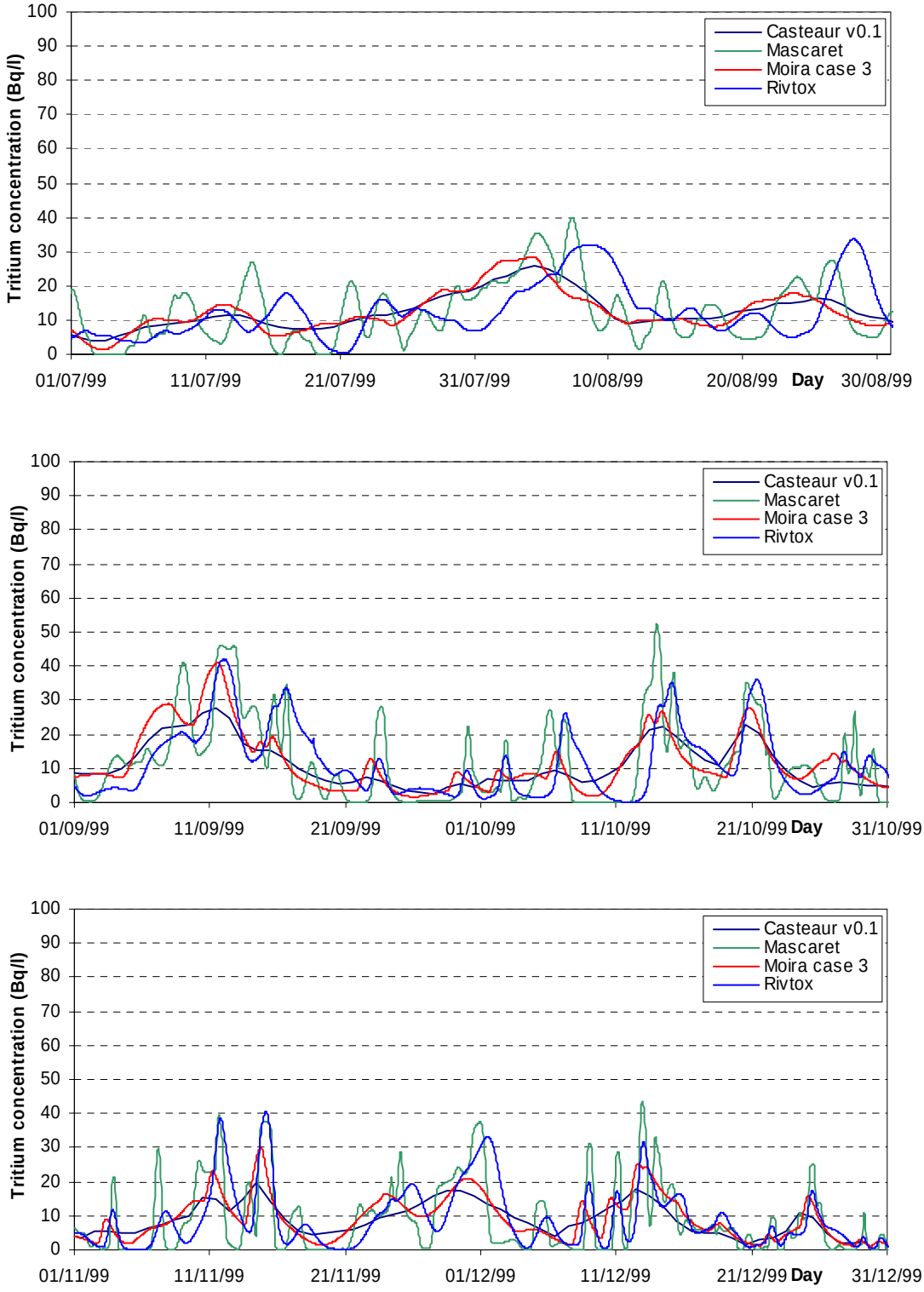

Fig. 4.8. Inter-comparison of the calculated tritium concentrations at Angers.

The comparison with CASTEAUR v0.1 shows an acceptable approximation of the real situation. CASTEAUR v0.1 is a dynamic box model, therefore its calculations can be assumed to reproduce the average conditions at the scales of the considered temporal and spatial steps: one day and the length of the reaches for these calculations. As the empirical data corresponds to instantaneous values measured with a temporal step of height hours, the first and simpler improvement of this model is to reduce the temporal and spatial calculation steps.

4.3.1.2. MASCARET – module Tracer

The calculated tritium concentrations resulting from the application of MASCARET to the Loire River are in good agreement with the measured concentrations at Angers.

The module Tracer represents quite well the high tritium discharges of short duration, with a low numerical dispersion. It seems particularly suitable for high flow rates (for example in November and December 1999), when physical dispersion is less important than advection (which is the main process).

Nevertheless, for low flow rates, when physical dispersion becomes important compared to advection, even if the mean levels of tritium concentration is reproduced, the peaks of tritium concentrations are not enough smoothed and the module predicts too high values of the tritium concentration (as seen from the results of July and August 1999).

4.3.1.3. MOIRA – module Marte

As seen from Figure 4.3, in general the results of the model applications are apparently in reasonable agreement with the measured data. It is obvious that the performances of the model improve when more site-specific information relevant to the hydrologic regime of the river are used.

It seems that water velocity and water fluxes are the most important factors to be accounted for a reliable prediction of the migration of tritium through the river. Therefore, the performances of the model are essentially controlled by appropriate estimates of those quantities.

4.3.2. Improvements of the models and new tests

In a second step of the study, after presentation of the results of the blind test (at the EMRAS WG meeting of November 2004), some participants made new tests, with improvements of their models or with new models.

The participants who have presented new computations on the scenario and the models they tested are listed in Table 4.4. Obviously, these further applications were not blind tests.

Table 4.4. Participants who improved their models or tested new models.

Models used for the exercise	Organization	Country
CASTEAUR version v0. 1, with improvement of the numerical method and the spatial discretization, and for different couple (time step, space step)	IRSN	France
ET-model, without/with smoothing	ENEA	Italy
RIVTOX, with a different method for hydraulics calculation	IMMSP	Ukraine

4.3.2.1. CASTEAUR

On the basis of the results of the blind test, some improvements have been implemented in CASTEAUR v0.1. These improvements concern two levels: the numerical methods and the spatial discretisation.

For the blind test, the hydraulic module was solved with an explicit semi-unsteady method and the radioecological model by a pure implicit mode. Now, all the models are solved with this last method. This allows to obtain a more realistic propagation of the water masses (and so of the pollutants) and to improve the numerical stability of the system. Particularly, this last point allows to apply and to test different associations between spatial and temporal steps.

A further improvement was the integration of methods to refine the spatial resolution. For the user, it is now possible to define a spatial resolution allowing to refine the discretization of the spatial grid to a scale lower than the one of the river reaches.

From these evolutions and with exactly the same parameters than the ones used for the blind test, four computations are presented in view to test the influence of the spatial and temporal discretizations:

- two computations with a resolution in space at the scale of the river reaches and with a time step of 1 day and 1 hour (taking into account only the first evolution of CASTEAUR v0.1),
- two examples of different computations made with different couple (time step ; spatial resolution) taking into account the two evolutions of CASTEAUR v0.1: the first with a couple (δt = 1 hour ; δx = 1 km), the second with a couple (δt = 0.5 hour ; δx = 0.5 km).

Figure 4.9 presents the comparisons between these computations and the measurements at Angers. Significant improvements of the predicted concentrations are obtained when the space grid is refined and the time resolution reduced. This behaviour has to be associated to the theoretical bases of the box approaches. In these approaches, the objectives are not to compute punctual values in space and time but to compute integrated values on a spatio-temporal domain.

Considering that the targets are some instantaneous values punctually measured at Angers, these results confirm the previous remarks about the behaviour of the box models. The more the spatio-temporal scales are refined, the best the results are. Nevertheless, considering that the diffusion process is not implicitly considered in CASTEAUR v0.1, it could be surprising to obtain a precision equivalent to this of numerical tools as MASCARET or RIVTOX where this process is taken into account. It can be deduced that for the temporal and spatial scales associated to this scenario, the dominant transfer's processes are the dilution and the advection.

In comparison to complex models, it can be noted that the simplified parameterization, the calculation time (one to some seconds on a personal computer) and the precision of the results justify using this type of box model for equivalent scenarios.

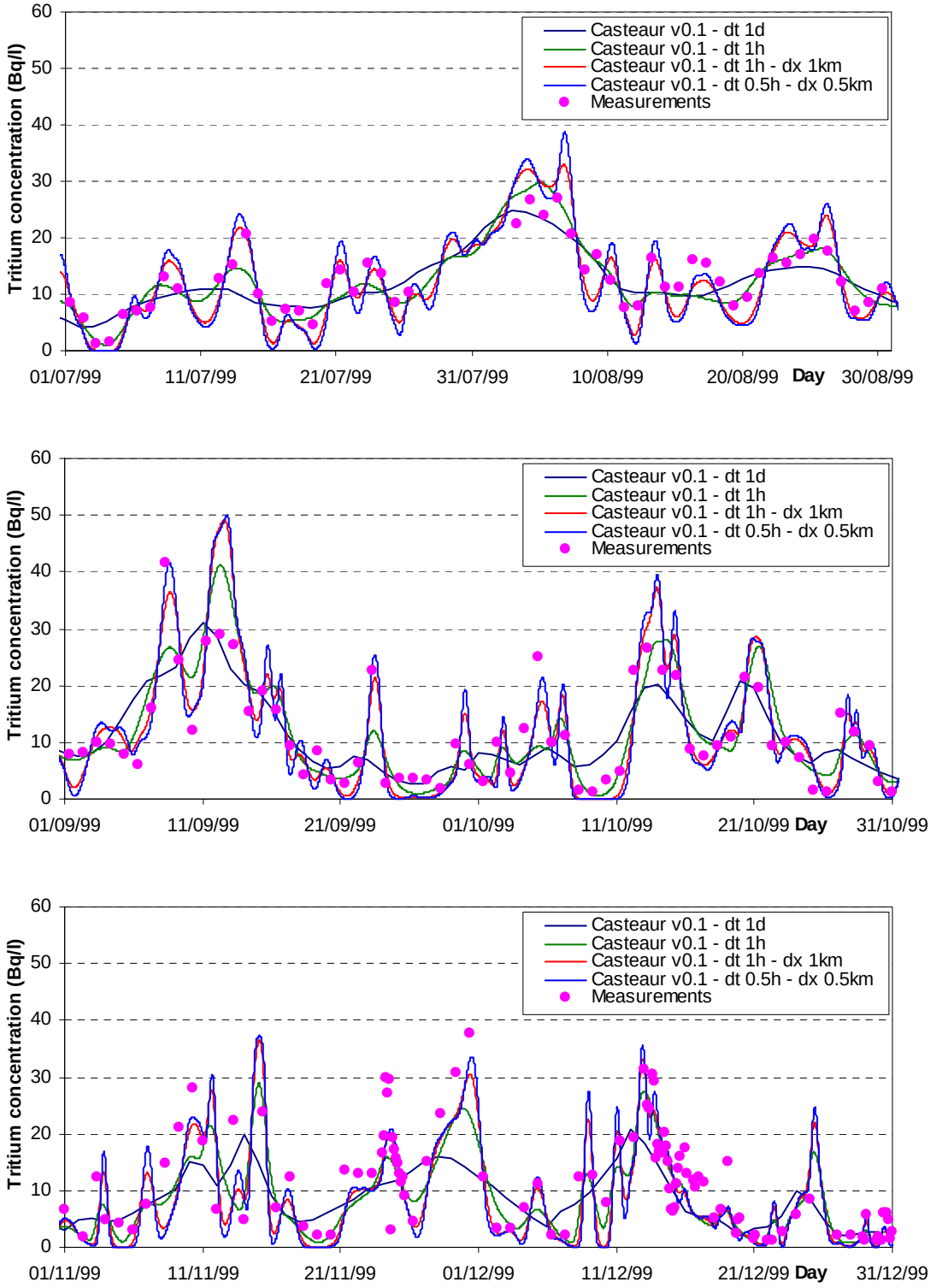

Fig. 4.9. Comparison between improved calculated and measured tritium concentration at Angers for CASTEAUR v0.1

4.3.2.2. Easy Tool (ET) model

The application of a simple transport/dilution model (ET = Easy Tool) was made by ENEA to predict the migration of tritium through the Loire River.

This model is based on transport and dilution processes. Tritium concentration at Angers is simply calculated by the following equation:

$$C(t) = \frac{\sum_i F_i(t - \tau_i)}{\Phi(t)} \tag{4.1}$$

where C(t) (Bq/m3) and Φ(t) (m^3/s) are, respectively, the concentration of tritium and the water flux at Angers at instant t, $F_i(t)$ (Bq/s) is the input flux of tritium into the Loire River at source point i and at time t. The argument $(t-\tau_i)$ of function F_i accounts for the delay due to the transport of the contaminant from the release point to Angers.

The delay time is:

$$\tau_i = \frac{x_i}{v} \tag{4.2}$$

where v (m/s) is the average water velocity, x_i (m) is the distance of Angers from the ith source point.

An average value of v = 0.67 m/s was used for the present application.

The dispersion of radionuclide due to turbulent diffusion was simulated by a time-moving average to smooth the output.

The model was solved by a simple Excel file.

The model was applied by using different time intervals for averaging the concentrations of radionuclide in water at Angers (smoothing procedure):

- Order of smoothing = 0 hours;
- Order of smoothing = 11 hours;
- Order of smoothing = 41 hours;
- Order of smoothing = 121 hours;
- Order of smoothing = 201 hours.

The present applications of ET model clearly demonstrate (Figure 4.10) that the water transport and the dilution due to the river water fluxes are the most important processes controlling, from a quantitative point of view, the behaviour of dissolved contaminants in water when the interaction with sediments is negligible. The comparison of the results of ET with other more advanced models suggests that appropriate quantitative evaluations of these processes are necessary to assure acceptable performances of a model.

It seems, therefore, that the predictive power of a migration model for assessing the transport of (non reactive) dissolved substances in a water body is mainly related to the accuracy that characterise the simulation of the above processes.

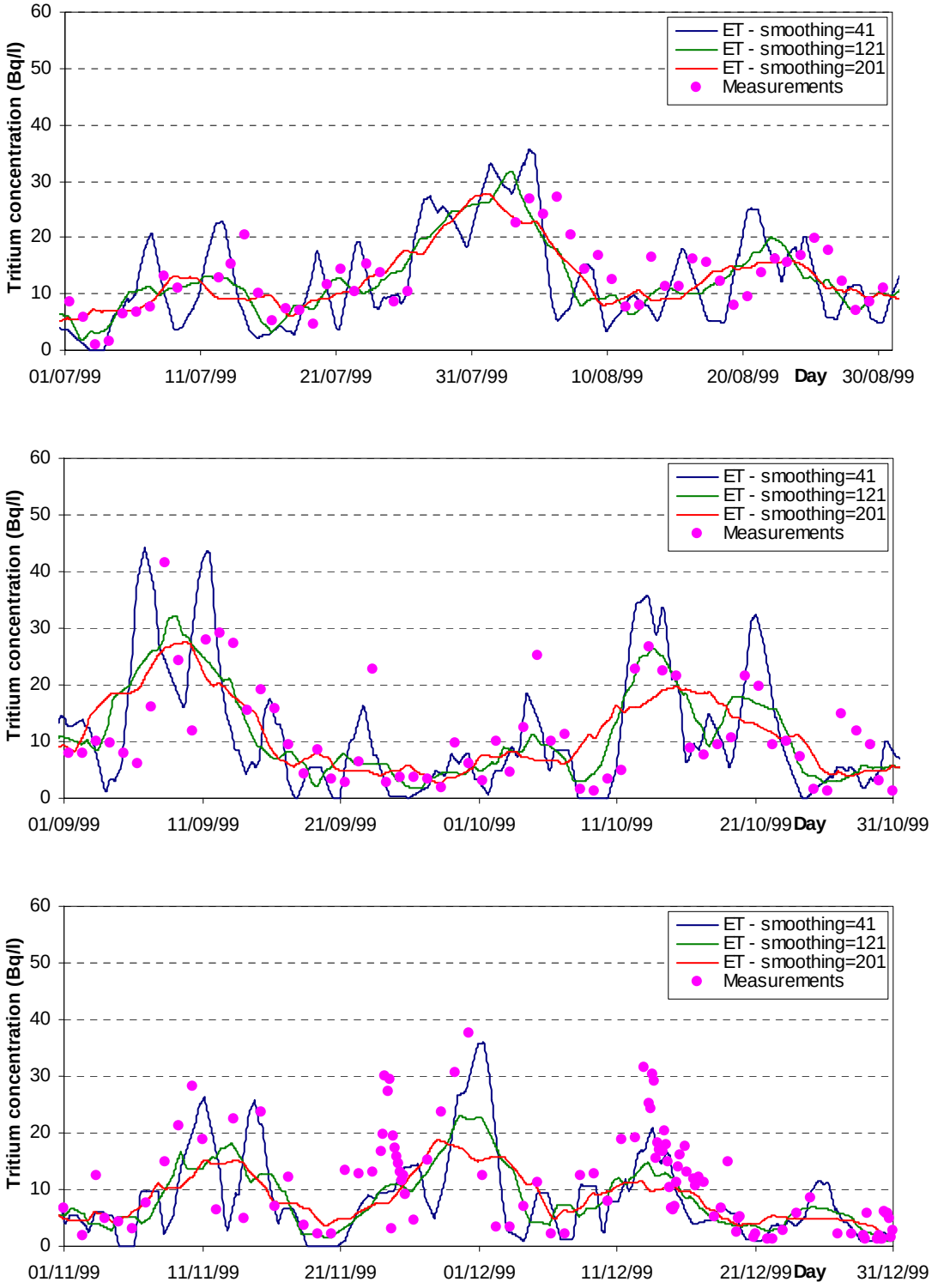

Fig. 4.10. Comparison between calculated and measured tritium concentration at Angers for T model.

4.3.2.3. RIVTOX

A new computation, with a different method for hydraulics calculation, has been made.

For the blind test, Saint-Venant equations were used without taking into account the water level-discharges relations on the dams, but with a simplified approach, as dam effects imitation by "artificial thresholds" in bottom level.

A new calculation was provided without any dam effects in hydraulics calculations, using the same Saint-Venant equations. The same equation of tritium transport, with the same dispersion coefficient, was used. So, the only difference between the two computations concerns the hydraulics calculation that was provided on a "natural way", without artificial thresholds on the dam places.

This new computation gives results in good agreement with the measurements (Figure 4.11), and shows that river hydraulics should be calculated without simplification or dam effects, but by their proper descriptions by discharge level relations on the dams.

4.3.2.4. UNDBE model

After presentation of the results of the blind test, IGE (Ukraine), that did not participated in the blind test scenario, presented the results of model UNDBE.

The comparison of results of the exercise shows that box model UNDBE gives coincidence with measurements not worse of the more complicated 1D models. UNDBE taking into account time of water transport and partial mixing in box gives the possibility to obtain results equivalent to 1D models or box models with small temporal and spatial discretisation, without small discretisation and peak smoothing.

4.3.3. Further exercise: models inter-comparisons for a hypothetical realistic pulse-type release

A further exercise for comparing the performances of the different models in case of a single event of radionuclide release, considering various realistic water flux conditions and release dynamics of tritium was carried out (Appendix I).

EDF-LNHE was responsible for the preparation of the relevant input data for this schematic scenario. The description of the results of this scenario are presented hereafter.

Obviously, the results of the models participating in this exercise (hypothetical realistic pulse-type release) could not be compared with measurements.

This exercise consists in modelling the dispersion of Belleville NPP tritium discharges in the Loire River (from Belleville to MontJean, which represents a domain length of about 350 km) for 4 different situations (corresponding to real situations of routine releases), covering each a period of time between 9 and 24 days:

- Case 1: low flow rates, long duration tritium release,
- Case 2: low flow rates, short duration tritium release,
- Case 3: increasing flow rates, long duration tritium release,
- Case 4: high flow rates, short duration tritium release.

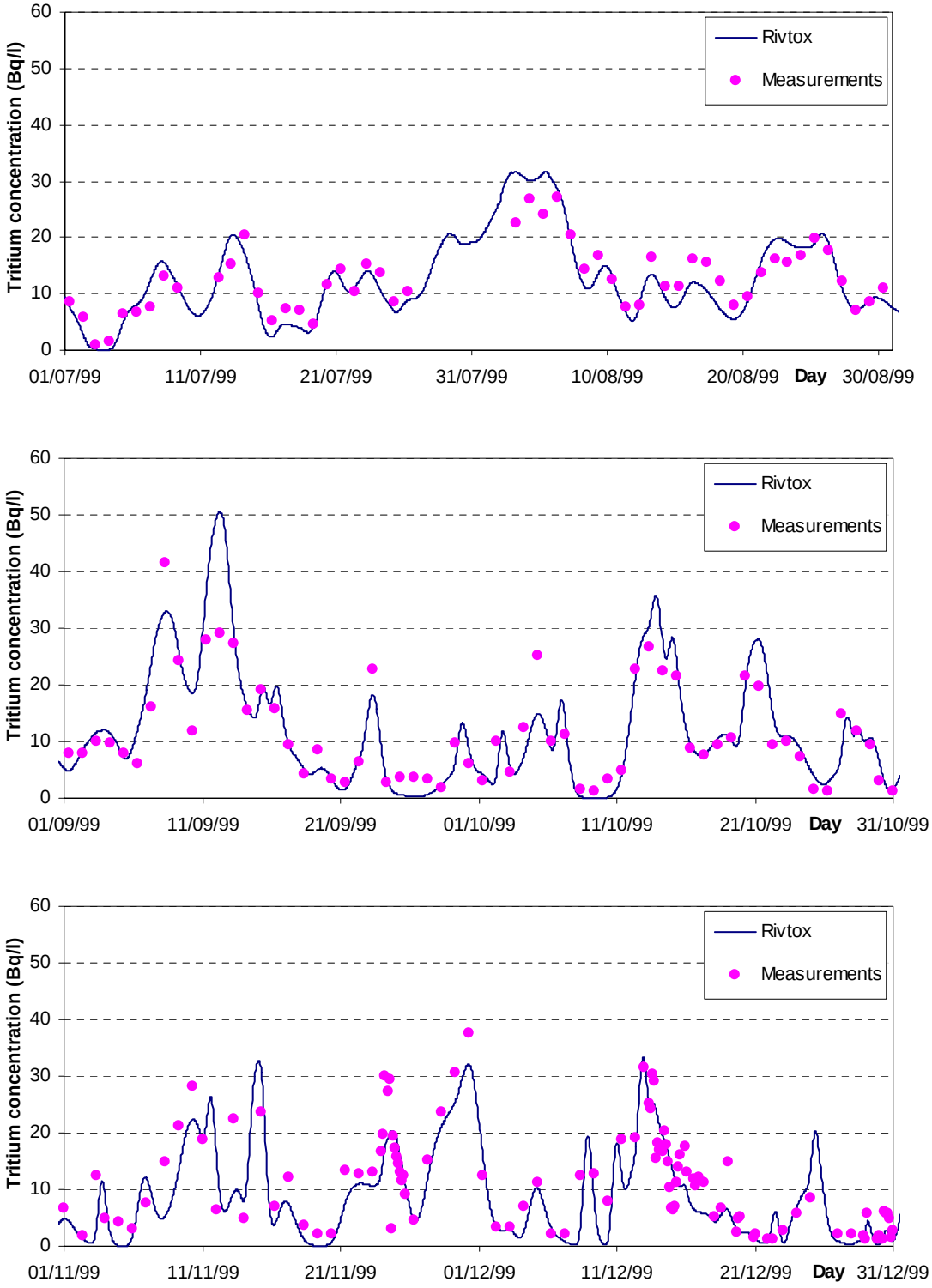

Fig. 4.11. Comparison between calculated and measured tritium concentration at Angers for RIVTOX.

The hydraulic boundary conditions were similar to those used for the blind test (real hydraulic conditions, from the 1st of July to the 31st of December 1999), with all water discharges from the tributaries taken into account.

Concerning the tritium discharges, we only considered the tritium releases at Belleville nuclear power plant (the first NPP, situated upstream of the Loire River). We selected 4 releases among the real tritium discharge conditions of the considered period (from the 1st of July to the 31st of December 1999).

New model versions were tested. These new model versions (CASTEAUR 1D model and MASCARET version 5.1) are shortly described hereafter (the descriptions of CASTEAUR v0.1, MASCARET – module Tracer, MOIRA – module Marte, ET, RIVTOX and UNDBE models and their customisation to the Loire River are described in Appendix II).

4.3.3.1. CASTEAUR 1D model

The one-dimensional model is derived from the box approach. The topographic and hydraulic models are like in CASTEAUR, whereas the radionuclide migration equation is given by:

$$\frac{\partial(S\cdot[r])}{\partial t}+\frac{\partial(Q\cdot[r])}{\partial x}=\frac{\partial}{\partial x}\left(S\cdot K\cdot\frac{\partial[r]}{\partial x}\right)+S\cdot\sigma-S\cdot\lambda\cdot[r] \qquad (4.3)$$

where:

[r] is the dionuclide concentration (Bq.m^{-3});
S is the wet section (m^2);
Q is the water flow (m^3.s^{-1});
K is the global diffusion coefficient (m^2.s^{-1});
σ is the release (Bq.m^{-3}.s^{-1}); and
λ is the radionuclide decay constant (s^{-1}).

This equation is resolved with an implicit difference finite method, the calculation points being centred on the reaches defined in function of a space step dx (m).

Two different modelling of the global diffusion coefficient are possible:

— Graf approach $K=6\cdot h\cdot u_*$

— Fischer approach $K=0.011\cdot\frac{l^2\cdot u^2}{h\cdot u_*}$

where:

h is the water depth (m);
u_* is the friction velocity (m.s^{-1}); and
l is the river width (m);

The friction velocity is given by: $u_*=\sqrt{i\cdot g\cdot R_h}$,

where:

i is the slope (m.m^{-1});
g is the gravitational acceleration (m.s^{-2}); and
R_h is the hydraulic radius (m).

4.3.3.2. MASCARET – module Tracer version 5.1

In its version 5.1, the module Tracer can solve the 1D advection-diffusion equation in its conservative form:

$$\frac{\partial(AC)}{\partial t} + \frac{\partial(uAC)}{\partial x} = \frac{\partial}{\partial x}\left(A \cdot k \cdot \frac{\partial C}{\partial x} \right) + A \cdot S \tag{4.4}$$

where:

C is the tracer concentration (kg/m^3) u flow velocity (m/s);
A is the river section (m^2) S sources of tracer (kg/m^{3}s^{-1}); and
k is the dispersion coefficient (m^2/s).

The resolution is still (as in version 5.0) made by a method with fractional steps: a convection step and a diffusion step, but the convection step is now solved by a finite volumes method (order 1), as described by Godunov [23].

Inter-comparisons of the results provided on the 4 studied cases by the different models at different points along the Loire River are reported in Figures 4.13–4.15.

We choose to use the first calculations of IRSN, ENEA and EDF, to be coherent with the calculations made for the blind test. As a result, the calculations appearing on the figures with the name "CASTEAUR", "MOIRA" and "MASCARET" are the one relevant to CASTEAUR v0.1 "box model", MOIRA – module Marte with customised hourly data (MOIRA case 3) and MASCARET v5.0.

The peak durations and amplitudes obtained with the different models at Angers are compared in the Table 4.5 (after 320 km of transport). In this table, we also indicate the ratio between the maximal and the minimal values obtained for peak duration (period over which the tritium concentration is not equal to zero) and maximal concentration.

We can note that:

— the dispersion of the results obtained by the different models for peak durations at Angers is conditioned both by release characteristics and hydraulics conditions;
— the dispersion of the results obtained by the different models for maximal concentrations at Angers seems to be mainly influenced by release duration. For long releases, all the model give quite similar maximal concentrations in Angers; for short releases (~ 1 day releases, corresponding to realistic conditions), some models give a maximal concentration 2.8 times lower than others.

Table 4.5. Comparison of peak durations and amplitudes at Angers.

Case	Peak duration	Maximal concentration
1	12–18 days (ratio 1.5)	15–18 Bq/l (ratio 1.2)
2	4–10 days (ratio 2.5)	4–11 Bq/l (ratio 2.8)
3	5–11 days (ratio 2.2)	13–14 Bq/l (ratio 1.2)
4	2–6 days (ratio 3.0)	2–6 Bq/l (ratio 2.8)

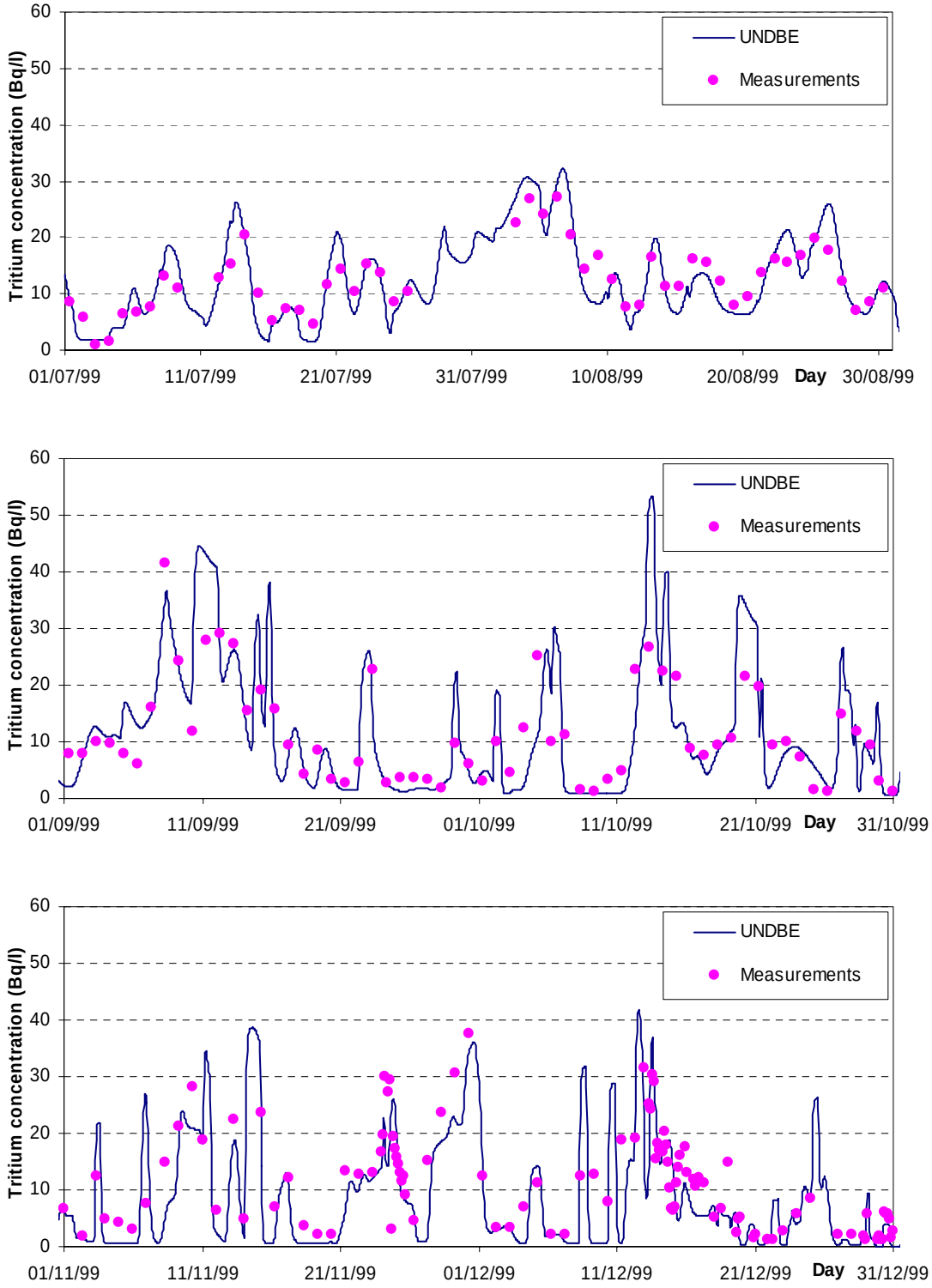

Fig. 4.12. Comparison between calculated and measured tritium concentration at Angers for UNDBE.

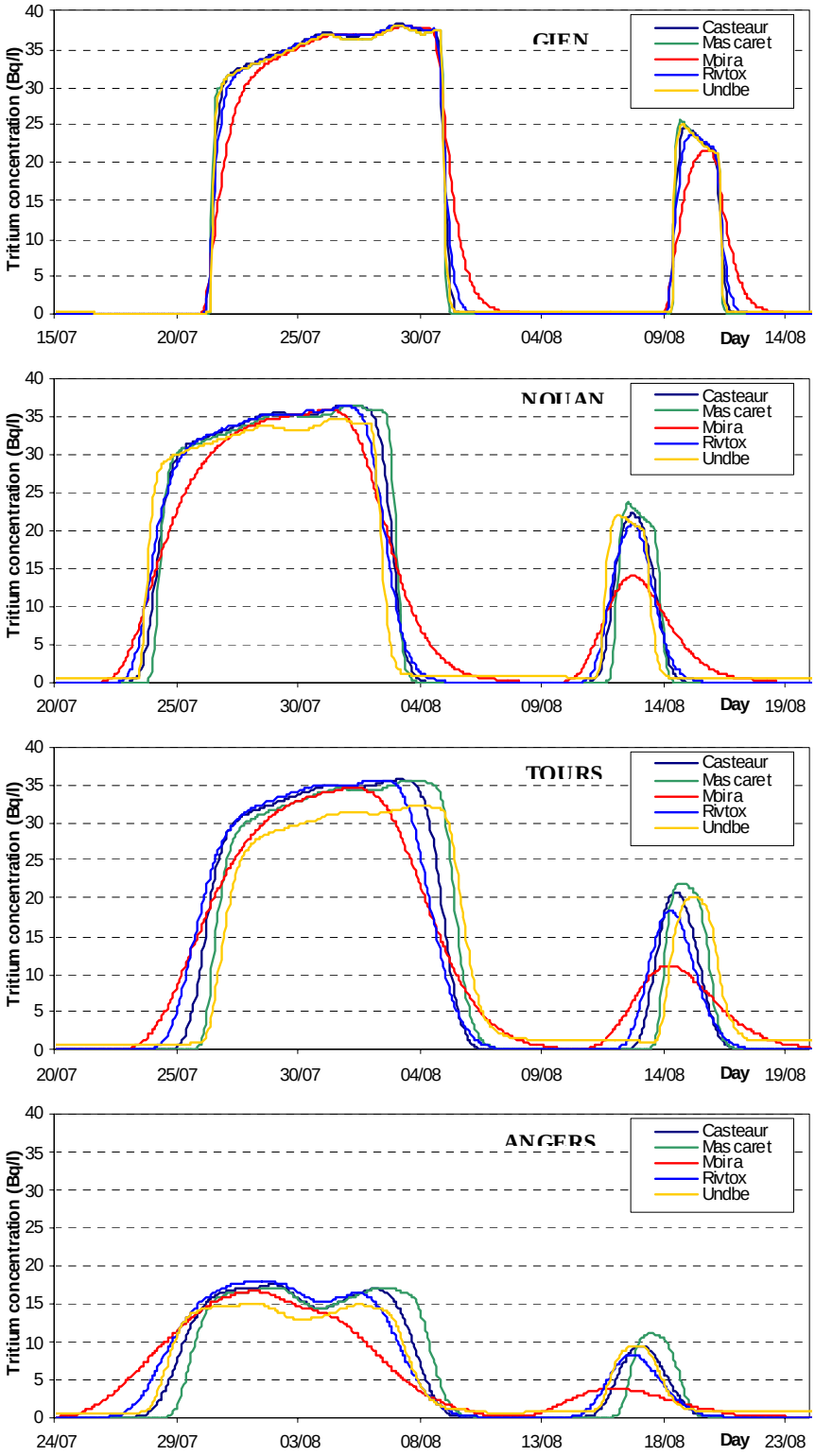

Fig. 4.13. Inter-comparison of the calculated tritium concentrations on Cases 1 and 2.

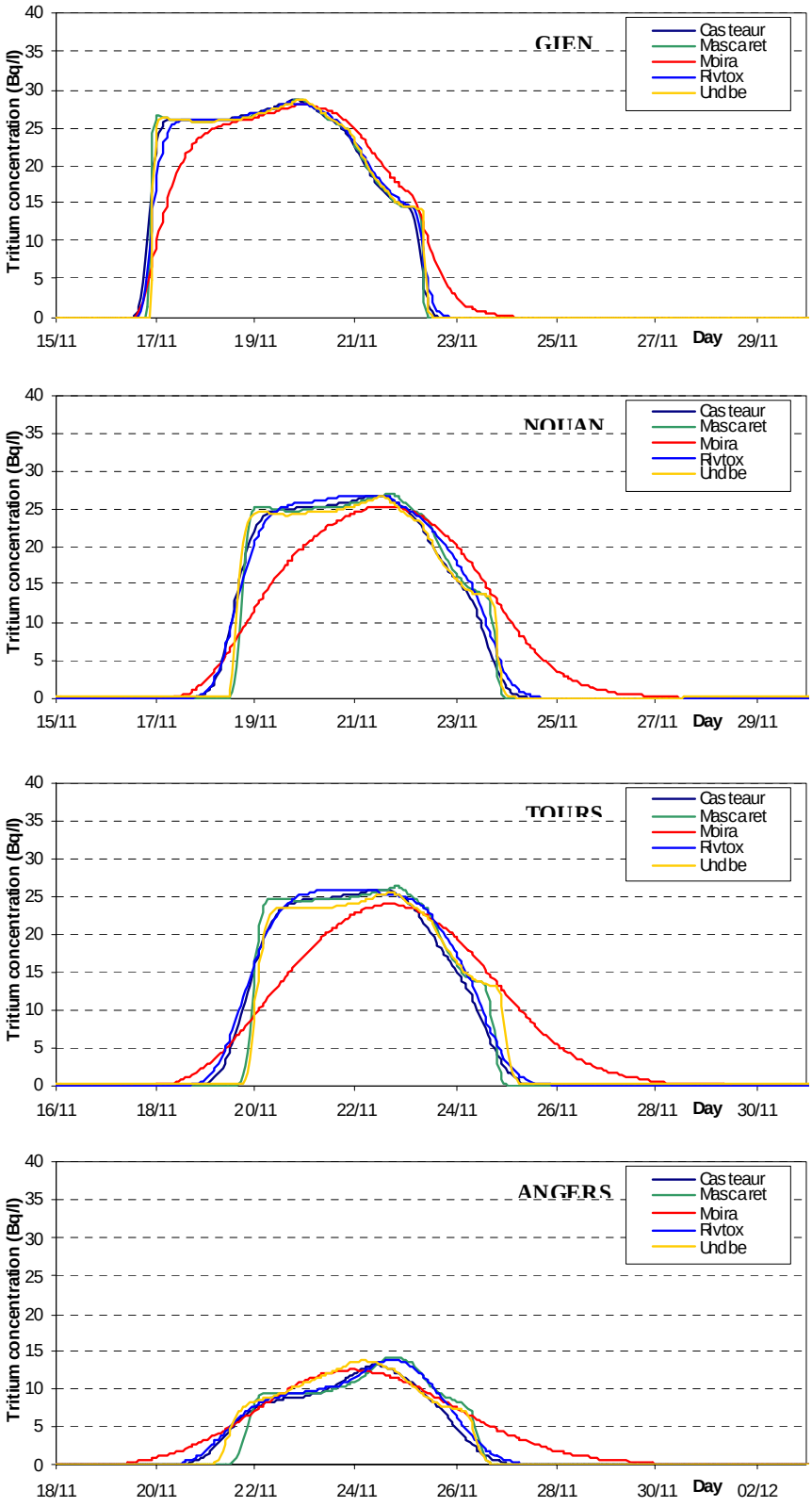

Fig. 4.14. Inter-comparison of the calculated tritium concentrations on Case 3.

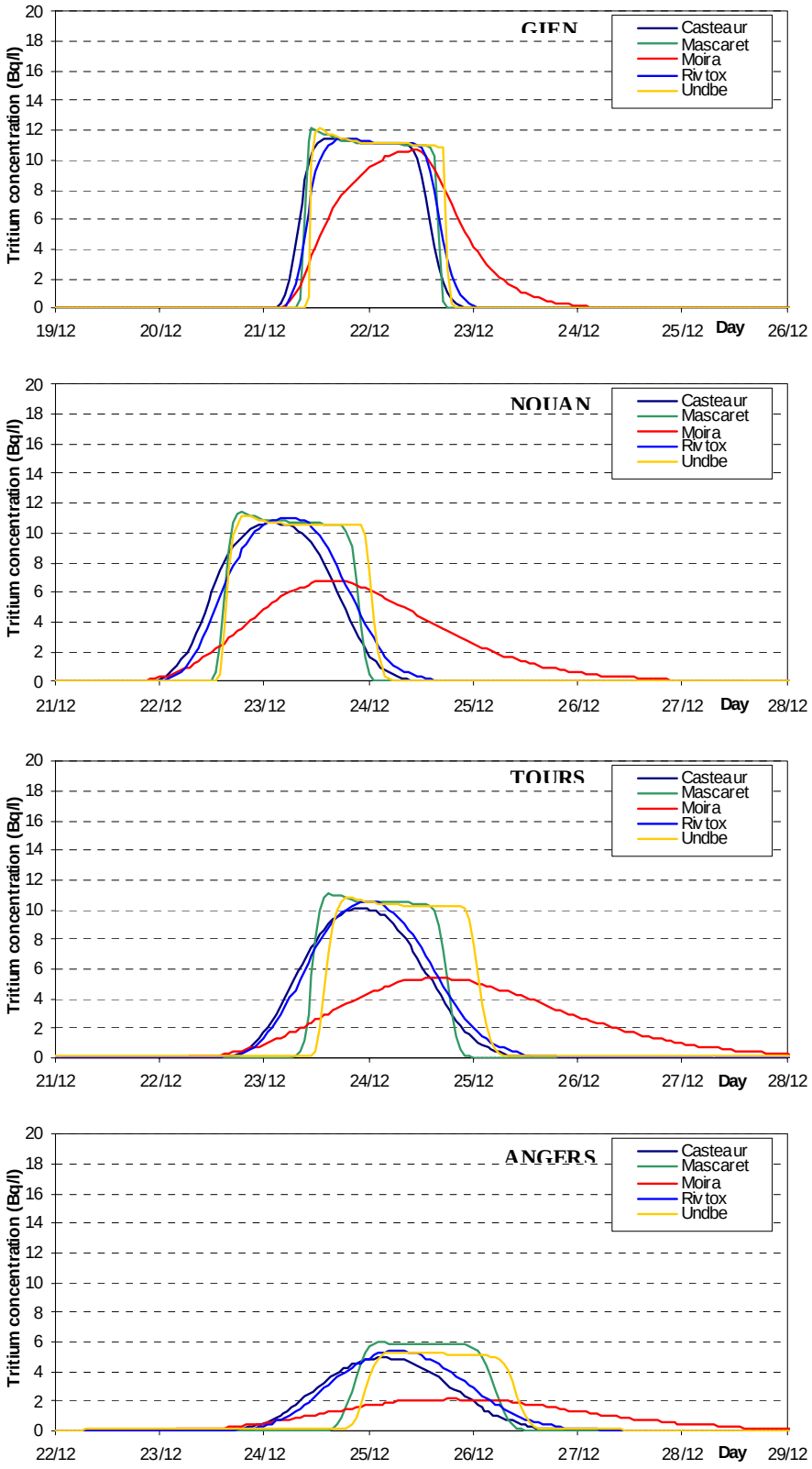

Fig. 4.15. Inter-comparison of the calculated tritium concentrations on Case 4.

Table 4.6. Relative error on the tritium quantities for each model on the schematic scenario (in %).

Model	Gien	Nouan	Tours	Angers
CASTEAUR v0.1				
"Box model" (considered in the original Loire scenario)	-0.3	-0.3	-0.4	-0.4
1D model (with Graf modelling of the diffusion)	-0.3	-0.3	-0.3	-0.2
1D model (with Fischer modelling of the diffusion)	-0.3	1.0	1.3	7.8
MASCARET – module Tracer				
version 5.0 (non conservative form, characteristics method)	-0.6	-0.6	-0.7	1.8
version 5.1 (conservative form, finite volumes method of order 1)	< 0.1	< 0.1	< 0.1	< 0.1
MOIRA – module Marte, with customised hourly data	3.4	9.4	11.0	10.6
RIVTOX	-0.2	-0.2	-0.3	-0.7
UNDBE	0.4	1.2	1.4	1.3

For this schematic scenario, we decided to give information on the tritium mass balance. Each modeller had to evaluate the quantity of tritium passed at the four studied stations, by an integral over time of the tritium flux at each station (with a time step of one hour for the flux). Then, the relative error on tritium mass balance was evaluated by comparing these quantities to the quantity of tritium coming from the releases of Belleville NPP (in %). These estimations of the relative error at each station, presented in Table 4.6, enable to give an idea of the models' conservativity.

4.4. Conclusions

The common conclusion of the study is that the models used by the participating Institutes, namely 1D models (MASCARET, RIVTOX) and models based on a schematic hydraulic (CASTEAUR, MOIRA, UNDBE), are reliable tools for tritium transport modelling and, consequently, for the simulation of advection and diffusion of non-reactive pollutants in rivers. In the blind test, all the models give results in good agreement with the measurements in Angers.

The refinement of the discretisation allows a better accuracy for sharp release of pollutants and a better adaptation to the hydraulic variability. The box models MOIRA and CASTEAUR v0.1 are indeed more diffusive and consequently the peaks are smoothed, particularly on the schematic scenario.

The importance of proper and detailed hydrological data for the appropriate prediction of pollutant migration in water is demonstrated by the examples provided during this study:

— MOIRA "case 3" run, based on the site specific hourly averaged data on water discharges, provides results closer to the experimental data than MOIRA "case 1" run and MOIRA "case 2" run, that are based on generic monthly averaged data and site specific monthly averaged data respectively (Figure 4.3) .

— RIVTOX without "artificial dams" in the hydraulics module, that provides hydrological data close to the reality, provides better results in comparison with measurements than the version with the "artificial dams" that has been used in the initial blind test, without any changes in tritium transport module (Figures 4.4 and 4.11).

— The comparison of the results of MOIRA with 20 boxes against the other results with more refined spatial discretisation in case of the schematic test case emphasizes the different mathematical features of the model solutions.

— Implementation of box models with small temporal and spatial discretisation is, in principle, equivalent to finite-difference approximation of 1D partial differential advection equation. Therefore the results of both kinds of models can be comparable. The main differences are due to numerical diffusion of the various finite-difference schemes and to the presence of a physical dispersion term in 1D models (see CASTEAUR results for different size of the boxes, Figure 4.9).

Therefore 1D models or box models with small spatial resolution (scale of hundred of meters) have ad hoc advance for the process simulation, compared to the models that used "rough" spatial resolution. The schematic test case allows to enhance and refine these previous conclusions.

Hydrological model are common tools for hydrological forecasting. The hydrological input data necessary for the radionuclide transport model (results of simulations or empirical time series) could be obtained in each country by contacts between radiological and hydrological experts/institutions.

The steadily increasing performance of conventional spread computers (PC) provides new possibilities to use pre-customized 1D numerical models for simulation of emergency releases of radionuclide into rivers that was not possible earlier. Nevertheless, box models continue to be main tools for quick analysis of radionuclide transport in rivers on the basis of generic or limited sets of input data by the expert community.

The comparison of the results of the different models applied to the short-term release scenarios (realistic conditions of routine releases) of tritium in water enlightened the marked differences of the mathematical characteristics of the model solutions. The blind test demonstrated that these differences, although apparent in the exercise, also in view of the uncertainty of the empirical data, were not similarly significant for model applications to the real contamination scenario when multiple, time-dependent releases were considered and the inherent uncertainty of realistically available hydrological information and of the contamination input data influenced the model results.

When the conditions of pollutant releases approach the steady state on a river with a quite regular geometry, very simple models based on evaluations of radionuclide dilution (contaminant input rate in water divided by the water flow) and peak transport due to the water velocity (transport time = distance from the contaminant source divided by the water average velocity) can supply results that are in reasonable agreement with the other models as demonstrated by the applications of model ET (Figure 4.10).

CHAPTER 5. RADIOACTIVE CONTAMINATION OF THE TECHA RIVER BY ^{90}SR, ^{137}CS AND ^{239,240}PU (SOUTH URALS, RUSSIA)

Kryshev I., SPA "Typhoon", Obninsk, Russia; Boyer P. ,IRSN, Cadarache, France; Dzyuba N., IMMSP, Kiev, Ukraine; Krylov A., ISDAE, Moscow, Russia; Kryshev A., SPA "Typhoon", Obninsk, Russia; Nosov A., AEP, Moscow, Russia; Sanina K., SPA "Typhoon", Obninsk, Russia; Zheleznyak M., IMMSP, Kiev, Ukraine.

5.1. Introduction

The objective of the Techa Scenario is to test models for radioactive contamination of river water and bottom sediments by ^{90}Sr, ^{137}Cs and ^{239,240}Pu. The Scenario is based on data from the Techa River (South Urals, Russia), which was contaminated mainly in 1949–1952 as a result of discharges of liquid radioactive wasters into the river. One of the most heavily contaminated rivers in the world, the Techa River is a suitable aquatic system for assessment of radioactive safety of human population and natural environment, dose reconstruction and risk estimation, management of protective measures and studying the processes of radionuclide migration and accumulation.

The complete Scenario description is given in Section I.4 of Appendix I. Here, information on the starting points, and endpoints of Techa Scenario is summarized.

The Techa River is part of the hydrological system Techa-Iset'-Tobol-Irtysh-Ob' belonging to the Kara Sea basin. Prior to operation of the Mayak nuclear materials production complex, the Techa River flowed out of Lake Irtyash and then through Lake Kyzyltas (Figure 5.1). Following the commissioning of the Mayak complex, the upper reaches of the Techa River were considerably affected due to the construction of the system of industrial water bodies and bypass canals (Figure 5.2). At present, a tail reach of the dam of water body 11 must be taken as the source of the Techa River. The Techa River is the right tributary of the Iset' River The catchment area of the Techa River is located to the west of the Ural range of mountains.

The Techa River is 207 km long, and its catchment area is 7600 km^2. The river depth varies from 0.5 m to 2 m, and its width is, on the average, 15–30 m. The average water flow in the river mouth is about 7 m^3/s. The maximum water flow is observed in April amounting, on the average, to 29 m^3/s in the river mouth. In April 1951, the average monthly water flow was 60 m^3/s. In its hydrochemical regime, the Techa River belongs to the bicarbonate-calcium type.

The upper part of the river channel (upstream of the village of Muslyumovo) is heavily overgrown with aquatic plants. The river channel is meandering. The river width amounts to 30 m, and its depth varies from 0.5 m to 2 m. The current is slow. Peat-silt and clay deposits prevail in bottom sediments. The bogs stretch along the river channel. The most waterlogged parts of the floodplain (Asanov bogs) are located near the inflow of the Zuzelga River and in front of the village of Muslyumovo. The width of the waterlogged floodplain varies from 300 m to 1 km. The central part of the floodplain is formed of peat-bog soils and its edges of soddy meadow soils. The peat layer depth varies from 0.1 m to 3 m. The underlying grounds for peat are primarily clay and loam.

Fig. 5.1. Map of the Techa River [24]. Scale: 1 cm = 12.5 km.

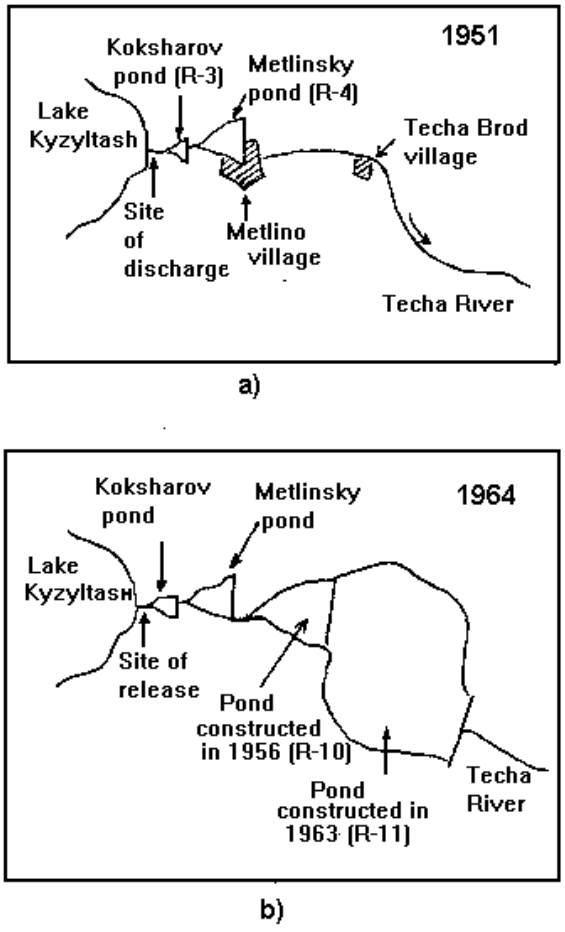

Fig. 5.2. Map of the upper reaches of the Techa River in (a) 1951 and (b) 1964.

In the middle and lower reaches of the river (downstream of the village of Muslyumovo) the banks of the Techa River are steep, and its channel is well defined. The river width is, on the average, 20 m and its depth 0.5–1 m. The floodplain is weakly water-logged. In the middle reaches of the river the floodplain width decreases to a few tens of meters, whereas near the mouth of the river it extends to 3 km. The dry floodplain is formed primarily of soddy meadow soils. The river bed is covered in sand and silt or sand and gravel. Rapids and sand bars are of frequent occurrence. The flow velocity is 0.3–0.8 m/s. A time it takes for the water to pass along the river from its source to the mouth is about 8 days.

The main hydrological and hydrochemical parameters of the Techa River are presented in Appendix I.

Since March 1949, waste waters from the radiochemical plant "Mayak" have been discharged to the Techa River. The site of discharge was at a distance 200 m from Lake Kyzyltash downstream the Techa River, and the contaminated waters flowed through Kaksharovsky and Metlinsky ponds (water bodies R-3 and R-4). The nearest riparian settlement (Metlino) was located at a distance of 7 km from the site of discharge. The scheme of the upper reaches of the Techa River in 1949–1951 is shown in Appendix I.

The main sources of radioactive contamination of the Techa River were discharges of radionuclides in the period 1949–1956 . In this period, about 10^{17} Bq of radionuclides entered the river ecosystem, including 1.2×10^{16} Bq of ^{90}Sr and 1.3×10^{16} Bq of ^{137}Cs . The total volume of radioactive discharges was about 76 mln.m^3. Alpha releases were relatively low, amounting to about 2 TBq, including both Pu and U-isotopes.

In the period of the most intensive discharges from March 1950 to November 1951, their radionuclide composition (in %) was the following: ^{89}Sr – 8.8, ^{90}Sr – 11.6, ^{137}Cs – 12.2, ^{95}Zr and ^{95}Nb – 13.6, ^{103}Ru and ^{106}Ru – 25.9, and the other isotopes – 27.9.

The following three periods with different intensity of discharges can be distinguished within the period 1949–1956:

- January–November 1949, with a total discharge of beta-emitters of $1.85\text{x}10^{15}$ Bq. The contribution of ^{90}Sr and ^{137}Cs to the activity of discharges was about 4% and 11%, respectively.
- December 1949–November 1951, with a maximum activity of discharges of about 10^{17} Bq for the total beta-emitters. The contribution of ^{90}Sr and ^{137}Cs to the activity of discharges was 12–15% and 12–21%, respectively
- December 1951–December 1956, with the total activity of discharges of beta-emitting nuclides decreased considerably to 5.2×10^{14} Bq. The contribution of ^{90}Sr and ^{137}Cs to the activity of discharges was 17–38% and 4–15%, respectively.

5.1.1. Exposure of the population

In 1949, 39 riparian settlements were located on the banks of the Techa River area. The total numbers of population was 124 000. For the local population the Techa River was the main (and sometimes, the only) source of household and drinking water supply. There were few wells in the area, and only part of the population used them for limited purposes because the well water was not as good to taste as the river water. The Techa River was used for watering of cattle, breeding of waterfowl, irrigation of agricultural crops, catching of fish, swimming and bathing, laundering, etc.

An extraordinary powerful flood in April to May 1951 led to the radioactive contamination of the land ajacent to the river. The floodlands were used by inhabitants of the riparian settlements for cattle-breeding and making hay. Up to this point radionuclides had been ingested mainly with water, since 1951 contaminated food began to play a role, especially milk and vegetables from flooded kitchen gardens.

In the summer of 1951, during the radiation survey of all areas adjacent to PA "Mayak" it was found that the Techa River bed and floodplain were highly contaminated with radionuclides. This led to enhanced radiation impact on the population residing on the banks and especially in the upper reaches of the river. Some riparian settlements located in the upper reaches of the Techa River were evacuated in 1953–1956.

In 1953 it was officially banned to use the Techa River for all household and drinking needs, as well as for catching of fish, breeding of waterfowl and bathing. The most contaminated part of the floodplain was removed from land utilization. Simultaneously, the digging of wells was initiated but it was carried out off and on. By the end of 1954, all population and livestock on the banks of the Techa River were provided with water from underground sources. However, the river water consumption and the use of the Techa River for other household purposes continued, although on a smaller scale, even after setting up a special "river police" in 1956.

As is evident from the description of the radiation situation, the population of riparian settlements was exposed both to external radiation due to the increased gamma radiation background near the river and to internal radiation from the mixture of radionuclides entering the human organism with water and food products. The main nuclides responsible for the internal exposure to the population living on the shore of the Techa River are ^{90}Sr and ^{137}Cs.

5.1.2. Countermeasures

In the initial period of operation of the Mayak complex, radioactive wastes were discharged to the Techa River. Waste waters from the radiochemical plant were discharged to Koksharovsky pond (water body R-3) located at a distance of about 1.5 km from the site of discharges. Contaminated water from this pond entered Metlinsky pond (water body R-4) and then to the Techa River through the dam locks of water body R-4 (Figure 5.2).

Water bodies R-3 and R-4 were the settling reservoirs with the water contaminated by radionuclides, which remained there for a few days. Due to radioactive decay and sorption of radionuclides on suspended matter and in bottom sediments, the water activity decreased by a factor of ten and over by the time of its intake to the Techa River. However, part of the activity, which did not settled in water bodies R-3 and R-4, turned out to be sufficient for intensive contamination of the Techa and Iset' Rivers.

In 1951 repositories of the radiochemical plant were filled with high-activity wastes, and an internal-drainage Lake Karachai (water body R-9) began to be used for discharge of technological radioactive solutions. In the following five years, radioactive discharges to the Techa River system decreased drastically. In 1952 they amounted to 3.5×10^{14} Bq year^{-1}, and in the period from 1953 to 1956 to $2\times10^{13} - 8\times10^{13}$ Bq year^{-1}.

To reduce the radionuclide transport, a system of bypasses and industrial reservoirs for storage of low-activity liquid wastes has been constructed in the upper reaches of the Techa River in 1956–1965.

In addition to already existing reservoirs R-3 and R-4, in 1956 the Techa River was dammed in the vicinity of the village of Asanovo and the reservoir R-10 with an area of 18.6 km^2 was constructed. As a consequence, the intake of radioactive substances to the river decreased to 7.3×10^{12} Bq $year^{-1}$.

In 1963, the reservoir R-11 with an area of 48.5 km^2, immediately adjacent to the reservoir 10 and the end in the cascade of industrial reservoirs, was constructed. The construction of the left-bank and right-bank bypasses for interception of surface run-off was completed in this period.

The total volume of the cascade of technological water bodies is 400 millions m^3. The annual water filtration from reservoir R-11 to the Techa River is about 10 millions m^3.

5.1.3. Current sources of the radionuclide input to the Techa River

A number of factors are contributed to the current radioactive contamination of the Techa River with ^{90}Sr, ^{137}Cs and Pu: runoff of radionuclides from the waterlogged floodplain; runoff of radionuclides through the bypass canals; filtration of radionuclides through the dam 11.

The assessments of current sources of radioactive contamination of the Techa River are presented in Appendix I.

The endpoints of the scenario were the model predictions of the activity concentrations of ^{90}Sr, ^{137}Cs and $^{239,240}Pu$ in water and bottom sediments of the Techa River at different locations downstream of the dam 11. The input data included: assessments of inventories of ^{90}Sr, ^{137}Cs and $^{239,240}Pu$ in the floodplain of upstream part of Techa River, intake of ^{90}Sr to the river as a result of runoff from bypass canals and filtration through the dam 11, the estimated annual runoff of ^{90}Sr, ^{137}Cs and $^{239,240}Pu$ from upstream part of Techa River, data on the precipitation, hydrological and hydrochemical characteristic of the river.

5.2. Main characteristics of the models

Calculations for Techa Scenario were performed 5 participant teams from France, Ukraine and Russia using different models (see Table 5.1). For all the endpoints, model predictions were compared against test data. Tables of model predictions and test data are presented in Section 4. Model descriptions, equations and parameters are reported in Appendix II.

Table 5.1. Models and participants in the Techa Scenario testing.

Model	Participants	Organization	Radionuclides	Components of river system
CASTEAURv0.1	P. Boyer	IRSN Cadarache, France	^{90}Sr, ^{137}Cs, $^{239,240}Pu$	Water Bottom sediments
TRANSFER-2	A. Nosov	AEP (Atomenergoproject) Moscow, Russia	^{90}Sr, ^{137}Cs, $^{239,240}Pu$	Water Bottom sediments
CASSANDRA	A. Krylov	ISDAE (Institute of Safety Development of Atomic Energy) Moscow, Russia	^{90}Sr, ^{137}Cs, $^{239,240}Pu$	Water Bottom sediments
GIDRO-W	A. Kryshev K. Sanina	SPA “Typhoon” Obninsk, Russia	$^{239,240}Pu$	Water
RIVTOX	N. Dzyuba, M. Zheleznyak	IMMSP Kiev, Ukraine	^{90}Sr, ^{137}Cs, $^{239,240}Pu$	Water Bottom sediments

5.2.1. Model CASTEAURv0.1

Four box modelling modules of the code CASTEAURv0.1 are involved: hydrographical, hydraulic, sedimentary and radioecological for the water and the solids matters.

The hydrographical model describes the geometry of the river. Based on a succession of reaches, constituting a linear hydrographic network, the aim of the model is to give a linear grid in function of a space step precise by the user. At this end, a simplified trapezium bathymetric form is considered to describe the sections. The variables are the hydrographical parameters at each space step: length, width, bank angle, slope. The input data are a linear succession of reach.

The hydraulic module assesses the spatial and temporal evolutions of the water column. The modelling is based on the two equations allowing the determination of the water flow and of the water depths.

The sedimentary model calculates the stocks and the fluxes of matters in the water column and the bottom sediment. The model can take into account several classes of matter and considers three bottom sediment layers: an interface, an active and a passive. The interface layer is a very fine layer constituted of recent deposit not compacted yet. It is supposed that whatever the matters, their behaviour in this layer is always non-cohesive. The active layer results from the compaction of the interface. It is called active because the interstitial water remains enough mobile to allow the dissolved radionuclide phases to be exchanged with the column by interstitial diffusion. The compaction of the active layer feeds the passive layer. In this third layer the consolidation becomes strong enough to reduce the mobility of interstitial water and the exchanges of dissolved radionuclide phases become negligible.

The bottom sediment layers are characterized by: maximal thickness of the interface layer, water content of the interface layer, maximal thickness of the active layer, water content of the active layer, coefficient of consolidation of the active layer, water content of the passive layer, coefficient of consolidation of the passive layer.

The radioecological model uses the results provided by the hydraulic and sedimentary models to compute spatio-temporal distributions of the radionuclides activities (Bq) under their dissolved and solid forms in the different compartments: water column, interface, active and passive layers. Considering the small thickness of the interface layer, an equilibrium hypothesis between this layer and the water column is assumed. So, these two compartments are combined in the radioecological model.

The variables of the radioecoligical model are the activities in the different components: dissolved and particulate activities in the water column, in the interface, active and passive layers.

The input data are: radioactive decay, coefficient of equilibrium between dissolved and solid phases, specific radionuclide import under particulate and dissolved phases.

Two kinds of radionuclide fluxes are taken into account: (i) between reaches and components; and (ii) between solid and dissolved phases.

The parameterization is based on the Techa Scenario (Appendix I). It can be noted that the application involves two calibrations: Ks, the strickler coefficient and Kd_r, the coefficient of equilibrium between the solid and liquid phases. All the others parameters are input data.

5.2.2. Model TRANSFER-2

For calculating the radionuclides concentrations in water in the Techa River in the case of stationary discharges from the nuclear facility a stationary two components model TRANSFER-2 for transport of radioactive material in the one-dimensional flow was used. The model is based on the turbulent diffusion equation and accounts for the interaction of radioactive substances between the water mass (solution, suspended material) and bottom sediments. The model is based on several assumptions:

- The exchange of radioactive material between water and bottom sediments is proportional to the radionuclide concentration in the liquid and solid phases;
- Sorption and desorption of radionuclides between the solution and solid phase is considered to be instantaneous, and obey the linear isotherm with a constant distribution coefficient;
- Exchange between the bottom and water mass occurs within the accessible upper layer of bottom sediments with depth h;
- It is assumed that the channel does not get silted;
- In water, radioactive material is transported by the water flow and dispersed due to longitudinal turbulent dispersion. Radioactive material is distributed uniformly by river depth and account is taken only of the longitudinal component of convective dispersion

The morphometric characteristics of the channel are invariable over the whole section of the river. The total water discharge of the lateral tributaries is negligible as compared to that of the main channel. Variations in the water discharge along the length of the river are due to changes in the flow velocity by the linear law.

5.2.3. Model CASSANDRA

The integrated information modeling system CASSANDRA based on using geoinformation technologies is designed to predict and estimate the consequences of radioactive contamination of rivers and water bodies.

The system is composed of:

- a geographical information system *Komponovka*;
- a model predicting radionuclide behavior in water bodies with a weak flow and models of long-term transport of radionuclides in river channel is integrated within the computer model *Basin*; and
- a model predicting internal and external doses (aquatic pathways of exposures) for different population groups, estimates of radiation risk for developing appropriate recommendations is integrated in the computer model *Inter*.

Komponvka is the core of the system. It is used for entering, storing, processing and representation of spatially distributed information. The computer model *Basin* is designed for predicting the contamination of water bodies.

Within the computer model *Basin* several different eco-mathematical models have been integrated. A model is selected for prediction of contamination depending on the type of water body, radionuclides, and some other conditions.

The system is arranged in such a way that results of calculations can be replaced by experimental data (if available). For example, a measured radionuclide concentration in bottom sediments can be used instead of the concentration estimated by the model.

The radionuclide transport model (included in the computer model *Basin*) accounts for

- radiation decay;
- advective transport of radionuclides;
- variance;
- exchange processes between radionuclides in dissolved and adsorbed forms;
- redistribution and transport of radionuclides; and
- migration of radionuclides down the bottom sediments.

The principal assumptions made in the model are the following:

- The radionuclide concentration and all river characteristics have been averaged over the river lateral cross section. In other words, the mixing in the river channel perpendicular to the channel is instantaneous and uniform.
- The longitudinal river averaging scale is taken to be much greater than the river width.
- The processes of radionuclides sorption and desorption by suspended particles and bottom sediments are instantaneous, reversible and described by a linear isotherm with a constant distribution coefficient K*d*.
- Dynamic factors (currents) have no impact on the radionuclide mass exchange diffusion coefficient.
- The leading role in the processes of interaction of bottom sediments is played by the effective layer of bottom sediments, the thickness of which is estimated or determined experimentally.
- The activity of biomass activity is negligible as compared with the levels of radionuclides in bottom sediments.

5.2.4. Model GIDRO-W

The model GIDRO-W for long-term transport of radionuclides in the river channel is based on the model accounting for radioactive decay, advective transport of radionuclides, dispersion, exchange between radionuclides adsorbed on suspended particles in the water column and those occurring in bottom sediments, removal of radionuclides from the river due to evaporation, filtration losses and flow of radionuclides to the river from different sources, diffusion down the profile of bottom sediments.

For calculating radionuclide transport in the Techa River from Muslyumovo point to the river mouth the model of piston displacement has been used (one-dimension model of radionuclide migration). In this model lateral variance of pollutant was neglected.

The radionuclide concentration in water was calculated from the village Muslyumovo (44 km from water reservoir 11) to the estuary of the river (207 km) with the interval of 3 km. The mean annual transport of ^{239}Pu through the Techa cross section near Muslyumovo is accounted to be $(8 \pm 4)\cdot 10^7$ Bq/year.

5.2.5. Model RIVTOX

The model RIVTOX of river hydraulics for simulation cross sectional averaged flow velocity and water elevation in a network of river canals includes continuity equation (mass conservation law) and momentum equation. The friction slope is calculated using one of the empirical resistance laws, such as Chezy's or Manning's. Techa hydrology (cross sectional averaged velocities) was calculated with help of one-dimensional Saint-Venant equations.

The suspended sediment transport in river channels is described by the 1-D advection-diffusion equation that includes a sink-source term describing sedimentation and resuspension rates.

The fluxes are calculated as a difference between actual and equilibrium suspended sediment concentration multiplied on fall velocity of sediment grains. The equilibrium suspended sediment concentration (flow capacity) can be calculated by empirical formula.

This submodel of radionuclide transport describes the advection-diffusion transport of the cross section averaged concentrations of radionuclides in the solution, the concentration of radionuclides on the suspended sediments and the concentration in the top layer of the bottom depositions. The adsorption/desorption and the diffusive contamination transport in the systems "solution – suspended sediments" and "solution – bottom deposition" is treated via the K_d approach for the equilibrium state, additionally taking into account the exchange rates between solution and particles for the more realistic simulation of the kinetic processes.

The present version of this model uses different values of the sorption and desorption rates for the system "water-suspended sediment" and for the system "water-bottom deposits" because this fits better with the real physical-chemical behaviour of radionuclides in the water systems.

5.3. Model results

5.3.1. Model CASTEAUR

The calculation domain is 207 km long from the dam 11 to the river mouth. The domain is characterized by an average slope of 0.0006 m/m. The hydrographical data divide the domain into 18 reaches to represent, from 0 to 207 km an increase of the width by step of 1m, from 18–35 m. The bank angle is put at 45° all along the domain.

For the calculations, this domain is divided with a space step 1 km.

At the entrance of the domain, the imports of water are equalized to the average monthly values given at Muslyumovo. Between 44 and 180 km, the waters discharges are defined by four contributions regularly distributed between 78 and 180 km.

The river depth is varying from 0.5–2 m. To obtain this range with the considered geometrical and the specific water inflow data, the calibration of the Strickler coefficient gives a value of 10 $m^{1/3}.s^{-1}$.

For the suspended matter, the scenario gives the monthly average turbidity at Pershinskoe and the granulometric distribution for the diameters 4, 8, 16, 32, 63, 125, 250, 500 and 1000 μm.

For this exercise, the erosive fluxes of the active and passive layers have been annihilated.

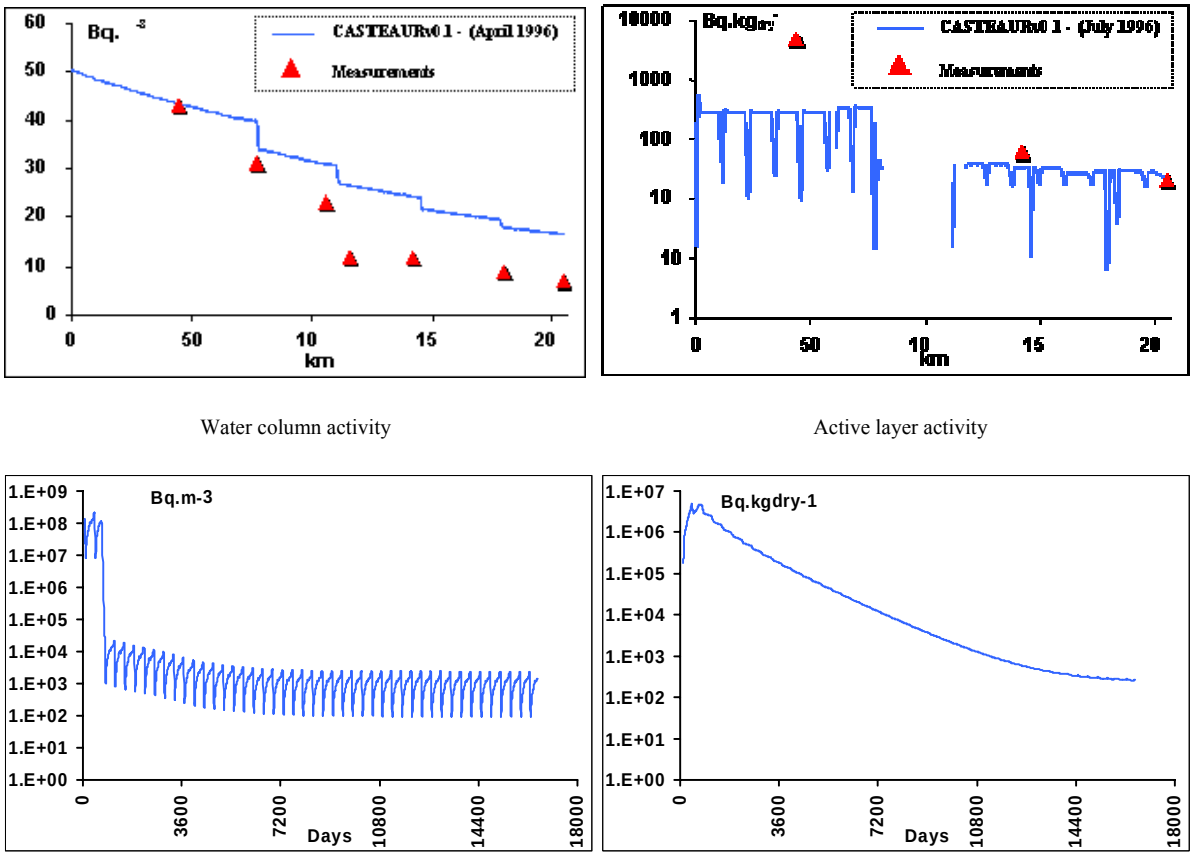

Fig. 5.3. Results of calculating by model CASTEAURv0.1 for ^{90}Sr in water and bottom sediments of the Techa River.

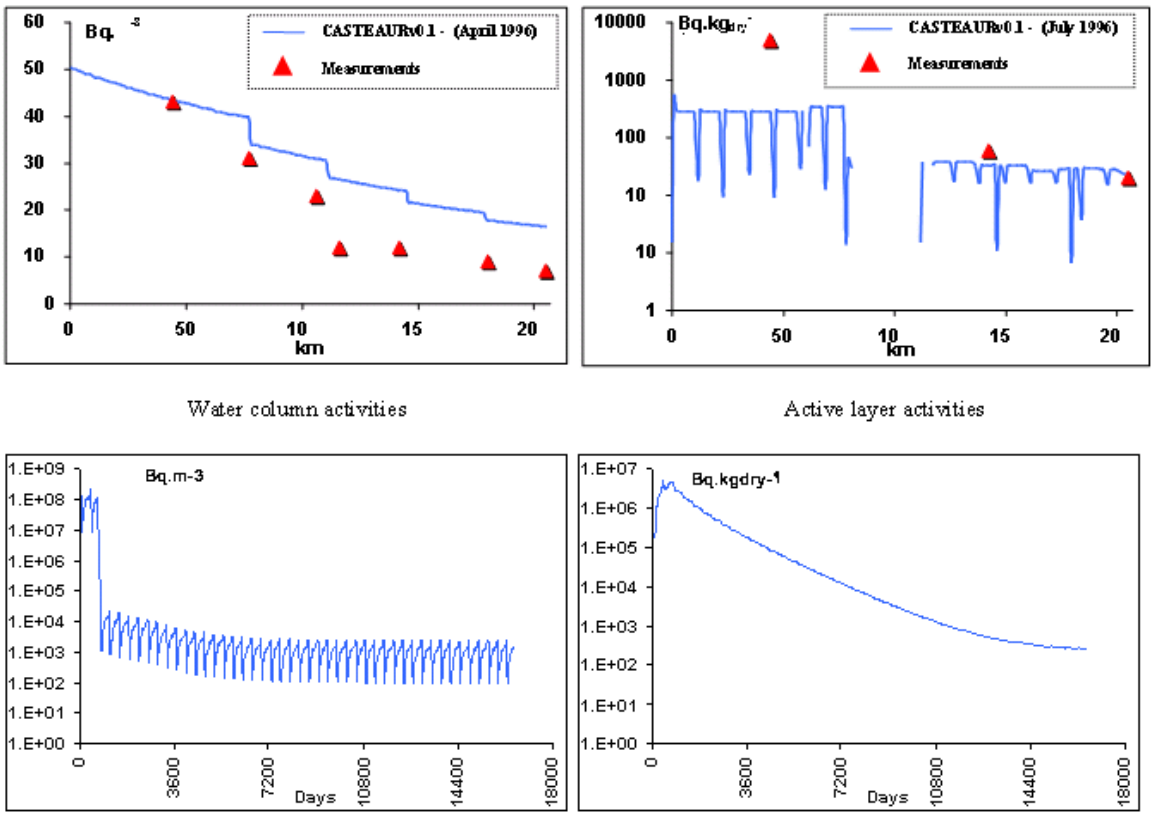

Fig. 5.4. Results of calculating by model CASTEAURv0.1 for ^{137}Cs in water and bottom sediments of the Techa River.

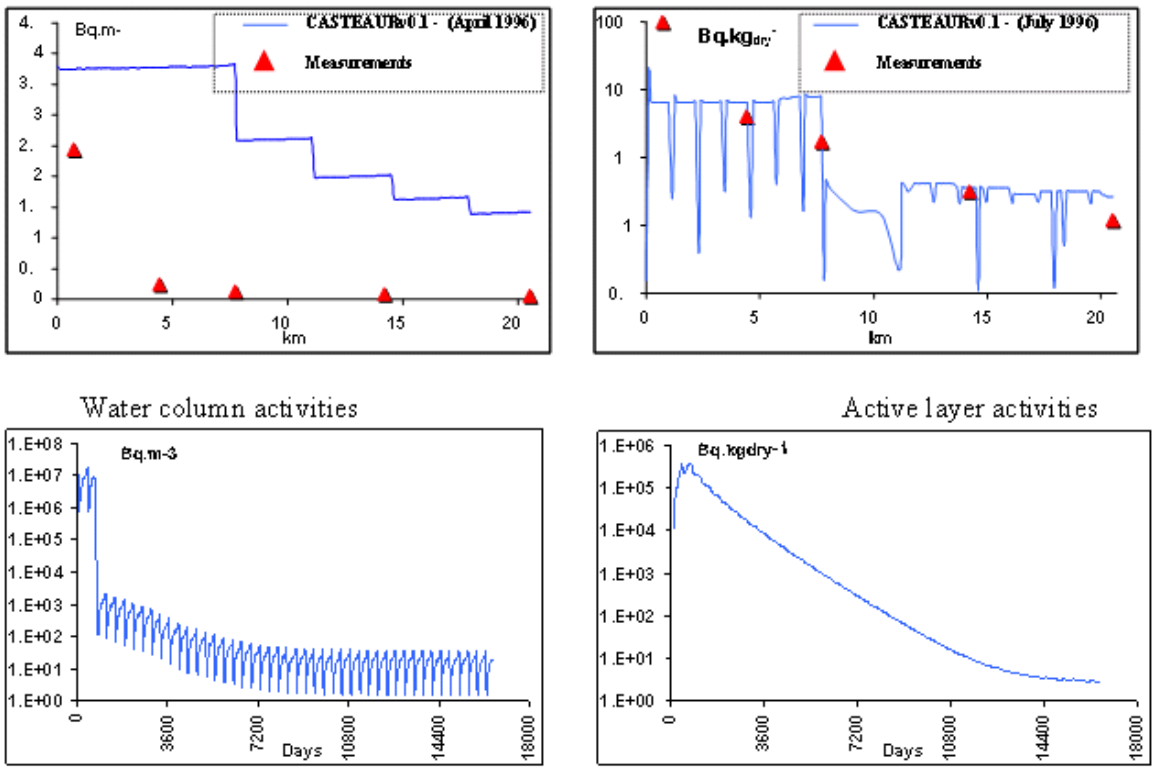

Fig. 5.5. Results of calculating by model CASTEAURv0.1 for ^{239,249}Pu in water and bottom sediments of the Techa River.

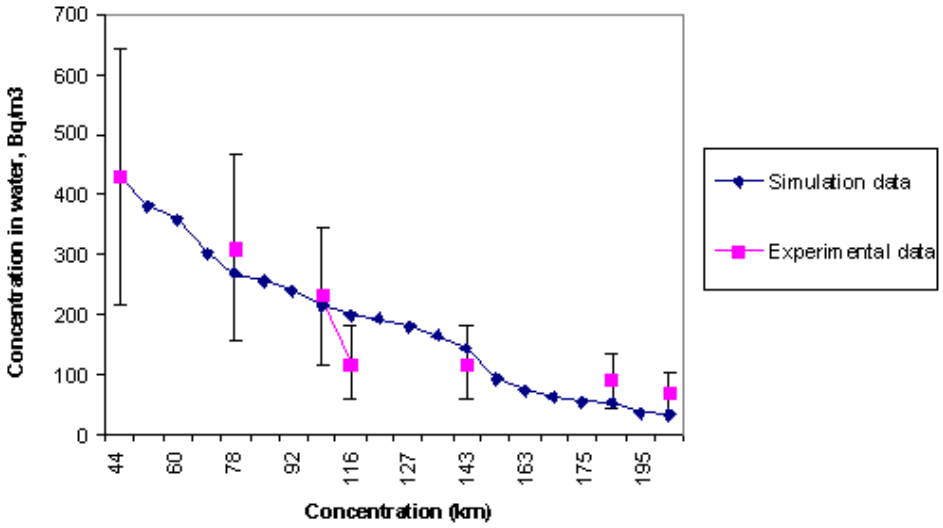

Fig. 5.6. Variations in the ^{137}Cs concentrations in water along the whole length of the Techa. Estimates versus measurements (Model TRANSFER-2).

Table 5.2. Values of K_d used in model CASTEAUR.

Radionuclides	Kd ($m^3.kg^{-1}$)
^{90}Sr	0.3
^{137}Cs	15
$^{239,240}Pu$	10

Table 5.3. Values of the calculation parameters in CASTEAUR.

Period	January 1950 to December 1996
Duration	16560 days
Time step	10 days
Space step	1 km

Each imports of water is associated to a concentration for each class of suspended matter. These concentrations are deduced from the turbidity and from the contributions. The scenario considers three radionuclides: ^{90}Sr, ^{137}Cs, $^{239,240}Pu$.

The imports are described considering three periods of release: (1) January 1950 to February 1950, (2) March 1950 to November 1951 and (3) November 1951–December 1996. Whatever the period, all the imports are situated at the entrance of the domain.

The Kd_r values were adjusted to obtain the best agreement between the calculation and the measurements and are shown in Table 5.2. The parameters for the calculation are given in Table 5.3.

For the sediments, results are given for the active layer which corresponds to the first 2 cm associated to the measurements in the scenario.

The empirical data of the scenario correspond to spatial distribution in the water column and in the two first centimetres of the bottom sediment. The date associated to these distributions is not precise (just the year, 1996). As the CASTEAUR calculations give the results with a temporal resolution of 10 days, the following comparisons are given for the periods associated to the best agreement during 1996. To illustrate the temporal evolution of the calculus, these evolutions at 200 km are also presented (Figures 5.3–5.5).

5.3.2. Model TRANSFER-2

Calculations were performed for water and bottom sediment contamination with ^{90}Sr, ^{137}Cs and $^{239,240}Pu$ along the Techa under normal operational condition. In doing so, an assumption was made that there are no external sources of ^{90}Sr and ^{137}Cs to the river, i.e., the concentrations of the radionuclides in the Techa are attributed only to the contamination of bottom sediments and transport of ^{90}Sr with the Techa waters merging downstream of the Muslyumovo and for ^{137}Cs – the Techa water of the upper parts. The initial concentrations in the bottom sediments were estimated under the assumption of the equilibrium between the radionuclides in bottom sediments and in water. Results of modeling suggest that the estimates are in good agreement with the measurements (Figure 5.6), the errors not exceeding 50%. The distribution coefficients are selected assuming the equilibrium between the radionuclides occurring in water and in bottom sediments. The exchange with the underflow was set to be zero, with the assumption that as a result of long-term discharges of ^{90}Sr the underflow concentrations of the radionuclide are not lower than those in the channel flow. Table 5.4 includes results of calculations.

Table 5.4. Comparison of estimates and measurements for the Techa River. Model TRANSFER-2.

x, km	^{239,240}Pu				^{90}Sr				^{137}Cs			
	water, Bq/m^3		sediments, Bq/kg		water, Bq/m^3		sediments, Bq/kg		water, Bq/m^3		sediments, Bq/kg	
0	0.65		–		26 000		705		1800		13830	
Point	C	M	C	M	C	M	C	M	C	M	C	M
Muslyumovo, 44 000	0.25	2.5	2.7	40	17 850	18 000	484.1	670	590	430	49 000	4540
Brodokalmak, 77 000	0.15	0.13	1.6	16.6	14 400	14 000	390.6	–	313	310	2405	–
143 000	0.07	0.092	0.7	1.04	10 380	11 000	280.5	150	120	120	903	590
Zatechenskoe, 205 000	0.04	0.055	0.4	0.43	8147	8000	221.0	200	60	70	446	200

C = Calculated; M = Measured.

It can be concluded that calculation results for different radionuclides are dependent, to a great extent, on ζ – the coefficient of radionuclides exchange between the main flow and the underflow and on the value of the coefficient *a* representing the linear increase in the velocity (discharge), given the invariable river cross section along the length of the river. Considering that over the time of the "Mayak" operations the river underflow was contaminated with radionuclides to a different extent, it can be assumed that for some radionuclides (^{90}Sr and partly ^{137}Cs) this flow serves as a source of radioactivity, like the Asanov swamps. For others (^{239,240}Pu) the underflow is a sink to which the radionuclides keep entering.

5.3.3. Model CASSANDRA

Calculations with the CASSANDRA model were performed for the part of the Techa River situated downstream the Muslyumovo settlement. It was assumed that the external sources do not make any contribution to the radioactive contamination of the Techa River, and the radionuclide content in the river water is caused only by migration of radioactivity from bottom sediments and from the upstream parts of the river. The measured level of activity concentration of radionuclides in water near Muslyumovo was taken as an initial value for model calculations, as well as activity concentration of ^{90}Sr in bottom sediments. For ^{239}Pu and ^{137}Cs the activity concentrations in sediments were estimated taking into consideration activity concentrations of these radionuclides in water.

There are some differences between approaches of the analytical model and the numerical CASSANDRA model. The CASSANDRA model considered several parameters, for example, water flows, river width, distribution coefficients K_d for ^{239}Pu and ^{137}Cs, to be in dependence of a distance downstream the river.

The results of calculations by model CASSANDRA in comparison with observation data are presented on Figures 5.7–5.12. Comparison of the CASSANDRA model results with the test data led to the following conclusions:

- Model calculations of plutonium concentrations in water are in good agreement with the test data for all considered part of the Techa River. At the same time for plutonium in sediments at the upper part of the river this model provides underestimated values.
- Model results of ^{137}Cs concentrations in water and sediments are, in general, in agreement with the test data.
- Model results of ^{90}Sr concentrations in water and sediments are in good agreement with the test data at upper and lower reaches of the Techa River, but differ from the test data at the middle reaches.

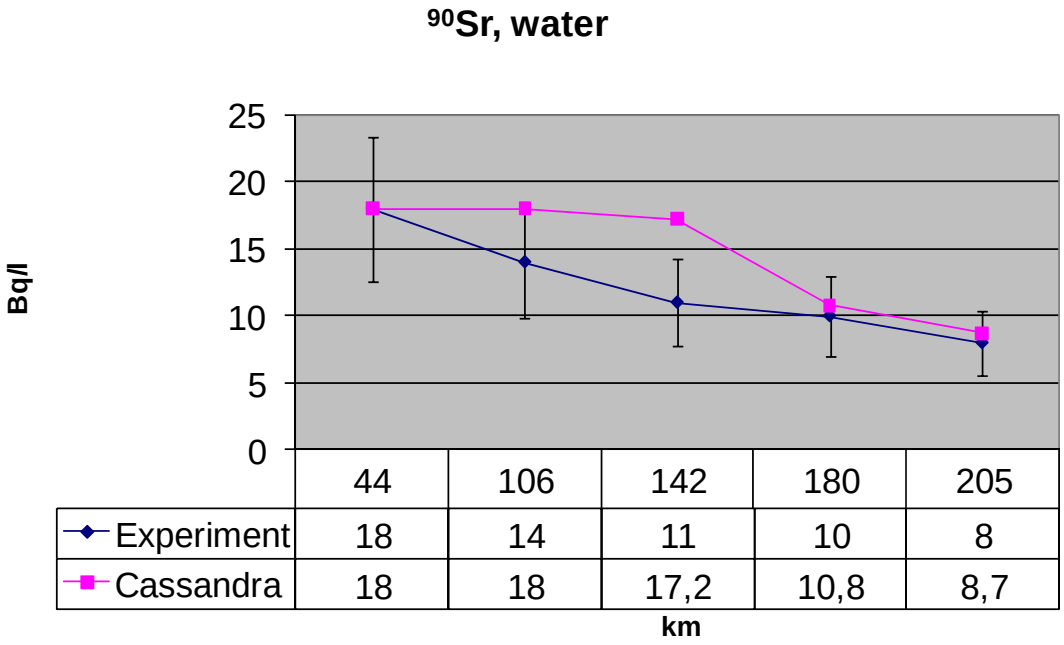

Fig. 5.7. Results of calculating by model CASSANDRA for ^{90}Sr in water of the Techa River.

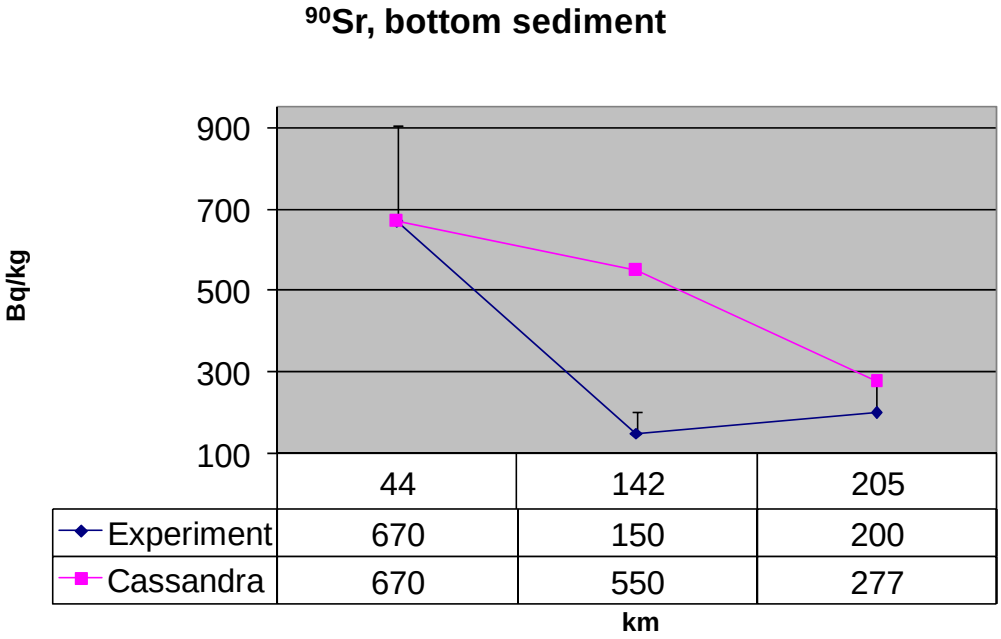

Fig. 5.8. Results of calculating by CASSANDRA for ^{90}Sr in bottom sediments of the Techa River.

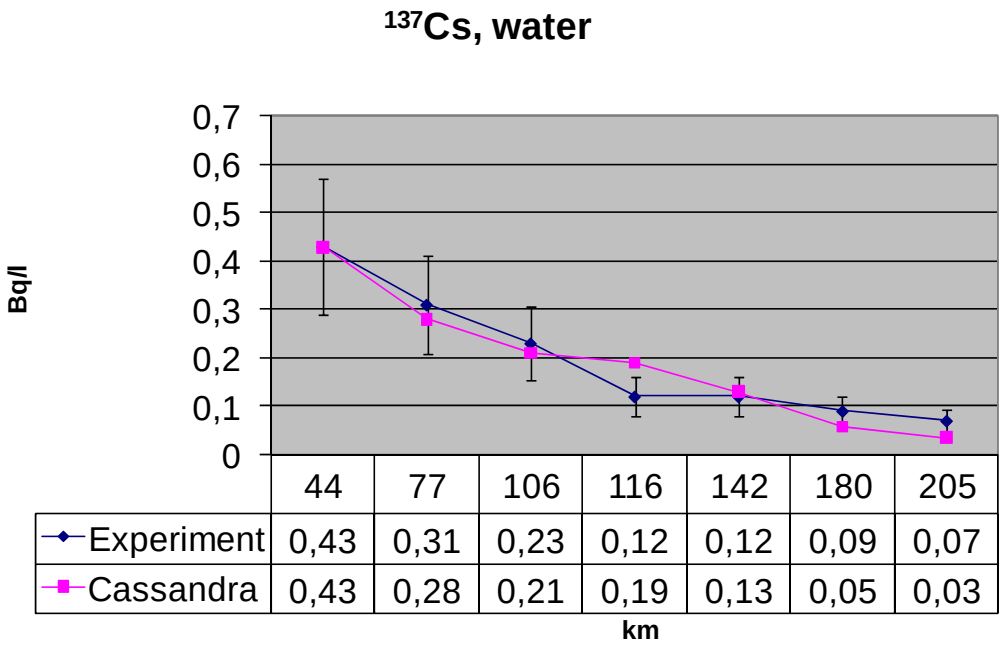

Fig. 5.9. Results of calculating by model CASSANDRA for ^{137}Cs in water of the Techa River.

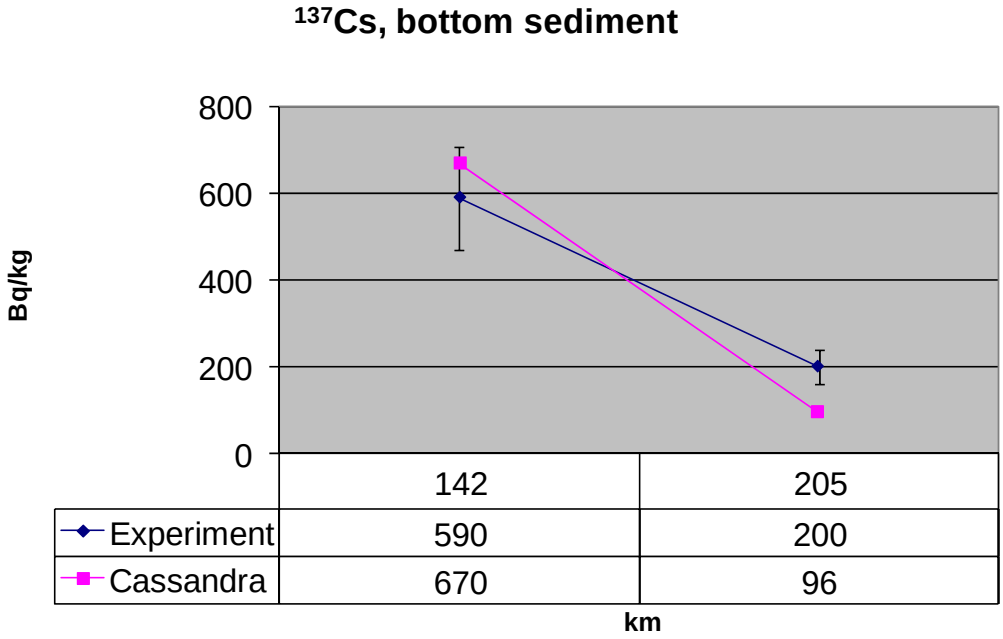

Fig. 5.10. Results of calculating by CASSANDRA for ^{137}Cs in bottom sediments of the Techa River.

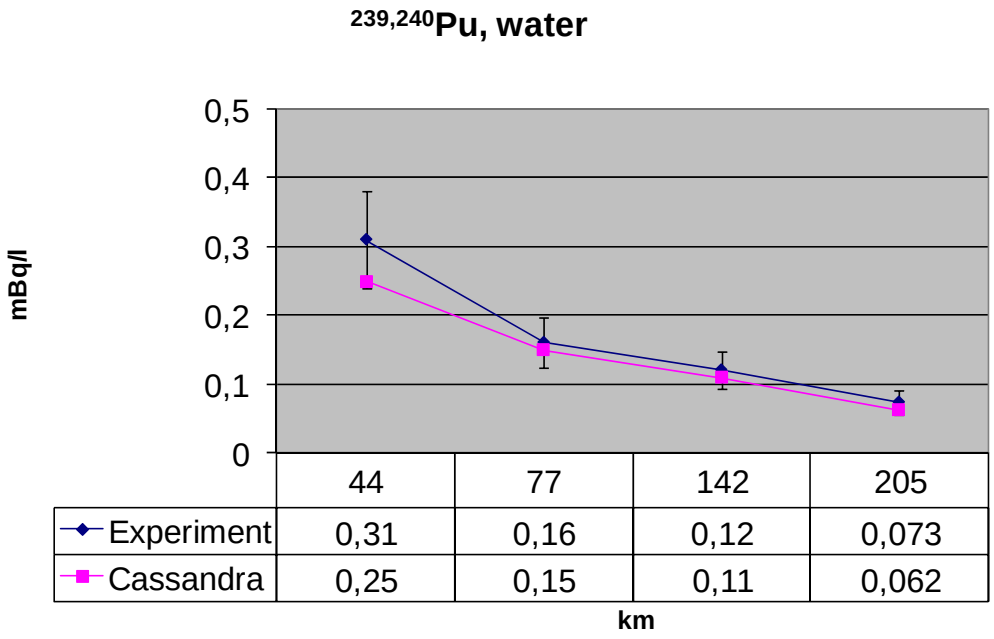

Fig. 5.11. Results of calculating by model CASSANDRA for ^{239,240}Pu in water of the Techa River.

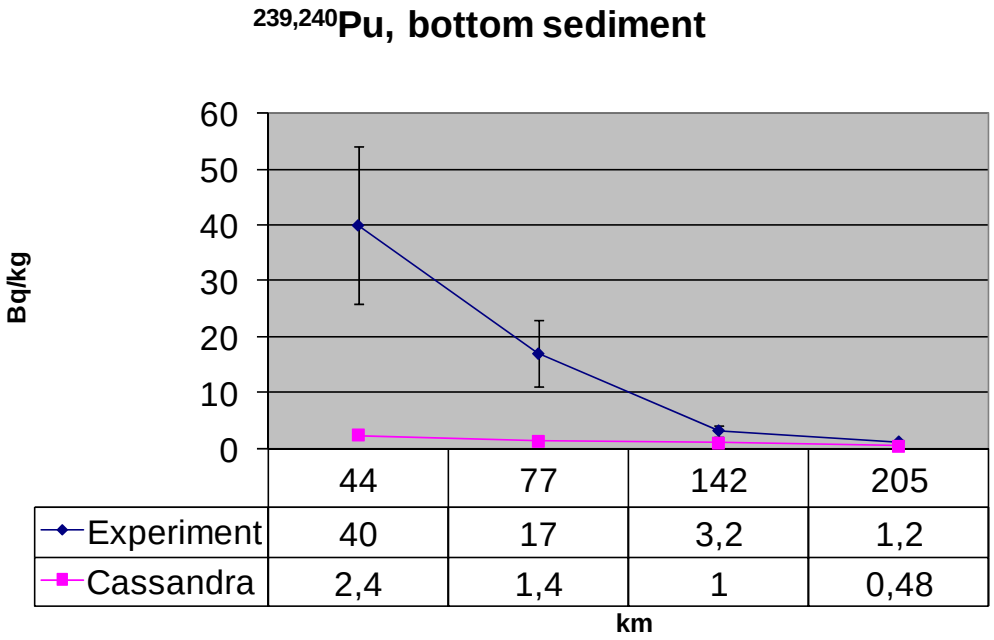

Fig. 5.12. Results of calculating by model CASSANDRA for ^{239,240}Pu in bottom sediments of the Techa River.

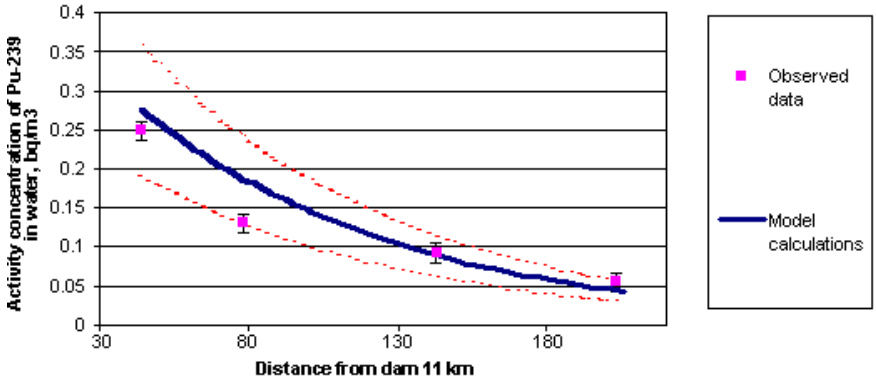

Fig. 5.13. Activity concentration of ^{239}Pu in the water of the Techa River, comparison of the calculations and experimental data. Model GIDRO-W.

5.3.4. Model GIDRO-W

The model GIDRO-W was calibrated with empirical data for plutonium transport in the river system. The validation was carried out for two model parameters whose estimates were characterized by the greatest uncertainty, which are the sedimentation velocity U of suspended matter and the coefficient of radionuclide distribution in the system water-suspended matter (K_d). Good agreement between the calculated values and the measured decrease in the activity concentration of the radionuclide in water with distance downstream was achieved with the parameters taken for U=0.1 m/day, and K_d=500 m^3 kg^{-1}.

Figure 5.13 shows the model estimates of the activity concentration of ^{239}Pu in water and the observed water concentrations of plutonium in the Techa River.

The comparison of the estimated activity concentration of ^{239}Pu in river water at different distances from the river source with the empirical data shows that the model supplies reliable results when the selected values of the parameters are used.

5.3.5. Model RIVTOX

According to the Scenario on Model Validation Radioactive Contamination of the Techa River, the ^{90}Sr, ^{137}Cs and ^{239,240}Pu concentrations in solution and bottom sediment were calculated on the base of Scenario input data (Appendix I), namely:

Assessments of inventories of ^{90}Sr, ^{137}Cs and ^{239,240}Pu in the floodplain of upstream part of Techa River, intake of ^{90}Sr to the river as a result of runoff from bypass canals and filtration through the dam 11 the estimated annual runoff of ^{90}Sr, ^{137}Cs and ^{239,240}Pu from upstream part of Techa River, data on the precipitation, hydrological and hydrochemical characteristic of the river (see Table I.1 in Appendix I). Also information about average sediment transport and turbidity in the Techa River at Pershinskoe and average granulometric composition of suspended matter in Techa River at Pershinskoe (Table I.9–I.11 in Appendix I) were used for modeling sediment transport. Initial conditions for radionuclides concentrations in solution

and suspended sediments were equal to 0. For initial conditions in bottom sediments the Table I.3 of Scenario described in Appendix I was used.

For modeling purposes the river network presents the part of the Techa River from dam 11 to Techa mouth and is equal to 207 km. This distance is fragmented on three branches with tributaries in their junctions in this way to provide given discharges in Muslyumovo and Pershinskoe according with data in the Scenario and to get the best correspondence with real geographical map. So first tributary is associated with Zuzelga at the distance of 10 km from dam 11, second with Shutiha, at the distance of 163 km from dam 11. River bed bathymetry corresponds to description of hydrological data in paragraph 3 of Scenario. The external boundary conditions at the dam 11 for discharge corresponds the data from Table I.4 of Scenario for 1996 year (Appendix I). For modeling suspended sediments transport the data from Table I.9 of Scenario were taking into account.

In Figure 5.14 the comparison of calculated and measured discharge in Pershinskoe is presented. Figure 5.15 presents the turbidity in Pershinskoe.

For calculation the ^{239,240}Pu concentrations in solution and bottom sediments of the Techa River the following additional assumption about zero Pu intake from bypass canals and filtration through the dam 11 was made. Result of calculations of ^{239,240}Pu concentrations in solution and bottom sediments of the Techa River and comparisons with measured data at different locations from dam 11 are shown in Figures 5.16 and 5.17. Parameters of exchange used for calculation are presented at the Table 5.5.

For calculation the ^{137}Cs concentrations in solution and bottom sediments of the Techa River the same additional assumption about zero ^{137}Cs intake from bypass canals and filtration through the dam 11 was made. Result of calculation ^{137}Cs concentrations and there comparison with measured data at different locations from dam 11 are presented in Figures 5.18 and 5.19. Parameters of exchange used for calculation are presented at the Table 5.6.

For calculation the ^{90}Sr concentrations the strontium intake from bypass canals and filtration through the dam 11 was taking into account as boundary condition. Result of calculation ^{90}Sr concentrations and there comparison with measured data at different locations from dam 11 are presented in Figures 5.20 and 5.21. Parameters of exchange used for calculation are presented at the Table 5.7.

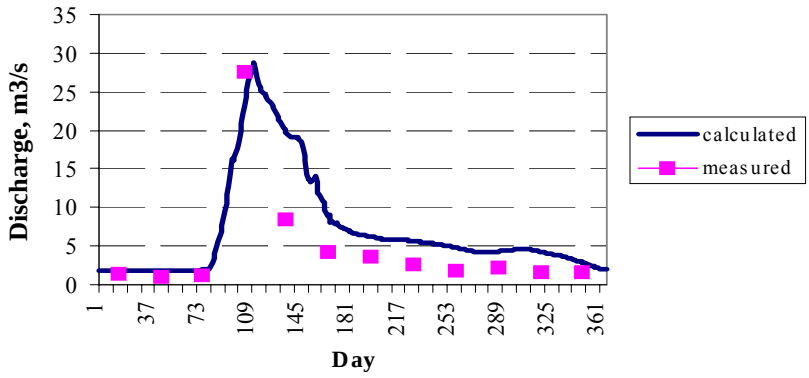

Fig. 5.14. Comparison of calculated and measured discharge in Pershinskoe. Model RIVTOX.

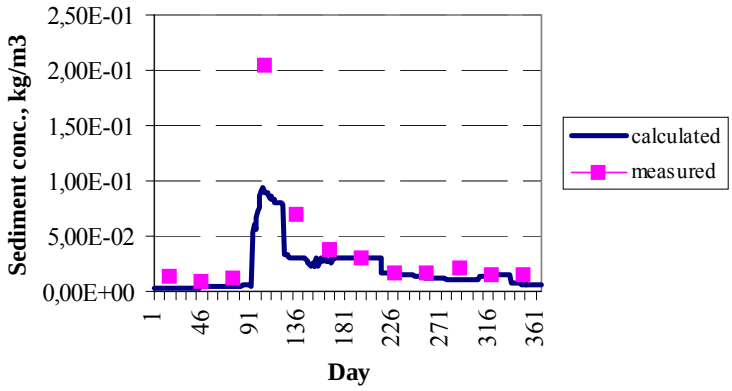

Fig. 5.15. Comparison of calculated and measured turbidity (sediment concentration) in Pershinskoe. Model RIVTOX.

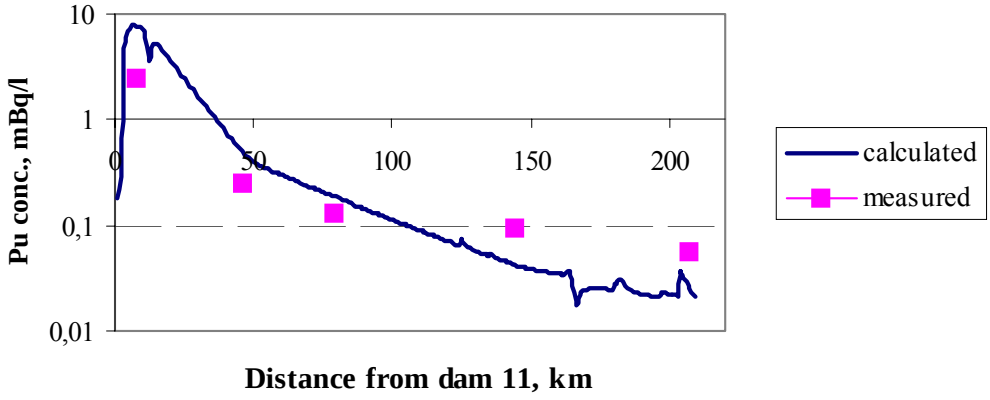

Fig. 5.16. Concentrations of ^{239,240}Pu in water along the Techa River, 1996. Model RIVTOX.

Table 5.5. Exchange parameters for ^{239,240}Pu.

Symbol	Value	Parameter
K_{db}	100 m^3/kg	Equilibrium water-bottom coefficient
K_{ds}	150 m^3/kg	Equilibrium water-suspended sediment coefficient
a_{12}	1 day^{-1}	Exchange rate between water and suspended sediment
a_{21}	0.01 day^{-1}	Exchange rate between suspended sediment and water
a_{13}	0.01 day^{-1}	Exchange rate between water and bottom sediment
a_{31}	0.003 day^{-1}	Exchange rate between bottom sediment and water

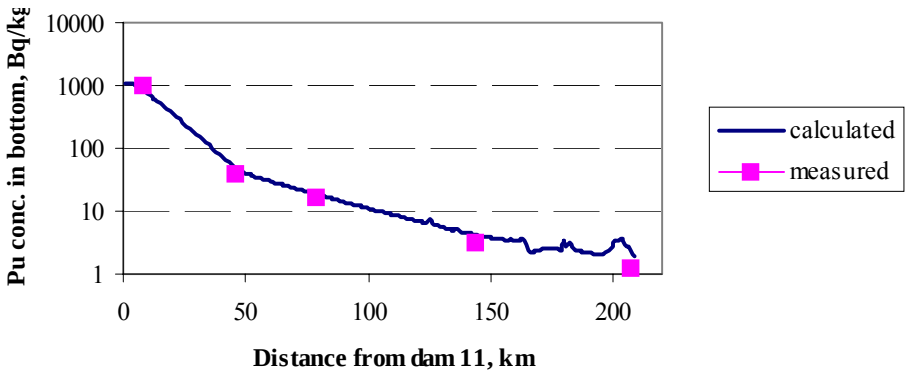

Fig. 5.17. Concentrations of ^{239,240}Pu in bottom sediment along the Techa River, 1996. Model RIVTOX.

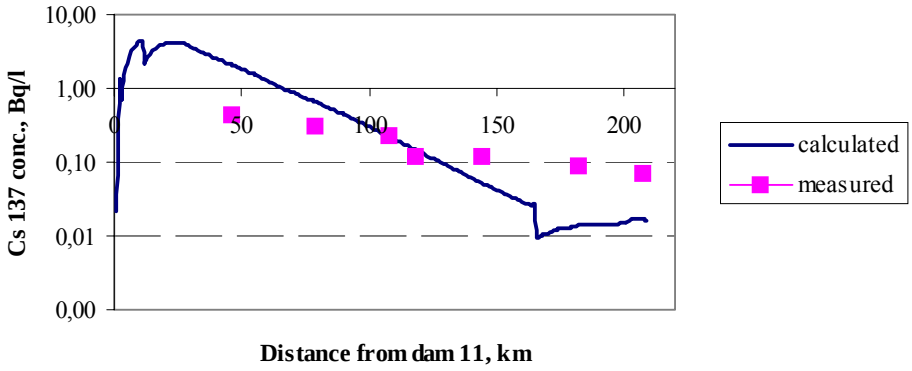

Fig. 5.18. Concentrations of ^{137}Cs in solution along the Techa River, 1996. Model RIVTOX.

Table 5.6. Exchange parameters for ^{137}Cs.

Symbol	Value	Parameter
K_{db}	20 m^3/kg	Equilibrium water-bottom coefficient
K_{ds}	25 m^3/kg	Equilibrium water-suspended sediment coefficient
a_{12}	1 day^{-1}	Exchange rate between water and suspended sediment
a_{21}	0.02 day^{-1}	Exchange rate between suspended sediment and water
a_{13}	0.01 day^{-1}	Exchange rate between water and bottom sediment
a_{31}	0.0027 day^{-1}	Exchange rate between bottom sediment and water

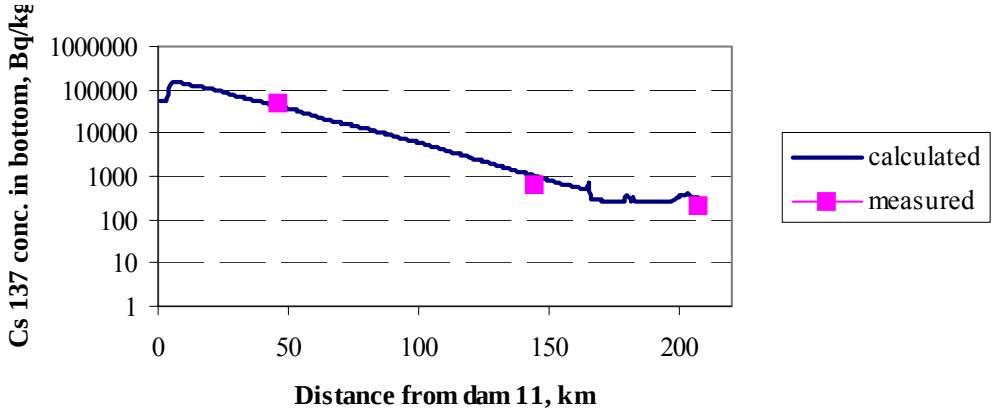

Fig. 5.19. Concentrations of ^{137}Cs in bottom sediment along the Techa River, 1996. Model RIVTOX.

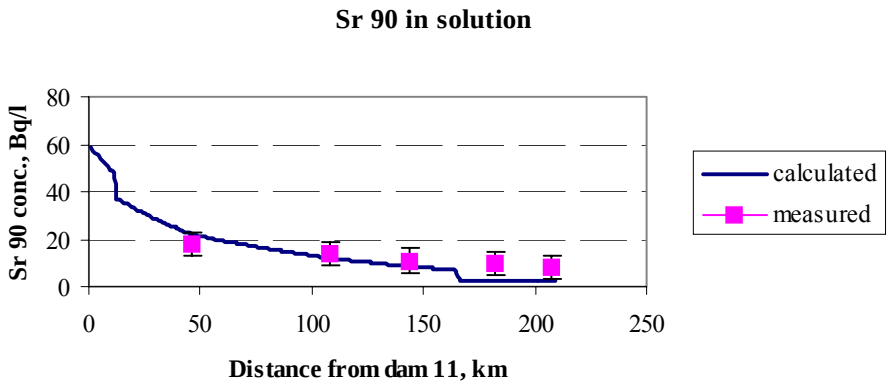

Fig. 5.20. Concentrations of ^{90}Sr in solution along the Techa River, 1996. Model RIVTOX.

Table 5.7. Exchange parameters for ^{90}Sr.

Symbol	Value	Parameter
K_{db}	0.1 m^3/kg	Equilibrium water-bottom coefficient
K_{ds}	0.8 m^3/kg	Equilibrium water-suspended sediment coefficient
a_{12}	1 day^{-1}	Exchange rate between water and suspended sediment
a_{21}	0.02 day^{-1}	Exchange rate between suspended sediment and water
a_{13}	0.01 day^{-1}	Exchange rate between water and bottom sediment
a_{31}	0.0027 day^{-1}	Exchange rate between bottom sediment and water

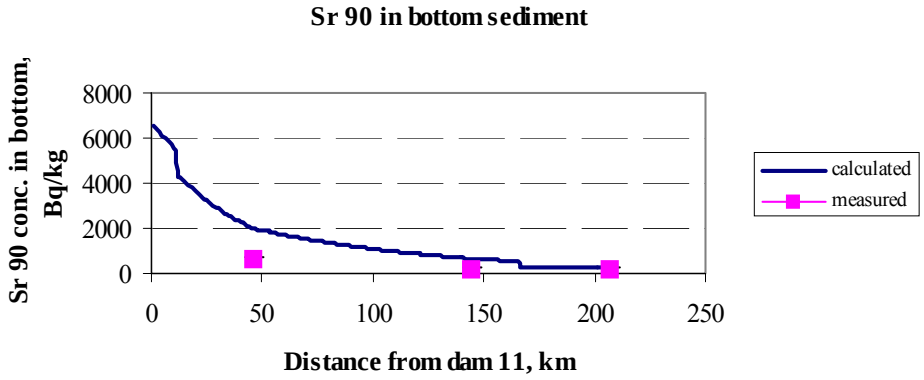

Fig. 5.21. Concentrations of ^{90}Sr in bottom sediment along the Techa River, 1996. Model RIVTOX.

5.4. Discussion

5.4.1. Comparison of the model calculations with empirical data: radionuclides in water

5.4.1.1. ^{90}Sr

Model estimates of the ^{90}Sr specific activity in water in the Techa at different distances from the river source (dam 11) are shown in Table 5.8. The error in determining ^{90}Sr in water, according to empirical data, is about 30%.

The comparison of model estimates with the empirical data suggests that the prediction error for the CASTEAUR model does not exceed the measurement error and on the average is estimated to be 9%, varying from 4–23% for different observational points. The differences are the least in the upper and middle parts of the river (observational points 44, 106, and 142 km). As to the lower river section (180 and 205 km), the error in estimating the specific activity of ^{90}Sr somewhat increases, but does not go beyond the empirical data uncertainty.

For the model TRANSFER-2 the error in determining ^{90}Sr in water, on the average, is 7%, varying from 3–19%. The difference from the observational data is only 3–4% throughout the river down to its mouth and increases to 19% at the mouth only.

For the model CASSANDRA the error, on the average, is 19%, i.e., does not exceed the measurement error either. The errors involved in model estimates range from 0 to 56%. The largest discrepancy with the observational data is seen in the middle part of the river and the smallest in the upper part and at the mouth.

For the model RIVTOX the error in determining ^{90}Sr in water, on the average, is 30%, varying from 7–50%. The largest discrepancy with the empirical data is seen in the upper part of the river and mouth, and the smallest in the middle part.

On the whole, it can be concluded that all tested models are in good agreement with the empirical data of the ^{90}Sr specific activity in the Techa water.

Table 5.8. Model calculations of the ^{90}Sr specific activity in the Techa water as compared with empirical data at different distances from the river source (dam 11), Bq/l.

Model/empirical data	44 km	106 km	142 km	180 km	205 km
CASTEAUR	18.8	13.4	10.5	7.7	7.1
TRANSFER-2	17.3	13.4	11.5	10.3	9.5
CASSANDRA	18.0	18.0	17.2	10.8	8.7
RIVTOX	25	15	10	5	5
Empirical data	18±5	14±4	11±4	10±3	8±2

5.4.1.2. ^{137}Cs

Model estimates of the ^{137}Cs specific activity at different distances from the river source (dam 11) are shown in Table 5.9. The error in determining ^{137}Cs in water by empirical data, on the average, is about 27%.

For the model CASTEAUR the error in the model predictions is, on the average, 70%, varying for different observational points from 10 to 130%. In the upper part of the river, the modeling error does not exceed the measurement error, while in the middle and lower parts of the river the model estimates are about twice as high as those associated with experimental data.

For the model TRANSFER-2 the error in determining ^{137}Cs in water is on the average 18%, varying from 0 to 67%. For most of the points the modeling error is 0–14% and does not exceed the measurement error. The greatest differences with the empirical data are seen for the middle part of the river at the distance of 116 km from the river source.

For the model CASSANDRA the prediction error is, on the average, 25%, with the range of modeling variations being 0–58%. The discrepancy with the empirical data is the greatest in the middle part of the river (116 km from the river source) and at the river mouth.

For the model RIVTOX the error in determining ^{137}Cs in water is on the average 100%, varying from 0 to 360%. For most of the points the modeling error exceeds the measurement error. The greatest differences with the empirical data are seen for the upper part of the river and at the river mouth.

It can be generally concluded that the tested models TRANSFER-2 and CASSANDRA are in a relatively good agreement with the data of monitoring the ^{137}Cs specific activity in the Techa River water. The model CASTEAUR also describes fairly realistically the distribution of this radionuclide along the river channel, overestimating, however, the specific activity in the middle and lower part of the river. For the model RIVTOX the modeling error exceeds the measurement error.

Table 5.9. Modeling estimates of the ^{137}Cs specific activity in the Techa water as compared with empirical data at different distances from the river source (dam 11), Bq/l.

Model/ empirical data	44 km	77 km	106 km	116 km	142 km	180 km	205 km
CASTEAUR	0.43	0.34	0.31	0.26	0.24	0.18	0.16
TRANSFER-2	0.59	0.31	0.23	0.20	0.12	0.085	0.06
CASSANDRA	0.43	0.28	0.21	0.19	0.13	0.057	0.034
RIVTOX	2.0	0.60	0.23	0.18	0.06	0.015	0.018
Empirical data	0.43±0.12	0.31±0.11	0.23±0.09	0.12±0.03	0.12±0.03	0.09±0.02	0.07±0.01

Table 5.10. Modeling estimates of the ^{239,240}Pu specific activity in the Techa River water as compared with empirical data at different distances from the river source (dam 11), mBq/l.

Model/empirical data	44 km	77 km	142 km	205 km
TRANSFER-2	0.27	0.17	0.07	0.04
CASSANDRA	0.25	0.15	0.11	0.062
GIDRO-W	0.34	0.23	0.11	0.06
RIVTOX	0.42	0.20	0.05	0.04
Empirical data	0.31±0.06	0.16±0.05	0.12±0.04	0.073±0.024

5.4.1.3. ^{239,240}Pu

Table 5.10 shows the model estimates of the ^{239,240}Pu specific activity in the Techa water at different distances from the river source (dam 11). The error in determining ^{239,240}Pu in water by empirical data is, on the average, 29%. For the model TRANSFER-2 the error in determining ^{239,240}Pu in water is, on the average, 26%, varying from 6–45%. The greatest discrepancies with the empirical data of 42 and 45%, respectively were reported for the middle part of the river (142 km from the source) and at the river mouth, while the least (6–12%) – in the upper part of the river. For the model CASSANDRA the error in determining ^{239,240}Pu in water is, on the average, 12%, varying from 6–19%., do not exceed measurement errors. For the model GIDRO-W the error in estimating the plutonium specific activity in river water, on the average, is 20%, with the variations of 10–44%, i.e., it practically does not exceed the measurement error. The largest discrepancy with the empirical data is seen over the river section at the distance of 77 km from the river source (dam 11). For the model RIVTOX the error in determining the plutonium specific activity in water is on the average 40%, varying from 25–60%. The greatest discrepancies with the empirical data were reported for the middle part of the river and at the river mouth, while the least – in the upper part of the river.

On the whole, it can be concluded that the tested models TRANSFER-2, CASSANDRA and GIDRO-W are in good agreement with empirical data of the ^{239,240}Pu specific activity in the Techa water. Model RIVTOX underestimates the plutonium specific activity in water in the upper part of the river. The model CASTEAUR overestimates the plutonium levels in river water.

5.4.2. Comparison of the model calculations with empirical data: radionuclides in bottom sediments

5.4.2.1. ^{90}Sr

Table 5.11 shows the model estimates of the specific activity of ^{90}Sr in bottom sediments of the Techa at different distances from the river source (dam 11). The error in determining ^{90}Sr in bottom sediments based on the empirical data is on the average about 35%.

For the model CASTEAUR the errors in model predictions is, on the average, 26%, varying from 8–59% in different empirical points. The least discrepancies with the empirical data within 8–11% are reported for the lower parts of the river (observational points 44 and 205 km), the largest difference (59%) – on the middle part of the river.

Table 5.11. Modeling estimates of the ^{90}Sr specific activity in bottom sediments of the Techa as compared with the empirical data at different distances from the river source (dam 11), Bq/kg dry weight.

Model/empirical data	44 km	142 km	205 km
CASTEAUR	721	239	178
TRANSFER-2	480	410	260
CASSANDRA	670	550	277
RIVTOX	2000	500	200
Empirical data	670±190	150±60	200±72

For the model TRANSFER-2 the error in determining ^{90}Sr in bottom sediments is on the average 76%, varying from 30 to 170%. As is the case with the model CASTEAUR, the least discrepancy with the observational data (about 30%), not exceeding the measurement errors, occur in the upper and lower parts of the river and the largest – in the middle part.

For the model CASSANDRA the error, on the average, is 100%. The errors associated with model estimates vary within 0–270%. The discrepancy with empirical data is the largest in the middle part of the river.

For the model RIVTOX the error in determining ^{90}Sr in bottom sediments is on the average 140%, varying from 0 to 230%.

It can generally be concluded that the model CASTEAUR is in good agreement with the observations of the specific activity of ^{90}Sr in bottom sediments of the Techa. The models TRANSFER-2 and CASSANDRA also account in a realistic way for the distribution of ^{90}Sr in bottom sediments of the upper and lower parts of the Techa, but give estimates going beyond the measurement error for the middle part of the river. For the model RIVTOX the discrepancy with empirical data is the largest in the upper and middle parts of the river.

All tested models overestimate the specific activity of ^{90}Sr in bottom sediments, and this is particularly the case with the models RIVTOX and CASSANDRA.

5.4.2.2. ^{137}Cs

The model estimates of the ^{137}Cs specific activity in bottom sediments of the Techa at different distances from the river source (dam 11) are shown in Table 5.12. The error in determining ^{137}Cs in bottom sediments, based on empirical data, is on the average 32%.

For the model CASTEAUR the error in model predictions is on the average 30%, varying from 16–44%. The largest discrepancy with the empirical data occurs in the middle part of the river.

As to the model TRANSFER-2 the error in determining ^{137}Cs in bottom sediments on the average is 65%, varying from 41–90%. The difference from the observational is the largest for the lower part of the river.

The error associated with the model CASSANDRA is on the average 32%. The range of variations in the estimate errors is 13–52%. The discrepancy with the empirical data is the largest in the lower part of the river.

Table 5.12. Model estimates of the ^{137}Cs specific activity in the Techa as compared with empirical data at different distances from the river source (dam 11), Bq/kg dry weight.

Model/empirical data	44 km	142 km	205 km
CASTEAUR	2830*	328	232
TRANSFER-2	4540*	830	380
CASSANDRA		670	96
RIVTOX	43 000	1000	200
Empirical data	49 000±6000	590±170	200±70

Note. * estimates were not considered in testing the models

As to the model RIVTOX the error in determining ^{137}Cs in bottom sediments on the average is 27%, varying from 0 to 70%. The difference from the observational is the largest for the middle part of the river.

On the whole, it can be concluded that the models CASTEAUR and RIVTOX are in a relatively good agreement with the empirical data of the ^{137}Cs specific activity in bottom sediments of the Techa. The models TRANSFER-2 and CASSANDRA provide realistic estimates for the middle part of the river, but their estimates for the lower part go beyond the range of measurement errors. It should be noted that in testing the models no account was taken of the empirical data of the levels of ^{137}Cs in the upper part of the river for which the scenario includes abnormally high specific activity from a contamination spot. At the same time model RIVTOX in contrast to other models provides realistic estimate for the ^{137}Cs contamination spot in the upper part of the river.

5.4.2.3. ^{239,240}Pu

The model estimates of the ^{239,240}Pu specific activity in bottom sediments of the Techa at different distances from the river source (dam 11) are shown in Table 5.13. The error in determining ^{239,240}Pu in bottom sediments based on the empirical data is on the average about 40%.

For the model CASTEAUR the error in model predictions is on the average 67%, varying from 12–117%. The discrepancy with the empirical data is the largest for the lower part of the river.

For the model TRANSFER-2 the error in determining ^{239,240}Pu in bottom sediments is on the average 82%, varying from 67–93%. The discrepancy with the empirical data is the largest for the upper part of the river.

As to the model CASSANDRA the error in the model predictions is on the average 79%, varying from 60 to 94%. The discrepancy with the empirical data is the largest for the upper part of the river.

For the model RIVTOX the error in determining ^{239,240}Pu in bottom sediments is on the average 25%, varying from 18–33%.

It can be generally concluded that the model RIVTOX provides realistic estimations for plutonium contamination of the bottom sediments along a whole length of the Techa River. For the other tested models the estimates of the plutonium specific activity in bottom sediments in most of the points go beyond the measurement errors.

Table 5.13. Model estimates of the ^{239,240}Pu specific activity in the Techa as compared with empirical data at different distances from the river source (dam 11), Bq/kg dry weight.

Model/empirical data	44 km	77 km	142 km	205 km
CASTEAUR	67	4.5	3.6	2.6
TRANSFER-2	2.6	1.6	0.7	0.4
CASSANDRA	2.4	1.4	1.0	0.48
RIVTOX	50	20	4.0	1.6
Empirical data	40±12	17±6	3.2±1.1	1.2±0.7

5.4.3. Intercomparison of the tested models and empirical data

One of the ways to evaluate the model ability to reproduce adequately empirical data is using the mean ratio of model estimates and experimental data (Table 5.14).

In addition, most of tested models provides adequate results for ^{239,240}Pu distribution between water and bottom sediments of the Techa River. The ratio between the calculated and observed activity concentrations of ^{239,240}Pu in water is equal to 0.77 for the TRANSFER-2 model, 0.88 for CASSANDRA model and 1.07 for GIDRO-W model. At the same time the ratio between the calculated and observed activity concentrations of ^{239,240}Pu in bottom sediments is equal to 1.3 for CASTEAUR model, 0.18 for the TRANSFER-2 model, 0.21 for CASSANDRA model.

The analysis of model results and the test data leads us to the following conclusions:

- All tested models provide an adequate description of the distribution of ^{137}Cs in water and bottom sediments of the Techa.
- The models CASTEAUR and TRANSFER-2 provide an adequate description of the distribution of ^{90}Sr in water and bottom sediments of the Techa.
- The model CASTEAUR is in good agreement with the observations of the distribution of ^{90}Sr and ^{137}Cs, both in water and bottom sediments, practically over all sections of the Techa River, but this model overestimates the plutonium levels in water.
- The model TRANSFER-2 is the best from the standpoint of agreement with empirical data on the distribution of ^{90}Sr, ^{137}Cs and plutonium in river water. It accounts for the distribution of ^{90}Sr, ^{137}Cs and plutonium with a lesser accuracy, and considerably underestimates the plutonium levels in bottom sediments.
- The model CASSANDRA is in good agreement with the observations of the distribution of ^{90}Sr, ^{137}Cs and plutonium in river water, less accurate in describing the distribution of ^{90}Sr, ^{137}Cs and plutonium in bottom sediments.
- The model RIVTOX in contrast to other models provides realistic estimate for the ^{137}Cs contamination spot in the bottom sediments of the upper part of the river.

Table 5.14. Comparison of the model estimates of the ^{90}Sr and ^{137}Cs activity concentrations in water and bottom sediments of the Techa with the empirical data.

Model	Water		Bottom sediments	
	^{90}Sr	^{137}Cs	^{90}Sr	^{137}Cs
CASTEAUR	0.92	1.70	1.2	0.86
TRANSFER-2	1.04	1.12	1.6	1.7
CASSANDRA	1.20	0.94	2.0	0.81
RIVTOX	0.90	1.40	2.4	1.2

Thus, all tested models have both strengths and weaknesses in terms of reproducing empirical data and none of them agrees with the observations of ^{90}Sr, ^{137}Cs and $^{239,240}Pu$ in the system river water-bottom sediments. Modelling the $^{239,240}Pu$ distribution provided the most diffiuclties, because most of models have not been previously tested or validated for these radionuclides, in contrast with ^{137}Cs and ^{90}Sr.

The primary reason for the discrepancy of predictions and empirical radionuclide concentration in sediments is that the modelers had no true parameters governing sorption and migration of radionuclides under modeling. These parameters include the distribution coefficients for water-suspended particles and porous water- bottom sediments and a number of parameters controlling the transport of radionuclides by suspended particles- their composition and grain size, sedimentation rate etc. For determining correctly the radionuclides concentrations in bottom sediments these parameters are better to be determined experimentally.

Let us now consider the mean errors in the estimates of the tested models as compared with the experimental results presented in Table 5.15.

On a whole, the data of Table 5.15 are in agreement with those of Table 5.14. This is indicative of the absence of any significant compensation effect in averaging the ratios of model estimates and experimental values. The exception is the RIVTOX estimates of the ^{137}Cs specific activity in water and ^{90}Sr in bottom sediments. The increase in the relative error in the estimates of the CASSANDRA and GIDRO-W model do not go beyond the measurement error. Mean errors in the model estimates for $^{239,240}Pu$ in the river water as compared with the test data are equal to 26% for the TRANSFER-2 model, 12% for CASSANDRA model and 20% for GIDRO-W model. At the same time the mean errors in the model estimates for $^{239,240}Pu$ in bottom sediments as compared with the test data are equal to 67% for CASTEAUR model, 82% for the TRANSFER-2 model and 79% for CASSANDRA model.

As mentioned above, the tested models account for the radionuclides concentrations in two components of the river system: water and bottom sediments. Therefore there may be another way to measure the models adequacy: the coefficient R_d representing the ratio of the specific activities of radionuclides in bottom sediments (Bq/kg dry weight) and in water (Bq/l).

The model and experimental estimates of this coefficient for ^{90}Sr, ^{137}Cs and $^{239,240}Pu$ over different parts of the river are shown in Tables 5.16–5.18.

The best agreement in estimates of R_d for CASTEAUR, TRANSFER-2 and CASSANDRA is seen for ^{90}Sr (Table 5.16). For this radionuclide the model estimates of the coefficient R_d are virtually in complete agreement with those based on the observations in the upper and lower

parts of the river and somewhat higher the experimental values for the middle part. The model RIVTOX overestimates this coefficient for ^{90}Sr for all parts of the river by 1.6–3.5 times.

For ^{137}Cs the model CASTEAUR underestimates R_d by 2.0–3.6 times, the model TRANSFER-2 overestimates R_d by 1.4–2.2 times and CASSANDRA underestimates R_d by 2.9 times for the lowest part of the river (Table 5.17). Note also that CASSANDRA uses the variable values of R_d along the river channel and is in better agreement with the empirical data for the middle part of the river. The model RIVTOX overestimates R_d for ^{137}Cs by 3.5 times.

For ^{239,240}Pu significant differences can be seen between the calculated R_d and the empirical data for all tested models besides some assessments by model RIVTOX (Table 5.18).

Table 5.15. Mean errors in the estimates of the tested models as compared with the experimental results (%).

Model	Water		Bottom sediments	
	^{90}Sr	^{137}Cs	^{90}Sr	^{137}Cs
CASTEAUR	9	70	26	30
TRANSFER-2	7	18	76	65
CASSANDRA	20	25	100	32
RIVTOX	28	100	140	34

Table 5.16. Comparison of the model estimates of coefficient Rd for ^{90}Sr in bottom sediments of the Techa with the empirical data over different parts of the river (dam 11).

Model/empirical data	44 km	142 km	205 km
CASTEAUR	38	23	25
TRANSFER-2	28	36	27
CASSANDRA	37	32	32
RIVTOX	80	50	40
Empirical data	37±15	14±7	25±11

Table 5.17. Comparison of the model estimates of coefficient Rd for ^{137}Cs in bottom sediments of the Techa with the empirical data over different parts of the river (dam 11).

Model/empirical data	142 km	205 km
CASTEAUR	1370	1450
TRANSFER-2	6920	6330
CASSANDRA	5150	2800
RIVTOX	17 000	11 000
Empirical data	4900±1700	2900±1700

Table 5.18. Comparison of the model estimates of coefficient Rd for ^{239,240}Pu in bottom sediments of the Techa with the empirical data over different parts of the river (dam 11).

Model/empirical data	44 km	77 km	142 km	205 km
CASTEAUR	17600	1200	1800	1860
TRANSFER-2	9600	9400	10 000	10 000
CASSANDRA	9600	9300	9100	7700
RIVTOX	120 000	100 000	80 000	40 000
Empirical data	130 000±40 000	110 000±43 000	27 000±10 000	16 000±10 000

5.5. Conclusions

Calculations for Techa Scenario were performed 5 participant teams from France, Ukraine and Russia using different models.

All tested models have both strengths and weaknesses in terms of reproducing empirical data and none of them agrees with the observations of all three radionuclides (^{90}Sr, ^{137}Cs and ^{239,240}Pu) in the system river water bottom sediments.

All tested models provide an adequate description of the distribution of ^{137}Cs in water and bottom sediments of the Techa River.

The models CASTEAUR and TRANSFER-2 provide an adequate description of the distribution of ^{90}Sr in water and bottom sediments of the Techa.

The model RIVTOX provides realistic account of the plutonium distribution in the two component system water bottom sediments.

The model RIVTOX in contrast to other models provides realistic estimate for the ^{137}Cs contamination spot in the bottom sediments of the upper part of the river.

The models TRANSFER-2, CASSANDRA, GIDRO-W, RIVTOX is in good agreement with the observations of the distribution of plutonium in river water.

The model CASTEAUR accounts best of all for the distribution of radionuclides in bottom sediments of the Techa.

The distribution of plutonium in bottom sediments of the Techa River seems to be the most difficult to estimate for most of tested models.

CHAPTER 6. MODELLING ^{226}RA SELF-CLEANING IN THE HUELVA ESTUARY

R. Periañez, Departamento Fisica Aplicada, University of Sevilla, Spain; N. Goutal, Electricité de France, R&D, France; S. Kivva Institute of Mathematical Machines and System Problems, Ukraine; M. Luck, Electricité de France, R&D, France; L. Monte, ENEA, Italy; F. Siclet, Electricité de France, R&D, France; M. Zheleznyak, Institute of Mathematical Machines and System Problems, Ukraine

6.1. Introduction

The Huelva estuary is located at the southwest of Spain. It consists of a tidal, fully mixed, estuary formed by the Odiel and Tinto Rivers, which surround the town of Huelva (Figure 6.1). Both rivers join at the Punta del Sebo. From this point, they flow together through the same channel towards the Atlantic Ocean. An industrial area, including a complex dedicated to the production of phosphoric acid and phosphate fertilizers, is located by the Odiel River. The fertilizer plants have been the main source of natural radionuclides to the estuary: it is well known that the phosphate rock used as raw material by this industry contains significant amounts of natural radionuclides, mostly U, Th and Ra. The industrial processing of the phosphate rock leads to a redistribution of radioactivity. For instance, during the wet process for phosphoric acid production, 86% of U and 70% of Th present in the rock are transferred to the phosphoric acid itself, while 80% of the Ra content follows the so called phosphogypsum path. This is a form of impure calcium sulfate removed as a precipitate during the process. Phosphogypsum is usually disposed into open air piles or discharged into rivers or estuaries, giving rise to a local radioactive impact. During 1990, for instance, 2×10^6 tons were processed and 3×10^6 tons of phosphogypsum were produced [25]. These wastes were partially released directly into the Odiel River (20%) and conveyed with water through a pipeline to phosphogypsum piles (remaining 80%) located by the Tinto River (see Figure 6.1), where such material was stored in the open air. The gypsum piles cover some 12 km^2 of the Tinto River margin. Since 1998 wastes are not released directly into the Odiel River due to new regulations from the EU, although phosphogypsum is still being disposed of in the piles by the Tinto River. These new piles, however, are surrounded by dykes to prevent leaching to the river.

In Absi et al. [25], the time evolution of ^{226}Ra activities in water and sediments over years 1999–2002 was studied. Results indicated that a self-cleaning process was taking place in the estuary as a consequence of the new waste policy, since a systematic and continuous decrease in activities was found in the water column and in bed sediments. The objective of this scenario was to study the self-cleaning process that has been observed in the Huelva estuary by means of different models.

The estuary is very shallow (maximum depth around 19 m) and also well mixed vertically due to the strong tidal currents of the order of 1 ms^{-1}. Moreover, the stream flows of the rivers are very low (normally ranging from 0.5–70 m^{3}s^{-1} in the Odiel River and even lower in the Tinto River) and a rapid dispersion of fresh water into a much larger volume of salt water occurs [26]. This mixing takes place upstream of the studied area and the salinity across the estuary may be considered constant and typical of seawater. Residual currents, due to the river discharges, are of the order of 1 cm s^{-1} over the estuary.

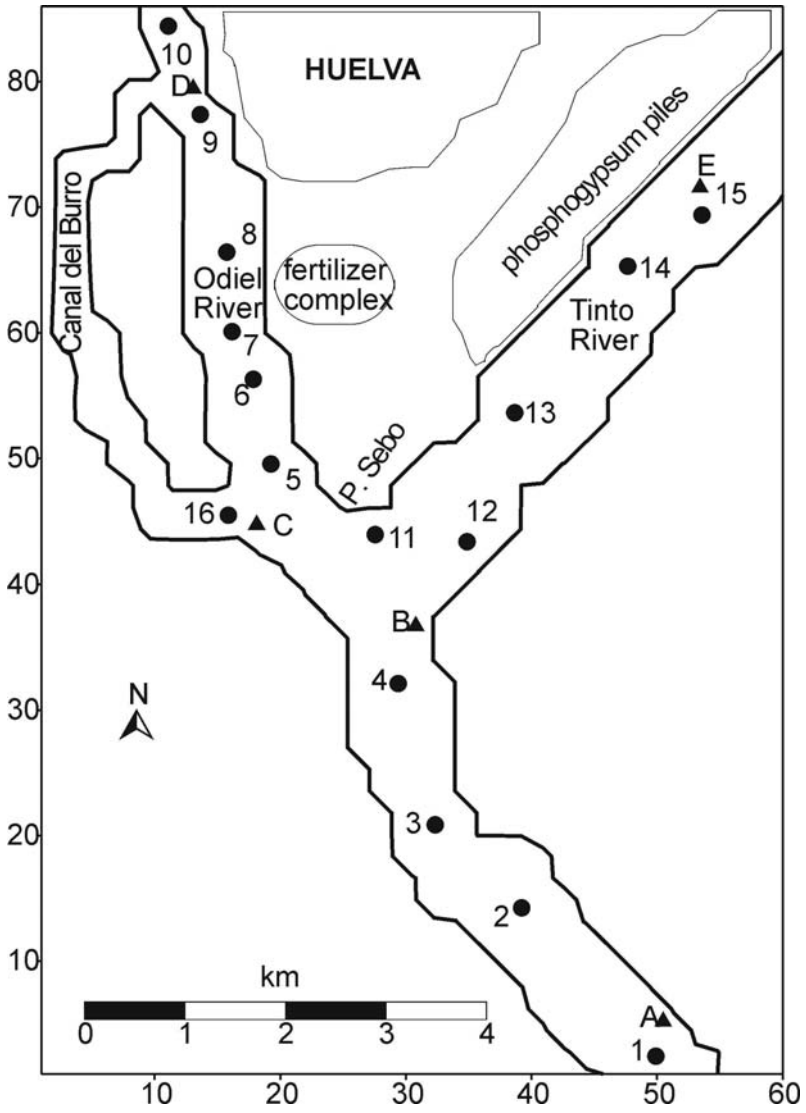

Fig. 6.1. Map of the Huelva estuary showing points where samples were collected (circles) and points where current measurements are available (triangles). The location of the fertilizer complex and of the phosphogypsum piles is also shown. The Atlantic Ocean is approximately 1 km to the south of point 1. Each unit in the axes corresponds to 125 m.

The concentrations of suspended sediments in the estuary depend on tidal state. Thus minimum concentrations are expected during high and low water due to sedimentation during slack water periods. During ebb and inflowing periods, stronger currents produce some erosion of the bed sediment. Seasonal variations must be expected as well. Nevertheless, net sedimentation rates are low and these processes have been neglected in previous modelling studies. Indeed, suspended matter concentrations of the order of a few mg l^{-1} have been measured along the estuary.

Limited information is available on the bottom sediment characteristics. In some of the sampling points indicated in the map of Figure 6.1, bulk density, organic matter content and fraction of muds (particles <63 μm) were measured for samples collected in 1991.

The information provided with the scenario is the following:

- Water depths with (grid) resolution 125 m.
- Initial conditions were concentrations of ^{226}Ra in the bed sediments and in the water column throughout the estuary. These concentrations have been obtained from a run of a model developed at the University of Seville and correspond to concentrations when direct releases from the fertilizer complex were stopped. Initial conditions also provide the partition of Ra in the bed sediment between a fast and a slow exchangeable phase.
- Boundary conditions consist of the measured concentrations at the three open boundaries of the domain.
- Physical characteristics of the estuary: averaged monthly river flows, sediment characteristics and suspended matter concentrations.
- Kinetic rates for radium exchange (obtained from laboratory experiments) and average distribution coefficient in the estuary, enabling the modeller to decide between using a distribution coefficient or a kinetic model for describing the interactions between the dissolved and solid phase.

The endpoint of the exercise consisted of providing the time evolution of the total ^{226}Ra inventory in the bed sediment and the time evolution of the concentration in the water column. Models are started from the initial conditions and the system evolves without any external source of radionuclides. Thus, it may be assessed if a self-cleaning process of the system is actually predicted by the model. The time scale at which this process occurs is also of interest.

6.2. Main characteristics of the models

The following models have been applied in the exercise:

MASCARET (Electricé de France R&D, France)

MASCARET is a 1-D hydrodynamic system for simulating hydrodynamic flows, water quality and sediment transport [27]. In the present application the hydrodynamic and pollutant transport modules of the model have been used. The hydrodynamic module has been modified with respect to the Loire River model application to account for tides. The interactions of dissolved radionuclides with the bed sediments have been described by means of two different approaches: a kd-based model and a kinetic model consisting of two consecutive reversible reactions [28].

COASTOX (Institute of Mathematical Machines and System Problems, Ukraine)

COASTOX is a 2-D depth-averaged model that has been applied to the Pripyat River floodplain exercise [29]. As in MASCARET, the hydrodynamics, including tides, and dispersion modules are solved online (simultaneously). To diminish the computational time (calculation time step scale of minutes) the simulation was provided for the periods 10 –12 days for some values of the river discharges and then these hydrodynamics were replicated for other periods with the similar discharges.

The interaction of dissolved radionuclides with the bed sediment was described by means of a desorption coefficient and an adsorption coefficient that was deduced from the kd and the desorption coefficient. Thus, this was a kinetic model consisting of a single reversible reaction.

USEV (University of Seville, Spain)

The USEV model (2-D depth-averaged) is essentially the same as applied to the Pripyat River floodplain exercise. The main difference is that tides were accounted for in boundary conditions of the hydrodynamic module. Dispersion and hydrodynamics were solved offline and standard tidal analysis [30] was used to calculate tidal constants (amplitudes and phases) over the domain. These constants were stored and later read by the dispersion module for a fast computation of tidal currents. Thus, one year of dispersion calculations with a temporal resolution of 60 s took a few minutes on an up-to-date PC. The interactions of dissolved radionuclides with the bed sediments were described through a kinetic model consisting of two consecutive reversible reactions [28].

ENEA (Italian National Agency for New Technologies, Energy and the Environment, Italy)

The ENEA model is a box model based on quantitative evaluations and balance of radionuclide contents in the water system components (surface water, deep water, bottom sediment) accounting for the fluxes among these. The model structure is conceptually similar to the one adopted for the sub-model MARTE (Model for Assessing Radionuclide Transport and countermeasure Effects in complex catchment) [11] implemented in the Computerised Decision Support Systems MOIRA [31]. The water body is divided into three sectors. Each sector is sub-divided into three compartments: surface water, deep water and bottom sediment. A fourth compartment representing the sediment interface between the bottom sediment and the water is considered to simulate the quick interaction processes of radionuclide with particulate matter. The first order differential equations of the model were obtained by calculating the radionuclide budget in the system compartments from the balance between input and output radionuclide fluxes. These are assumed to be proportional to the amount of radionuclide in the respective "source" compartment. Eddy diffusion is simulated by two way fluxes that are calculated from the difference between radionuclide concentrations in two contiguous sectors. The radionuclide absorption by suspended matter and by the sediment interface layer is modelled according to the k_d concept.

6.3. Results and discussions

The time evolution of the computed ^{226}Ra inventory in the sediments of the complete estuary and the mean concentration in the water column obtained with the different models may be seen in Figure 6.2.

All the models predict a decrease of activity in both phases. Different behaviours may be observed for the sediment phase between models that use two step kinetics (USEV and MASCARET 2 reactions) and models that use a single reaction or a distribution coefficient. In the former case, the first rapid reaction followed by a slower redissolution is clearly seen. In the latter case, a continuous reduction in the inventory was obtained. A detailed view of the initial phase of the process is presented in Figure 6.3, as well as the time evolution of the bed inventory after this initial phase on a logarithmic scale.

It is worth commenting that there is a slight difference in the initial inventory in the bed sediment between MASCARET and the other models. This is due to the fact that MASCARET is a 1D model, thus ^{226}Ra concentrations in the bed provided in the scenario as 2D data had to be converted into a 1D structure and some activity was missed in the process.

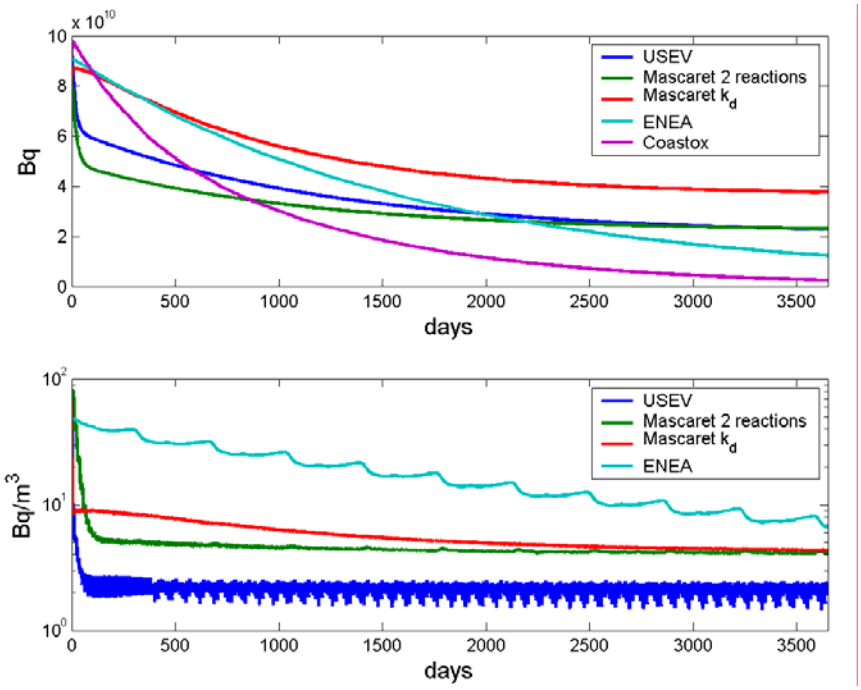

Fig. 6.2. Computed evolution of total ^{226}Ra inventory in bed sediments (upper) and average concentration in the water column (lower).

From measurements in the estuary, Absi et al. [25] determined that the sediment half-time (time in which the ^{226}Ra sediment inventory decreases by a factor 2) was 630 days. The values of this half-time obtained with the different models may be seen in Table 6.1. Computed half-times range between some 400 and 1400 days, thus all models predict that a self-cleaning process of the estuary is occurring, and the order of magnitude of the process time scale is also correctly estimated. Nevertheless, there were differences between the models, especially in the initial stages of the process. Due to the difficulty in simulating this initial phase, that is strongly dependent on the kind of model adopted to describe water sediment interactions, the trends shown in Figure 6.3 have been fitted to exponential decay curves and the corresponding half-times derived from them are also given in Table 6.1. Thus, model behaviours after the initial phase may be compared.

Ideally, the system contamination reaches a quasi steady state in the long term due to the assumed constant values of radionuclide concentrations at the open boundaries, as reported in the scenario description. This condition was predicted, to different degrees, by all models. It is worthwhile to note that four of the five models calculated long-term sediment inventories ranging within a factor less than 4. These results can be deemed in acceptable agreement for the long-term application of the models in view of the uncertainty that generally affects such kind of assessment. For a proper evaluation of the self-cleaning capacity of the Huelva estuary it is necessary to account for the influence of the long-term conditions on the model outputs. Therefore, to estimate the sediment half-time the following equation was used for the numerical fitting mentioned above:

$$I(t) = A + B \cdot \exp(-k \cdot t) \qquad (6.1)$$

where *I(t)* is the inventory at time *t*; *A* and *B* are constants (*A* is the long-term "quasi steady-state" value of the inventory); and the sediment half-time is Ln 2/*k*.

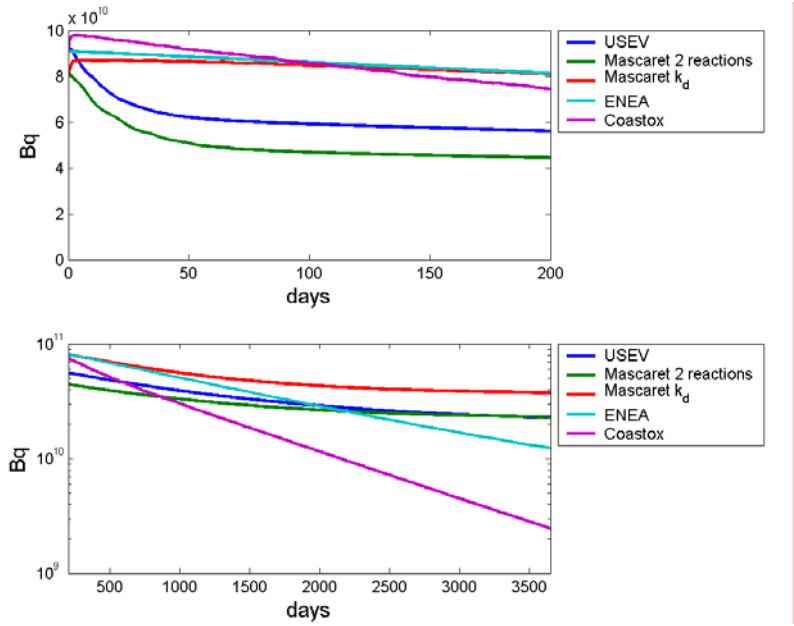

Fig. 6.3. Time evolution of computed inventories in the bed sediment at different time scales.

All models gave very similar results on a longer time scale, if the initial phase of redissolution is not considered, with halving times ranging from 617–844 days.

It may be questioned which is the most suitable water sediment interaction description. Recent experimental [28] and modelling [21] evidence suggests that a 2-reaction kinetic model is more appropriate than a k_d or a 1-reaction model to describe both radionuclide uptake and release from contaminated sediments, since the latter produce dissolution rates that are faster than those deduced from experiments and field measurements. However, no clear conclusion can be derived from this work. Indeed, all models produce acceptable values for the sediment half-time. The main differences between models appear in the initial stages of the redissolution process, but no experimental data are available to test which ones provide the most realistic answer.

Sensitivity tests have been carried out to study the model response to changes in some of the parameters involved (Figure 6.4). One of the parameters is the sediment mixing depth (the sediment depth that interacts with the dissolved phase). Since ^{226}Ra concentrations in the surface sediment at the initial time are provided with the scenario description, reducing the mixing depth from the nominal value, 10 cm, to 1 cm clearly implies a reduction of the inventory in the initial time by a factor 10. Nevertheless the model output remains essentially the same, showing a self-cleaning process occurring at the same rate (results for the USEV model are shown). The Coastox model has been tested with the nominal average sediment bulk density provided with the scenario (700 kg m^{-3}, from measurements) and a more standard value (1480 kg m^{-3}). Apart from the obvious change in the initial inventory, a similar cleaning process is obtained for both model runs. Finally, the MASCARET model has been tested with two k_d values. The mean value of the ^{226}Ra k_d measured in the estuary (36 samples), and provided with the scenario, is 9×10^3. The model has also been tested with a k_d of 1×10^3, which is closer to the value recommended by the IAEA [32] based upon a 20% of exchangeable Ra in coastal sediments (0.7×10^3). A reduction of the distribution coefficient makes the radionuclide more soluble and as a consequence there is a faster self-cleaning process over the first 500 days.

Table 6.1. Computed sediment half-times obtained from the full simulations and after the initial dissolution phase (from t=200 days on).

Model	Half-time (days) Full simulation	Half-time (days) After initial phase
Coastox	597	632
USEV	510	758
MASCARET 2 reactions	405	617
MASCARET k_d	1405	629
ENEA	1186	844

6.4. Conclusions

Different models have been applied to simulate the self-cleaning process that has been observed in an estuary formerly affected by ^{226}Ra releases from a fertilizer complex. The models are very different in structure and resolution, from box models in which the complete estuary is divided into 3 compartments, to high resolution two-dimensional models that explicitly solve tidal circulation processes. Water sediment interactions are also described in different ways: distribution coefficients and kinetic models are used. In spite of these differences, all models predict that a self-cleaning process occurs and that the time scale of the process ranges between some 400 and 1400 days, i.e., a few years. The main differences between models appear during the initial phase of the cleaning process. A very good agreement between models is obtained if half-times are calculated after the initial phase. In this case they range from 617–844 days, in rather good agreement with the 630 days half-time deduced from actual measurements in the estuary. This exercise also shows, as already stated [3, 4], that a multi-model approach can be useful for the management of complex environmental assessment problems. Such an approach clarifies what are the conclusions that obtain the greatest consensus among modellers and what are the ones that should be treated with caution.

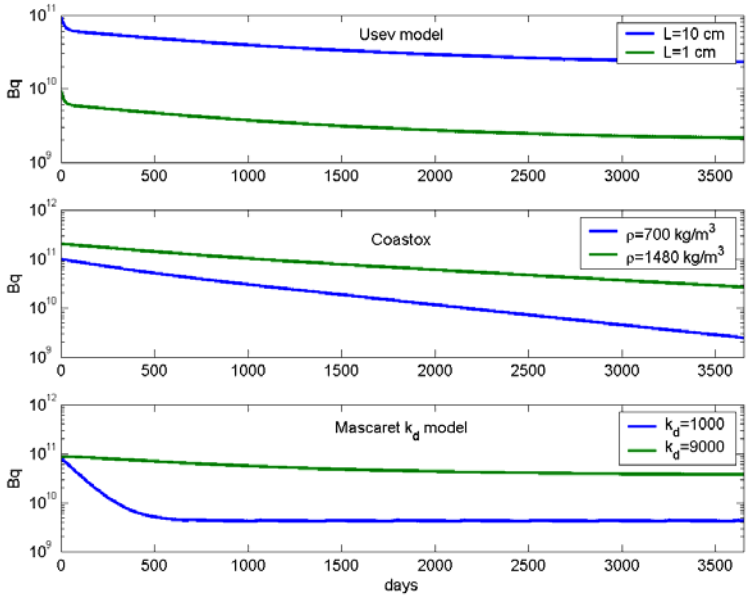

Fig. 6.4. Sensitivity of models to selected parameters. The time evolution of the total ^{226}Ra inventory in the bed sediment is shown. Up: sensitivity to the sediment mixing depth. Middle: sensitivity to the sediment bulk density. Down: sensitivity to the distribution coefficient.

CHAPTER 7. SIMULATION OF ^{90}SR WASH-OFF FROM THE CONTAMINATED PRIPYAT RIVER FLOODPLAIN USING COMMERCIALLY AVAILABLE SOFTWARE

Gennady Laptev, Ukrainian Institute for Hydrometeorology, UHMI, Ukraine

7.1. Introduction

Two-dimensional depth-averaged-type models, distributed through commercial networks as a part of software packages, are widely used at the present time for solving different tasks in computational hydrodynamics of the free-flow systems. Among them the most popular are MIKE-21 (Danish Hydraulics Institute), TELEMAC (Laboratory of Hydraulics, EDF, France), and SMS (Environmental Modeling Research Laboratory at Brigham Young University, USA). All above models have a well developed computer code implemented in software modeling environment with user friendly graphical interface for pre- and post-processing the input data and results of simulation, and can be run either on PC or work station under different operational platforms.

A common feature of this software is the focus on sophisticated hydrodynamical submodel, whereas water quality simulation is supported by the simple model for mainly conservative transport of contaminant. Processes of greater complexity, including those controlled by adsorption/desorption reaction, cannot be modeled by this type of a simple model.

In Ukrainian Hydrometeorological Research Institute over the long time he SMS (Surface Water modeling System) have been being used for simulation of ^{90}Sr radionuclide wash-off from contaminated areas on the Pripyat River floodplain after the Chernobyl accident [33, 34]. Because of the mentioned limitation, only ^{90}Sr transfer from land and transport in watercourse can be correctly simulated, other radionuclides, such as ^{137}Cs, to large extent show reactive feature and therefore transport and interaction between dissolved and particulate phases should be considered together.

Adaptation of the SMS for simulation of ^{90}Sr wash-off in UHMI is considered to be successful, mostly due to capability of the system to achieve the hydrodynamical solution with precise tracing the wetting/drying boundary conditions over the contaminated area and therefore accounting for temporal variation of the source term strength (flux) which is of crucial importance when the source of radioactivity is spatially distributed.

Here we present the results obtained using SMS software for simulation of ^{90}Sr wash-off during the historical flood of 1999, the highest recorded in Chernobyl zone since the 1986 accident [35].

7.2. Main characteristics of the models

The modelling engineering tool (software) SMS is based on user friendly graphical interface designed, among others features, for constructing the conceptual framework for numerical models from well known TABS package developed by Corps of Civil Engineers, USA. TABS comprises models RMA-2V (2-D water surface elevation and flow velocity calculation), SED2D (suspended and bed-loaded sediment calculation) and RMA-4V (water quality model) [36, 37].

RMA-2 is a finite element model designed for simulating one- and two-dimensional depth-averaged hydrodynamic systems. The dependent variables are velocity and water depth, and the equations solved are the depth-averaged Navier Stokes equations. Reynolds assumptions are incorporated as an eddy viscosity effect to represent turbulent energy losses:

$$\frac{\partial u}{\partial t}+u\frac{\partial u}{\partial x}+v\frac{\partial u}{\partial y}-\frac{1}{\rho}\left(\varepsilon_{xx}\frac{\partial^2 u}{\partial x^2}+\varepsilon_{xy}\frac{\partial^2 u}{\partial y^2}\right)+g\frac{\partial a}{\partial x}+g\frac{\partial h}{\partial x}+g\frac{n^2 u\left(u^2+v^2\right)^{1/2}}{h^{4/3}}=0,$$

$$\frac{\partial v}{\partial t}+u\frac{\partial v}{\partial x}+v\frac{\partial v}{\partial y}-\frac{1}{\rho}\left(\varepsilon_{yx}\frac{\partial^2 v}{\partial x^2}+\varepsilon_{yy}\frac{\partial^2 v}{\partial y^2}\right)+g\frac{\partial a}{\partial y}+g\frac{\partial h}{\partial y}+g\frac{n^2 v\left(u^2+v^2\right)^{1/2}}{h^{4/3}}=0, \qquad (7.1)$$

$$\frac{\partial h}{\partial t}+\frac{\partial}{\partial x}(hu)+\frac{\partial}{\partial y}(hv)=0.$$

where all terms accounting for the Coriolis effect and surface wind stress are omitted, and *u* and *v* are the components of velocity vector, ρ is the fluid density, ε is the tensor of turbulent viscosity, *g* is the gravity constant, *a is* the bottom elevation, *h* is the flow depth, and *n* is the Manning's roughness coefficient.

RMA-4v is a finite element model designed for simulating one- and two-dimensional transport in flow of conservative constituents with the possibility of accounting for decay It is based on hydrodynamical solutions of velocity vectors and water depth achieved with the RMA-2V, and calibrated turbulent diffusion for the specific constituent. The main governing equation of convective-diffusion transport in RMA-4V is:

$$\frac{\partial \mathrm{C}}{\partial \mathrm{t}}+\mathrm{u}\frac{\partial \mathrm{C}}{\partial \mathrm{x}}+\mathrm{v}\frac{\partial \mathrm{C}}{\partial \mathrm{y}}-\mathrm{D_x}\frac{\partial^2 \mathrm{C}}{\partial \mathrm{x}^2}\mathrm{D_y}\frac{\partial^2 \mathrm{C}}{\partial \mathrm{y}^2}-\sigma+\mathrm{kC}=0 \qquad (7.2)$$

where *C* is the concentration (Bq m^{-3}, in case of radionuclide) of pollutant in unit volume of fluid, D_x and D_y are the components of turbulent diffusion coefficient, σ is the source term (can be either defined for node or element of the mesh), *k* is the decay constant.

7.2.1. Model set-up procedures

All models share the same finite-element mesh, which can be designed using embedded software tools. The finite-element mesh is generally optimized to adequately meet the area orography and topography (bathymetry).

For the Pripyat River floodplain this was achieved by incorporating taken from GIS layer of watercourses and other water boundary lines, topography features e.g., dikes and floodplain outer margins. The finite-element mesh shown in Figure 7.1 contains 4300 nodes organized in 2000 triangular and quadrilateral elements. The proportion of individual elements was verified with requirements to maintain stability of the model run to finding right solution.

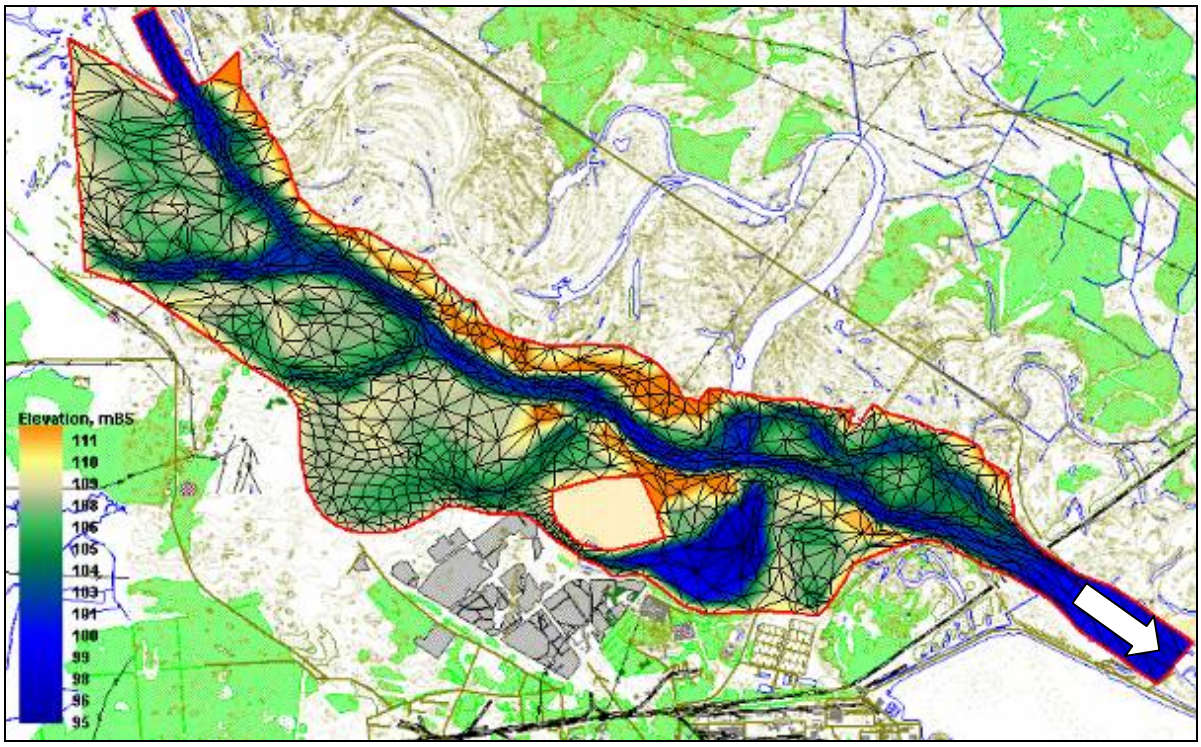

Fig. 7.1. Pripyat River floodplain GIS layer and Finite-element mesh.

Once the finite-element mesh was constructed and optimized, the specific parameters and boundary conditions were defined in order to run the hydrodynamical model RMA-2V. Specific parameters are necessary to run the model in dynamic mode and, alongside with verified proportions of the calculation mesh, maintaining calculational stability of the numerical scheme:

- time step – 1.5 hrs from 0 to 2184 (01/03/1999 – 31/05/1999);
- steady state depth convergence – 0.0025m;
- dynamic depth convergence – 0.015m;
- water temperature – 10^{o}C;
- nodal dry depth for wet/dry element check – 0.084m;
- nodal active depth for wet/dry element check – 0.183m;
- initial water surface elevation – 107.15m;
- Peclet number – 35;
- Estimated flow velocity – 1 m s^{-1}; and
- Eddy viscosity ratio (isotropic) – 10.

Boundary conditions were defined from the datasets supplied by EMRAS Flood-1999 Scenario – empirical measurements of water discharge (in m^3s^{-1}) for the input cross section, and water surface elevation (in mBS) for the output cross section (Figure 7.1).

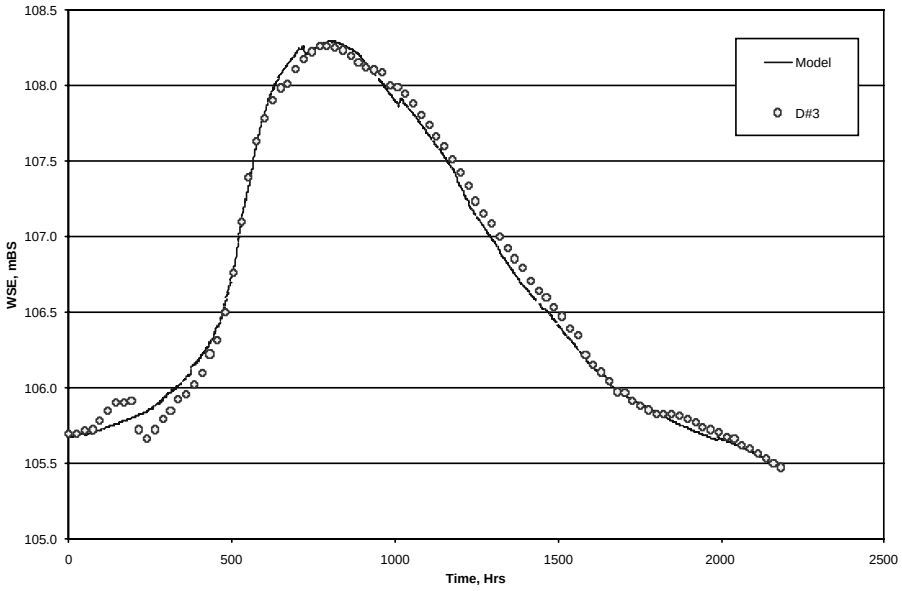

Fig. 7.2. Simulated versus empirical Water Surface Elevation at gauge station Dike#3.

7.3. Results, discussion and conclusions

Hydrodynamic numerical solution contain scalar datasets – water surface elevation (WSE), water depth (WD), flow velocity (FV) magnitude and vector datasets – *Vx*- and *Vy*-component of the velocity vector in each node for every time-step interval. The validity of the numerical solution was verified with best correspondence between calculated and measured water surface elevations (level) at the interior gauging station Dike#3 (Figure 7.2).

Alongside the calculated values for hydrodynamics, the model also traces continuity of the wet/dry elements boundary. This is very important for water quality modeling when the source is spatially distributed. Suggested boundary of area being submerged with water at the climax of the water surface level rise (800 hrs of simulation, 3/04/1999) is shown in Figure 7.3. The main pattern of the flow circulation (direction and magnitude) can also be seen.

A hydrodynamic solution is then used in RMA-4 model to simulate dispersion of the constituent in fluid flow in conservative mode (no decay/ no reactions). Each node or element (or group of them) from the finite-element mesh can be assigned as a source term for constituent transfer to the flowstream. Source flux is measured in pollutant unit per second from a unit area and must to be defined in a control file (operational card). In our case for ^{90}Sr simulation this parameter, in Bq s^{-1} m^{-2}, was defined for every element of the mesh with material type "floodplain". Because of individual character of geometrical properties of every element this requires calculation of the inventory of radionuclide inside each individual element. The standard tools of SMS do not allow this procedure to be executed in an automated mode. To overcome this problem a utility program was developed in UHMI which facilitated calculation of the constituent inventory within groups of elements in accordance with the specific logical constrains. Once inventory was calculated, further procedure was to convert itto source strength parameters in order to enter it into the model control file. The source strength ($Bqs^{-1}m^{-2}$) of any *i*-element, as a function of time, is defined as:

$$V_{source} = a \cdot S_{triangle} \cdot k_{ex} \cdot k_{migr} \cdot z_0 \cdot \exp(-\frac{\Delta t \cdot \ln(2)}{T}) \quad (7.3)$$

where $S_{triangle}$ is the i-element area; a is the mass-exchange constant (s^{-1}); k_{ex} is the fraction of readily exchangeable form of radionuclide in soil; k_{migr} is the burial (downward migration) fraction of radionuclide in soil; Z_o is the average contaminant inventory inside *i*-element (Bqm^{-2}); Δt is the time between referenced date and simulation time; T is the decay half-life of radionuclide.

For the Flood 1999 Scenario ^{90}Sr calculations the following values have been used: k_{migri} = 0.75, k_{Ex} = 0.75 , a_i =1.16×10^{-7} s^{-1}. Some modelers tend to use effective parameter which is product of all above terms (in this case effective parameter equal to 4.75×10^{-8} s^{-1}), but at least three among listed are subject for variation with time (and space) and, from our point of view, should be estimated independently.

Other boundary conditions were: (a) ^{90}Sr concentration at the inflow cross section (taken from the Scenario description); and (b) initial concentration for different water masses:

Material Type	**Feature**	**^{90}Sr Initial Conc., Bq L^{-1}**
River Channel	River Channel	0.25
Floodplain	Soil	0.00
	Sandy Dike	0.00
Branches	Side Branches	20.00
	Lake	25.00

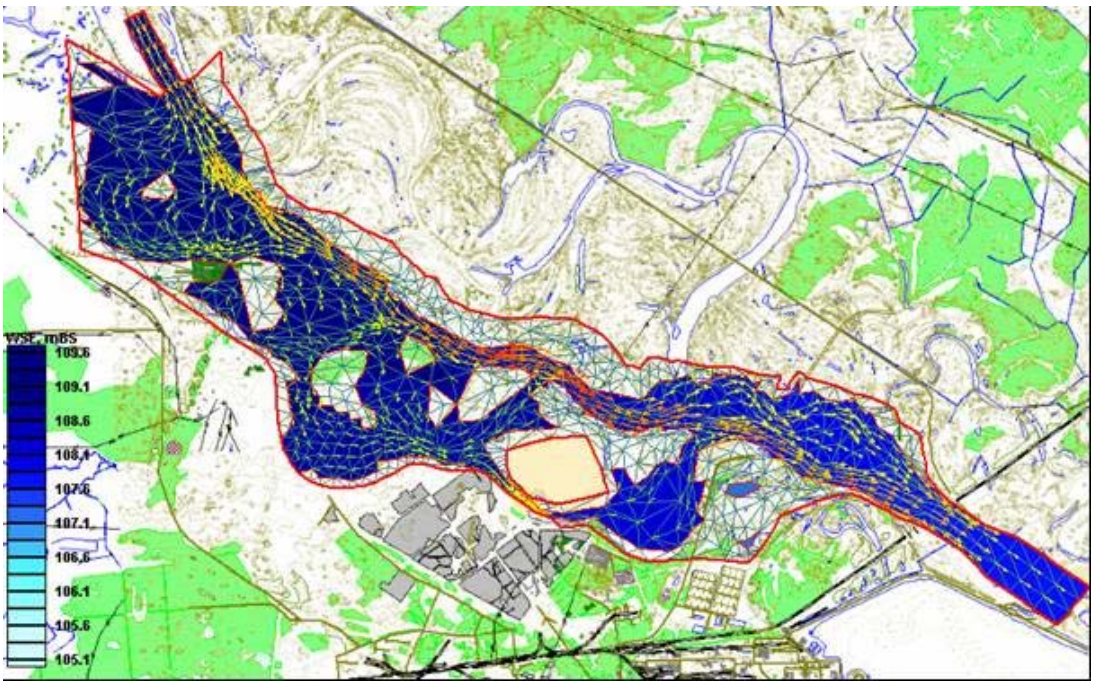

Fig. 7.3. Simulated flooded area and flow circulation at peak WSE ($Time_{sim}$=800 hrs).

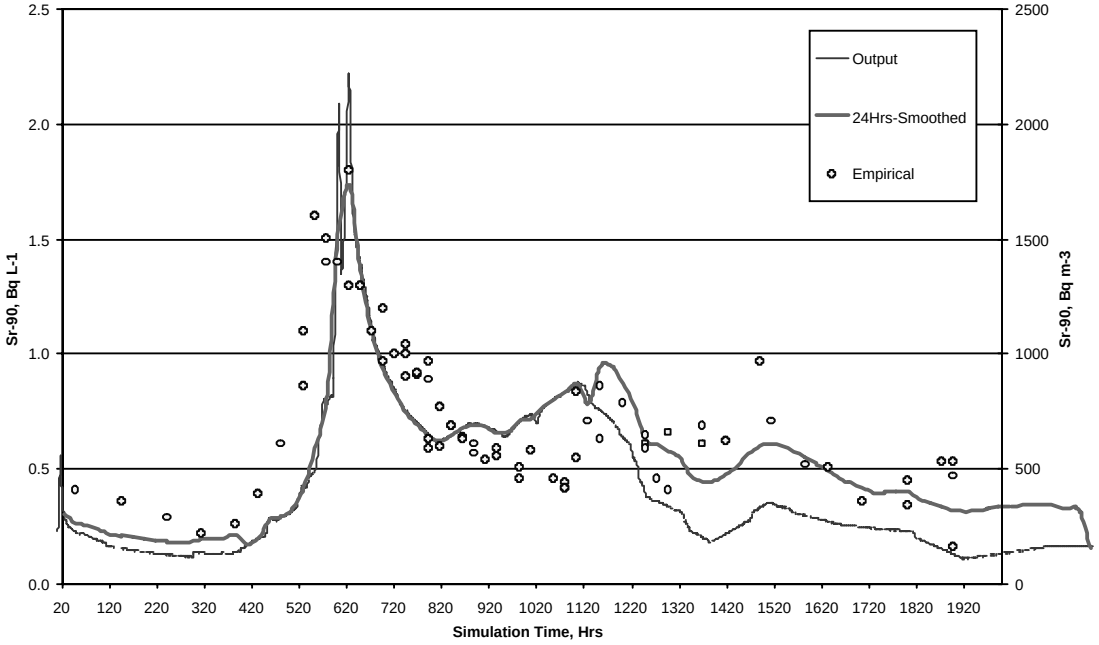

Fig. 7.4. Simulated ^{90}Sr concentration at the output cross section Yanovskyi Bridge vs empirical data for Chernobyl cross section during Flood 1999. (Red – floodplain only; Blue – smoothed floodplain and Dike-7)

^{90}Sr concentrations simulated by RMA-4 model at the outflow cross section are shown in Figure 7.4 with bold line, while the empirical data for Chernobyl cross section are presented as open circles.

We have processed primary modeling data through a 24 hour smoothing filter and this allowed the elimination of non-physical concentration jump effect and significantly narrowed the discrepancy between the magnitude of the simulated and empirical data (Figure 7.4).

Another feature noticed from the initial model run is that, after 1200 hrs of simulation, the predicted concentration declined much faster than the observed values. As was stated in the Scenario description empirical dataset correspond to the Chernobyl Town cross section located some 15 km downstream of the floodplain area we focus on. A number of controlled sources contribute to the secondary contamination of the Pripyat River between the Yanov Bridge (the floodplain outcome cross section) and Chernobyl, among them Sakhan River, Glinitsa Stream, streams fed by seepage water from the Chernobyl NPP Cooling Pond, and polder drainage water discharged via the floodgate hatch at Dike-7 etc.. Analysis of monitoring data inferred the most likely important source affecting concentration of ^{90}Sr in the river is discharge over Dike-7 and this was accounted for in order to provide the predicted concentration with appropriate correction. Water discharges and concentration of ^{90}Sr in polder drainage water (Table 7.1) were added as point source in the model boundary conditions. The results of the model run with this altered boundary conditions and processed with 24 hour smoothing filter are also shown in Figure 7.4.

Comparing the two curves one can notice that such a simple input data modification and model arrangement ultimately produced a much better correspondence between model predictions and the empirical dataset.

It is obvious that model satisfactorily described the dynamics of increased ^{90}Sr concentrations in the Pripyat River due to flooding of the contaminated floodplain. Another feature worth mentioning is that the discrepancy between simulated values and observations at low water conditions are definitely caused by not accounting for the presence of extra sources of secondary contamination of the river water in the conceptual model. By propagating the ^{90}Sr concentration wave further downstream 15 km from the area of concern with a correct assessment of the contribution from other sources of radioactive contamination of the Pripyat River, it is possible to significantly improve the quality of the model results.

Table 7.1. Water Discharge and ^{90}Sr Concentration at Dike-7, Flood 1999.

Date	**Water Discharge, m^3s^{-1}**	**^{90}Sr concentration, Bq L^{-1}**
26.02.99	1.47	25.0
12.03.99	2.40	23.0
18.03.99	Hatch closed	
31.03.00	–	46.0
06.04.99	–	21.0
16.04.99	Hatch open	38.0
19.04.99	7.14	60.0
25.04.99		53.0
05.05.99	5.05	63.0
12.05.99	3.06	50.0
20.05.99	3.27	55.0
26.05.99	3.25	52.0
02.06.99	2.06	43.0

CHAPTER 8. CONCLUSIONS

Several state-of-the-art models were assessed in the frame of the present project. A number of consolidated modelling procedures and approaches are widely accepted by modellers and can be framed in a general, harmonised perspective. Indeed, available state-of-the-art models for predicting the behaviour of radioactive substances through fresh water systems are, in general, based on a common overall structure.

The basic components of state-of-the-art models for predicting the behaviour of radionuclides in the abiotic compartments of aquatic systems are: (1) hydrological sub-models (and related transport-diffusion sub-models); (2) sub-models for predicting the radionuclide interaction of radionuclides with sediments and suspended matter; and (3) sub-models for predicting the migration of radionuclides from contaminated catchments. The uncertainty of models is related, to different degrees, to the features of these components.

Nevertheless, the models showed different levels of complexity from those based on simple box-type approach to those making use of the Navier-Stokes and transport-diffusion equations. Similarly, the complex processes controlling the interaction of radionuclides with sediments were approached at different levels of detail by the models. Although different approaches, simplifications and approximations are used by the models, there are some conceptual and structural similarities that are apparent in an overall perspective. An obvious example is the modelling of radionuclide interaction with suspended matter and bottom sediments by means of a compartmental approach.

Conceptually, such submodels assume that three main active compartments are involved in the processes of radionuclide interactions with sediments and suspended matter. Most state-of-the-art models evaluate the radionuclide migration to and from sediments (suspended matter) by including, in a pragmatic way, three active compartments and seven main "aggregated" radionuclide transformation/transfer processes from water to sediments or suspended matter and vice versa.

The active compartments are:

- Dissolved radionuclide in water (C_w);
- Particulate radionuclide – rapid exchange component (D_f);
- Particulate radionuclide – slow exchange component (D_s).

A fourth "passive compartment" (deep sediment) is used to represent the radionuclide subject to non-reversible removal processes from the active sediments. It is generally hypothesised that the exchanges of radionuclide between different compartments are first order processes.

In principle, the migration of radionuclide to bottom sediments can be predicted by accounting for the processes of contaminant sedimentation/resuspension/remobilisation and for the migration through the sediment due to the diffusion. This approach leads to a complex partial differential equation (the diffusion equation) that allows one to assess the radionuclide concentrations at different depths within the bottom sediment layer. To model the above processes in the sediment interstitial water, the sediment density, and the sediment water content are required. Moreover, it is necessary to model the complex mechanisms of interaction of radionuclide in dissolved form with sediment particles. All the above quantities, in principle, are functions of the depth from the sediment surface and some of them can depend on the seasonal conditions. As sufficient data and information are not ever available, it

is often preferable, in view of practical applications, to make use of models that are based on spatial and process aggregations as the state-of-the-art models here assessed.

As tritium does not interact with sediments, the only processes that controls the migration of this radionuclide are diffusion and transport by the current. Therefore, exercise c) was an important test to evaluate the reliability of the modules for the simulation of the hydrological and the diffusion transport processes in the assessed models.

The tritium exercise showed that the results from box-type models are consistent with those obtained by models based on one-dimension shallow water fluid dynamics and advection-dispersion equations to simulate water flow and radionuclide transport. In conclusion, this "blind test" exercise showed that the behaviour of radionuclides that scarcely react with suspended matter and sediments is generally predicted within acceptable levels of accuracy by models even if based on relatively simple hydrological sub-models and on a "box-type" approach for predicting the migration of contaminant through the watercourse.

In contrast, the results of sub-models for predicting the behaviour of radionuclides strongly interacting with sediment and soil particles are affected by significant levels of uncertainty. Exercise a) was crucial in this respect. This blind test showed that models properly predicted the remobilisation of strontium from the contaminated Pripyat River floodplain, whereas they significantly overestimated the remobilisation of radiocaesium. The modelling of the complex dynamics of extreme hydrological events, such as inundation of large flood plains, was also recognised as an important source of uncertainty for reactive radionuclides. Indeed, the concentration of re-mobilised radionuclides in water depends on the time of inundation and on the proportion of water flowing on more or less contaminated areas. In many circumstances these quantities cannot be predicted with sufficient accuracy and, therefore, have a major influence on overall model uncertainty.

Generally, the sub-models for assessing the interaction of radionuclides with sediments and the migration from the catchments are the most significant source of uncertainty. These conclusions were confirmed by the results of exercises d) and e) that also dealt with these complex problems. In particular, the application of the models to the scenario based on the contamination of Techa River by ^{90}Sr, ^{137}Cs and $^{239,240}Pu$ demonstrated the uncertainties inherent to the assessment of the sediment contamination by highly reactive substances.

In spite of the uncertainty of the model results, the exercises presented and discussed here clearly demonstrate that the models supplied much coherent information that achieved general agreement among modellers. For instance, in the exercise b) the models reliably predicted the different time behaviour of radiocaesium and radiostrontium in estuary waters. It is well known that these radionuclides show significantly different degrees of mobility in the aquatic environment. The potential for radiocaesium migration from the contaminated catchment of the estuary was significantly lower than radiostrontium. Therefore, the direct deposition of ^{137}Cs was a significant source of contamination of the estuary. Due to the relatively fast dynamics of the estuarine water, radiocaesium concentrations showed a marked decline with time. The direct initial atmospheric deposition of radiostrontium onto the estuary was negligible and the increase of radiostrontium concentration in water was due to the delayed transport to the estuary from the heavily contaminated area around Chernobyl.

It is interesting to note that models applied at a regional scale gave results showing these different behaviours in the same range as the results of the other more local models.

In this respect, the models can be considered as "behavioural", in other words, although affected by inherent uncertainty, the model results reproduce the characteristic features of the different time behaviour of radionuclides in the environmental system.

Similar conclusions concerning the ability of models to reproduce the behaviour of the environmental processes were drawn from the application of models to the Huelva estuary scenario to predict the self-cleaning process that has been observed in an estuary formerly affected by ^{226}Ra releases from a fertilizer complex. ^{226}Ra is a naturally occurring radioactive material (NORM) usually associated to the processing of phosphate rock containing significant amounts of natural radionuclides, mostly U, Th and Ra. The discharges of ^{226}Ra to the Odiel River were concluded in 1998 as a result of EU regulations. The models applied were very different in structure and resolution, from box models in which the complete estuary was divided into 3 compartments, to high-resolution two-dimensional models that explicitly solved tidal circulation through 1D-models based on shallow-water equations. Water-sediment interactions were also assessed in different ways by using distribution coefficients and/or kinetic models. In spite of these differences, all models predict that a self-cleaning process occurs and that the time scale of the process ranges between some 400 and 1400 days, i.e., a few years.

To take account of such "behavioural" aspects is an essential characteristic of models for applications aimed at supporting the management of the aftermath of nuclear accidents.

Furthermore, it is important to note that, in case of accidental introduction of radioactive substances onto the environment, the uncertainty associated with the empirical assessment of the source term can considerably affects the model results. This can be crucial especially in the "emergency" phase if sufficient data and information have not yet been acquired.

In conclusion, some recommendations for the proper application of models aimed at predicting the contamination levels of the fresh water environment can be derived from the present study. The sub-models for predicting the dispersion of contaminant in water are not the most significant source of the overall model uncertainty. Simple approaches to predict, for screening purposes, hydrological and transport-diffusion processes (like those suggested by the IAEA [38]) can be sufficiently reliable also in in view of the higher levels of uncertainty of the sub-models for predicting the interaction of radionuclides with sediments and the migration from contaminated catchments. It is obvious that, in case of radionuclides characterised by high levels of reactivity with sediments, the uncertainty of sub-models for the adsorption-desorption and the fixation process can considerably influence the results of radionuclide concentration in water. The use of site-specific values for radionuclide sedimentation, remobilisation and fixation to buried sediments can improve the performances of models for predicting the migration of radionuclides in the aquatic environment. When these values are not available, the uncertainty levels of model output can be high. Nevertheless, some important time dependent features of the environmental contamination can be satisfactory predicted by state-of-the-art models as demonstrated by the application to the estuary of the Dnieper River. It should be noted that such a scenario involved the assessment of radionuclide migration through the catchment of one of the largest rivers in Europe. The use of different models to assess the evolution over time of the environmental contamination can be useful to clarify the model outcomes that attain the largest consensus by modellers. Moreover, the range of results obtained by different models can supply information about the model uncertainty given the current level of understanding of environmental process.

REFERENCES

[1] SWEDISH RADIATION PROTECTION INSTITUTE, BIOMOVS 1990, On the validity of environmental transfer models, Proceedings of a Symposium, 8–10 October 1990, ISBN 91-630-0437-2, Stockholm (1990).

[2] INTERNATIONAL ATOMIC ENERGY AGENCY, Modelling of the transfer of radiocaesium from deposition to lake ecosystems, Report of the VAMP Equatic Working Group, IAEA-TECDOC-1143, IAEA, Vienna (2000).

[3] MONTE, L., PERIAÑEZ, R., KIVVA., S., LAPTEV, G., ANGELI, G., BARROS, H, ZHELEZNYAK, M., Assessment of state-of-the-art models for predicting the mobilisation of radionuclides following the flooding of heavily contaminated areas: the case of Pripyat River floodplain, Journal of Environmental Radioactivity 88, 267–288 (2006).

[4] MONTE, L., HÅKANSON, L., PERIANEZ, R., LAPTEV, G., ZHELEZNYAK, M., MADERICH, V., ANGELI, G., KOSHEBUTSKY, V., Experiences from a case study of multi-model application to assess the behaviour of pollutants in the Dnieper-Bug Estuary, Ecological Modelling 195, 247–263 (2006).

[5] GOUTAL, N., LUCK, M., BOYER, P., MONTE, L., SICLET, F., ANGELI, G., Assessment, validation and intercomparison of operational models for predicting tritium migration from routine discharges of nuclear power plants: the case of Loire River, Journal of Environmental Radioactivity 99, 367–382 (2008).

[6] ZHELEZNYAK, M., DEMCHENKO, R., KHURSIN, S., KUZMENKO, Y., TKALICH, P., VITIUK, N., Mathematical modeling of radionuclide dispersion in the Pripyat-Dnieper aquatic system after the Chernobyl accident, The Science of the Total Environment 112, 89–114 (1992).

[7] ZHELEZNYAK, M., Multiple scale analyses of radioactive contamination for rivers and reservoirs after the Chernobyl accident – Multiple Scale Analyses and Coupled Physical Systems, Proc. Saint-Venant Symposium, 28-29 August 1997, Presses de l'ecole nationale des ponts et chaussees, Paris, p.p. 45–52 (1997).

[8] MCHENRY, J.R., RITCHIE, J.C., Physical and chemical parameters affecting transport of ^{137}Cs in arid watershed, Water Resources Research, 13, 923–927 (1977).

[9] FRISSEL, M.J., PENNDERS, R., Models for the accumulation of ^{90}Sr, ^{137}Cs, ^{239,240}Pu and $^{241.1.1}$m in the upper layers of soil, In: Coughtrey, P.J. (ed.), Ecological Aspects of Radionuclide Release, Blackwell, Oxford, pp. 63–72 (1983).

[10] LIVENS, F.R., RIMMER, D.L., Physico-chemical controls on artificial radionuclides in soil, Soil Use and Management, 4, 63–69 (1988).

[11] MONTE, L., A generic model for assessing the effects of countermeasures to reduce the radionuclide contamination levels in abiotic components of fresh water systems and complex catchments, Environmental Modelling and Software 16, 669–690 (2001).

[12] NATIONAL INSTITUTE OF RADIATION PROTECTION, BIOMOVS 1991, Scenario A5, Dynamics within lake ecosystems, Technical Report 12, NRPI, Stockholm (1991).

[13] MONTE, L., BOYER, P., BRITTAIN, J.E., HÅKANSON, L., LEPICARD, S., SMITH, J.T., Review and assessment of models for predicting the migration of radionuclides through rivers, Journal of Environmental Radioactivity 79, 273–296 (2005).

[14] KANIVETS, V.V., VOITSEKHOVICH, O.V., SIMOV, Radioactive contamination of the Black and Azov seas, In: Voitsekhovich, O.V. (ed.) Radioecology of water objects of the Chernobyl NPP accident impact area., Chernobylinterinform, Kiev, 127–151, in Russian (1997).

[15] KATRICH, I.YU., NIKITIN, A.I., MEDINETS, V.I., LEPESHKIN, V.I., KABANOV, A.I., SEMKO, N.N., BAZHANOV, V.N., Dynamics of the radioactive contamination caused by CNPP accident on observed data 1986–1990, In: Borzilov V.A., Kryshev I.I., Ecological and hydrophysical consequences of the nuclear accidents, Hydrometerological Publ., Moscow, p. 57–61, in Russian (1992).

[16] DE CORT, M., DUBOIS, G., FRIDMAN, S.D., GERMENCHUK, M.G., et al., Atlas of Caesium deposition on Europe after the Chernobyl accident, EUR 16733 Luxemburg, Office for Official Publication of the European Communities, ISBN 92-828-3140-X (1998).

[17] MONTE, L., BRITTAIN, J., E., HÅKANSON, L., HELING, R., SMITH, J., T., ZHELEZNYAK, M., Review and assessment of models used to predict the fate of radionuclides in lakes, Journal of Environmental Radioactivity 69, 177–205 (2003).

[18] PERIAÑEZ, R., ABRIL, J.M., GARCÍA-LEÓN, M., Modelling the dispersion of non conservative radionuclides in tidal waters, Part 1: conceptual and mathematical model, Journal of Environmental Radioactivity 31, 127–141 (1996).

[19] EISMA, D., Suspended Matter in the Aquatic Environment, Springer Verlag, Berlin (1993).

[20] PERIAÑEZ, R., Modelling the suspended matter dynamics in a marine environment using a three dimensional s coordinate models: application to the eastern Irish Sea, Applied Mathematical Modelling 26, 583–601 (2002).

[21] PERIAÑEZ, R., Testing the behaviour of different kinetic models for up-take/release of radionuclides between water and sediments when implemented in a marine dispersion model, Journal of Environmental Radioactivity 71, 243–259 (2004).

[22] DYER, K.R., Estuarine oceanography, In: Parker, S.P. (ed.), McGraw-Hill Encyclopedia of Environmental Science, McGraw-Hill Book Company, New York (1980).

[23] GODUNOV, S.K., A Finite Difference Method for the computation of Discontinuous Solutions of Fluid Dynamics, Mat. Sb. 47, pp. 357–393 (1959).

[24] NORWEGIAN RADIATION PROTECTION AUTHORITY, Sources Contributing to Radioactive Contamination of the Techa River and Areas Surrounding the “Mayak” Production Association, Urals, Russia, Published by the Joint Norwegian-Russian Expert Group for Investigation of Radioactive Contamination in the Northern Areas, NRPA, Osteras, pp. 1-134 (1997).

[25] ABSI, A., VILLA, M., MORENO, H.P., MANJÓN, G., PERIÁÑEZ, R., Self-cleaning in an estuarine area formerly affected by ^{226}Ra anthropogenic enhancements, Science of the Total Environment 329, 183–195 (2004).

[26] BORREGO, J., PENDÓN, J.G., Algunos ejemplos de la influencia de los procesos antrópicos en el medio sedimentario: la ría de Huelva, Henares Revista de Geología 2, 299–305 (1988).

[27] LUCK, M., GOUTAL, N., Système Mascaret: note de principe de l’outil (transport de traceurs) et des modules de qualité d’eau O2, biomass, eutro, micropol et thermic. Rapport EDF-LNHE-HP-75/03/047/A (2003).

[28] CIFFROY, P., GARNIER, J.M., PHAM, M.K., Kinetics of the adsorption and desorption of radionuclides of Co, Mn, Cs, Fe, Ag and Cd in freswater systems: experimental and modelling approaches, Journal of Environmental Radioactivity 55, 71–91 (2001).

[29] MARGVELASHVILI, N., MADERICH, V., YUSCHENKO, S., ZHELEZNYAK, M., 3D modelling of the mud and radionuclide transport in Chernobyl cooling pond and Dnieper-Boog Estuary, Fine Sediments Dynamics in the Marine Environment Proceedings of INTERCOH-2000, J.C. Winterwerp and C. Kranenburg (eds.), Elsevier, p. 595–610 (2002).

[30] PERIÁÑEZ R., Modelling the dispersion of radionuclides in the marine environment, Springer, Heidelberg (2005).

[31] APPELGREN, A., BERGSTRÖM, U., BRITTAIN, J., GALLEGO DIAZ, E., HÅKANSON, L., HELING, R., MONTE, L., An outline of a model-based expert system to identify optimal remedial strategies for restoring contaminated aquatic ecosystems: the project MOIRA, ENEA, RT/AMB/96/17, Rome (1996).

[32] INTERNATIONAL ATOMIC ENERGY AGENCY, Sediment distribution coefficients and concentration factors for biota in the marine environment Technical Reports Series No. 422, IAEA, Vienna (2004).

[33] LUTKOVSKYI, V.V., MINGALEVA, E.S., Application of modern modelling system with distributed parameters BOSS SMS for simulation of wash-off and transport of radionuclides from Prypyat River floodplain, Proceedings UHMI 247 , 171–183, in Russian (1999).

[34] BILYI, I.Y., VOITSEKHOVICH, O.V., ONISHI, Y., GRAVES, R., Modelling of Sr-90 wash-off from the Prypyat River floodplains by four-year flood, In: Proceedings of Symposium on Isotopes in Water Resources Management, IAEA, Vienna, 20–24 March 1995, v.1, pp. 117–126 (1996).

[35] VOITSEKHOVICH, O.V., Analysis: 1999 flood on Prypyat River and remediation activity in Chernobyl exclusion zone – consequences for the Dnieper system, Bulletin of Ecological State of the Chernobyl Exclusion Zone, 14 October 1999, pp.13–18, in Ukrainian (1999).

[36] DONNELL, B.P., LETTER, J.V., MCANALLY, W.H., et al., "Users Guide for RMA2 Version 4.5" http://chl.erdc.usace.army.mil/chl.aspx?p=s&a=SOFTWARE; 14 (2005).

[37] LETTER, J.V., DONNELL, B.P., et al., Users Guide for RMA4 Version 4.5, http://chl.erdc.usace.army.mil/chl.aspx?p=s&a=ARTICLES;481 (2003).

[38] INTERNATIONAL ATOMIC ENERGY AGENCY, Generic Models for Use in Assessing the Impact of Discharges of Radioactive Substances to the Environment, Safety Reports Series No. 19, IAEA, Vienna (2001).

APPENDIX I. SCENARIO DESCRIPTIONS

I.1. Wash-off of Chernobyl ^{90}Sr and ^{137}Cs from the floodplain into the Pripyat River

I.1.1. Description of the floodplain scenario

In the present scenario, the Pripyat River floodplain is understood as a small embanked part of the floodplain, 12 km long and 4 km wide, adjacent to the Chernobyl NPP in the northwest (see Figure I.1). The Pripyat River enters the considered area near the exclusion zone boundary (Input cross section) and flows out near the Yanov Bridge (Output cross section). The floodplain was subjected to the heaviest impact of radioactive contamination after the Chernobyl accident in 1986 and became an object for regular radiological monitoring, since it plays a key role in formation of contamination of the Pripyat River [I.1].

I.1.1.1. Description of events

1991 Ice jam

In January 1991, an ice jam formed in the Pripyat River channel between Yanov Bridge and the town of Chernobyl. The water level in the Pripyat River upstream of the jam increased abruptly. As a result, a significant part of the Pripyat floodplain near the NPP became flooded for the first time since the accident. This caused washout of radionuclides to the river with the flood water. Even though only 30% of the whole area was flooded, it was enough for the ^{90}Sr activity concentration in the Pripyat River near the town of Chernobyl to increase up to the critical level.

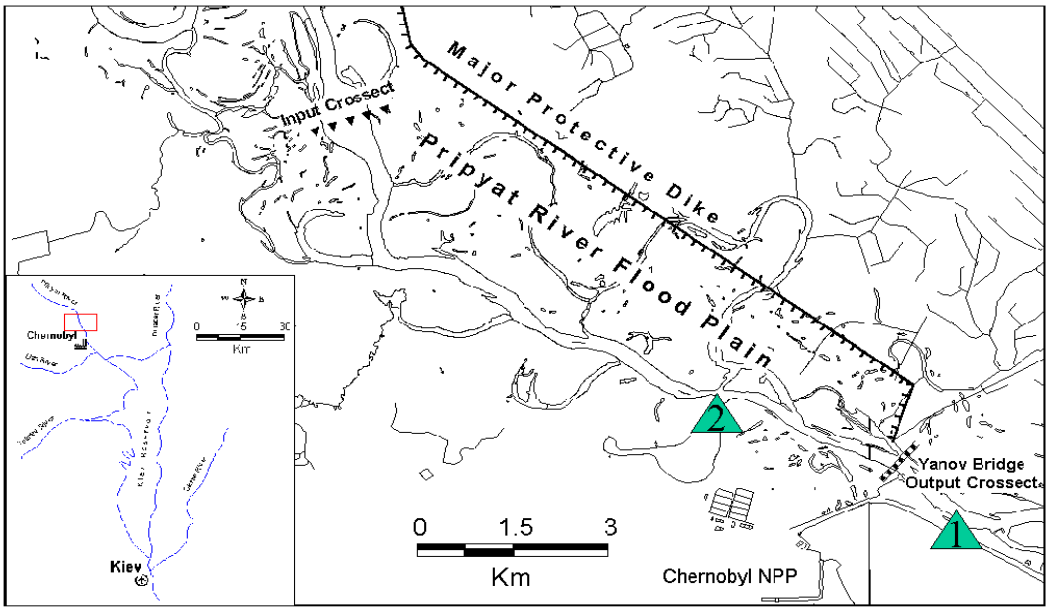

1 - Gauge Station BNS; 2 - Gauge Station D3

Fig. I.1. Scheme of the Pripyat River floodplain in the vicinity of Chernobyl NPP (before 1992).

After unsuccessful aircraft bombing of the jammed ice cover, it was decided to clear this part of the river channel using an ice-breaker. As a result, the water level rapidly decreased to normal values.

1994 Ice jam during spring flood

The 1994 event was similar to the ice jam of 1991. The principal difference was that the ice jam and partial flooding of the floodplain in 1994 occurred in the final phase of the winter low water and the initial phase of spring flood, rather than in the period of deep winter low water with low water discharge in the river channel. As a result, the wash-off of radionuclides from the floodplain surface after destruction of the ice jam was coincident with the beginning of the rise in water level of the river. Due to this fact, the influx of radionuclides from the floodplain was more protracted in time, and dilution of contaminated runoff entering the river by cleaner waters of the Pripyat River was more effective than that in 1991.

Moreover, a protective sand dike on the left bank of the Pripyat River floodplain was built in 1992, and the left bank part of the floodplain was not flooded thereafter. Therefore, the source of contamination in 1994 was the right bank part of the floodplain, rather than its whole area.

1999 Spring flooding

It was after the completion of the left bank dam on the Pripyat River that an extremely high spring flood occurred in 1999. The maximum water discharges in the river were as high as 3000 $m^3 s^{-1}$ and were the highest reported in the river since the historically high flood of 1979 (4500 $m^3 s^{-1}$). By 1999, the construction of the dam on the right bank was already under way; this dam was meant to cut off the most contaminated floodplain areas on the right bank. The construction, however, was not complete (see Section I.1.1.2 below), and part of the right bank floodplain was flooded for 2 weeks, primarily due to dam overflow. Therefore, the dam did not prevent wash-off from the floodplain, but only lengthened the formation of floodplain flows and reduced a possibly higher peak in the river contamination, which could have occurred with more rapid flow of water from the floodplain.

It is proposed that 2 sources of radionuclide contamination of the river be considered for the 1999 flood:

Areas on the right bank floodplain with elevation below 107.5 m which were flooded as a result of the dam overflow. The contaminated water from these areas entered the river after the decrease in water level by filtration through the dam and by washed out channels.

The Yanov Bay, which was filled with water during the water level increase through the stone filtration dam built in 1987. The runoff from the bay started on 4 April and continued to the end of May. Over this time, between 0.8×10^6 and 1.0×10^6 m^3 of water containing about 37 Bq L^{-1} ^{90}Sr and about 2–3 Bq L^{-1} of ^{137}Cs was discharged. The water discharges were roughly the following: 50–75 L s^{-1} on 4–6 April, 100 L s^{-1} on 10–12 April, 350 L s^{-1} on 15 April, 600–700 L s^{-1} on 16–18 April, 300 L s^{-1} on 22 April and 100 L s^{-1} on 30 May.

I.1.1.2. Description of countermeasures

After the event of 1991, construction of water protective facilities was initiated. These facilities were intended to change the conditions of water flow in the river floodplain and radionuclide wash-off from the surface. These changes should be kept in mind when generating input files accounting for the contamination source in the scenarios for 1994 and 1999.

(a)

(b)

(c)

Fig. I.2. Modification of the Pripyat River Floodplain in Chernobyl Exclusion Zone (SPOT Satelite Images). (a) 1986, Original shape; (b) 1994, embankment of the left bank sandy dike; (c) 1999, embankment of the right bank sandy dike.

By the end of 1992, a left bank dam was built, as is shown on the satellite images shown in Figure I.2. The construction involved bringing sand from the river bed and the drainage channel on the inside of the dam. The dam width at the foundation was up to 200 m, and the elevation was 111 m BS. This elevation excludes overflow of water even in case of realization of the scenario providing for water discharge up to 6000 m^3 s^{-1}, the frequency of which is once in 100 years. The filtration flows from the dammed area are also very small, as the purposely built drainage system and regulation of water regime in this area make it possible to keep it dry during the entire year.

By the beginning of the 1999 flood, the right bank dam was partially built. It was anticipated that the highest level of the dam would be not less than 109 m. However, by the spring of 1999, its height in many parts was not more than 107–107.5 m. When the water level increased above this height, dam overflow occurred, and the right bank was flooded (see Figure I.3). The dam was built by bulldozer and using sacks, and, therefore, first, its filtration ability was rather high, and second, it was not very strong. Because of this, after a sharp decrease in the river water level during the flood of 1999, the contaminated water was flowing vigorously through the dam via washed out parts and filtration prisms.

I.1.1.3. Description of input data (http://www-ns.iaea.org/projects/emras/emras-aquatic-wg.htm)

The topography of the floodplain was given to the modelers in its original state (before implementation of countermeasures) in three commonly used formats:

(1) Plain ASCII XYZ file "FP_GK5.xyz" (developed at UHMI). The file has the following structure:

1st Column	2nd Column	3rd Column
X coordinate (m)	Y coordinate (m)	Altitude (m)

Statistics for the floodplain topography calculated using Surfer Software procedures and the FP_GK5.xyz file as an input are reported in the web-site.

(2) TABS(RMA2) compatible file "FP_GK5.geo". This file contains a triangulated mesh of the floodplain area developed at UHMI.

(3) MapInfo format set of files (extracted from a digital map of the Chernobyl Exclusion Zone):

Dotted isolines of the altitude with 1 m increment:

FP_Topo10.tab
FP_Topo10.id
FP_Topo10.dat
FP_Topo10.map

Basic shape of the Pripyat River cross sections in ASCI and MAPINFO formats:

FP_Channel10.tab
FP_Channel10.id
FP_Channel10.dat
FP_Channel10.map

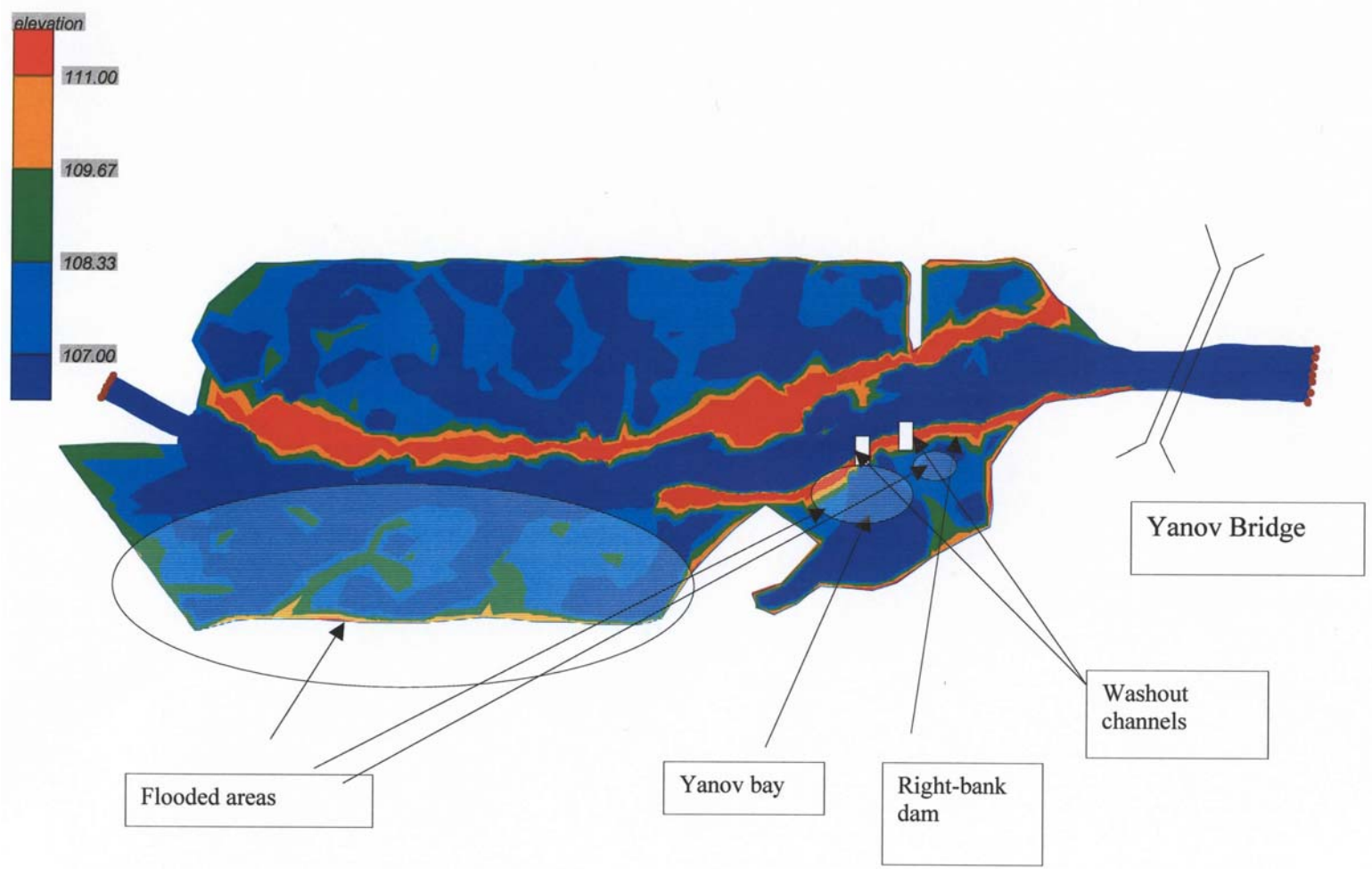

Fig. I.3. Scheme of the Pripyat River floodplain area in 1999.

Table I.1. Distribution of radionuclide deposition by elevation in the floodplain area.

Level		Area		Volume		^{90}Sr		^{137}Cs	
m		km^2	%	10^3 km^3	%	Ci	%	Ci	%
Channel[a]	0[b]	4.3	12.5	9.4	4.9	–	0.0	–	0.0
0	1	6.3	18.3	16.0	8.3	519	8.6	441	7.2
0	2	9.2	26.7	25.3	13.1	1293	21.4	1089	17.8
0	2.5	11.4	33.1	31.4	16.2	1792	29.7	1556	25.5
0	3	14.3	41.5	38.8	20.0	2511	41.6	2282	37.4
0	3.5	18.7	54.3	48.1	24.8	3580	59.3	3358	55.0
0	4	24.5	71.1	59.9	30.9	4793	79.4	4682	76.7
0	6	32.6	94.7	122.9	63.4	5736	95.0	5854	95.9
0	8	34.3	99.7	193.8	100.0	6035	99.9	6103	100.0
0	10	34.5	100.0	–	0.0	6039	100.0	6106	100.0

[a] Including the river's main channel and other internal surface depressions below "0" level.
[b] "0" level corresponds to 104 m BS (Baltic System), the normal level of the river for the Output cross section (Yanov Bridge) under winter hydrological conditions (flow < 400 m^3 s^{-1}).

All the coordinates in the presented maps are given in Gauss-Kruger (the 5th zone). The right bank of the input cross section in this coordinate system is 5 708 700 m and 5 707 400 m; the right bank of the output cross section is 5 717 600 m and 5 702 300 m.

The user must adjust the topographic map to the specific shape after different countermeasures were applied using standard software and procedures. The information required for doing this is given in the section "Description of countermeasures" and in Figures I.1–I.13.

The deposition density of ^{137}Cs and ^{90}Sr (Ci km^{-2}) in the area is given in the files "FP_CS137.DAT" and "FP_SR90.DAT", respectively. The structure of these files is the same as for "FP_GK5.xyz", but the estimated density of deposition of ^{137}Cs or ^{90}Sr for each grid node is presented instead of elevation. Distributions of radionuclides on the surface at different elevations are included in Table I.1.

Hydrological and meteorological data are given in Tables I.2–I.4 for the events of 1991, 1994 and 1999, respectively. The tables contain data on water levels for the gauge stations D3 and BNS, located upstream and downstream of the Output cross section, respectively. The water surface levels upstream of the point D3 can be estimated in several ways.

The levels can be estimated by the methods of channel hydraulics using input data available in files "FP_Channel10.tab", "FP_Channel10.id", "FP_Channel10.dat" and FP_Channel10.map".

For approximate estimates, data on river surface slopes can be used; these are calculated using data on river levels at points D3 and BNS (Tables I.2–I.4).

It is possible to use results of hydraulic calculations performed earlier by UHMI. It was shown that for the period of low water in the considered river section upstream of the measuring section D3, the increment in the water surface level is 12–15 cm for each running km; in the period of downstream levels during ice jams and at the peak of flooding, the increment is 3–5 cm per running km.

Table I.2. Hydrological and meteorological data and activity concentrations of ^{90}Sr and ^{137}Cs in the Input cross section during the ice jam event in January–February 1991.

Date	Water level[a] m BS		Discharge[b] $m^3 s^{-1}$	Suspended sediment[b] $g L^{-1}$	T[c] °C	Precipitation[c] mm	^{137}Cs $Bq m^{-3}$		^{90}Sr $Bq m^{-3}$
	D3	BNS					Particulate	Dissolved	Dissolved
1 Jan 91		105.12	494	0.0097	-0.6		88.9	181.5	666.7
2 Jan 91		105.15	493	0.0095	0.0	1.5	88.9	177.8	666.7
3 Jan 91		105.15	493	0.0093	-1.0	5.4	88.9	174.1	703.7
4 Jan 91		105.15	492	0.0092	1.2		88.9	170.4	703.7
5 Jan 91		105.15	491	0.009	3.3	3.6	88.9	166.7	740.7
6 Jan 91		105.23	490	0.0088	0.6	0.0	85.2	159.3	740.7
7 Jan 91		105.30	489	0.0107	1.9		85.2	155.6	711.1
8 Jan 91		105.30	488	0.0125	2.4	0.4	85.2	151.9	681.5
9 Jan 91		105.36	487	0.0144	1.8		85.2	148.1	651.9
10 Jan 91		105.44	487	0.0163	3.1		85.2	148.1	655.6
11 Jan 91		105.60	486	0.0182	8.1		85.2	148.1	655.6
12 Jan 91		105.75	486	0.0201	5.4	0.6	85.2	151.9	659.3
13 Jan 91		105.65	486	0.0219	2.2		85.2	151.9	659.3
14 Jan 91	105.96	105.68	486	0.0238	-3.1	0.2	85.2	151.9	663.0
15 Jan 91	105.96	105.70	485	0.0257	-3.4		85.2	151.9	663.0
16 Jan 91	105.96	105.66	485	0.0276	-6.5		85.2	151.9	666.7
17 Jan 91	105.97	105.66	485	0.0295	-2.6		85.2	151.9	666.7
18 Jan 91	105.97	105.60	484	0.0313	-3.9		85.2	155.6	670.4
19 Jan 91	105.97	105.70	484	0.0332	-4.5		85.2	155.6	670.4
20 Jan 91	106.10	105.78	484	0.0351	-5.1		85.2	155.6	674.1
21 Jan 91	106.31	106.21	484	0.0370	-6.4		81.5	155.6	674.1
22 Jan 91	106.66	106.50	483	0.0389	-4.4	0.5	81.5	155.6	677.8
23 Jan 91	106.95	106.49	483	0.0407	-0.3		81.5	159.3	677.8
24 Jan 91	106.98	106.42	483	0.0426	0.5	0.3	81.5	159.3	703.7
25 Jan 91	107.00	106.49	482	0.0445	-1.3		81.5	159.3	703.7
26 Jan 91	106.98	106.46	482	0.0464	1.9	0.4	81.5	159.3	777.8
27 Jan 91	106.95	106.42	482	0.0483	-6.4		81.5	159.3	851.9
28 Jan 91	106.80	106.35	481	0.0502	-10.7		81.5	159.3	925.9
29 Jan 91	106.61	106.15	481	0.0520	-3.1	1.8	81.5	163.0	1000.0
30 Jan 91	106.48	106.00	481	0.0539	-13.2	1.5	81.5	163.0	740.7
31 Jan 91	106.37	105.85	481	0.0558	-19.6		81.5	163.0	525.9

[a] Water levels were measured at the gauge stations D3 and BNS, located upstream and downstream, respectively, of the Output cross section (Figure I.1).
[b] Water discharges and suspended sediment load are given for the Output cross section.
[c] Temperature and precipitation were registered at the Chernobyl meteostation.

Table I.2. (Continued)

Date	Water level[a] m BS		Discharge[b] $m^3 s^{-1}$	Suspended sediment[b] $g L^{-1}$	T[c] °C	Precipitation[c] mm	^{137}Cs Bq m^{-3}		^{90}Sr Bq m^{-3}
	D3	BNS					Particulate	Dissolved	Dissolved
1 Feb 91	106.21	105.75	480	0.0577	-17.1		66.7	137.0	518.5
2 Feb 91	106.19	105.68	480	0.0596	-10.8	0.4	55.6	114.8	555.6
3 Feb 91	106.17	105.65	480	0.0614	-11.2	0.5	40.7	88.9	592.6
4 Feb 91	106.15	105.60	465	0.0633	-14.1	1.1	70.4	148.1	777.8
5 Feb 91	106.13	105.60	449	0.0652	-15.7		59.3	122.2	518.5
6 Feb 91	106.09	105.54	434	0.0671	-13.9		51.9	100.0	481.5
7 Feb 91	106.06	105.50	418	0.0690	-11.7	0.4	40.7	74.1	407.4
8 Feb 91	106.05	105.50	403	0.0708	-8.5	0.0	70.4	129.6	518.5
9 Feb 91	106.00	105.45	388	0.0727	-9.8		96.3	185.2	1037.0
10 Feb 91	105.98	105.40	372	0.0746	-8.4	3.5	77.8	200.0	555.6
11 Feb 91	105.96	105.40	357	0.0765	-5.0	2.7	63.0	211.1	277.8
12 Feb 91	105.94	105.30	356	0.0784	-2.4		44.4	225.9	518.5
13 Feb 91	105.91	105.25	355	0.0802	-1.0	2.7	55.6	233.3	607.4
14 Feb 91	105.92	105.25	354	0.0821	-3.8	0.8	63.0	244.4	692.6
15 Feb 91	105.93	105.25	353	0.0840	-6.6		88.9	251.9	666.7
16 Feb 91	105.86	105.25	352	0.0859	-5.9	10.2	111.1	259.3	629.6
17 Feb 91	105.84	105.25	351	0.0878	-6.5	8.3	74.1	100.0	425.9
18 Feb 91	105.81	105.20	350	0.0896	-3.2	1.9	77.8	100.0	422.2
19 Feb 91	105.80	105.20	349	0.0915	-7.3	0.0	74.1	174.1	418.5
20 Feb 91	105.65	105.15	347	0.0934	-5.3		70.4	181.5	414.8
21 Feb 91	105.50	105.12	346	0.0953	-5.3		63.0	188.9	414.8
22 Feb 91	105.46	105.10	345	0.0972	-1.5		59.3	200.0	411.1
23 Feb 91	105.44	105.05	344	0.0991	-3.8		55.6	207.4	407.4
24 Feb 91	105.41	105.03	343	0.1009	-3.8		48.1	214.8	425.9
25 Feb 91	105.38	105.03	342	0.1028	2.5		44.4	222.2	444.4
26 Feb 91	105.39	105.02	341	0.1047	2.1	1.2	40.7	207.4	463.0
28 Feb 91	105.40	105.02	346	0.1085	-0.3	3.1	40.7	207.4	407.4
27 Feb 91	105.39	105.02	340	0.1066	0.6	0.9	37.0	192.6	481.5

[a] Water levels were measured at the gauge stations D3 and BNS, located upstream and downstream, respectively, of the Output cross section (Figure I.1).
[b] Water discharges and suspended sediment load are given for the Output cross section.
[c] Temperature and precipitation were registered at the Chernobyl meteostation.

Table I.3. Hydrological and meteorological data and activity concentrations of ^{90}Sr and ^{137}Cs in the Input cross section in January–April 1994.

Date	Water level[a] m BS		Discharge[b] $m^3 s^{-1}$	Suspended sediment[b] $g L^{-1}$	T[c] deg. C	Precipitation[c] mm	^{137}Cs $Bq m^{-3}$		^{90}Sr $Bq m^{-3}$
	D3	BNS					Particulate	Dissolved	Dissolved
1 Jan 94	104.50	104.05	370	0.0609	0.6		22.2	144.4	151.9
2 Jan 94	104.51	104.05	380	0.0619	1.1		22.2	148.1	151.9
3 Jan 94	104.53	104.08	391	0.0629	-0.4	2.4	18.5	151.9	151.9
4 Jan 94	104.56	104.10	401	0.0638	-0.3	0.6	18.5	155.6	151.9
5 Jan 94	104.57	104.10	411	0.0648	0.6	0.4	18.5	159.3	148.1
6 Jan 94	104.58	104.16	422	0.0658	2.3	4.6	18.5	163.0	148.1
7 Jan 94	104.59	104.15	432	0.0668	1.7		14.8	166.7	148.1
8 Jan 94	104.60	104.14	440	0.0678	-0.3		14.8	170.4	148.1
9 Jan 94	104.60	104.14	457	0.0687	-0.5		14.8	174.1	155.6
10 Jan 94	104.61	104.17	475	0.0697	-0.3		14.8	177.8	163.0
11 Jan 94	104.62	104.12	488	0.0707	0.6		14.8	181.5	170.4
12 Jan 94	104.57	104.16	500	0.0717	-0.2		14.8	185.2	177.8
13 Jan 94	104.57	104.16	513	0.0726	0.6	2.5	14.8	188.9	188.9
14 Jan 94	104.53	104.12	526	0.0736	4.0	4.7	14.8	192.6	196.3
15 Jan 94	104.65	104.20	538	0.0746	2.7	4.2	14.8	196.3	203.7
16 Jan 94	104.74	104.25	551	0.0756	0.9		14.8	200.0	211.1
17 Jan 94	105.13	104.68	563	0.0766	0.2	0.3	14.8	203.7	218.5
18 Jan 94	105.16	104.70	576	0.0775	-2.1	5.4	14.8	207.4	225.9
19 Jan 94	105.08	104.71	579	0.0785	-3.1	2.8	18.5	200.0	222.2
20 Jan 94	105.20	104.75	582	0.0795	-5.7		22.2	192.6	218.5
21 Jan 94	105.24	104.85	585	0.0805	-4.2		25.9	188.9	214.8
22 Jan 94	105.26	105.00	587	0.0814	0.0		29.6	181.5	211.1
23 Jan 94	105.29	105.07	590	0.0824	1.7		33.3	174.1	207.4
24 Jan 94	105.43	105.15	593	0.0834	1.1	3.8	37.0	166.7	203.7
25 Jan 94	105.39	105.13	598	0.0844	0.4	0.6	40.7	163.0	200.0
26 Jan 94	105.35	105.08	603	0.0854	-1.3	0.8	40.7	155.6	196.3
27 Jan 94	105.38	105.08	607	0.0863	1.3	1.5	44.4	148.1	192.6
28 Jan 94	105.49	105.12	612	0.0873	2.8	3.4	48.1	140.7	188.9
29 Jan 94	105.51	105.12	617	0.0883	1.1		51.9	133.3	185.2
30 Jan 94	105.50	105.09	615	0.0893	-4.2	1.2	55.6	129.6	181.5
31 Jan 94	105.53	105.12	614	0.0902	-2.0	3.9	59.3	122.2	177.8
1 Feb 94	105.59	105.29	612	0.0912	-0.2	0.0			
2 Feb 94	105.74	105.38	603	0.0922	-0.7		51.9	114.8	174.1
3 Feb 94	105.69	105.40	593	0.0932	0.2	3.1	48.1	107.4	174.1
4 Feb 94	105.70	105.39	584	0.0942	0.0	0.0	44.4	100.0	177.8

[a] Water levels were measured at the gauge stations D3 and BNS, located upstream and downstream, respectively, of the Output cross section (Figure I.1).
[b] Water discharges and suspended sediment load are given for the Output cross section.
[c] Temperature and precipitation were registered at the Chernobyl meteostation.

Table I.3. (Continued)

Date	Water level[a] m BS		Discharge[b] $m^3 s^{-1}$	Suspended sediment[b] $g L^{-1}$	T[c] deg. C	Precipitation[c] mm	^{137}Cs Bq m^{-3}		^{90}Sr Bq m^{-3}
	D3	BNS					Particulate	Dissolved	Dissolved
5 Feb 94	105.69	105.40	575	0.0951	-5.7		40.7	92.6	177.8
6 Feb 94	105.72	105.40	565	0.0961	-10.2		37.0	85.2	181.5
7 Feb 94	105.87	105.58	556	0.0971	-6.7	7.8	33.3	77.8	181.5
8 Feb 94	106.08	105.75	549	0.0981	-11.8		29.6	70.4	185.2
9 Feb 94	106.59	106.30	542	0.0990	-13.8		25.9	63.0	185.2
10 Feb 94	107.08	106.65	530	0.1000	-8.2	3.6	22.2	85.2	200.0
11 Feb 94	106.90	105.57	530	0.1010	-8.4	0.5	22.2	107.4	214.8
12 Feb 94	106.83	106.53	525	0.1020	-19.1		51.9	111.1	188.9
13 Feb 94	106.56	106.30	521	0.1030	-19.2		77.8	114.8	163.0
14 Feb 94	106.43	105.95	518	0.1039	-11.6	0.2	74.1	103.7	174.1
15 Feb 94	106.40	105.90	515	0.1049	-12.8		74.1	88.9	181.5
16 Feb 94	106.39	105.90	512	0.1059	-12.3		70.4	77.8	255.6
17 Feb 94	106.44	105.93	509	0.1069	-7.0		70.4	70.4	325.9
18 Feb 94	106.49	105.92	506	0.1078	-7.8		66.7	59.3	325.9
19 Feb 94	106.54	106.03	503	0.1088	-2.8	0.7	66.7	51.9	325.9
20 Feb 94	106.58	106.07	500	0.1098	-4.5		63.0	40.7	325.9
21 Feb 94	106.62	106.13	498	0.1108	-4.1		63.0	55.6	325.9
22 Feb 94	106.62	106.14	497	0.1118	-4.2		63.0	70.4	318.5
23 Feb 94	106.63	106.15	496	0.1127	-3.7	0.8	66.7	85.2	318.5
24 Feb 94	106.63	106.16	495	0.1137	-0.4	1.9	66.7	96.3	348.1
25 Feb 94	106.58	106.15	495	0.1147	-0.1	2.3	66.7	111.1	377.8
26 Feb 94	106.55	106.13	495	0.1157	-1.5	0.7	66.7	125.9	407.4
27 Feb 94	106.54	106.10	495	0.1166	-5.2	0.0	70.4	137.0	392.6
28 Feb 94	106.53	106.08	495	0.1176	-0.6		77.8	148.1	381.5
1 Mar 94	106.45	106.02	496	0.1186	1.7		81.5	159.3	366.7
2 Mar 94	106.42	106.00	497	0.1196	-3.8	4.4	81.5	151.9	337.0
3 Mar 94	106.41	105.97	498	0.1206	-3.7	13.0	85.2	148.1	307.4
4 Mar 94	106.38	105.93	499	0.1215	-4.0	8.8	85.2	140.7	281.5
5 Mar 94	106.35	105.90	501	0.1225	-5.2	1.5	88.9	137.0	251.9
6 Mar 94	106.31	105.85	502	0.1235	-7.1		88.9	129.6	222.2
7 Mar 94	106.23	105.85	505	0.1245	-3.6		92.6	125.9	211.1
8 Mar 94	106.27	105.83	507	0.1254	1.1		92.6	118.5	200.0
9 Mar 94	106.26	105.83	515	0.1264	2.8		96.3	114.8	188.9
10 Mar 94	106.27	105.80	524	0.1274	4.4		96.3	107.4	174.1

[a] Water levels were measured at the gauge stations D3 and BNS, located upstream and downstream, respectively, of the Output cross section (Figure I.1).
[b] Water discharges and suspended sediment load are given for the Output cross section.
[c] Temperature and precipitation were registered at the Chernobyl meteostation.

Table I.3. (Continued)

Date	Water level[a] m BS		Discharge[b] $m^3 s^{-1}$	Suspended sediment[b] $g L^{-1}$	T[c] deg. C	Precipitation[c] mm	^{137}Cs Bq m^{-3}		^{90}Sr Bq m^{-3}
	D3	BNS					Particulate	Dissolved	Dissolved
11 Mar 94	106.24	105.81	532	0.1284	3.7	3.6	100.0	103.7	163.0
12 Mar 94	106.27	105.83	540	0.1294	1.2		100.0	96.3	151.9
13 Mar 94	106.26	105.79	550	0.1303	1.1		81.5	111.1	188.9
14 Mar 94	106.22	105.70	560	0.1313	1.1	12.0	63.0	125.9	222.2
15 Mar 94	106.20	105.75	570	0.1323	2.8	3.2	44.4	137.0	259.3
16 Mar 94	106.20	105.74	580	0.1333	-0.2	5.6	25.9	151.9	292.6
17 Mar 94	106.28	105.79	610	0.1342	1.1	2.6	25.9	185.2	396.3
18 Mar 94	106.38	105.85	640	0.1352	1.9	2.9	29.6	218.5	503.7
19 Mar 94	106.46	105.93	670	0.1362	2.3	3.1	29.6	251.9	607.4
20 Mar 94	106.50	106.02	700	0.1372	4.7	0.5	33.3	285.2	714.8
21 Mar 94	106.55	106.19	750	0.1382	2.0	0.3	33.3	318.5	818.5
22 Mar 94	106.39	106.08	790	0.1391	-1.3		37.0	355.6	925.9
23 Mar 94	106.28	105.96	860	0.1401	0.2	7.2	37.0	388.9	1029.6
24 Mar 94	106.29	105.93	950	0.1391	5.5	0.0	37.0	422.2	1133.3
25 Mar 94	106.36	106.00	1070	0.1381	4.8	3.1	40.7	455.6	1240.7
26 Mar 94	106.50	106.12	1218	0.1371	6.4		40.7	488.9	1344.4
27 Mar 94	106.78	106.35	1365	0.1361	2.7		44.4	522.2	1451.9
28 Mar 94	106.99	106.55	1500	0.1351	0.0	1.0	44.4	555.6	1555.6
29 Mar 94	107.14	106.65	1544	0.1341	0.0		66.7	518.5	1388.9
30 Mar 94	107.14	106.72	1660	0.1331	0.0	0.5	85.2	518.5	1222.2
31 Mar 94	107.17	106.72	1638	0.1321	5.5	0.1	81.5	518.5	1185.2
1 Apr 94	107.15	106.71	1660	0.1311	7.4	9.8	74.1	481.5	1148.1
2 Apr 94	107.15	106.70	1650	0.1301	8.3	0.6	70.4	481.5	1111.1
3 Apr 94	107.15	106.69	1630	0.1291	8.0		55.6	381.5	911.1
4 Apr 94	107.12	106.66	1600	0.1281	7.4		44.4	281.5	714.8
5 Apr 94	107.03	106.64	1580	0.1271	2.8		29.6	181.5	514.8
6 Apr 94	107.06	106.60	1560	0.1261	8.3	0.6	14.8	81.5	314.8
7 Apr 94	107.03	106.59	1540	0.1251	7.5	0.3	14.8	174.1	403.7
8 Apr 94	107.02	106.56	1510	0.1241	10.6		14.8	263.0	492.6
9 Apr 94	107.00	106.55	1490	0.1212	5.6		18.5	355.6	577.8
10 Apr 94	106.95	106.50	1470	0.1183	6.7		18.5	444.4	666.7
11 Apr 94	106.91	106.47	1440	0.1153	9.7		37.0	377.8	666.7
12 Apr 94	106.88	106.43	1410	0.1124	11.4		51.9	307.4	703.7
13 Apr 94	106.83	106.40	1380	0.1095	15.6		70.4	240.7	740.7

[a] Water levels were measured at the gauge stations D3 and BNS, located upstream and downstream, respectively, of the Output cross section (Figure I.1).
[b] Water discharges and suspended sediment load are given for the Output cross section.
[c] Temperature and precipitation were registered at the Chernobyl meteostation.

Table I.3. (Continued)

Date	Water level[a] m BS		Discharge[b] $m^3 s^{-1}$	Suspended sediment[b] $g L^{-1}$	T[c] deg. C	Precipitation[c] mm	^{137}Cs Bq m^{-3}		^{90}Sr Bq m^{-3}
	D3	BNS					Particulate	Dissolved	Dissolved
14 Apr 94	106.80	106.36	1350	0.1066	14.3	9.4	70.4	192.6	740.7
15 Apr 94	106.77	106.32	1330	0.1036	12.3		66.7	148.1	777.8
16 Apr 94	106.70	106.26	1300	0.1007	12.1		66.7	100.0	777.8
17 Apr 94	106.65	106.23	1270	0.0978	14.8		51.9	122.2	777.8
18 Apr 94	106.63	106.19	1240	0.0949	15.7	3.0	33.3	148.1	777.8
19 Apr 94	106.59	106.15	1210	0.0919	4.7	2.4	18.5	170.4	777.8
20 Apr 94	106.53	106.07	1180	0.0890	5.3		25.9	137.0	685.2
21 Apr 94	106.48	106.02	1150	0.0861	9.2		33.3	100.0	592.6
22 Apr 94	106.45	106.00	1120	0.0832	9.3		40.7	66.7	500.0
23 Apr 94	106.39	105.90	1090	0.0802	6.9	1.3	48.1	29.6	407.4
24 Apr 94	106.29	105.84	1060	0.0773	8.3		48.1	40.7	392.6
25 Apr 94	106.23	105.77	1034	0.0744	10.9	8.0	44.4	48.1	374.1
26 Apr 94	106.18	105.74	1008	0.0714	12.2	0.8	40.7	59.3	359.3
27 Apr 94	106.10	105.69	982	0.0685	13.7		37.0	66.7	340.7
28 Apr 94	106.04	105.60	962	0.0656	14.4		40.7	92.6	333.3
29 Apr 94	105.93	105.53	942	0.0627	16.1		40.7	122.2	329.6
30 Apr 94	105.94	105.49	923	0.0597	15.4		44.4	148.1	322.2

[a] Water levels were measured at the gauge stations D3 and BNS, located upstream and downstream, respectively, of the Output cross section (Figure I.1).
[b] Water discharges and suspended sediment load are given for the Output cross section.
[c] Temperature and precipitation were registered at the Chernobyl meteostation.

Table I.4. Hydrological and meteorological data and activity concentrations of ^{90}Sr and ^{137}Cs in the Input cross section in January–April 1999.

Date	Water level[a] m BS		Discharge[b] $m^3 s^{-1}$	Suspended sediment[b] $g L^{-1}$	T[c] deg. C	Precipitation[c] mm	^{137}Cs $Bq m^{-3}$		^{90}Sr $Bq m^{-3}$
	D3	BNS					Particulate	Dissolved	Dissolved
1 Jan 99	105.91	105.52	591	0.020	-4.3		37.0	55.6	137.0
2 Jan 99	105.90	105.52	599	0.020	-2.8	0.2	40.7	51.9	144.4
3 Jan 99	105.91	105.52	607	0.020	-1.8		40.7	51.9	148.1
4 Jan 99	105.92	105.55	610	0.020	-0.3		44.4	48.1	155.6
5 Jan 99	105.91	105.55	614	0.020	1.5	0.0	48.1	44.4	163.0
6 Jan 99	105.89	105.54	617	0.020	3.3	2.7	48.1	40.7	166.7
7 Jan 99	105.90	105.54	620	0.020	4.7		51.9	40.7	174.1
8 Jan 99	105.88	105.52	623	0.020	1.4	0.8	51.9	37.0	181.5
9 Jan 99	105.86	105.51	627	0.020	-2.1	1.6	48.1	40.7	170.4
10 Jan 99	105.86	105.50	630	0.020	-1.5	3.6	44.4	48.1	159.3
11 Jan 99	105.85	105.49	633	0.020	-8.9		40.7	51.9	151.9
12 Jan 99	105.85	105.49	637	0.021	-7.1	5.1	33.3	59.3	140.7
13 Jan 99	105.80	105.49	640	0.021	-0.2	3.7	29.6	63.0	133.3
14 Jan 99	105.80	105.50	643	0.021	-1.0	0.3	25.9	66.7	122.2
15 Jan 99	105.80	105.48	647	0.021	-2.2	0.0	22.2	74.1	111.1
16 Jan 99	105.79	105.48	650	0.021	-0.1	0.9	14.8	77.8	103.7
17 Jan 99	105.79	105.49	653	0.021	-4.3		11.1	85.2	92.6
18 Jan 99	105.78	105.47	656	0.021	-3.6		7.4	88.9	81.5
19 Jan 99	105.78	105.47	660	0.021	-5.0		7.4	96.3	81.5
20 Jan 99	105.78	105.47	663	0.021	-5.6		7.4	103.7	81.5
21 Jan 99	105.78	105.46	665	0.022	-5.8		7.4	111.1	81.5
22 Jan 99	105.77	105.46	667	0.022	-5.6		7.4	118.5	81.5
23 Jan 99	105.76	105.46	669	0.023	-0.5		7.4	125.9	81.5
24 Jan 99	105.74	105.44	672	0.024	-0.5		7.4	133.3	81.5
25 Jan 99	105.73	105.43	674	0.024	0.1	0.4	7.4	140.7	77.8
26 Jan 99	105.71	105.39	676	0.025	3.2		0.2	4.0	2.1
27 Jan 99	105.70	105.39	678	0.025	1.3	5.4	11.1	155.6	77.8
28 Jan 99	105.69	105.39	680	0.026	0.4	1.8	11.1	163.0	77.8
29 Jan 99	105.67	105.40	682	0.027	-1.6	1.2	11.1	170.4	77.8
30 Jan 99	105.65	105.36	685	0.027	-10.2	0.0	11.1	163.0	77.8
31 Jan 99	105.63	105.39	687	0.028	-10.3	7.6	11.1	155.6	77.8
1 Feb 99	105.72	105.44	689	0.028	-7.3	2.9	11.1	151.9	77.8
2 Feb 99	105.74	105.46	691	0.029	-1.8	0.8	11.1	144.4	81.5
3 Feb 99	105.76	105.48	690	0.032	-11.0		11.1	137.0	81.5
4 Feb 99	105.78	105.48	690	0.035	-6.6	0.3	11.1	129.6	81.5

[a] Water levels were measured at the gauge stations D3 and BNS, located upstream and downstream, respectively, of the Output cross section (Figure I.1).
[b] Water discharges and suspended sediment load are given for the Output cross section.
[c] Temperature and precipitation were registered at the Chernobyl meteostation.

Table I.4. (Continued)

Date	Water level[a] m BS		Discharge[b] $m^3 s^{-1}$	Suspended sediment[b] $g L^{-1}$	T[c] deg. C	Precipitation[c] mm	^{137}Cs Bq m^{-3}		^{90}Sr Bq m^{-3}
	D3	BNS					Particulate	Dissolved	Dissolved
5 Feb 99	105.79	105.50	689	0.038	2.5	3.6	14.8	122.2	81.5
6 Feb 99	105.80	105.50	688	0.042	0.5	1.4	14.8	118.5	81.5
7 Feb 99	105.80	105.50	688	0.045	-3.4	4.2	14.8	111.1	85.2
8 Feb 99	105.79	105.45	687	0.048	-6.1		14.8	103.7	85.2
9 Feb 99	105.79	105.47	687	0.051	-2.2	6.0	14.8	96.3	85.2
10 Feb 99	105.79	105.47	686	0.054	-7.3	1.3	14.8	88.9	85.2
11 Feb 99	105.78	105.46	685	0.057	-2.9	5.3	14.8	85.2	85.2
12 Feb 99	105.78	105.46	685	0.061	-1.9	1.6	14.8	77.8	88.9
13 Feb 99	105.77	105.46	684	0.064	-0.4	1.1	14.8	77.8	88.9
14 Feb 99	105.78	105.46	683	0.067	-0.7		14.8	77.8	88.9
15 Feb 99	105.78	105.46	683	0.070	-0.6	4.0	18.5	74.1	92.6
16 Feb 99	105.78	105.39	682	0.073	-1.9	2.4	18.5	74.1	92.6
17 Feb 99	105.78	105.40	692	0.078	-1.7	1.7	18.5	74.1	92.6
18 Feb 99	105.78	105.42	702	0.083	-2.6		18.5	74.1	96.3
19 Feb 99	105.78	105.42	712	0.088	-4.3		18.5	74.1	96.3
20 Feb 99	105.77	105.40	723	0.092	-4.5	0.2	18.5	74.1	96.3
21 Feb 99	105.78	105.40	733	0.097	-2.1	1.4	18.5	74.1	100.0
22 Feb 99	105.78	105.39	743	0.101	-0.4	0.2	18.5	74.1	100.0
23 Feb 99	105.78	105.35	753	0.105	1.4	8.0	18.5	74.1	100.0
24 Feb 99	105.77	105.36	763	0.109	0.1	1.1	18.5	70.4	103.7
25 Feb 99	105.76	105.32	773	0.113	-1.2	0.9	18.5	70.4	103.7
26 Feb 99	105.72	105.30	783	0.117	-2.0	1.8	18.5	70.4	103.7
27 Feb 99	105.71	105.32	793	0.121	0.1	1.8	22.2	70.4	107.4
28 Feb 99	105.70	105.25	804	0.124	2.7		22.2	70.4	107.4
1 Mar 99	105.69	105.24	814	0.135	2.7		22.2	70.4	107.4
2 Mar 99	105.69	105.24	824	0.146	3.2	2.7	22.2	74.1	114.8
3 Mar 99	105.71	105.28	834	0.156	1.9		25.9	81.5	118.5
4 Mar 99	105.72	105.30	844	0.166	6.3		25.9	88.9	125.9
5 Mar 99	105.78	105.30	854	0.176	6.0		25.9	92.6	133.3
6 Mar 99	105.84	105.31	864	0.182	7.5	0.9	29.6	100.0	137.0
7 Mar 99	105.90	105.35	874	0.188	4.5		29.6	103.7	144.4
8 Mar 99	105.90	105.48	885	0.194	3.1	1.1	33.3	111.1	148.1
9 Mar 99	105.91	105.55	895	0.200	0.1	1.6	33.3	118.5	155.6
10 Mar 99	105.72	105.35	905	0.205	-1.3	1.7	37.0	122.2	163.0

[a] Water levels were measured at the gauge stations D3 and BNS, located upstream and downstream, respectively, of the Output cross section (Figure I.1).
[b] Water discharges and suspended sediment load are given for the Output cross section.
[c] Temperature and precipitation were registered at the Chernobyl meteostation.

Table I.4. (Continued)

Date	Water level[a] m BS		Discharge[b] $m^3 s^{-1}$	Suspended sediment[b] $g L^{-1}$	T[c] deg. C	Precipitation[c] mm	^{137}Cs Bq m^{-3}		^{90}Sr Bq m^{-3}
	D3	BNS					Particulate	Dissolved	Dissolved
11 Mar 99	105.66	105.35	915	0.211	1.8	6.3	37.0	129.6	166.7
12 Mar 99	105.72	105.36	925	0.216	0.9	4.2	40.7	133.3	174.1
13 Mar 99	105.79	105.46	1013	0.228	-1.1	2.2	40.7	140.7	177.8
14 Mar 99	105.84	105.46	1100	0.238	-1.2	0.8	40.7	144.4	185.2
15 Mar 99	105.92	105.55	1139	0.257	-2.6	0.4	44.4	151.9	188.9
16 Mar 99	105.95	105.62	1178	0.274	-2.8	3.0	44.4	159.3	196.3
17 Mar 99	106.02	105.63	1216	0.291	-1.8		48.1	163.0	203.7
18 Mar 99	106.09	105.72	1255	0.306	-0.6		48.1	170.4	207.4
19 Mar 99	106.22	105.80	1294	0.321	0.8		51.9	174.1	214.8
20 Mar 99	106.31	105.93	1333	0.335	2.2		51.9	181.5	218.5
21 Mar 99	106.50	106.10	1371	0.348	0.0	4.0	51.9	185.2	251.9
22 Mar 99	106.76	106.37	1410	0.360	0.1	0.6	55.6	192.6	285.2
23 Mar 99	107.09	106.70	1550	0.347	4.0		55.6	200.0	318.5
24 Mar 99	107.39	107.00	1690	0.337	3.9	3.7	59.3	203.7	351.9
25 Mar 99	107.63	107.21	1970	0.305	4.0		59.3	211.1	429.6
26 Mar 99	107.78	107.38	2147	0.335	5.8		74.1	259.3	459.3
27 Mar 99	107.90	107.47	2323	0.362	8.1		85.2	311.1	488.9
28 Mar 99	107.98	107.53	2320	0.414	9.3		63.0	425.9	688.9
29 Mar 99	108.01	107.60	2355	0.446	9.8		40.7	540.7	892.6
30 Mar 99	108.11	107.66	2390	0.460	10.1		40.7	555.6	914.8
31 Mar 99	108.17	107.70	2570	0.445	10.8		40.7	570.4	940.7
1 Apr 99	108.22	107.74	2600	0.457	9.5		44.4	307.4	896.3
2 Apr 99	108.26	107.77	2690	0.477	10.3		48.1	40.7	851.9
3 Apr 99	108.26	107.80	2780	0.468	9.6		63.0	259.3	807.4
4 Apr 99	108.25	107.74	2755	0.465	7.5		77.8	481.5	759.3
5 Apr 99	108.23	107.70	2730	0.390	2.2		51.9	251.9	514.8
6 Apr 99	108.19	107.68	2630	0.382	5.9		25.9	25.9	270.4
7 Apr 99	108.15	107.65	2530	0.374	11.5	5.4	3.7	111.1	118.5
8 Apr 99	108.12	107.63	2430	0.365	8.3	6.5	14.8	144.4	155.6
9 Apr 99	108.10	107.60	2330	0.355	9.2		29.6	181.5	188.9
10 Apr 99	108.08	107.57	2253	0.341	10.1		29.6	229.6	251.9
11 Apr 99	108.00	107.53	2177	0.326	10.4	1.9	70.4	203.7	288.9
12 Apr 99	107.99	107.50	2100	0.309	9.2	4.3	111.1	181.5	329.6
13 Apr 99	107.94	107.43	2085	0.283	7.5		77.8	148.1	263.0

[a] Water levels were measured at the gauge stations D3 and BNS, located upstream and downstream, respectively, of the Output cross section (Figure I.1).
[b] Water discharges and suspended sediment load are given for the Output cross section.
[c] Temperature and precipitation were registered at the Chernobyl meteostation.

Table I.4. (Continued)

Date	Water level[a] m BS		Discharge[b] $m^3 s^{-1}$	Suspended sediment[b] $g L^{-1}$	T[c] deg. C	Precipitation[c] mm	^{137}Cs Bq m^{-3}		^{90}Sr Bq m^{-3}
	D3	BNS					Particulate	Dissolved	Dissolved
14 Apr 99	107.88	107.38	2070	0.257	11.6	2.5	48.1	114.8	196.3
15 Apr 99	107.80	107.30	2013	0.234	12.7	1.7	14.8	81.5	129.6
16 Apr 99	107.74	107.24	1957	0.211	14.3		11.1	59.3	240.7
17 Apr 99	107.66	107.15	1900	0.186	16.2		14.8	77.8	244.4
18 Apr 99	107.59	107.11	1825	0.184	14.5	5.0	14.8	100.0	251.9
19 Apr 99	107.51	107.03	1750	0.182	15.6		18.5	118.5	255.6
20 Apr 99	107.42	106.95	1675	0.180	8.5	4.3	22.2	140.7	259.3
21 Apr 99	107.33	106.86	1600	0.177	9.1		18.5	129.6	218.5
22 Apr 99	107.23	106.78	1527	0.174	12.6		18.5	118.5	174.1
23 Apr 99	107.15	106.68	1453	0.171	12.5		18.5	111.1	129.6
24 Apr 99	107.08	106.60	1380	0.168	13.0		14.8	100.0	125.9
25 Apr 99	107.00	106.55	1370	0.163	14.0	1.4	11.1	92.6	125.9
26 Apr 99	106.92	106.46	1360	0.158	15.7		11.1	81.5	122.2
27 Apr 99	106.85	106.39	1350	0.153	16.9		7.4	74.1	118.5
28 Apr 99	106.79	106.33	1330	0.148	16.8		7.4	85.2	151.9
29 Apr 99	106.70	106.25	1310	0.144	13.9	1.7	11.1	100.0	185.2
30 Apr 99	106.64	106.20	1290	0.140	10.8	0.9	11.1	114.8	214.8

[a] Water levels were measured at the gauge stations D3 and BNS, located upstream and downstream, respectively, of the Output cross section (Figure I.1).
[b] Water discharges and suspended sediment load are given for the Output cross section.
[c] Temperature and precipitation were registered at the Chernobyl meteostation.

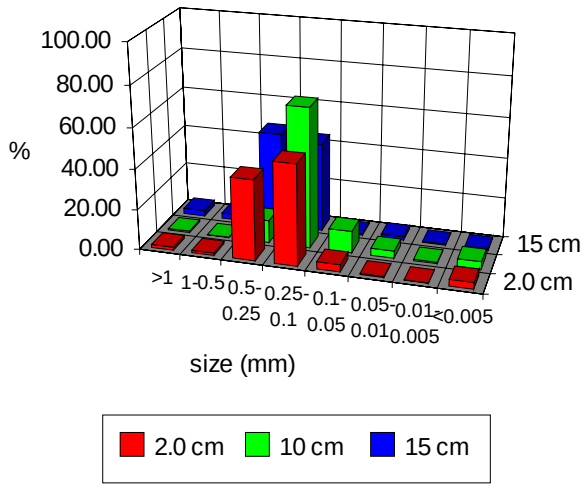

Fig. I.4. Particle size distribution of alluvial acid soddy soil of the Pripyat River floodplain.

Data on water discharge and suspended sediment load in the Output cross section, and air temperature and precipitation measured at the Chernobyl Meteostation, are also provided in Tables I.2–I.4. All data are presented with 1 day resolution.

Activity concentrations of ^{137}Cs (the dissolved and particulate states) and ^{90}Sr (the dissolved state) in the Input cross section are given in Tables I.2–I.4 for the events of 1991, 1994 and 1999, respectively, with 1 day resolution.

The chemical composition of the Pripyat River and of internal lakes, the granulometric characteristics of the Pripyat River suspended sediment for winter conditions, typical values of activity concentrations in water bodies of the floodplain area and values for the Manning n-roughness coefficient are presented in Table I.5–I.8, respectively.

The major part of the floodplain area is represented by alluvial acid soddy soils; however, soddy sand gley soils occur at elevated sites. The typical physico-chemical characteristics of the upper horizon for the alluvial acid soddy soil are given in Table I.9. The main physical properties of the upper 10 cm layer of this soil are as follows: soil density, 1.45 g cm^{-3} dry weight; soil porosity, 45 cm^3 per cm^3; hydraulic conductivity, 0.33 mm min^{-1}. The depth of soil freezing on the eve of the flooding was more than 50 cm. Groundwater table depth for the end of winter is about 1.0 m. Typical particle size distribution of the alluvial acid soddy soil from the floodplain area is given in the web-site (Figure I.4). The main type of floodplain vegetation is mixed meadow grasses. An insignificant part of the floodplain area (largely at a high level) is covered by thin oak and willow planting.

To obtain kinetic parameters of radionuclide exchange in a flooded soil-water system, experimental data [I.2] can be used. The data were obtained for soils collected just before the flooding in 1991, using original methodology presented by Bulgakov et al. [I.3]. According to Laptev and Voitsekhovich [I.2], the rate constant of radionuclide exchange between soil and water during a flooding event varies in the range of 0.01–0.04 day^{-1}, with a mean value of 0.02 day^{-1}.

Table I.5. Typical hydrochemical composition of Pripyat River and internal lakes for winter conditions.

Chemical species	Units	Pripyat River	Internal lakes
NO_2^-	mg L^{-1}	N/O[a]	N/O
NO_3^-	mg L^{-1}	N/O	N/O
HCO_3^-	mg L^{-1}	192.76	109.80
Cl^-	mg L^{-1}	21.30	10.65
SO_4^-	mg L^{-1}	28.25	27.33
Ca^{2+}	mg L^{-1}	48.09	28.06
Mg^{2+}	mg L^{-1}	6.81	5.84
$(Na + K)^+$	mg L^{-1}	31.27	17.24
NH_4^+	mg L^{-1}	0.45	0.60
Mineralisation	mg L^{-1}	336.71	199.53
Hardness	mg-eq L^{-1}	2.96	1.88
pH	–	7.49	7.4
eH	mV	438	427
O_2	mg L^{-1}	17.55	12.95
O_2	%	181	128
Cu	µg L^{-1}	11	9
Zn	µg L^{-1}	7	14
Permanganate oxidation	mg O_2 L^{-1}	17.4	12.3

[a] N/O = not observed.

Table I.6. Typical size distributions (%) of suspended sediment in the Pripyat River near Chernobyl for different hydrological seasons.

Hydrological conditions	Size of particles, mm							d_{ave}
	1–0.5	0.5–0.2	0.2–0.1	0.1–0.05	0.05–0.01	0.01–0.005	< 0.005	
Winter drought period	0.10	1.43	1.87	0.83	21.6	11.1	63.1	0.019
Increasing of spring flood	0.95	12.7	23.3	14.8	23.6	11.1	13.5	0.110
Peak of spring flood	4.63	34.7	33.6	6.41	11.0	4.41	5.7	0.219
Abatement of spring flood	2.45	13.2	8.74	6.58	33.7	14.0	14.2	0.096
Increasing of summer and autumn flood	0.0	0.65	8.35	9.98	28.0	28.6	1.6	0.039
Abatement of summer and autumn flood	0.0	0.30	3.28	4.23	49.9	16.4	1.0	0.026
Summer and autumn drought period	0.77	1.58	1.41	2.29	43.8	18.6	26.0	0.033

Table I.7. Activity concentrations of ^{90}Sr and ^{137}Cs in selected internal lakes.

Date	^{137}Cs particulate pCi L^{-1}	^{137}Cs dissolved pCi L^{-1}	^{90}Sr dissolved pCi L^{-1}
25 January 1991	88.8	–	3490
10 February 1991	79.1	–	2830
25 February 1991	432	494	5010

Table I.8. Values for the Manning n-roughness coefficient.

Type of channel and description	% of cover (averaged)	Minimum	Normal	Maximum
Area of the floodplain covered by:				
(a) sandy soils and poor grass	20	0.025	0.03	0.035
(b) sandy soils and reach grass and vegetation	30	0.03	0.035	0.05
(c) sandy soils covered by willow bushes	50	0.06	0.12	0.18
Main stream channel			0.025–0.035	

Table I.9. Typical physico-chemical composition of the alluvial acid soddy soil in the floodplain area.

Parameter	Units	Value
Horizon		A_D
Depth	cm	0–7
pH		5.0
SEC	meq/100 g	6.7
Humus	%	2.1
Macro-cations in exchangeable complex	meq/100 g	
Ca^{2+}		3.1
Mg^{2+}		0.25
K^{+}		0.09
Na^{+}		0.03
Sr^{2+}		0.003

I.1.1.4. Data for model testing

The following types of data will be made available for model testing at a later date:

- vertical distribution and chemical speciation of ^{90}Sr in the alluvial acid soddy soil in 1991;
- vertical distribution and chemical speciation of ^{137}Cs in the alluvial acid soddy soil in 1991;
- activity concentrations of dissolved and particulate ^{137}Cs in the Output cross section with 1 day resolution for each event; and
- activity concentrations of dissolved ^{90}Sr in the Output cross section with 1 day resolution for each event.

I.1.2. Experimental details

Radiocaesium activity on the soil surface was estimated by utilising the data of helicopter surveys using an onboard-installed γ-spectrometer. The flight routes were taken to be parallel to the dike with 200 m distance to each other, which made it possible to obtain detailed information.

Activity of ^{90}Sr was determined based on radiochemical analysis of spatially distributed samples, with further comparison of the $^{137}Cs/^{90}Sr$ ratio in samples and the radiocaesium data obtained by γ-survey. Results of more than 50 samples were used for this purpose.

The vertical distribution of radionuclides in soil was determined by taking two soil cores from two plots located on the left bank of the floodplain [I.4]. The cores were taken 23 July 1991 using steel cylinders of 7.5 cm diameter and 15 cm length. The plot 1 and 2 coordinates are 52.4517 N, 30.0504 E and 51.4379 N, 30.0688 E, respectively.

ACKNOWLEDGEMENTS

The Floodplain Scenario was developed by Alexei Konoplev and Anatoly Bulgakov of the Centre for Environmental Chemistry of SPA "Typhoon", Obninsk, Russia, and Oleg Voitsekhovich, Gennady Laptev, and Vladimir Lutkovsky of the Ukrainian Hydrometeorological Institute, Kiev, Ukraine.

I.2. "Dnieper-Bug" (Dnieper-Southern Boug) Estuary case study

I.2.1. Description of the scenario

In this working material the description of dataset on hydrological and meteorological regime of Dnieper-Bug Estuary is presented. Most information in this appendix were obtained from the scientific literature [I.5–I.8]. The scenario datasets were made available to the modelers for the modelling exercise.

The Dnieper-Bug Estuary (DBE) is the largest of all the Black Sea estuaries (see Figure I.5) with a surface area of 1006.3 km^2, and a volume of 4.24 km^3. The DBE water system consists of the Dnieper Estuary with the adjoining Bug Estuary. The length of the DBE is 63 km with a width of up to 15 km. The DBE is connected with the Black Sea through the Strait of Kirnburn. The bathymetry of north-western part of the Black sea and DBE is given in Figure I.6. The average depth of the DBE is 4.4 m [I.5]. There is a narrow, 10–12 m deep channel suitable for shipping along the Dnieper and Bug estuaries from the Black Sea to ports of Mykolayiv and Kherson. The bottom is covered mainly by clay (50%) and sand. The main factor affecting the regime of the system is the process of mixing fresh river waters with saline marine waters. This forms the saline wedge in the estuary, which in the summer months can reach Kherson city. Stratification in the estuary ranges from almost none in the eastern part at the Dnieper mouth to a defined two layer system in the western marine part of the DBE. These processes are highly season-dependent. The regime of this drowned river estuary varies from stratified to partially mixed. The monthly average discharge of the Dnieper ranges from about 400 $m^3 s^{-1}$ to about 6000 $m^3 s^{-1}$ in spring whereas monthly average discharge of the Southern Bug ranges from 80 to 1000 $m^3 s^{-1}$. The Dnieper discharge, unlike the Southern Bug, is not simple seasonal because it is regulated from Kakhovka reservoir dam placed at 70 km from Dnieper mouth (Figure I.5). Therefore in the summer the saline wedge penetrates much further into the estuary than in the spring. Also, the concentration of salinity of the upper stratum in the summer is much higher than in the spring. In addition to the fresh water input, other key factors governing the transport of contaminants are air temperature, wind and sea level variability. Together they force complicated three dimensional time-dependent stratified flows in DBE.

To simulate radionuclide contamination in DBE the input data were prepared:

- Bathymetry;
- Discharges of the Dnieper River and Southern Bug 1984–1987;
- Sea level in Kinbourn Strait (Ochakiv) 1986–1987;
- Sea surface temperature and salinity in Ochakiv 1986–1987; and
- Meteorological parameters in Ochakiv 1986–1987.

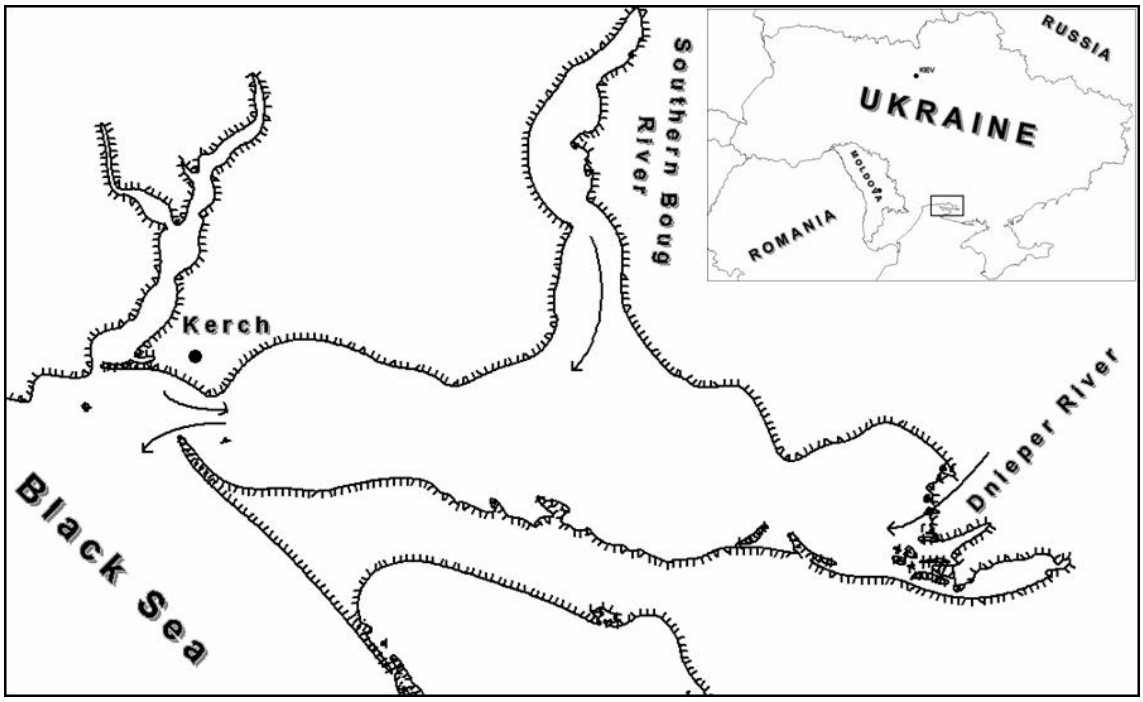

Fig. I.5. Dnieper-Bug Estuary.

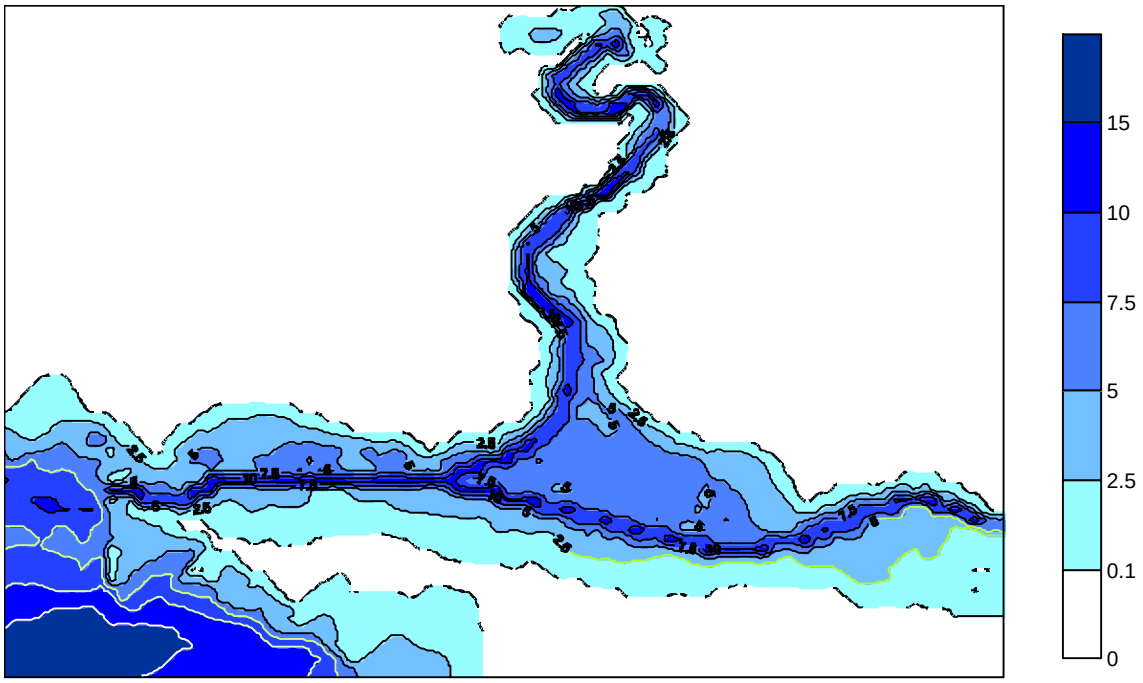

Fig. I.6. Bathymatry of DBE and coastal area of the Black Sea.

Other parameters of DBE hydrology are unavailable (temperature in the Dnieper River and Bug River, temperature and salinity profiles in the Kinbourn Strait). The relevant recommendations are given on their seasonal change.

Bathymetry

Bathymetry of DBE and coastal area of the Black Sea is provided on grid 2 km as DBE+BlackSea.dat and DBE+BlackSea.grd files. The bathymetry of DBE only with 1 km resolution is given in DBE.dat and DBE.grd files.

Discharges of the Dnieper River and Southern Bug River

Daily discharges of Dnieper River and S. Bug River in 1984–1987 are given in file Dnieper discharge.xls and S Bug discharge.xls.

Sea level in Kinbourn Strait (Ochakiv) 1986–1987

Daily sea level in Kinbourn Strait (Ochakiv) 1986–1987 are given in files sea level 1986.xls and sea level 1987.xls. The level is in cm relatively to some zero value.

Temperature and salinity in Kinbourn strait (Ochakiv)

Daily temperature and salinity (ppt.) at surface are given in files SST in Ochakiv 1986.xls and SST in Ochakiv 1987.xls. There are not systematic measurements of profiles of temperature and salinity in Kinbourn strait. Therefore it is proposed to use two layer approximation of profile with upper layer thickness 3 m. The recommended values for the bottom layer are given in file Bottom T and S in Ochakiv.xls. At winter the DBE is covered by ice.

Temperature in the Dnieper and Southern Bug Rivers

There are not data on the temperature in the Dnieper and Southern Bug Rivers. It is recommended to use surface temperature data from files SST in Ochakiv 1986.xls and SST in Ochakiv 1987.xls. At winter the rivers are covered by ice.

Atmospheric forcing

Three hour values of wind, air temperature, relative humidity and cloudiness (0–10) are given in files Meteorology 1986.xls and Meteorology 1987.xls.

Surveys

To validate hydrodynamics the data of surveys in DBE are given in files Surveys 1986.xls and Surveys 1987.xls. Coordinates of survey stations are given in file Coordinates.xls. In survey data 1986 the measurements of temperature and salinity are given, whereas in survey 1987 also velocities were measured.

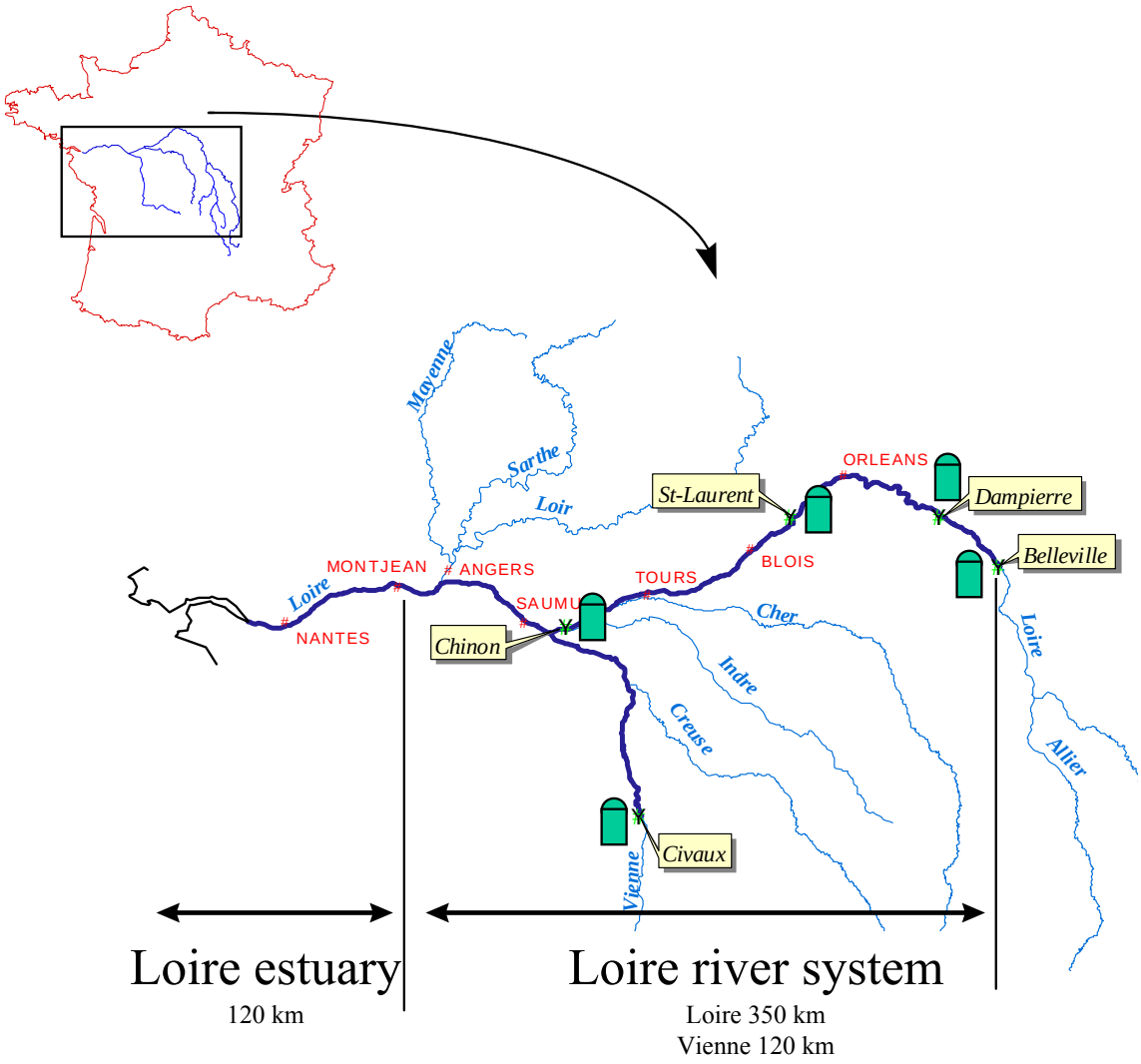

Fig. I.7. The Loire River system.

I.3. Migration of Tritium in the Loire River

I.3.1. Description of the blind test scenario

The Loire scenario was a blind test of models aimed at assessing the dispersion of tritium releases in the Loire River (France), on a large domain (~ 350 km) and on a period of six months, and to compare the results obtained by the different models to measurements of tritium concentration made in Angers, a city along the Loire River.

The exercise consists in modelling the dispersion of tritium in the Loire River:

- from Belleville (abscissa = 532 820 m) to MontJean (abscissa = 885 370 m), which represents a domain length of about 350 km;
- on a period of six months, from the 1st of July to the 31st of December 1999; and
- taking into account water discharges from tributaries and tritium discharges from 4 nuclear power plants (by using real hydraulic conditions of the year 1999).

Figure I.7 presents a general view of the Loire River system. The data given for this exercise are:

- the abscissa of all the objects describing the Loire River: upstream/downstream model boundary, profiles, weirs, tributaries, corrections of flow rate, tritium discharges and points used in the files given for calibration (associated to French city names);
- the geometry of the Loire River (~ 370 transversal profiles gathered by the DIREN Centre, with a spacing of approx. 1 km);
- the description of the singularities (18 weirs and little dams along the river), through their crest height and the corresponding hydraulic law (law Z = f(Q), where Z is the water level (m) and Q the flow rate (m^3/s));
- the hydraulic boundary conditions: the upstream hydraulic condition (flow rate at Belleville), the flow rates of the 4 main tributaries, the corrections of flow rate corresponding to little tributaries and exchanges with underground water, and the downstream hydraulic law (law Z = f(Q) at MontJean-sur-Loire. Flow rates were given with a time step of one hour, from the 1st of June to the 31st of December 1999; so, it allowed to compute an initial state in the river with the data of the month of June because the simulation exercise starts only at the 1st of July.
- the tritium discharges for each nuclear power plant, expressed by a tritium flux in kBq/s, and the concentration of tritium coming from the Vienne River (where another NPP is located), with a time step of one hour, from the 1st of June to the 31st of December 1999.
- hydraulic data for calibration: water level measurements and flow rates data collected by the DIREN Centre at low, medium and high flow regimes, and data coming from field water tracings made by the CEA and by EDF, providing information about mean velocities in different parts of the Loire River.

I.3.1.1. Endpoints of the exercise

Water samples were collected every 8 hours in the downstream section of the river basin (city of Angers) from July to December 1999, and were analysed for tritium concentrations.

The results of the modelling (temporal series of the tritium concentration with a time step between one hour and one day) were compared to measurements of tritium concentration made in Angers, located downstream of all the tritium discharges (approx. 59 km downstream of the last nuclear power plant and 52 km downstream of the confluence with the Vienne River).

Intercomparisons of the results provided by the different models at different points along the Loire River were also made.

I.3.2. Information about the measurements

Several locations around Angers (upstream and downstream of the confluence with the Maine River) were studied so as to find the best location for the measurements of tritium and suspended matter concentrations (particularly regarding the transversal homogeneity of the concentrations). Parameters like pH, temperature, dissolved oxygen, conductivity, chlorophyll and particulate organic matter concentration were also analysed.

The most favourable location for collecting samples was the water production plant of the city of Angers, upstream of the confluence with the Maine River.

Water was supplied to the sampling device by a small water pipe on one of the raw water feeder pipes of the plant. Photographs and a schematic view of the setup is given in Figure I.8.

Automatic samplings (by ISCO automatic samplers located in the water treatment plant) were usually made every 8 hours (at 0:00, 08:00 and 16:00) and the analysis was made on a daily composite. When the Loire flow rate was growing up (flow rate day D > flow rate day D-1 and > 1000 m^3/s), the samplings were made every 3 hours, as long as the flow rates were growing up, and the analysis were made on each sample. When the Loire flow rate was decreasing (flow rate day D < flow rate day D-1), even if flow rates were greater than 1000 m^3/s, the samplings were made every 8 hours and the analysis were made on a daily composite.

After filtration of the samples on a 0.45 µm pore-size filter, tritium concentrations were measured, by liquid scintillation counting.

Parameters like pH, temperature, dissolved oxygen, conductivity, chlorophyll and particulate organic matter concentration were also weekly analysed in water collected in the Loire River, at the location of the water production plant.

Figure I.9 presents the measured tritium concentrations in the water of each sample collected at Angers, with their counting uncertainties.

The mean uncertainty of the measurement is 9 %, with values ranging from 0 to 19 %.

Fig. I.8. Snapshots (arrival at the river bank of the raw water feeder pipe of the plant in Loire, water intake for sampling) and schematic view of the experimental setup.

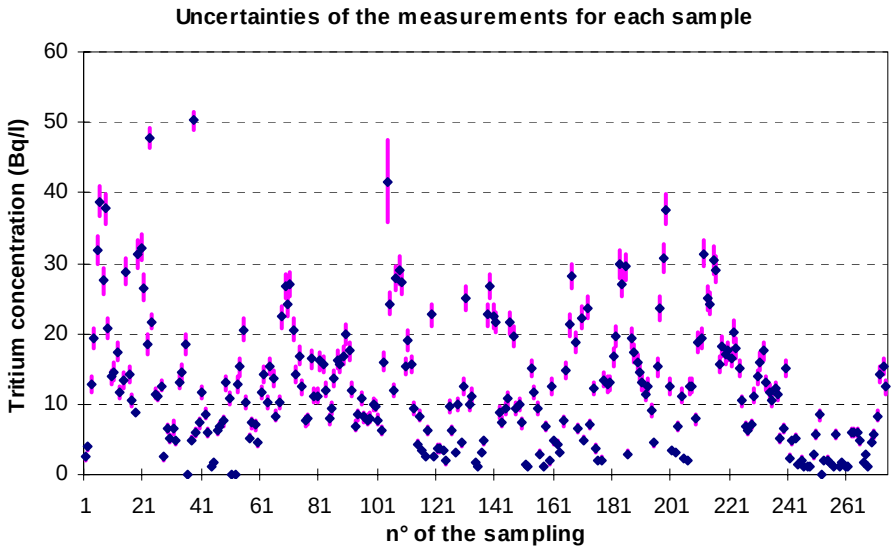

Fig. I.9. Tritium concentrations for each sample collected at Angers.

I.3.3. Description of the schematic scenario

This exercise consists in modelling the dispersion of Belleville NPP tritium discharges in the Loire River (from Belleville to MontJean, which represents a domain length of about 350 km) for 4 different situations (corresponding to real situations of routine releases), covering each a period of time between 9 and 24 days:

- Case 1: low flow rates, long duration tritium release;
- Case 2: low flow rates, short duration tritium release;
- Case 3: increasing flow rates, long duration tritium release; and
- Case 4: high flow rates, short duration tritium release.

The hydraulic boundary conditions are the same as the ones used for the blind test (real hydraulic conditions, from the 1st of July to the 31st of December 1999), with all water discharges from the tributaries taken into account.

Concerning the tritium discharges, we only consider the tritium releases of Belleville nuclear power plant (the first NPP, situated upstream of the Loire River). We selected 4 releases among the real tritium discharge conditions of the considered period (from the 1st of July to the 31st of December 1999).

The 4 studied cases are described in Table I.10 and the corresponding Loire upstream flow rates and Belleville tritium releases appear on the Figure I.10.

The geometric and hydraulic data used for this exercise are the same as the ones provided for the blind test (abscissa of all the objects describing the Loire River, geometry of the Loire River, description of the singularities, hydraulic boundary conditions).

Concerning Belleville tritium discharges, EDF-LNHE gave an input file compiling the 4 selected releases conditions.

Table I.10. Schematic scenarios for tritium migration in Loire River.

Case	Period	Hydraulic conditions	Tritium release conditions (only Belleville NPP)
1	From 20/07/1999 to 13/08/1999	Low flow rate (Loire upstream flow rate between 70 and 120 m^3/s)	Long release (~ 9.5 days)
2	From 08/08/1999 to 22/08/1999	Low flow rate (Loire upstream flow rate between 70 and 120 m^3/s)	Short release (~ 1.5 days)
3	From 16/11/1999 to 29/11/1999	Increasing flow rate (Loire upstream flow rate from 200 to 500 m^3/s)	Long release (~ 5.5 days)
4	From 20/12/1999 to 29/12/1999	High flow rate (Loire upstream flow rate between 500 and 800 m^3/s)	Short release (~ 1 day)

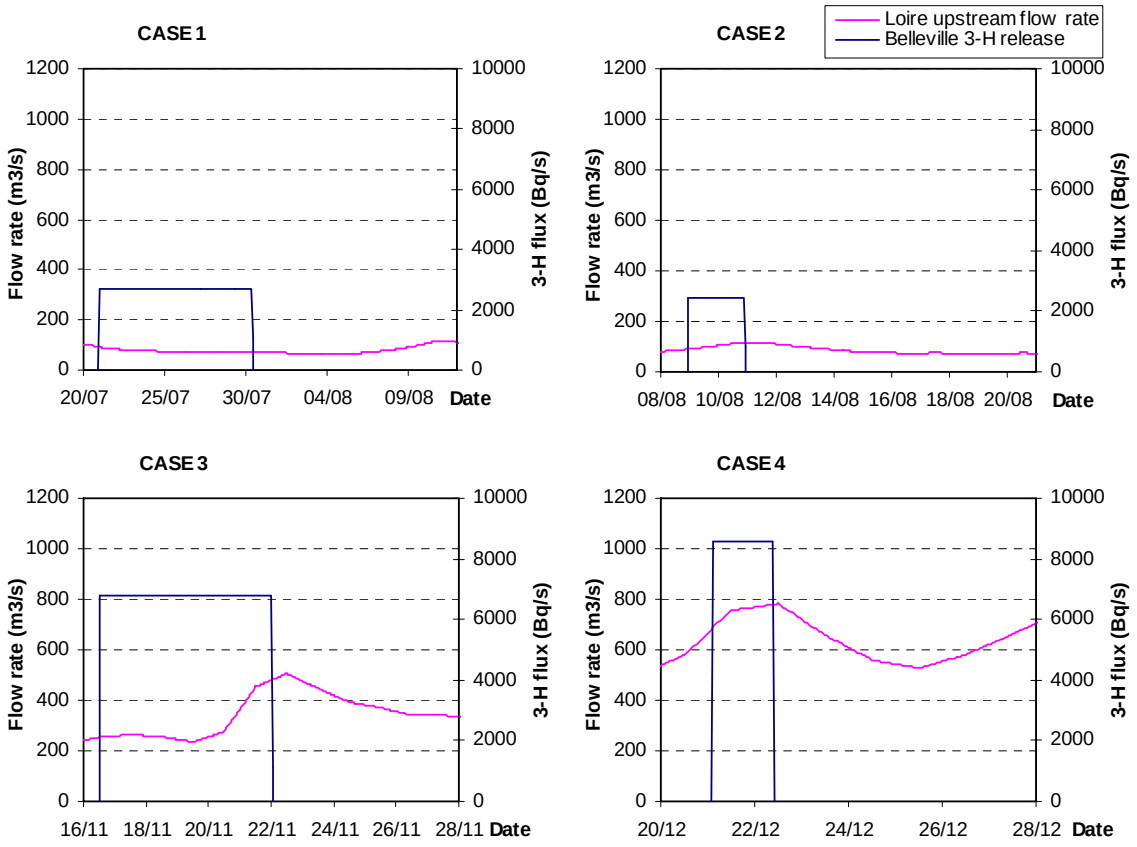

Fig. I.10. For each of the 4 studied cases, Loire upstream flow rate and Belleville tritium discharge.

There were two ways to proceed for this new exercise: either to make 4 simulations for the 4 cases described in Table I.10, or to make a single simulation covering the whole period from the 1st of July to the 31st of December 1999 with the given input file for Belleville discharge (file compiling the 4 releases conditions).

I.3.3.1. Endpoints of the exercise

The end points of this new exercise are the temporal series of tritium concentrations (with a time step of one hour) at 4 different points along the Loire River:

- Gien (approximately 25 km downstream of Belleville nuclear NPP),
- Nouan (approximately 140 km downstream of Belleville NPP),
- Tours (approximately 200 km downstream of Belleville NPP),
- Angers (approximately 320 km downstream of Belleville nuclear power plant and 52 km downstream of the confluence with the Vienne River).

As decided with the participants to this schematic scenario, each participant could present the results of two different modelling.

I.4. Radioactive contamination of the Techa River

I.4.1. Introduction

In the period 1949–1952, about 10^{17} Bq (2.7 MCi) of liquid radioactive wastes was discharged into the Techa River. About 95% of the activity entered into the Techa River during the period from March 1950 to November 1951.

The average daily discharge during this period amounted to 1.5×10^{14} Bq d^{-1} (4000 Ci d^{-1}), with the following radionuclide composition: ^{89}Sr 8.8%; ^{90}Sr 11.6%; ^{137}Cs 12.2%; ^{95}Zr and ^{95}Nb 13.6%; ^{103}Ru and ^{106}Ru 25.9%; isotopes of the rare-earth elements 26.8%; Pu – less 1 %.

The site of discharge into the Techa River was at a distance 200 m downstream from Lake Kyzyltash, and the contaminated waters flowed through Koksharovsky and Metlinsky ponds (water bodies R-3 and R-4) (Figure I.11(a)).

Beginning in 1951, Lake Karachai was used for discharge of technological radioactive solutions. In the following years, radioactive discharges to the Techa River system decreased drastically.

To reduce the radionuclide transport, a system of bypasses and industrial reservoirs for storage of low activity liquid wastes was constructed in the upper reaches of the Techa River during the period 1956–1965 (Figure I.11(b)). General map of the Techa River are shown in Figure I.12.

A number of investigations have been carried out in the territory of the Techa River [I.9–I.40].

The results of these investigations have been used for the development of this Scenario.

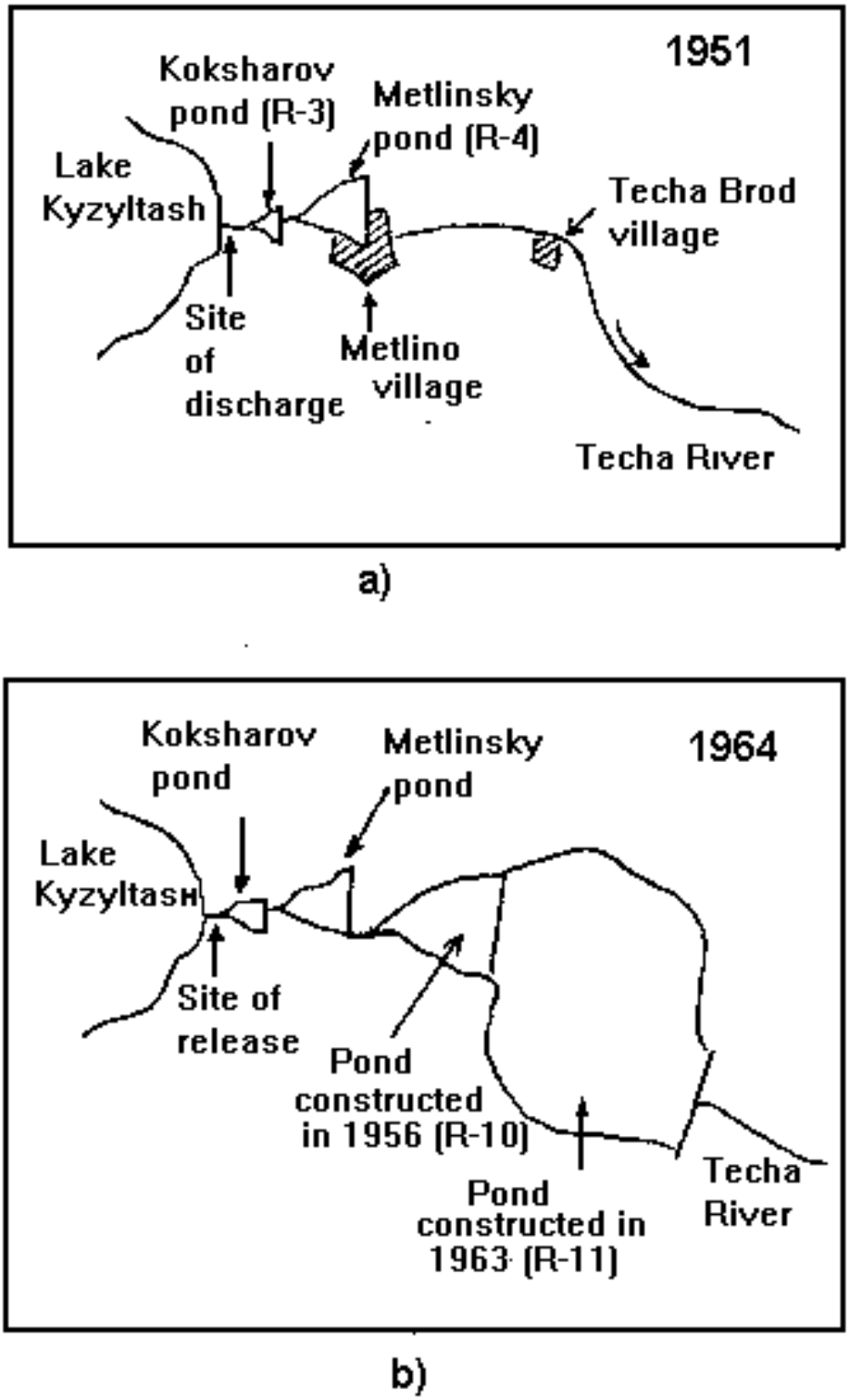

Fig. I.11. Map of the upper reaches of the Techa River in (a) 1951 and (b) 1964.

Fig. I.12. Map of the Techa River[I.39]. Scale: 1 cm = 12.5 km.

I.4.2. Current sources of radionuclide input to the Techa River

A number of factors are contributed to the current radioactive contamination of the Techa River with ^{90}Sr, ^{137}Cs and Pu:

- runoff of radionuclides from the waterlogged floodplain;
- runoff of radionuclides through the bypass canals; and
- filtration of radionuclides through the dam 11.

I.4.2.1. Runoff from the waterlogged floodplain

Downstream of the dam of water body R-11 the Asanov swamps are situated, with an area of about 30 km^2 contaminated with ^{90}Sr, ^{137}Cs and Pu. These swamps are the main source of current input of radionuclides to the Techa River.

The assessments of inventories of ^{90}Sr, ^{137}Cs and ^{239,240}Pu in the floodplain of upstream part of Techa River are presented in Table I.11 [I.10, I.33, I.39].

Densities of activity concentrations of ^{239,240}Pu in soil of the Techa floodplain in 1993 at different distances from the dam 11 are presented in Table I.12 [I.33].

Activity concentrations of ^{90}Sr, ^{137}Cs and ^{239,240}Pu in river bottom sediments are given in Table I.13 [I.33, I.35, I.37, I.41].

Table I.11. The assessments of inventories of ^{90}Sr, ^{137}Cs and $^{239,240}Pu$ in the floodplain of upstream part of Techa River (0–40 km from dam 11) in 1990–1991[I.10, I.33, I.39].

Radionuclide	Inventory, TBq	Interval of uncertainty, TBq
^{90}Sr	40	28–52
^{137}Cs	210	150–270
$^{239,240}Pu$	0.36	0.13–1.67

Table I.12. Density of activity concentrations of $^{239,240}Pu$ in the floodplain soil at the Techa River, kBq/m^2 [I.33].

Distance from dam 11 (km)	Distance from the shoreline (m)		
	0–20	22–40	40–100
4	86 ± 28	3.1 ± 1.7	0.90 ± 0.36
8	37 ± 11	2.9 ± 1.1	0.81 ± 0.42
12	26 ± 2.7	1.4 ± 0.5	0.62 ± 0.45
16	32 ± 13	3.2 ± 1.6	0.63 ± 0.27
20	50 ± 26	3.5 ± 1.3	1.5 ± 1.1
24	100 ± 72	13 ± 11	0.71 ± 0.43
28	160 ± 70	27 ± 4	0.72 ± 0.18
32	130 ± 80	26 ± 16	1.0 ± 0.41
36	54 ± 31	18 ± 9	2.3 ± 1.8
40	90 ± 85	12 ± 11	1.9 ± 1.2
Background (Ural)		0.054 ± 0.036	

Table I.13. Activity concentrations of radionuclides in bottom sediments of the Techa River [I.33, I.35, I.37, I.41].

Distance from dam 11, km	^{137}Cs, kBq/kg	^{90}Sr, kBq/kg	Pu, kBq/kg
7	170	2.5	0.99
14	140	2.1	0.82

I.4.2.2. Runoff through bypass canals

The bypass canals were constructed to regulate the runoff from the catchment area near the technical water bodies. The water runoff from the Kasli-Irtyash system of lakes to the Techa River occurs through the left bank canal constructed in 1963. The runoff of the Mishelyak River occurs now through the right bank canal constructed in 1972. Water entering the Techa River through the bypass canals is contaminated with ^{90}Sr [I.34].

Table I.14 shows the annual water entries from the left bank and right bank canals, and from filtration through the dam 11. Table I.15 shows the annual inputs of ^{90}Sr to the upper part of the Techa River as a result of runoff through bypass canals and filtration through the dam 11.

I.4.2.3. Filtration through dam 11

Activity concentration of ^{90}Sr in the water of water body R-11 is about 2200 Bq/L [I.39]. The dam of water body R-11 does not completely prevent the filtration of water from the water body. During the period 1991–1994, the runoff of ^{90}Sr as a result of filtration through dam R-11 was, on the average, 1.85×10^{10} Bq y^{-1} (Table I.15).

Table I.14. Water balance for the upper reaches of the Techa River (from Dam 11 to Muslyumovo village), 1976–1998, 106 m^3/year [I.35, I.39].

Year	Entering				Water flow (Muslyumovo)
	from LBC	from RBC	with filtration water through Dam 11	total	
1976	2.8	1.5	0.04	4.3	16.8
1977	0.13	3.5	0.04	3.7	9.9
1978	13.4	1.9	0.04	15.3	24.0
1979	21.0	3.6	0.05	24.6	27.4
1980	21.6	16.6	0.05	38.2	43.9
1981	14.5	6.0	0.060	20.5	56.5
1982	10.2	6.3	0.060	16.6	19.6
1983	12.8	9.5	0.065	22.4	46.6
1984	17.1	7.1	0.077	24.3	41.7
1985	14.6	7.5	0.068	22.2	59.6
1986	18.5	10.3	0.084	28.9	55.8
1987	90.1	7.6	0.102	97.8	164.4
1988	51.4	9.5	0.114	61	106.3
1989	55.5	7.2	0.114	62.8	99.3
1990	14.3	12.0	0.113	155.1	224.0
1991	73.9	13.4	0.108	87.4	127.8
1992	101.2	8.9	0.096	110.2	151.8
1993	187.1	14.5	0.11	201.7	265.3
1994	196.5	12.2	0.098	208.8	267.3
1995				63.1	107.3
1996				43.8	70.0
1997				42.5	69.0
1998				37.6	60.5
1999				188.0	
2000				259.0	297.0
2001				235.0	249.0
2002				259.1	335.0
2003				166.3	216.2
2004				61.1	92/2

Note. LBC – Left bank canal, RBC – Right bank canal.

Table I.15. Input sources of ^{90}Sr to the Techa River during 1976–1994, GBq/year [I.39].

Year	LBC	RBC	Filtration through Dam No. 11	Total
1976	252	3.70	37	292
1977	7.40	7.40	0.74	15.5
1978	988	7.40	0.74	996
1979	1560	33.3	1.5	1595
1980	718	77.7	1.5	797
1981	370	4.81	1.7	377
1982	170	31.1	1.9	203
1983	130	50.7	2.6	183
1984	263	20.7	3.7	288
1985	185	29.9	4.4	274
1986	315	27.8	7.4	348
1987	592	24.0	12	629
1988	474	45.1	19	539
1989	685	74.0	21	780
1990	1106	180	16	1356
1991	293	238	18	549
1992	260	242	10	512
1993	455	522	27	1004
1994	437	451	19	907
1995				651
1996				418
1997				858
1998				670
1999				1090
2000				850
2001				2170
2002				2420
2003				1840
2004				1850

Note. LBC – Left bank canal, RBC – Right bank canal.

Table I.16. Estimated annual radionuclide runoff from upstream part of Techa River (0–40 km from dam 11) at Muslyumovo [I.22, I.39].

Radionuclide	Runoff, GBq/year
^{90}Sr	1850 (1100 – 4200)
^{137}Cs	74 (20 – 150)
$^{239,240}Pu$	0.11 (0.04 – 0.5)

I.4.2.4. Radionuclide runoff from upstream part of Techa River

The estimated annual radionuclide runoff from upstream part of Techa River (0–40 km from dam 11) at Muslyumovo are presented in Table I.16 [I.22, I.39].

The total ^{90}Sr discharge to the Techa River has been estimated 1.85 TBq/year, and the main part of this discharge is due to washout from the contaminated Asanov Swamp area. Additional inputs originate from surface run-off via the left and right bank channels and infiltration through dam 11.

The total ^{137}Cs flow through the cross-section at Muslyumovo is approximately 0.074 TBq/year, and $^{239,240}Pu$ is 0.11 GBq/year [I.22].

I.4.3. Hydrological data

At present, a tail reach of the dam of water body 11 must be taken as the source of the Techa River, the length from dam 11 to the river mouth is 207 km. Average slope of the of Techa River is 0.0006 [I.35]. Average altitude of the catchment area is 211 m. The river depth varies from 0.5 m to 2 m. Width of the Techa River varies in range 18–24 m at distances 0–180 km from the dam 11, and at distances 180–207 km from the dam 11 the river width increases to 28–35 m. Catchment area at different parts of the Techa River is: 3690 km^2 at Muslyumovo (44 km from dam 11), 4420 km^2 at Brodokalmak (77 km from dam 11), 7600 km^2 near the river mouth.

The catchment area of the Techa River is located to the west of the Ural range of mountains. The surface of the catchment area is a weakly elevated plain with lots of lakes and bogs. The most abundant soils in the catchment area are gray forest soils and leached black earth. Boggy peat and meadow soils are dominant in the waterlogged plots.

The climate is continental, with considerable variations in the air temperature. Winters are cold and last about 6 months; summers are hot and last about 3 months. The average annual rainfall is 429 mm/year, of which nearly half (up to 200 mm) falls in summer months and about 15% in winter [I.27, I.39]. Distribution of rainfall during a year is shown in Table I.17 [I.39].

The monthly average water flows at two different locations are presented in Table I.18 [I.22, I.25, I.35, I.42]. The maximum water flow is observed in April. Table I.19 shows the monthly average sediment transport and turbidity in the Techa River at Pershinskoe [I.35]. Tables I.20 and I.21 show the average granulometric composition of sediments and suspended matter in the Techa River at Pershinskoe [I.35].

In its hydrochemical regime, the Techa River belongs to the bicarbonate-calcium type. Table I.22 shows the main hydrochemical characteristics of the Techa water at locations Muslyumovo (44 km from dam 11) and Pershinskoe (180 km from dam 11) [I.35].

I.4.3.1. Endpoints for calculations

In Stage 1 of the Scenario, the endpoints are model predictions of the activity concentrations of ^{90}Sr, ^{137}Cs and $^{239,240}Pu$ in water and bottom sediments of the Techa River at different locations downstream of the dam 11.

The input data include: assessments of inventories of ^{90}Sr, ^{137}Cs and $^{239,240}Pu$ in the floodplain of upstream part of Techa River, intake of ^{90}Sr to the river as a result of runoff from bypass canals and filtration through the dam 11, the estimated annual runoff of ^{90}Sr, ^{137}Cs and $^{239,240}Pu$ from upstream part of Techa River, data on the precipitation, hydrological and hydrochemical characteristic of the river.

Endpoints for modelling are given in Tables I.23–I.28.

Table I.17. Distribution of rainfall during a year (averaged long term observations). Mean annual rainfall is 429 mm/year [I.39].

Month	I	II	III	IV	V	VI	VII	VIII	IX	X	XI	XII
Monthly rainfall, % of the annual rainfall	4.0	3.4	3.2	5.0	9.9	14.1	20.0	13.8	9.2	7.3	5.2	4.9

Table I.18. Average water flows on the Techa River at locations Muslyumovo (44 km from dam 11) and Pershinskoe (180 km from dam 11).

Month	Monthly average water flow at Muslyumovo, m^3/s	Monthly average water flow at Pershinskoe, m^3/s
January	0.72	1.48
February	0.56	0.93
March	0.76	1.14
April	9.44	27.5
May	4.71	8.37
June	2.30	4.28
July	2.24	3.58
August	1.68	2.52
September	1.05	1.86
October	1.41	2.24
November	1.03	1.67
December	0.89	1.61

Table I.19. Average sediment transport and turbidity in the Techa River at Pershinskoe (180 km from dam 11).

Month	Water flow, m^3/s	Monthly average sediment transport, kg/s	Turbidity, g/m^3
January	1.48	0.021	14.2
February	0.93	0.0086	9.2
March	1.14	0.013	11.4
April	27.5	5.6	204
May	8.37	0.58	69.3
June	4.28	0.16	37.4
July	3.58	0.11	30.7
August	2.52	0.058	23.0
September	1.86	0.032	17.2
October	2.24	0.046	20.5
November	1.67	0.026	15.6
December	1.61	0.025	15.5

Table I.20. Average granulometric composition of sediments in Techa River at Pershinskoe (180 km from dam 11).

Diameter of particles, mm	10	5	2	1	0.25
Percentage of particles with size less than this fraction, %	100	81	78	72.4	26.2

Table I.21. Average granulometric composition of suspended matter in Techa River at Pershinskoe (180 km from dam 11).

Diameter of particles, mm	0.004	0.008	0.0016	0.0032	0.063	0.125	0.25	0.5	1
Percentage of particles with size less than indicated, %	3.9	9.1	14.2	25.3	43.9	57.5	90.1	94.8	100

Table I.22. Hydrochemical characteristics of the Techa River.

Parameter	Muslyumovo	Pershinskoe
pH	7.3	7.3
Ca^{2+} (mg L^{-1})	Spring 36.6 Summer 63.2 Winter 64.1	Spring 41.0 Summer 58.7 Winter 63.2
Mg^{2+} (mg L^{-1})	Spring 13.3 Summer 31.2 Winter 19.3	Spring 15.9 Summer 51.1 Winter 21.3
$Na^{+} + K^{+}$ (mg L^{-1})	Spring 18.2 Summer 28.5 Winter 32.3	Spring 27.8 Summer 26.9 Winter 35.2

Table I.23. Activity concentrations of ^{239,240}Pu in water of the Techa River at different locations.

Point	Distance from the dam 11, km	Activity concentration of ^{239}Pu, mBq/L	^{240}Pu/^{239}Pu atom ratio
Asanov	7	2.44± 0.44	<0.03
Muslyumovo	44	0.25 ± 0.03	0.24
Brodokalmak	77	0.13 ± 0.03	0.21
Verkhnyaya Techa	142	0.092 ± 0.015	–
Zatecha	205	0.055 ± 0.007	0.32

Table I.24. Activity concentrations of ^{90}Sr in water of the Techa River at different locations.

Point	Distance from the dam 11, km	Activity concentration of ^{90}Sr, Bq/L
Muslyumovo	44	18 ± 5
Russkaya Techa	106	14 ± 4
Verkhnyaya Techa	142	11 ± 4
Pershinskoe	180	10 ± 3
Zatecha	205	8 ± 2

Table I.25. Activity concentrations of ^{137}Cs in water of the Techa River at different locations.

Point	Distance from the dam 11, km	Activity concentration of ^{137}Cs, Bq/L
Muslyumovo	44	0.43 ± 0.12
Brodokalmak	77	0.31 ± 0.11
Russkaya Techa	106	0.23 ± 0.09
N. Petropavlovka	116	0.12 ± 0.05
Verkhnyaya Techa	142	0.12 ± 0.04
Pershinskoe	180	0.09 ± 0.02
Zatecha	205	0.07 ± 0.02

Table I.26. Activity concentrations of ^{239,240}Pu in surface bottom sediments (0–2 cm) of the Techa River at different locations from dam 11.

Point	Distance from the dam 11, km	Activity concentration of ^{239,240}Pu, Bq/kg dry weight	^{240}Pu/^{239}Pu atom ratio
Asanov	7	990± 180	0.0188± 0.0053
Muslyumovo	44	40 ± 12	0.035± 0.0087
Brodokalmak	77	17 ± 6	0.0933± 0.0087
Verkhnyaya Techa	142	3.2 ± 1.1	–
Zatecha	205	1.2 ± 0.7	0.0995± 0.0078

Table I.27. Activity concentrations of ^{90}Sr in surface bottom sediments of the Techa River at different locations from dam 11.

Point	Distance from the dam 11, km	Activity concentration of ^{90}Sr, Bq/kg dry weight
Muslyumovo	44	670 ± 190
Russkaya Techa	106	
Verkhnyaya Techa	142	150 ± 60
Pershinskoe	180	
Zatecha	205	200 ± 72

Table I.28. Activity concentrations of ^{137}Cs in surface bottom sediments of the Techa River at different locations from dam 11.

Point	Distance from the dam 11, km	Activity concentration of ^{137}Cs, Bq/kg dry weight
Verkhnyaya Techa	142	590 ± 70
Zatecha	205	200 ± 10

I.5. Modelling ^{226}Ra self-cleaning in the Huelva Estuary

Note: Data files may be downloaded from the EMRAS web page (***http://www-ns.iaea.org/projects/emras/emras-aquatic-wg.htm***.

I.5.1. Description of the characteristics of the estuary

The estuary of Huelva is a tidal, full mixed estuary. The strength of tidal currents and the shallow waters, maximum depth around 20 m, produce an effective mixing in the vertical direction. Moreover, the flows of the Odiel and Tinto Rivers are very low, and a fast dispersion of fresh water into a much larger volume of sea water occurs. This mixing also occurs upstream of the area of interest of both rivers, thus horizontal gradients of salinity can be neglected as well. Indeed, average electrical conductivity of water over the estuary is 38.42±0.25 $mScm^{-1}$.

Tidal constants[1] for the two main constituents, M_2 and S_2 are given in Table I.29. The variability of river flows during a typical year is given in Table I.30.

Measured water currents are available for the M_2 tide at five points in the estuary. Such points are indicated in the map in Figure 1.5 as black triangles. The values measured for the currents are given in Table I.31.

The effects of winds can generally be neglected in comparison with mixing produced by tides. Residual (averaged) currents produced by river flows are typically of the order of 1 cm s^{-1}.

1 Tides can be represented as a number of harmonic functions (denoted constituents), each one characterized by its angular speed, amplitude and phase. Thus, the water surface elevation *z(t)* at any time *t* is given by $z(t)=\sum_{i=1}^{N} h_i \cos(w_i t - g_i)$ were *N* is the number of harmonics included and h_i, w_i and g_i are the amplitude, angular speed and phase, respectively, of each harmonic. In our practical case it is enough to include only the two main constituents, denoted as M_2 and S_2. The sub index 2 refers to the fact that there are two cycles each day. Thus they are denoted as semidiurnal tides.

The bathymetry is provided in file *depth.dat*, which is an ASCII file consisting of three colums *i,j,d(i,j)* where *i* and *j* are the indexes of the grid cell (column and row starting from the down left corner) and *d(i,j)* is the corresponding water depth in meters. Index *i* runs from 1 to 60 and index *j* runs from 1 to 86. Note that the depth is given as a negative number, while the corresponding value for a land cell is zero. The datum[2] is already included in the provided depths (1.85 m in the case of Huelva). Resolution of data is $\Delta x=\Delta y=125$ m. The bathymetric data are somewhat schematic due to the lack of information in some parts of the estuary, but is enough for the modelling purposes of the exercise.

I.5.2. Sediment characteristics

Limited information is available on this point. In some of the sampling points indicated in the map of Figure I.13, bulk density, organic matter content and fraction of muds (particles <63 μm) were measured for the samples collected in 1991. Results are given in Table I.32. A mixed surface sediment layer of 10 cm may also be assumed.

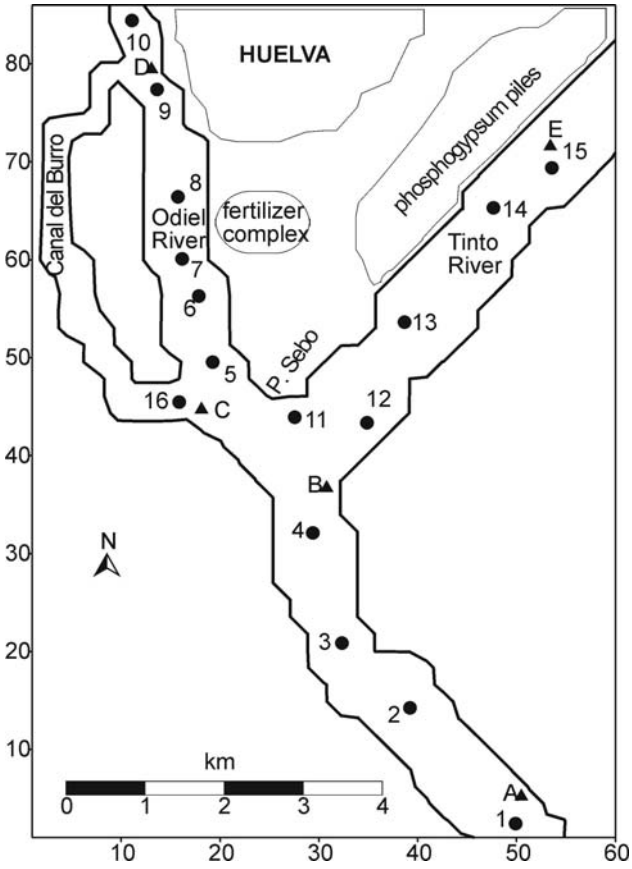

Fig. I.13. Map of Huelva estuary.

2 Water depths that can be read in all bathymetric charts are referred to the lowest water level that may occur. To obtain the average water depth, the datum must be added to the depth provided in the chart. In the case of Huelva, it is 1.85 m as mentioned above. Thus the datum is the difference between the average and minimum possible water levels.

Table I.29. Tidal angular speeds and constants for the two main constituents at the entrance of the estuary.

Tidal consituent	w (degree/h)	A (m)	g (degrees)
M_2	28.9841	1.20	45
S_2	30.0000	0.37	58

Table I.30. Water flows ($m^3\ s^{-1}$) for both rivers during a typical year.

River	January	February	March	April	May	June
Odiel	12	4	3	9	2	4
Tinto	0.2	0.1	0.09	0.4	0.04	0
River	**July**	**August**	**September**	**October**	**November**	**December**
Odiel	0.5	0.4	1	2	66	4
Tinto	0	0	0.3	0	2.7	0.3

Table I.31. Measured values of the M2 current magnitude and direction. The direction is measured anticlockwise from east.

Point	Current (m/s)	Direction (deg)
A	0.66	127
B	0.56	127
C	0.67	142
D	0.49	162
E	0.48	52

Table I.32. Bulk sediment density and contents of organic matter and muds for some sampling points indicated in Figure I.14 and for the 1991 campaign.

Sample	Density (gcm^{-3})	Organic matter (%)	Muds (%)
4	0.431	11.5	71
5	0.625	9.6	40
6	0.403	13.0	71
7	0.553	9.7	48
8	1.006	11.6	1
9	0.610	8.2	59
10	1.425	3.0	–
12	0.613	10.9	94
13	0.616	11.7	39
15	0.685	9.0	89

Table I.33. Suspended sediment concentrations measured along the estuary in 1991 for low water conditions. Errors are below 5% in all cases.

Sample	4	5	6	7	8	9	10	12	13	14
M (mg/L)	2.7	3.7	3.7	4.7	2.4	4.6	4.6	3.8	11.4	6.7

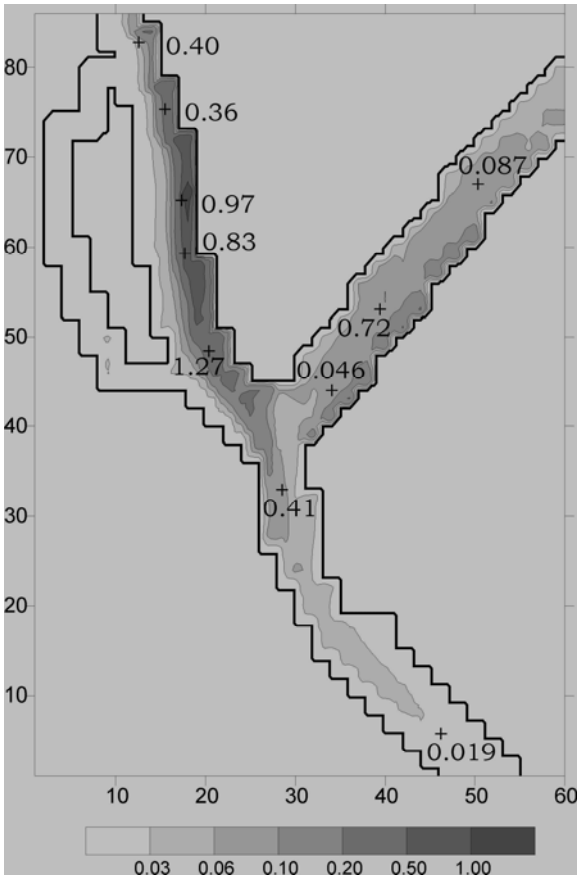

Fig. I.14. Initial conditions for the simulation; ^{226}Ra concentration in the bed sediment (Bq g^{-1}). Crosses indicate points where measurements were available and numbers correspond to the measured concentrations.

The concentrations of suspended sediments in the estuary depend on tidal state. Thus minimum concentrations are expected during high and low water due to sedimentation during slack water periods. During ebb and flood periods, higher currents produce some erosion of the bed sediment. Seasonal variations must be expected as well. Nevertheless, net sedimentation rates are small and these processes have been neglected in previous modelling studies. As an indication, suspended sediment concentrations along the estuary measured during low water in the 1991 campaign are given in Table I.33.

I.5.3. Transfer coefficients for water-sediment interactions

The k_d distribution coefficient for ^{226}Ra in the estuary has been measured along the Odiel and Tinto Rivers in sampling campaigns carried out in 1990 and 1991. The average value for both campaigns and the complete estuary is $(9\pm4)\times10^3$ L kg^{-1} (36 samples). The maximum value is $(132\pm12)\times10^3$ L kg^{-1} and the minimum one is $(0.216\pm0.018)\times10^3$ L kg^{-1}.

Kinetic rates have been obtained from experiments performed at the University of Seville using ^{133}Ba (chemical behaviour similar to radium) and water and sediment collected from the estuary. Experiments were carried out preserving the conditions of the estuary (pH, light, temperature) as close as possible to the natural conditions. The kinetic coefficient k_1 given below is normalized to a unit sediment concentration, since the uptake process depends on the amount of matter available to adsorb radionuclides. The release coefficient k_2 is not normalized. The following values were obtained:

$$k_1=4.21\times10^{-6}\ m^3\ s^{-1}\ kg$$
$$k_2=8.17\times10^{-6}\ s^{-1}$$

Experiments were carried out with a sediment concentration equal to 39 mg L^{-1}. Thus, the real value of k_1 for the experiment, with such particular sediment amount, is $1.64\times10^{-7}\ s^1$

It is also possible to use a kinetic model consisting of two reactions, a fast and a slow process. The first reaction describes a reversible isotopic or ion exchange process between dissolved radionuclides and some non-specific sites on particle surface. The second and slower process represents a reversible sorption from non-specific to more specific sites (consecutive reactions in this case). The second reaction is assumed to be governed by forward and backward rates k_3 and k_4 respectively. From experiments carried out with water and sediments collected from the estuary, the following values may be accepted:

$$k_3=1.4\times10^{-7}\ s^{-1}$$
$$k_4=1.4\times10^{-8}\ s^{-1}$$

I.5.3.1. Simulation endpoint

The objective of the present exercise is to simulate the self-cleaning process that has been observed after the fertilizer plants stopped releasing their wastes directly into the estuary. The result provided by the models should be a file consisting of three columns: time (days), concentration in solution averaged over all the estuary (Bq m^{-3}) and total inventory in the bed sediment (Bq).

I.5.3.2. Initial and boundary conditions

Initial conditions are provided in file *initial.dat* that consists of 5 columns: *i* and *j* indexes of the cell, specific activity in water (Bq m^{-3}), specific activity in the bed sediment (Bq g^{-1}) and activity fraction that is in the sediment in a slowly reversible phase (data required if a two reaction model is going to be applied). These initial conditions can be considered as the state of contamination over the estuary at the moment when the fertilizer complex stopped discharging wastes in 1998. They have been obtained from the University of Seville model when applied to simulate the contamination of the estuary using the releases from the complex as source term. Computed concentrations have been compared with available measured ^{226}Ra concentrations in the bed sediment [I.43] to assess that initial conditions are realistic (see Figure I.14). The different models participating in the exercise are run starting from these initial conditions and without any external source of Ra. Thus, it may be observed if the system evolution leads to a self-cleaning process.

Boundary conditions must be specified for the dissolved Ra concentrations along the three open boundaries of the domain. Measured concentrations may be used. They are given in Table I.34.

Table I.34. Measured ^{226}Ra concentrations in water at (or as close as possible) the three open boundaries of the computational domain.

Boundary	**Dissolved ^{226}Ra (Bq m^{-3})**
east	3.8±0.8
north	5.4±1.2
south	4.2±0.8

REFERENCES

[I.1] VOYTSEKHOVICH, O.V., BORZILOV, V.A., KONOPLEV, A.V., Hydrological Aspects of Radionuclide Migration in Water Bodies Following the Chernobyl Accident, Proceedings of Seminar on Comparative Assessment of the Environmental Impact of Radionuclides Released during Three Major Nuclear Accidents: Kyshtym, Windscale, Chernobyl, Luxembourg, 1–5 October 1990, 1, pp. 527–548 (1990).

[I.2] LAPTEV, G.V., VOITSEKHOVICH, O.V., Experimental studies of radionuclide washout from Pripyat floodplain soils in conditions of flooding, Proceedings of UHMI, 245, pp. 127–143 (1993).

[I.3] BULGAKOV, A.A., KONOPLEV, A.V., POPOV, V.E., SCHERBAK, A.V., Removal of long-lived radionuclides from the soil by surface runoff near the Chernobyl nuclear power station, Soviet Soil Sci., 23:124–131 (1991).

[I.4] POPOV, V.E., KUTNYAKOV, I.V., ZHIRNOV, V.G., VIRCHENKO, E.P., SIVERINA, A.A., BOBOVNIKOVA, TS.I., ^{90}Sr and ^{137}Cs chemical forms in alluvial soils of strontium spot on the left bank floodplain of Pripyat River in the vicinity of the Chernobyl NPP, Proceedings of Institute of Experimental Meteorology, 22 (158), pp. 180–189 (1993).

[I.5] KOSTYANITSYN, M.N., Hydrology of the Dnieper and Southern Bug Estuary, M. Gidrometeoizdat., 336 p (1964) (in Russian).

[I.6] ZHYKINSKY, V.N., The Dnieper and Bug Estuary Ecosystem, Kyiv, Naukova Dumka, 239 p (1989) (in Russian).

[I.7] KANIVETS V.V., VOITSEKHOVICH O.V., SIMOV, Radioactive contamination of the Black and Azov seas, In: Voitsekhovich O.V. (ed.) Radioecology of water objects of the Chernobyl NPP accident impact area, Chernobylinterinform, Kiev, 127–151 (1997) (in Russian).

[I.8] KATRICH I.YU., NIKITIN A.I., MEDINETS V.I., LEPESHKIN V.I., KABANOV A.I., SEMKO, N.N., BAZHANOV, V.N., Dynamics of the radioactive contamination caused by CNPP accident on observed data 1986–1990, In: Borzilov V.A., Kryshev I.I. Ecological and hydrophysical consequences of the nuclear accidents, Hydrometerological Publ., Moscow, p. 57–61 (1992) (in Russian).

[I.9] ACADEMY OF SCIENCE, Conclusion of the Commission on the estimation of the ecological situation in the region of production association “Mayak”, organized by the direction of the Presidium of the Academy of Science, Russia J. Radiobiology 31:436–452 (1991) (in Russian).

[I.10] AARKROG, A., TRAPEZNIKOV, A.V., MOLCHANOVA, I.V., YUSHKOV, P.I., POZOLOTINA, V.N., POLIKARPOV, G.G., DAHLGAARD, H., NIELSEN, S., Environmental modelling of radioactive contamination of floodplains and sorlakes along the Techa and Iset Rivers, J. Environmental Radioactivity 49:243–257 (2000).

[I.11] AKLEEV, A.V., KOSTYUCHENKO, V.A., PEREMYSLOVA, L.M., BATURIN, V.A., POPOVA, I.YA., Radioecological impacts of the Techa River contamination, Health Physics 79(1):36–47 (2000).

[I.12] AKLEYEV, A.V., KISSELJOV, M.F., (Eds.), Medical-Biological and Ecological Impacts of Radioactive Contamination of the Techa River, Russian Federation Health Ministry, Federal Office of Medical-Biological Issues and Emergencies, Urals Research Center for Radiation Medicine (URCRM), Chelyabinsk (2002).

[I.13] BURKART, W., GOLOSHAPOV, P., KONIG, K., MUNDIGL, S., ROMANOV, G.N., Intercomparison and validation exercises in the Southern Urals and the Kazakh Polygon, Radioprotection 32(2):197–208 (1997).

[I.14] CABIANCA, T., BEXON, A.P., POZOLOTINA, V., TRAPEZNIKOV, A., SIMMONDS, J., Preliminary assessment of current radiation doses to the population of Brodokalmak from contamination of the Techa River, J. Environmental Radioactivity 50:193–206 (2000).

[I.15] CHESNOKOV, A.V., GOVORIN, A.P., LINNIK, V.G., SHCHERBAK, S.V., ^{137}Cs contamination of the Techa River floodplain near village of Muslumovo, J. Environmental Radioactivity 50:179–191 (2000).

[I.16] CHUMICHEV, V.B., DEM'YANCHENKO, Z.A., Contamination with ^{90}Sr and radionuclide discharges into the Techa, Karabolka (1974–1990) and Ob' (1961–1990) Rivers, Environmental Radioactivity in the Arctic and Antarctic. Osteras, pp. 110–113 (1993).

[I.17] CHUMICHEV, V.B., NIKITIN A.I., KRYSHEV, I.I., Plutonium in the components of the river system Techa-Ob, In: Proceedings of the 5th International Conference on Radiation Researches, Section "Radioecology", 10–14 April 2006, Moscow (2006).

[I.18] DEGTEVA, M.O., KOZHEUROV, V.P., VOROBIOVA, M.I., General approach to dose reconstruction in the population exposed as a result of the release of radioactive wastes into the Techa River, The Science of the Total Environment 142:49–61 (1994).

[I.19] DEGTEVA, M.O., KOZHEUROV, V.P., BURMISTROV, D.S., VOROBIOVA, M.I., VALCHUK, V.V., BOUGROV, N.G., SHISHKINA, H.A., An approach to dose reconstruction for the Ural populations, Health Physics 71(1)71–76 (1996).

[I.20] ILYIN, L.A., GUBANOV, V.A., (Eds.), Severe radiation accidents: consequences and countermeasures, Izdat, Moscow, 752 pp (2001) (in Russian).

[I.21] ILYIN, L.A., GUBANOV, V.A., (Eds.), Large radiation accidents: consequences and protective countermeasures. Izdat, Moscow, 555 pp (2004) (in English).

[I.22] NORWEGIAN RADIATION PROTECTION AUTHORITY, Impacts on man and the environment in nirthern areas from hypothetical accidents at "Mayak" PA, Urals, Russia, Published by the Joint Norwegian-Russian Expert Group for Investigation of Radioactive Contamination in the Northern Areas, NRPA, Osteras, pp. 1–104 (2004).

[I.23] KRYSHEV, I.I., Some problems of the risk assessment for the Ural radioactive pattern, Russian Academy of Natural Sciences, Environmental Division (4):44–52 (1996a) (in Russian).

[I.24] KRYSHEV, I.I., Radioactive contamination of aquatic ecosystems in the areas of Nuclear Power Plants and other nuclear facilities in Russia, Radiochimica Acta 74:199–202 (1996b).

[I.25] KRYSHEV, I.I., (Ed.), Environmental Risk Analysis for the Ural Radioactive Pattern, Nuclear Society, Moscow, pp. 1–214 (1997).

[I.26] KRYSHEV, I.I., SAZYKINA, T.G., ISAEVA, L.N., Risk assessment from contamination of aquatic ecosystems in the areas of Chernobyl and Ural radioactive patterns, Radiation Protection Dosimetry 64(1/2):103–107 (1996).

[I.27] KRYSHEV, I.I., ROMANOV, G.N., SAZYKINA, T.G., ISAIEVA, L.N., KHOLINA, YU.B., Radioecological problems of the Southern Urals, Nuclear Society of Russia, Moscow, 118 pp (1997) (in Russian).

[I.28] KRYSHEV, I.I., ROMANOV, G.N., CHUMICHEV, V.B., SAZYKINA, T.G., ISAEVA, L.N., IVANITTSKAYA, M.V., Radioecological consequences of radioactive disharges into the Techa River on the Southern Urals, J. Environ. Radioactivity 38(2):195–209 (1998a).

[I.29] KRYSHEV, I.I., ROMANOV, G.N., SAZYKINA, T.G., ISAEVA, L.N., TRABALKA, J.R., BLAYLOCK, B.G., Environmental contamination and assessment of doses from radiation releases in the Southern Urals, Health Physics 74(6):687–697 (1998b).

[I.30] KRYSHEV, I.I., SAZYKINA T.G., MONTE, L., Scenario on River Techa contamination for model validation, Implementing computersed methodologies to evaluate the effectiveness of countermeasures for restoring radionuclide contaminated fresh water ecosystems, ENEA, ISSN/1120/5555, p. 51–65 (2001).

[I.31] KRYSHEV, I.I., RYAZANTSEV, E.P., Ecological Safety of the Nuclear Energy Complex of Russia. Izdat, Moscow (2000) (in Russian).

[I.32] MAKHON'KO, K.P., (Ed.), The Radiation Situation in the Territory of Russia and Contiguous States in 1992–1996, Yearbooks, Obninsk, SPA "Typhoon" (1993–1998) (in Russian)

[I.33] MARTYUSHOV, V.V., SPIRIN, D.A., BAZYLEV, V.V., POLYAKOVA, V.I., MEDVEDEV, V.P., MARTYUSHOVA, L.N., PANOVA, L.A., TEPLYAKOV, I.G., Radioecological aspects of the behavior of long-lived radionuclides in the floodplain landscapes of the Techa River upstream water, Ecology 5:341–368 (1997).

[I.34] MOKROV, YU.G., Prediction of the transfer of ^{90}Sr with the Techa River waters, Part 1, The Problems of Radiation Safety, No. 1, pp. 20–27 (1996) (in Russian).

[I.35] MOKROV, YU.G., Reconstruction of the Techa River Radioactive Contamination, Part 1, The Role of the Weighed Particles in the Process of the Techa River Radioactive Contamination Formation in 1949–1951, Library of the Journal "The Problems of Radiation Safety", No. 1. Ozersk, 172 pp (2002) (in Russian).

[I.36] MOKROV, YU., GLAGOLENKO, YU., NAPIER, B., Reconstruction of radionuclide contamination of the Techa River caused by liquid waste discharge from radiochemical production at the Mayak Production Association, Health Physics 79(1):15–23 (2000).

[I.37] OUGHTON, D.H., FIFIELD, L.K., DAY, J.P., CRESSWELL R.C., SKIPPERUD, L., DI TADA, M.L., SALBU, B., STRAND, P., DROZCHO, E., MOKROV, YU., Plutonium from Mayak: Measurement of isotope ratios and activities using accelerator mass spectrometry, Environmental Science and Technology, 34, 1938–1945 (2000).

[I.38] SKIPPERUD, L., SALBU, B., OUGHTON, D.H., DROZCHO, E., MOKROV, YU., STRAND, P., Plutonium contamination in soils and sediments at Mayak PA, Russia, Health Physics, 89, 3, 255–266 (2005).

[I.39] NORWEGIAN RADIATION PROTECTION AUTHORITY, Sources Contributing to Radioactive Contamination of the Techa River and Areas Surrounding the "Mayak" Production Association, Urals, Russia, Published by the Joint Norwegian-Russian Expert Group for Investigation of Radioactive Contamination in the Northern Areas, NRPA, Osteras, pp. 1-134 (1997).

[I.40] TRAPEZNIKOV, A.V., POZOLOTINA, V.N., CHEBOTINA, M.YA., CHUKANOV, V.N., TRAPEZNIKOVA, V.N., KULIKOV, N.V., NIELSEN, S.P., AARKROG, A., Radioactive Contamination of the Techa River, the Urals, Health Physics 65:481–488 (1993).

[I.41] TRAPEZNIKOV, A.V., POZOLOTINA, V.N., YUSKOV P.I., et al., Study of radioecological situation in the Rivers Techa and Iset contaminated by discharges of PA "Mayak", Problems of radioecology and boundary sciences, 2:20–66 (1999).
[I.42] Resources of Surface Water, Gidrometeoizdat, Leningrad (1986) (in Russian).
[I.43] ABSI, A., VILLA, M., MORENO, H.P., MANJÓN, G., PERIÁÑEZ, R., Self-cleaning in an estuarine area formerly affected by ^{226}Ra anthropogenic enhancements, Science of the Total Environment 329, 183–195 (2004).

APPENDIX II. DESCRIPTIONS OF THE MODELS

II.1. Wash-off of Chernobyl ^{90}Sr and ^{137}Cs from the floodplain into the Pripyat River

II.1.1. University of Seville Floodplain Model

Raul Periañez and Haydn Barros, Departamento Física Aplicada, E.U. Ingenieria Técnica Agrícola, Universidad de Sevilla, Spain

A 2D depth-averaged model has been used. The model solves the hydrodynamic equations over the domain to obtain water circulation. The output from the hydrodynamic model is used to solve the advection/diffusion dispersion equation for radionuclides, including exchanges with bed sediments. Depth-averaged shallow water hydrodynamic equations may be written in the form:

$$\frac{\partial z}{\partial t} + \frac{\partial}{\partial x}(Hu) + \frac{\partial}{\partial y}(Hv) = 0$$

$$\frac{\partial u}{\partial t} + u\frac{\partial u}{\partial x} + v\frac{\partial u}{\partial y} + g\frac{\partial z}{\partial x} - \Omega v + k\frac{u\sqrt{u^2+v^2}}{H} = 0$$

$$\frac{\partial v}{\partial t} + u\frac{\partial v}{\partial x} + v\frac{\partial v}{\partial y} + g\frac{\partial z}{\partial y} + \Omega u + k\frac{v\sqrt{u^2+v^2}}{H} = 0 \qquad \text{(II.1)}$$

where u and v are the components of the water current along x and y axis, H is depth of the water column and z is the displacement of the water surface: H=z-d, where d is topographic height read from the file "FP_GK5.xyz". Ω is the Coriolis parameter and k is a bed friction coefficient obtained from model calibration. Equations have been solved by finite differences on a grid covering the floodplain area with a resolution Δx=Δy=200 m. A steady-state approach has been assumed. Thus, the hydrodynamic model has been forced by constant surface elevations along input and output cross sections and calculations are continued until a steady-state for currents and elevations is obtained for the whole model domain. Elevations at input and output sections have been obtained from elevation at point D3 and assuming a water surface slope of 4 cm per running km, as shown by hydraulic calculations performed by UHMI. Once the steady-state is obtained, currents and depths over the domain are stored in a file that will be used by the radionuclide dispersion model.

The following open boundary conditions have been applied to the water current component that is normal to the boundary:

$$\frac{\partial q}{\partial \eta} = 0 \qquad \text{(II.2)}$$

where q is the current component normal to the boundary and η is the direction that is normal to the boundary.

The calibration of the bed friction coefficient has been made in the following form: it was changed by trial and error until the computed water discharge through the output section was as close as possible to the measured discharge. Using k=0.030 a discharge equal to 483.4 m^3/s is computed, that can be compared with discharge measured during the first flood event.

The computed steady-state currents for the first flood event (1991 ice jam) are shown in Figure II.1 as an example.

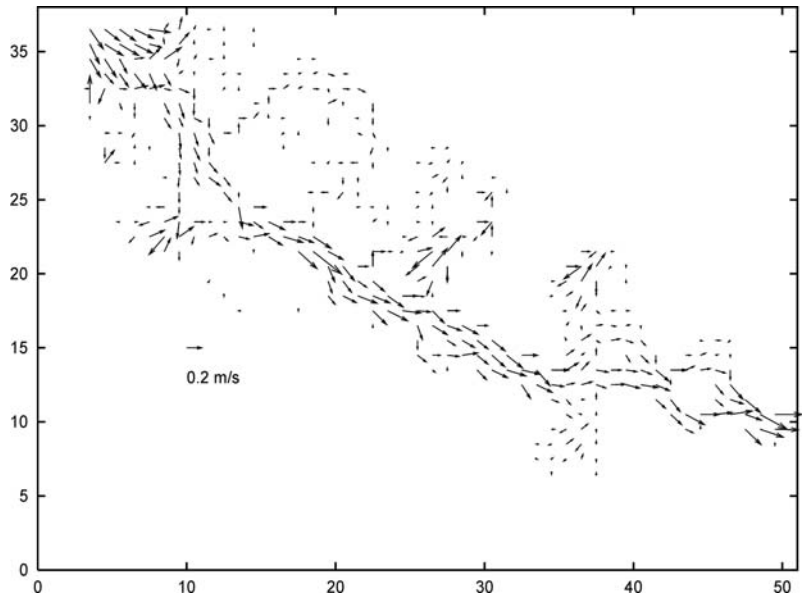

Fig. II.1. Computed steady currents. Each unit in the axis corresponds to 200 m.

The exchanges of radionuclides between the liquid and solid phases are described by means of kinetic coefficients. Thus, a k_1 coefficient governs the transfer from the dissolved to the solid phase and a coefficient k_2 governs the inverse process. Two kinetic models have been tested, a 1-step model consisting of a single reversible reaction and a 2-step model consisting of two consecutive reversible reactions.

The adsorption of radionuclides depends on the available surface of particles per water volume unit:

$$k_1 = \chi_1 S \tag{II.3}$$

where χ_1 is a coefficient with the dimensions of a velocity (denoted exhange velocity) and S is the specific surface (dimension L^{-1}). It can be written, assuming spherical particles with average radius R, and for the bed sediment as:

$$S = \frac{3L\Psi}{RH}(1-\Phi) \tag{II.4}$$

where L is the average mixing depth (the sediment depth to which the water fraction exchanges radionuclides with it), Φ is sediment porosity and Ψ is a correction factor that takes into account that not all the sediment particle surface is in contact with water (and in consequence available for exchanging radionuclides) since can be partially hidden by other sediment particles.

In the first model version (3C), suspended particles, deposition of these particles and erosion of the sediment/soil have not been included. As a consequence, the dispersion model solves the equations that give the time evolution of activity concentration in the water phase and in the sediment/soil. This model was applied to the 1991 flooding (blind test).

Advection and diffusion terms are written in the following form:

$$adv = -\frac{1}{H}\left(\frac{\partial(C_d H)}{\partial x} + \frac{\partial(C_d H)}{\partial y}\right)$$
$$dif = \frac{1}{H}\left(\frac{\partial}{\partial x}\left(HK\frac{\partial C_d}{\partial x}\right) + \frac{\partial}{\partial y}\left(HK\frac{\partial C_d}{\partial y}\right)\right) \quad \text{(II.5)}$$

where K is a horizontal diffusion coefficient. This coefficient depends on grid size, following classical relations, and results K=0.091 m^2/s.

The University of Seville 3C model considers that exchanges are governed by two consecutive reversible reactions. Surface adsorption is followed by another slower process that may be a slow diffusion of ions into pores and interlattice spacings, inner complex formation or a transformation such an oxidation. Thus, sediments/soils are divided in two phases: a reversible and a slowly reversible fraction. The equations that give the time evolution of activity concentrations in the three phases are:

$$\frac{\partial C_d}{\partial t} = (adv + dif) - k_1 C_d + k_2 \frac{A_r L\rho(1-\Phi)\Psi}{H}$$
$$\frac{\partial A_r}{\partial t} = k_1 \frac{C_d H}{L\rho_s} - k_2 A_r \Psi - k_3 A_r + k_4 A_{sr}$$
$$\frac{\partial A_{sr}}{\partial t} = k_3 A_r - k_4 A_{sr} \quad \text{(II.6)}$$

where the advection and diffusion terms are written as before and Ar and Asr are activity concentrations in the reversible and slowly reversible, respectively, fractions of sediments. k_3 and k_4 are the forward and backward rates governing the second reaction. Finally, ρ is particle density and $\rho s=\rho(1-\phi)$ is sediment bulk density.

Boundary conditions must also be provided to solve the dispersion equations. In the input section, activity concentrations in water are specified from the measurements. Along the output section, a condition of zero gradients along the normal direction (as in the case of water currents) is used. Activity concentrations in the bed are obtained from the file "FP_CS137.DAT". However, in the case of the main stream bed (sediments that are always covered by water) such values are not used since these sediments have been washed by the permanent water flow. Thus, their activity concentrations have been deduced from concentration in the water phase assuming equilibrium between them. Activity concentrations included in provided files have been corrected by radioactive decay.

The exchange velocity and k_2 are not free parameters, but are bound through the equilibrium distribution coefficient through the following relation:

$$k_d = \frac{\chi_1}{k_2}\frac{3}{\rho R} \quad \text{(II.7)}$$

where k_d is the equilibrium distribution coefficient. It has been found that parameter k_2 remains rather constant even for elements with a rather different geochemical behaviour. Thus, we have used the same value as in previous caesium modelling applications:

$k_2=1.16\times10^{-5}$ s^{-1}. Average particle radius, from provided information, has been fixed as 10 μm and a standard value for particle density is 2600 kg/m^3. Thus, from these parameters and a site-specific distribution coefficient is possible to have a site-specific value for the exchange velocity. The distribution coefficient has been taken, from literature, as 2000 L/kg. This implies an exchange velocity equal to 2.00×10^{-7} m/s. Due to the lack of site-specific information, kinetic rates for the second reaction in the 2-step model have been taken as in previous modelling applications: $k_2=1.20\times10^{-7}$ s^{-1} and $k_4=1.20\times10^{-8}$ s^{-1}. Sediment bulk density, assuming a sediment porosity of 0.5, is ρs=1300 kg/m^3.

There are two other parameters whose values have to be defined. They are the sediment mixing depth L and the correction factor Ψ. The sediment mixing depth is taken as L=5 cm. The value of the correction factor Ψ has been defined through calibration of the model, and was finally fixed as 0.1 since acceptable results are obtained with this setting.

The 4C model includes suspended matter particles as well. The terms describing radionuclide interactions between the liquid phase and suspended matter were added to the basic dispersion equations shown above. This improved model was applied to the second phase of the exercise (1999 flood event). However, following Konoplev et al., [II.1, II.2] it has now been assumed that the two reactions governing water-sediment interactions are parallel instead of consecutive. In the case of suspended matter particles, the second slower reaction has been neglected since the time taken by particles to travel along the floodplain area is too short to allow the second reaction to be significant. Also, erosion-deposition dynamics of suspended matter particles has been neglected.

In the case of suspended matter particles, the specific surface is written as:

$$S=\frac{3m}{\rho R} \tag{II.8}$$

where m is the suspended matter concentration. It is considered that kinetic coefficients and exchange velocities for suspended particles and bed sediments are the same. The differences arise from the different values of specific surfaces. Kinetic rates for the backwards reactions are considered constants, not depending on the particle specific surface.

The full form of the dispersion equations, when terms describing kinetic processes are included, also using different kinetic models involving several parallel and consecutive reactions [II.3]. However, they are summarized below for the present application:

$$\begin{aligned}
&\frac{\partial C_d}{\partial t}=(adv+dif)-\chi_{11}\frac{3m}{\rho R}C_d-(\chi_{11}+\chi_{12})\frac{3L\psi}{RH}(1-\phi)+k_{21}mC_s+\\
&+\frac{L\rho\psi}{H}(1-\phi)(k_{21}C_{sed1}+k_{22}C_{sed2})\\
&\frac{\partial C_s}{\partial t}=(adv+dif)+\chi_{11}\frac{3}{\rho R}C_d-k_{21}C_s\\
&\frac{\partial C_{sed1}}{\partial t}=\chi_{11}\frac{3\psi}{\rho R}C_d-k_{21}\psi C_{sed1}\\
&\frac{\partial C_{sed2}}{\partial t}=\chi_{12}\frac{3\psi}{\rho R}C_d-k_{22}\psi C_{sed2}
\end{aligned} \tag{II.9}$$

In these equations C_d and C_s are activity concentrations in the dissolved phase and suspended matter particles respectively, and C_{sed1} and C_{sed2} are activity concentrations in the sediments (exchangeable and slowly reversible fractions respectively). Also, indexes 11 and 21 correspond to the fast reaction and indexes 12 and 22 to the slower one.

In the works by Konoplev [II.1, II.2], cited above,, a third reaction was considered. It is an irreversible reaction describing the leaching of radionuclides from fuel particles deposited after the accident. However, Konoplev et al., [II.1] found that the characteristic time for the process of transformation of Cs from fuel to an exchangeable form is of the order of 2–4 years. Given that typical simulated times are of the order of a few days, this reaction has been neglected.

The speciation of radionuclides in sediments has been deduced from literature and information provided with the floodplain scenario. It is summarized in Table II.1 below.

Kinetic rates for desorption and the exchange velocities for the two parallel reactions included in the model must be defined. Some of them have been directly obtained from the works by Konoplev. Other can be deduced from algebraic relations between them [II.4] and some had to be finally fixed by model calibration. Values are summarized in Table II.2, where indexes 11 and 21 correspond to the fast reaction and indexes 12 and 22 to the slower one.

The kinetic model that has been finally adopted for describing the interactions between the dissolved phase and the soil is the proposed [II.1]. It consists of two parallel reversible reactions (a fast and a slow process).

Four kinetic rates are thus required to solve the equations. Some of them have been obtained from literature and some can be calculated from other parameters. The free parameters that could not be directly obtained from literature or measurements in the floodplain area are, in the case of ^{90}Sr, the following:

- characteristic time of the fast reaction;
- total distribution coefficient;
- geometry factor that takes into account that part of the soil particle surface may be hidden by other soil particles; and
- the objective of this sensitivity analysis consists of studying the model response to variations in the parameters.

Table II.1. Percentages of reversible and slowly reversible radionuclide phases.

	Cs	**Sr**
% slowly reversible	15	30
% exchangeable		
1991	10	50
1999	4	70

Table II.2. Transfer coefficient and exchange velocities of radionuclide sorption-desorption processes.

Parameter	**^{90}Sr**	**^{137}Cs**
χ_{11} (m/s)	8.9×10^{-6}	1.4×10^{-5}
χ_{12} (m/s)	8.9×10^{-7}	1.6×10^{-9}
k_{21} (s^{-1})	1.0×10^{-4}	1.2×10^{-5}
k_{22} (s^{-1})	1.8×10^{-5}	8.7×10^{-9}

The first test shows the model response to variations in the total distribution coefficient (including the whole soil, not only the exchangeable fraction) for ^{90}Sr. The nominal simulation is obtained with a distribution coefficient equal to 1.0 m^3/kg. Results are shown in Figure II.2.

Increasing the distribution coefficient of course enhances the fixation of radionuclides to the solid phases. Thus concentrations in the output section well below the measured levels are obtained. On the other hand, decreasing the distribution coefficient produces an increase in concentrations at the output section with respect to the nominal simulation. It can be observed that the peak in computed concentrations in the output section appears some 4 days before than in measurements. Also, the increase of concentrations is faster than observed. The reasons to explain these disagreements are two: first the water transit time from the output section to Chernobyl town (where measurements were made) is not considered. Secondly, due the steady state approximation that has been used, the radionuclide model is started from a floodplain area already flooded at t=0. This has to produce a faster increase in concentrations at the output section than if the area is flooded during a finite time.

The results concerning model sensitivity to the geometry factor are presented in Figure II.3.

Increasing the geometry factor also increases the water-soil interactions. As a consequence, a higher re-dissolution is produced. If the geometry factor is decreased, computed concentrations at the output section are well below observations. The nominal value that has been used (0.1) is the same that has been applied in other modelling studies.

The mixing depth in the soil, L, which is defined as the soil depth to which the water penetrates, has been taken as 5 cm. This value is similar to that used in other modelling works. Also, from observations in the area, it may range between 4 and 6 cm. Thus, an intermediate value of 5 cm was used. Model response to changes in this parameter between 4 and 6 cm is shown in Figure II.4.

Now the radionuclide concentration at the output section is inversely correlated to the mixing depth. Thus, lower concentrations are obtained as the mixing depth is increased. This is because the measured radionuclide density over the floodplain area soil (given in the file "FP_SR90.DAT" in Ci/km^2) has to be converted into concentrations in Bq/kg. Thus, it is assumed that radionuclides are homogeneously distributed over a depth equal to L. An increase in L implies a lower concentration per mass unit, and a lower redissolution as a consequence.

Finally, the characteristic time of the fast reaction must be of the order of some minutes. The nominal value that was finally adopted is 15 minutes. As an example of the effect of this parameter on model output, results of a simulation with a faster reaction (4 minutes characteristic time) are presented in Figure II.5. As expected, a faster kinetics produces a higher redissolution of radionuclides from the soil.

Once nominal values have been selected for these parameters, they have also been used in the case of ^{137}Cs. The only exception is the total distribution coefficient, which of course must be different.

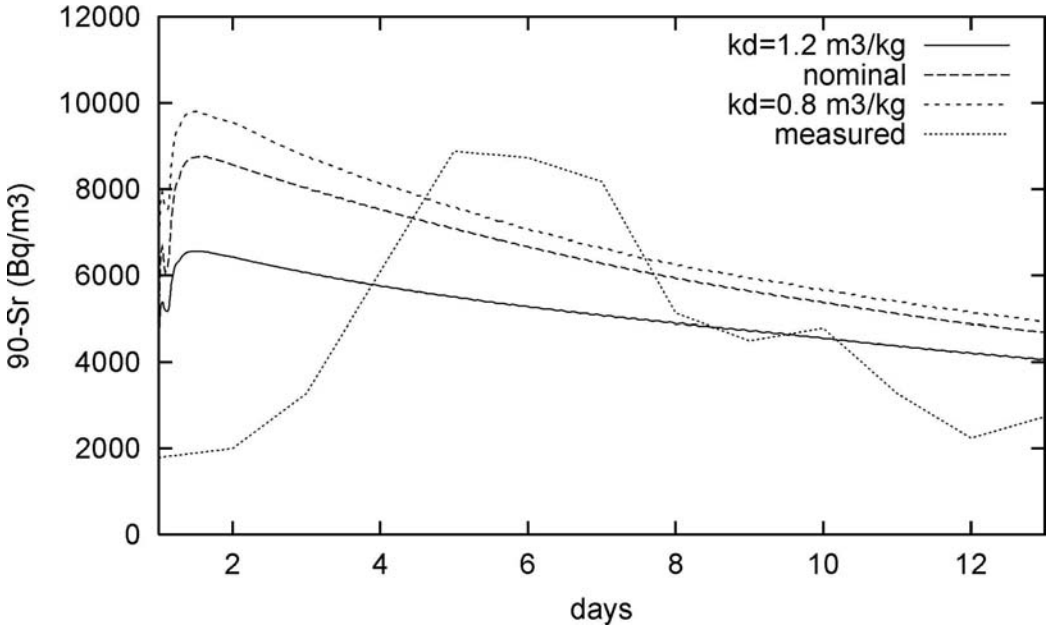

Fig. II.2. Sensitivity to the total distribution coefficient.

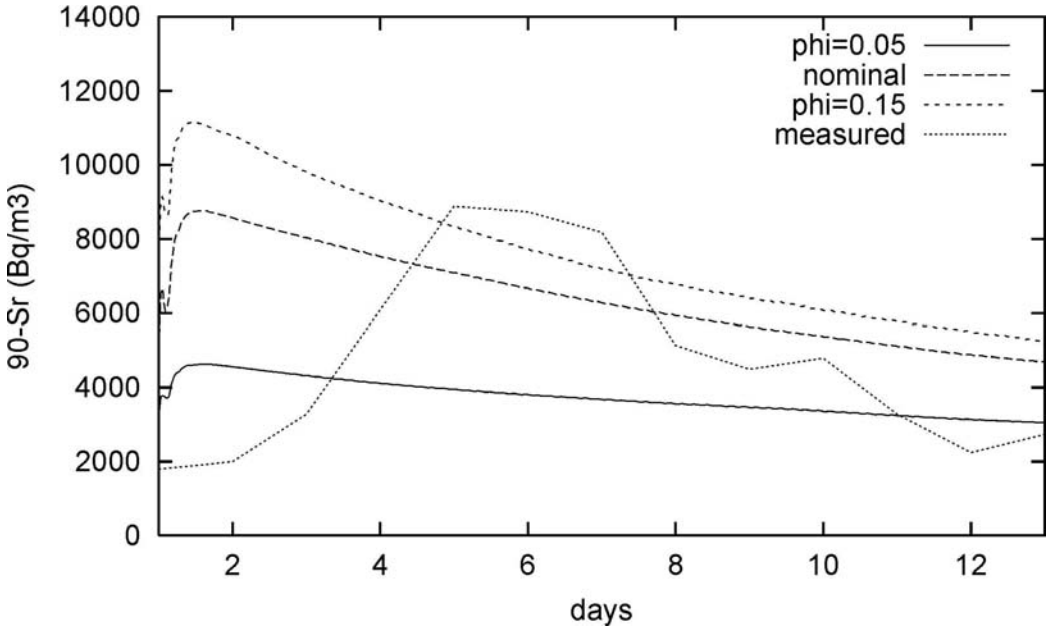

Fig. II.3. Model sensitivity to the geometry correction factor.

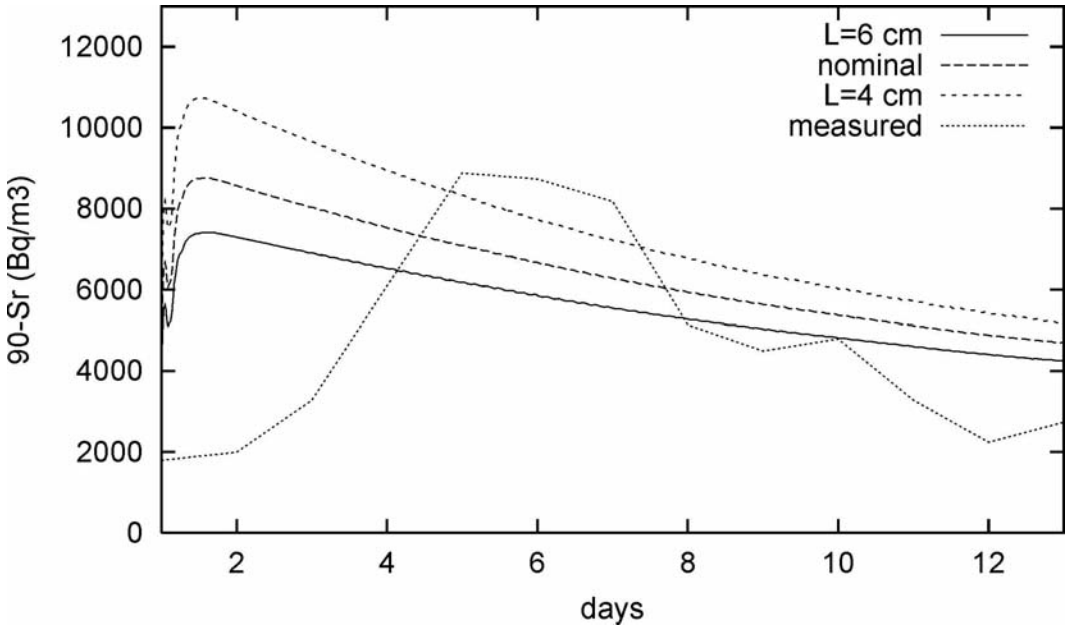

Fig. II.4. Sensitivity to soil mixing depth L.

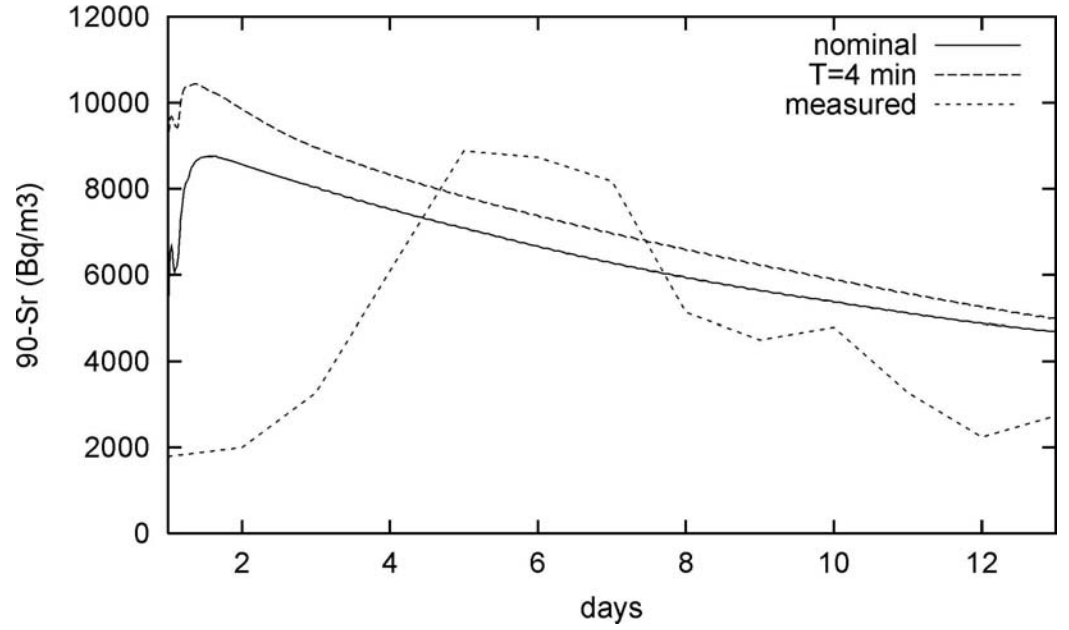

Fig. II.5. Sensitivity to the characteristic time of the fast reaction.

II.1.2. ENEA model
Luigi Monte, ENEA, Rome, Italy

The floodplain and the river are subdivided, respectively, into 3 and 12 sectors (see Figure II.6). These are characterised by different average elevations and specific contaminations (Bq m^{-2}) of soils (flood-plain) or of bottom sediments (river). The following equations were used to predict the total contents of radionuclide in the water (T_w) and in soil or sediment (D_s) of each sector i,j (a list of symbols is reported in Table II.3):

$$\frac{dT_w(i,j)}{dt} = -\frac{v_{ws}}{h} T_w(i,j) + K_{sw} D_s(i,j) - \lambda T_w(i,j) + I - O$$

$$\frac{dD_s(i,j)}{dt} = \frac{v_{ws}}{h} T_w(i,j) - (K_{sw} + K_{ds}) D_s(i,j) - \lambda D_s(i,j)$$

$$C_T(i,j) = \frac{T_w(i,j)}{V} \qquad \text{(II.10)}$$

I and O are, respectively, the radionuclide fluxes from and to the sectors contiguous to the target sector i,j:

$$I = \sum_s FI_s * C_{Ts} \qquad \text{(II.11)}$$

$$O = C_T \sum_s FO_s$$

where FI_s and FO_s are, respectively, the fluxes of water from and towards the sectors contiguous to the target sector i,j. C_{Ts} is the radionuclide concentrations in the contiguous sectors and C_T is the concentration of radionuclide in the target sector i,j. Figure I.7 shows the structure of the sub-model (10) (migration from water to sediment and vice-versa).

The diffusion of radionuclide between contiguous sectors is supposed: (a) directly proportional to the difference in radionuclide concentrations in the sectors; (b) directly proportional to the area of the interface between the sectors; and, (c) inversely proportional to the distance between the centres of the sectors.

Table II.3. List of symbols in Equations (II.10).

Symbol	Definition	Units
CT(i,j)	Concentration of radionuclide (total = dissolved + particulate form) in water	Bq m^{-3}
Ds(i,j)	Radionuclide deposit in the bottom sediment (total)	Bq
h	Depth of the water body	m
K_{sw}	Radionuclide migration rate from sediment to water	s^{-1}
K_{ds}	Radionuclide migration rate from bottom sediment to deep sediment	s^{-1}
T_w	Total amount of radionuclide in sector i,j	Bq
v_{ws}	Radionuclide migration velocity from water to sediment	m s^{-1}
λ	Radioactive decay constant	s^{-1}

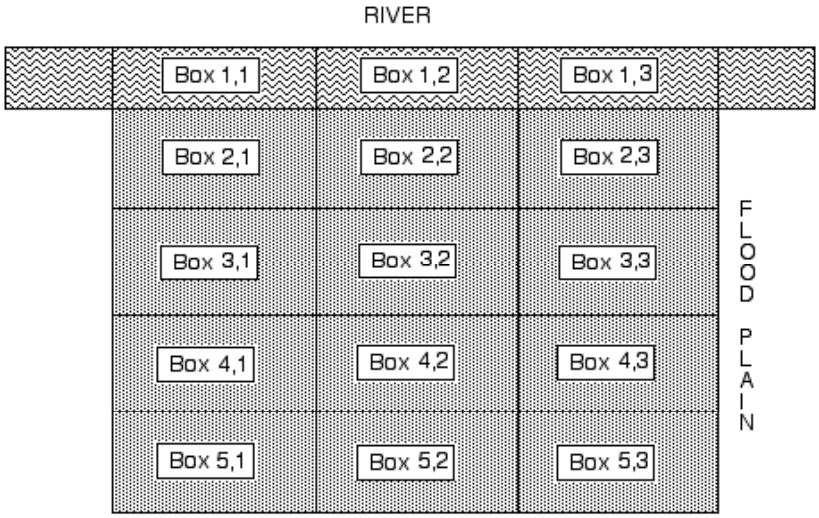

Fig. II.6. The floodplain is subdivided in 12 sectors. The river is supposed to composed of three sectors.

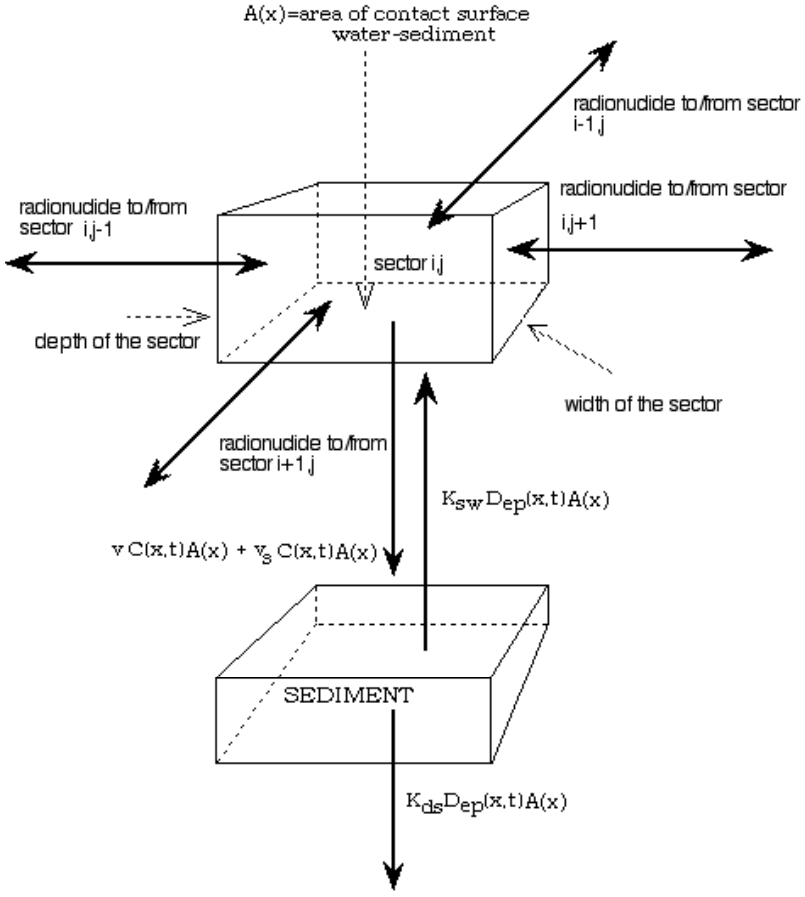

Fig. II.7. Structure of the sub-model for predicting the behaviour of radionuclide within the systems "water column – bottom sediment" in the river and the floodplain.

Table II.4. Values of the parameters of the "water-sediment" radionuclide migration sub-model [II.5, II.6].

Parameter	description	Units	^{90}Sr	^{137}Cs
V_{ws}	Radionuclide migration velocity to sediment (sedimentation velocity)	$m\ s^{-1}$	1.0×10^{-7}	1.6×10^{-6}
K_{sw}	Radionuclide resuspension rate from sediment to water (rate sediment to water)	s^{-1}	5.6×10^{-9}	1.5×10^{-8}
K_{ds}	Radionuclide migration rate to deep sediment (rate to deep sediment)	s^{-1}	8.8×10^{-10}	1.2×10^{-8}

The hydraulic model is a crude approximation of the complex processes controlling the water fluxes. Nevertheless it can be considered appropriate for the aim of the present model whose uncertainty is mainly related to the processes of migration of radionuclide from floodplain soils to water and vice-versa. Therefore, the fluxes of water between two contiguous sectors are supposed to be proportional to the differences in the water levels. Using this approximation the flooding of floodplain areas of different altitude levels can be simulated. The water volume in the "floodplain-river channel" system is calculated from the balance of the inflowing water and the water outflow.

The model was solved using Powersim ® version 2.5 software running on personal computer.

The values of the model parameters relevant to the processes of migration of radionuclide from the water column to the bottom sediments and vice-versa are reported in Table II.4.

II.1.3. COASTOX: 2-D model

Mark Zheleznyak and Vladimir Maderich, Institute of Mathematical Machines and System Problems, Kiev, Ukraine

The two dimensional lateral-longitudinal radionuclide transport model COASTOX have been used to simulate overland flow, suspended sediment transport and radionuclide transport both in the cooling pond and on the neighboring floodplain after the dam break. The model was tested within different studies of the radionuclide transport in the Chernobyl zone [II.7–II.9] and it is included into the Hydrological Dispersion Module of the EU decision support system RODOS [II.10]. The model has been recently applied to simulate radionuclide wash-off from small watersheds [II.11, II.12]. Within the project the numerical methods was refined for the model implementation for dam break problem.

The model consists of the modules describing overland flow; sediment transport; erosion/deposition processes; radionuclide transport in solute and on suspended sediments by the overland flow and contamination of upper soil layer.

II.1.3.1. Overland flow

Two-dimensional overland flow equations are obtained by vertically averaging the three-dimensional equations over flow depth and using the above kinematics boundary conditions. These equations consist of a continuity equation and two momentum equations. These equations can be expressed as follows:

$$\frac{\partial h}{\partial t} + \frac{\partial}{\partial x_i}(u_i h) = 0$$

$$\frac{\partial}{\partial t}(u_i h) + u_j \frac{\partial}{\partial x_j}(u_i h) + gh\frac{\partial \xi}{\partial x_i} + g\frac{n^2}{h^{1/3}} u_i \sqrt{u_1^2 + u_2^2} = 0 \qquad \text{(II.12)}$$

where t is the time variable (s); xi is the spatial Cartesian coordinates (m); h is the flow depth (m); ui is the flow velocity in the xi-direction (m s^{-1}); $\xi(x,y,t)$ is the free surface elevation (m); $\eta(x,y,t)$ is the bed surface elevation (m); g is the acceleration of the gravity (m s^{-2}); n is the Manning roughness coefficient (s $m^{-1/3}$).

II.1.3.2. Erosion/deposition and sediment transport

Change of the bed surface elevation is described by:

$$\rho_b (1-\phi)\frac{\partial \eta}{\partial t} = q_s - q_b \qquad \text{(II.13)}$$

where ϕ is the porosity of soil (dimensionless); ρ_b is the density of soil matrix (kg m^{-3}); q_s and q_b are the deposition and erosion rates (kg m^{-2} s^{-1}), respectively.

Mass conservation for sediment yields to:

$$\frac{\partial}{\partial t}(hS) + \frac{\partial}{\partial x_i}(u_i hS) = \frac{\partial}{\partial x_i}(hD_i\frac{\partial S}{\partial x_i}) - q_s + q_b \qquad \text{(II.14)}$$

where S is the suspended sediment concentration (kg m^{-3}); D_i is the coefficient of horizontal dispersion (m^2 s^{-1}).

The erosion rate and deposion rate are defined by the following relationships:

for non-cohesive sediments

$$q_s = \max\{0, w_0(S - S^*)\}; \qquad q_s = \max\{0, E_r w_0 (S^* - S)\} \qquad \text{(II.15)}$$

for cohesive sediments:

$$q_s = \max\left\{0, w_0 S(1 - \frac{\tau}{\tau_d})\right\}; \quad \text{for deposition [II.13]} \qquad \text{(II.16)}$$

$$q_b = \max\left\{0, M(\frac{\tau}{\tau_e} - 1)\right\} \quad \text{for erosion [II.14]} \qquad \text{(II.17)}$$

where S* is the concentration at equilibrium sediment transport capacity (kg m^{-3}); w_0 is the settling velocity of suspended particles (m s^{-1}); E_r is the overland flow erodibility coefficient; τ_d, τ_e are the critical shear stress for deposition and erosion, respectively; τ is the bed shear stress (N m^{-2}); M is experimentally determined constant.

The total load transport equation developed by Van Rijn [II.15, II.16] is used to compute the concentration at equilibrium transport capacity for non-cohesive sediments.

Cohesive sediments are different from non-cohesive sediments in two essential ways: aggregation and consolidation. Fine particles of cohesive sediments tend to form large, low density aggregates because of their surface ionic charges. Consequently, the settling velocity of muddy sediments is a function of concentration, salinity, and flow stress. After deposition, cohesive sediments will consolidate, leading to a progressive increase in density and shear resistance with depth and time. Due to our limited understanding of the erosion, deposition, and consolidation processes of cohesive sediments, the modelling of cohesive sediment transport is in its early stage. Recent advances in this field are summarized by Menta and Dyer [II.17].

II.1.3.3. Radionuclide transport by overland flow

The complex process of radionuclide transport in soluble phase and on suspended sediments is affected by many factors such as advection, diffusion and adsorption-desorption processes. The species transport equation is established by writing a mass balance over a stationary control volume through which the fluid is flowing. When diffusion effects are significant, the use of Fick's law results in the appearance of additional terms. The complete radionuclide transport in the aqueous phase and on suspended sediments by overland flow are described by the equations with the sink-source term describing physical-chemical interactions and erosion-deposition exchange processes

$$\frac{\partial}{\partial t}(hC)+\frac{\partial}{\partial x_i}(u_i hC)=\frac{\partial}{\partial x_i}(hD_i\frac{\partial C}{\partial x_i})-\lambda hC-a_s hS\left(\frac{k_d^s}{\rho}C-C_s\right)-(1-\phi)Z^* a_b\left(k_d^b\frac{\rho_b}{\rho}C-C_b\right)$$

$$\frac{\partial}{\partial t}(hSC_s)+\frac{\partial}{\partial x_i}(u_i hSC_s)=\frac{\partial}{\partial x_i}(hD_i\frac{\partial SC_s}{\partial x_i})-\lambda hSC_s+a_s hS\left(\frac{k_d^s}{\rho}C-C_s\right)+\frac{1}{\rho_b}q_b C_b-q_s C_s \qquad \text{(II.18)}$$

$$\frac{\partial}{\partial t}(hSC_s^f)+\frac{\partial}{\partial x_i}(q_i SC_s^f)=\frac{\partial}{\partial x_i}(hD_i\frac{\partial SC_s^f}{\partial x_i})-\lambda hSC_s^f+\frac{1}{\rho_b}q_b C_b^f-q_s C_s^f$$

$$\frac{\partial}{\partial t}(hSC_s^p)+\frac{\partial}{\partial x_i}(q_i SC_s^p)=\frac{\partial}{\partial x_i}(hD_i\frac{\partial SC_s^p}{\partial x_i})-\lambda hSC_s^p+\frac{1}{\rho_b}q_b C_b^p-q_s C_s^p$$

where C is the volumetric radionuclide activity in aqueous phase (Bq m^{-3}); C_s is the radionuclide activity in exchangeable phase on suspended sediment (Bq kg^{-1}); C_b is the volumetric radionuclide activity in exchangeable phase in upper soil layer (Bq m^{-3}); Z* is the thickness of active upper soil layer (m); λ is the radionuclide decay constant (s^{-1}); k_{ds} and k_{db} are the partition coefficients for "water-suspended sediment" and "water-upper soil layer" systems, respectively; a_s and a_b are the exchange rates for "water-suspended sediment" and "water-upper soil layer" systems (s^{-1}), respectively; C_{sf} and C_{sp} are the radionuclide activity in fixed phase and fuel particles on suspended sediment (Bq kg^{-1}), respectively; C_{bf} and C_{bp} are the volumetric radionuclide activity in fixed phase and fuel particles per soil solid volume in upper soil layer (Bq m^{-3}), respectively.

Table II.5. Parameters used in simulations.

Nuclide	k_d^b (L/kg)	k_d^s (L/kg)	a_b (1/day)	a_s (1/day)
^{90}Sr	0.3	–	0.0001	
^{137}Cs	4500	15 000	0.05	0.5

II.1.3.4. Contamination of upper soil layer

Contamination of the active upper soil layer is described by the equations:

$$\begin{aligned}
&\frac{\partial}{\partial t}(Z_* C_b) = a_b Z_* \left(k_d^b \frac{\rho_b}{\rho} C - C_b \right) - \lambda Z_* C_b - \frac{1}{1-\phi}\left\{ \frac{1}{\rho_b} q_b C_b - q_s C_s \right\} \\
&\frac{\partial}{\partial t}(Z_* C_b^f) = -\frac{1}{1-\phi}\left\{ \frac{1}{\rho_b} q_b C_b^f - q_s C_s^f \right\} \\
&\frac{\partial}{\partial t}(Z_* C_b^p) = -Z_*(\lambda + \alpha_p) C_b^p - \frac{1}{1-\phi}\left\{ \frac{1}{\rho_b} q_b C_b^p - q_s C_s^p \right\}
\end{aligned} \qquad \text{(II.19)}$$

where α_p is the first-order constant of radionuclide leaching from fuel particles (s^{-1}). The last equation is described the leaching of radionuclides from the fuel particles and erosion/deposition processes for the fuel particles.

The leaching of radionuclides from the fuel particles is described by the first term on right-hand side of the third equation.

II.2. Intercomparison of models for predicting the behaviour of ^{137}Cs and ^{90}Sr of Chernobyl origin in the Dnieper-Southern Boug (Dnieper-Bug) Estuary

II.2.1. The CoastMab-model (Uppsala University)
Lars Håkanson, Uppsala University, Sweden

This is a box model based on ordinary differential equations. For this model, one needs to define the borderlines which limit the given coastal areas and its boundaries towards the sea and/or adjacent coastal areas If such borderlines are drawn arbitrarily, one would get arbitrary volumes, areas and mean depths and the mass-balance model would loose predictive power [II.18, II.19].

The basic criteria to define a coastal area and the boundaries to the open water areas or adjacent coastal areas is to draw the boundary lines at the topographical bottlenecks where the exposure (Ex = 100·At/A) attains minimum values when different alternatives for settling the boundary lines are tested (At = section area; A = enclosed coastal area; method from [II.20]; see Figure II.8). Once the coastal area is defined, one can also define important variables for mass-balance calculations, such as the coastal volume (regulating the concentration of any given substance), and important morphometric parameters for internal fluxes, such as the mean depth and the water surface area, and key variables regulating the water exchange between the coast and the sea, such as the section area, the exposure and the filter factor. This method of defining coastal areas also opens a possibility to use empirical models to estimate, e.g., the theoretical water retention times of the surface water (see Table II.6) and the deep water, and the bottom dynamic conditions (regulating sedimentation, resuspension and diffusion) from morphometrical parameters (such as area, mean depth and section area).

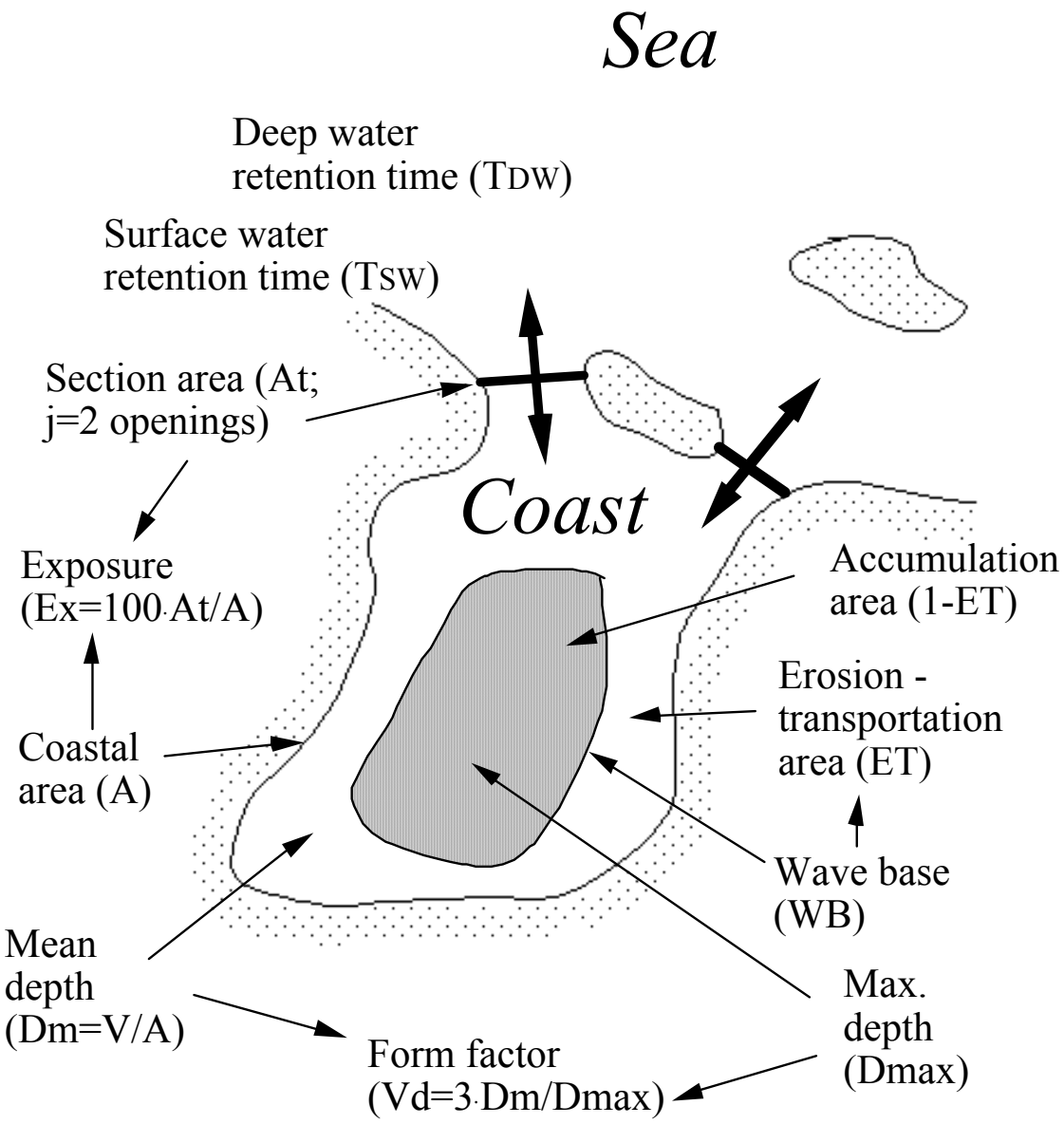

Fig. II.8. Illustration of key coastal parameters in mass-balance modelling. The most important criteria in this context is to define the boundary lines, i.e., where the coastal area ends and the sea or adjacent coastal area begins. The approach used in this work is to efine the boundary lines so that the topographical openness (the exposure, Ex, defined by the ratio between the section area, At, and the enclosed coastal area, A) attains a minimum value [II.18].

Table II.6. Empirical models used in this dynamic model to predict theoretical surface water and deep water retention times (TSW and TDW in days) and the fraction of ET-areas (ET) from morphometric parameters in archipelago areas and bays.

Regression	r^2	n	Reference
$\ln(T_{SW}) = (-4.33\cdot(\sqrt{Ex}) + 3.49)$	0.95	14	[II.21
$T_{DW} = (-251 - 138\cdot\log(At) + 269\cdot\log(Vd))$	0.79	15	[II.23]
$A = 1\text{-}ET = (D_{max}\text{-}D_{TA})/(D_{max} + D_{TA}\cdot EXP(3\text{-}Vd\text{^}1.5)))\text{^}(0.5/Vd)$ $D_{TA} = WB = Y_{ex1}\cdot(45.7\cdot(Area\cdot 10\text{^}(-6))\text{^}0.5/(21.4+(Area\cdot 10\text{^}(-6))\text{^}0.5)))$ If $D_{TA} \geq D_{max}$ then D_{max} else D_{TA} If $Ex < 0.003$ then $Y_{ex1} = 1$ else $Y_{ex1} = (Ex/0.003)\text{^}0.25$			[II.22]
Model domain: $0.002 < Ex < 1.3$; $0.0006 < At < 0.08$; $0.5 < Vd < 1.5$; data from coastal areas with very little tidal range; note that T_{SW} and T_{DW} are never permitted to be < 1 day and T_{DW} never > 120 days.			
Ex (exposure) = $100\cdot At/A$; Vd (the form factor) = $3\cdot D_m/D_{max}$; At = section area (km^2); A = coastal area (km^2); D_m = mean coastal depth (m); D_{max} = max. coastal depth (m); A = the fraction of A-areas; ET = the fraction of ET-areas; D_{TA} = WB = the wave base (m).			

Note that if reliable empirical data are at hand for a given coastal area on T_{SW}, T_{DW} or ET, such data should be used rather than the values predicted by these empirical models.

From the theoretical surface water retention time (TSW in months), one can calculate the surface water flux (QSW in m^3/month) as VSW/TSW, where VSW is the surface water volume (m^3) and the flux of the given substance, QSW·Csea in g/month, where Csea is the concentration of the substance in the sea outside the given coastal area (g/m^3).

The coastal model (see Figure II.9 for illustration; all equations are compiled in Table II.7) is modified from two validated models based on the same modelling principles and structures. One is the dynamic mass-balance model for suspended particulate matter (SPM; from [II.22], the other is the phosphorus model (see [II.23]).

The calculation time (dt) of the model is one month to reflect seasonal variations. An important demand, related to the practical utility of the model, is that it should be driven by variables readily accessed from standard monitoring programs or maps. The obligatory driving variables include four morphometric parameters (coastal area, section area, mean and maximum depth), latitude (to predict surface water and deep water temperatures, stratification and mixing) and the concentration of the given radionuclide in the sea outside the given coastal area, which is estimated in this paper using a simple approach based on the ecological half-life.

The model has four compartments. Two water compartments, surface water and deep water. The separation between these two compartments is done not in the traditional manner from measured water temperatures but from sedimentological criteria, as the water depth separating transportation areas from accumulation areas. The model also has two sediment compartments, the ET-areas, i.e., the erosion and transportation areas where fine sediments are discontinuously being deposited, and the A-areas, i.e., the accumulation areas where fine sediments are continuously being deposited. The processes accounted for are inflow and outflow via surface and deep water, direct fallout onto the water surface of the coastal area, sedimentation, burial (the transport from surficial A-sediments to underlying sediments), resuspension, diffusion and mixing between surface and deep water.

Table II.8 shows the input variable necessary to run the model.

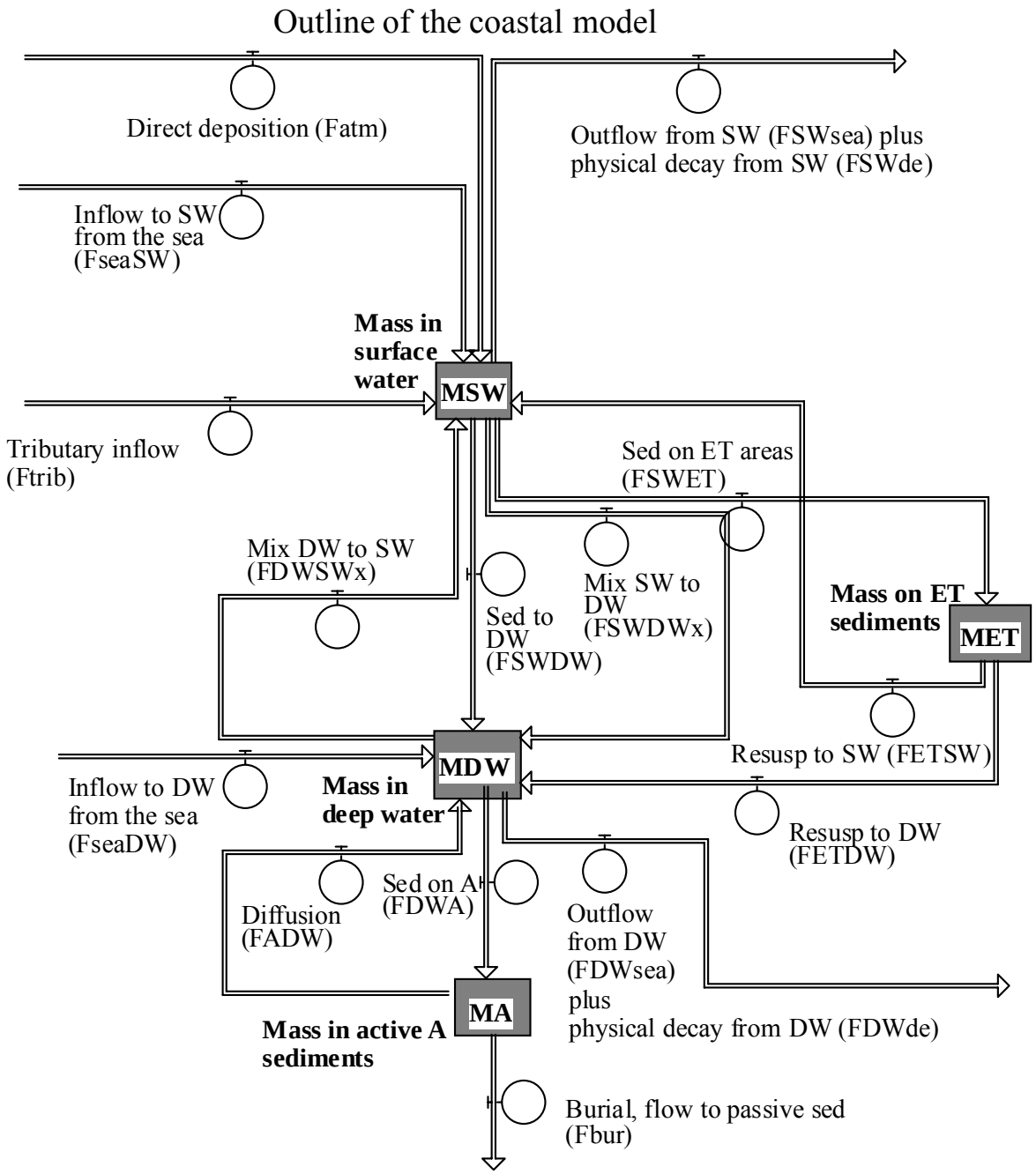

Fig. II.9. An outline of the mass-balance model for fluxes into (from rivers, from the sea or adjacent coastal areas or direct fallout onto the coastal area), out of the coastal area (via surface water or deep water exchange processes) and within coastal areas (sedimentation, resuspension from ET-areas either to surface water or deep water, diffusion from A-areas, mixing to and from the surface and the deep water compartments and burial).

Table II.7. Compilation of equations for the coastal model (for further information, see [II.18, II.22].

Compartment surface water:

$M_{SW}(t) = M_{SW}(t - dt) + (F_{seaSW} + F_{DWSWx} + F_{ETSW} + F_{trib} + F_{atm} - F_{SWsea} - F_{SWDW} - F_{SWET} - F_{SWDWx} - F_{SWde})\cdot dt$

$F_{seaSW} = Q_{SW}\cdot C_{sea}$ [flow from sea to SW]
$F_{DWSWx} = M_{DW}\cdot R_{mix}$ [mixing from DW to SW]
$F_{ETSW} = M_{ET}\cdot(1/T_{ET})\cdot(1\text{-}Vd/3)$ [resuspension from ET to SW]
F_{trib} = River inflow [from river model]
F_{atm} = Fallout·Area
$F_{SWsea} = M_{SW}\cdot(1/T_{SW})$ [flow from SW to sea]
$F_{SWDW} = M_{SW}\cdot PF\cdot(v/D_{SW})\cdot(1\text{-}ET)\cdot(1\cdot(1\text{-}DC_{SWres})+10\cdot DC_{SWres})$ [flow from SW to DW]
$F_{SWET} = M_{SW}\cdot PF\cdot(v/D_{SW})\cdot ET\cdot(1\cdot(1\text{-}DC_{SWres}s)+10\cdot DC_{SWres})$ [flow from SW to ET]
$F_{SWDWx} = M_{SW}\cdot R_{mix}$ [mixing from SW to DW]
$F_{SWde} = M_{SW}\cdot R_{de}$ [physical decay]

Compartment deep water:

$M_{DW}(t) = M_{DW}(t - dt) + (F_{SWDW} + F_{ETDW} + F_{SWDWx} + F_{seaDW} + F_{ADW} - F_{DWSWx} - F_{DWA} - F_{DWsea} - F_{DWde})\cdot dt$

$F_{SWDW} = M_{SW}\cdot PF\cdot(v/D_{SW})\cdot(1\text{-}ET)\cdot(1\cdot(1\text{-}DC_{SWres})+10\cdot DC_{SWres})$
$F_{ETDW} = M_{ET}\cdot(1/T_{ET})\cdot(Vd/3)$
$F_{SWDWx} = M_{SW}\cdot R_{mix}$
$F_{seaDW} = Q_{DW}\cdot C_{sea}$
$F_{ADW} = M_{A}\cdot R_{diff}$
$F_{DWSWx} = M_{DW}\cdot R_{mix}$
$F_{DWA} = M_{A}\cdot PF\cdot(v/D_{DW})\cdot(1\cdot(1\text{-}DC_{DWres})+ 10\cdot DC_{DWres})$
$F_{DWsea} = M_{DW}\cdot Q_{DW}/V_{DW}$
$F_{DWde} = M_{DW}\cdot R_{de}$

Compartment ET-sediments:

$M_{ET}(t) = M_{ET}(t - dt) + (F_{SWET} - F_{ETDW} - F_{ETSW} - F_{deET})\cdot dt$

$F_{SWET} = M_{SW}\cdot PF\cdot(v/D_{SW})\cdot ET\cdot(1\cdot(1\text{-}DC_{SWres})+10\cdot DC_{SWres})$
$F_{ETDW} = M_{ET}\cdot(1/T_{ET})\cdot(Vd/3)$
$F_{ETSW} = M_{ET}\cdot(1/T_{ET})\cdot(1\text{-}Vd/3)$
$F_{deET} = M_{ET}\cdot R_{de}$

Compartment A-sediments:

$M_{A}(t) = M_{A}(t - dt) + (F_{DWA} - F_{bur} - F_{ADW} - F_{deA})\cdot dt$

$F_{DWA} = M_{DW}\cdot PF\cdot(v/D_{A})\cdot(1\cdot(1\text{-}DC_{DWres})+10\cdot DC_{Dwres})$ [see also equation in Compartment deep water(above)
$F_{bur} = M_{A}/T_{A}$
$F_{ADW} = M_{A}\cdot R_{diff}$
$F_{deA} = MA\cdot R_{de}$

Concentration in sea:

$C_{sea}(t) = C_{sea}(t - dt) + (M_{Csea} - Out_{Csea})\cdot dt$

M_{Csea} = Fallout
$Out_{Csea} = C_{sea}/T_{sea}$

Notes: M = mass (Bq); F = flux (Bq/month); R = rate (1/month); C = concentration (Bq/m^3); DC = distribution coefficient (dim. less); T = age (months); V = volume (m3); de = decay; bur = burial; SW = surface water; DW = deep water; ET = ET-areas; A = A-areas; flux from SW to DW = FSWDW, etc.; concentration in SW = CSW, etc.; age of ET-sediments = TET, etc.; Table II.8 gives calculated values for many models constants for the default coastal area.

Table II.7. (Continued)

Other equations:

$T_A = 12 \cdot BF \cdot D_{AS}/Sed$ [BF = bioturbation factor (dim. less); D_{AS} = depth of active sediments in cm; sed = sedimentation in cm/month (see reference [II.22])]

$T_{ET} = 1$ [month]

$C = (M_{SW}+M_{DW})/V$ [Bq/m^3]

$C_{diss} = C \cdot (1\text{-}PF)$ [concentration in dissolved phase; Bq/m^3]

C_{sea} (initial) = Fallout/100 [the assumed default initial concentration in the sea outside the coast; Bq/m^3]

$C_{DW} = M_{DW}/V_{DW}$ [Bq/m^3]

$C_{SW} = M_{SW}/V_{SW}$ [Bq/m^3]

$u = 2.5$ [mean coastal current velocity; cm/s (see reference [II.18])]

$D_{DW} = (D_{max}\text{-}WB)/2$ [WB = wave base; the depth separating the SW and DW compartments; m]

$DC_{SWres} = (F_{ETSW})/(F_{ETSW}+F_{seaSW}+F_{DWSWx}+F_{trib}+F_{atm})$ [the resuspended fraction in SW; dim. less]

$Q_{DW} = V_{DW}/(T_{DWd}/30)$ [water flow into DW in m^3/month]

$DF = 1/(1+(Kd \cdot SPM)/1000000)$ [the dissolved fraction for ^{137}Cs (see reference [II.18])]

$D_{SW} = WB/2$ [the mean depth of the SW compartment; m]

$V_{DW} = V\text{-}V_{SW}$ [the SW water volume; m^3]

$Temp_{SW}$ = If ABS($Temp_{SW}$-$Temp_{DW}$)<4 then ($Temp_{SW}$+$Temp_{DW}$)/2 else $Temp_{SW}$ [temperatures; °C]

$Temp_{DW}$ = If < 4 then 4 else $Temp_{DW}$ [temperatures; °C]

ET = (1-A) [the fraction of ET-areas; dim. less]

$Ex = 100 \cdot At/Area$ [Exposure; At = section area in m^2; Area = coastal area; m^2]

$Vd = 3 \cdot D_m/D_{max}$ (the form factor, also often called the volume development; dim. less]

$T_{sea} = 3 \cdot 12$ [the assumed default ecological halflife of the radionuclide in the sea; months]

$C_K = C_{KURS} = (SPM_{URS}+1) \cdot 0.03)/0.0391$ [the estimated concentration of potassium in the coastal area and in the upstream river stretch; mg/l]

$Kd = 800000/C_K$ [Kd for ^{137}Cs (from reference [II.18])]

R_{mix} = if ABS($Temp_{SW}$-$Temp_{DW}$)<4 then $R_{mix} = 1$ else $R_{mix} = 1/ABS(Temp_{SW}\text{-}Temp_{DW})$ [the mixing rate; 1/month]

PF = (1-DF) (the particulate fraction of the radionuclide; dim. less]

$R_{de} = 0.693/(30.2 \cdot 12)$ [the physical decay rate for ^{137}Cs; 1/months]

$1/T_{SW}$ = if $(1/T_{SWbay})+(1/T_{SWtide})+(1/T_{SWu}) > 30$ days then $1/T_{SW} = 30$ else $1/T_{SW} = (1/T_{SWbay})+(1/T_{SWtide})+(1/T_{SWu})$

$v = v_0 \cdot Y_{SPM} \cdot Y_{sal}$ [the settling velocity for the particulate fraction; m/month]

$v_0 = 12/12$ [the default settling velocity for SPM; m/y]

SPM = if $SPM_{URS}/4 < 4$ mg/l then SPM = 4 else $SPM = SPM_{URS}/4$ [the suspended particulate matter concentration; mg/l]

$Q_{SW} = V_{SW}/T_{SW}$ [the water flux to the SW compartment; m^3/month]

V_{SW} = if WB = 0 or Temp = 100 then $V_{SW} = V$ else $V_{SW} = ((Area\text{-}Area_{WB}) \cdot WB/(3/Vd)+Area_{WB} \cdot WB)$ [volume of SW compartment; m^3]

T_{DWd} = if > 120 then T_{DWd} = 120 days else T_{DWd} [theoretical deep water retention time; days]

Tidal amplitude (amp) = (0+0.01) [cm]

T_{SWbay} = if $Ex \geq 1.3$ then $T_{SWbay} = T_{SWu}$ else $T_{SWbay} = T_{SW1}$ [theoretical SW retention time; months]

T_{SWu} = if $Ex < 1.3$ then $T_{SWu} = 100$ else $T_{SWu} = V_{SW}/(Y_{cur} \cdot u \cdot 0.01 \cdot 60 \cdot 60 \cdot 24 \cdot 30 \cdot 0.5 \cdot At)$

$T_{SWtide} = V_{SW}/(Area \cdot amp \cdot Y_{tide} \cdot 0.01 \cdot 30)$

T_{SW1} = If $EXP(3.49\text{-}4.33 \cdot (Ex^{0.5}))/30 < 1/30$ then $T_{SW1} = 1/30$ else $T_{SW1} = EXP(3.49\text{-}4.33 \cdot (Ex^{0.5}))/30$

Volume (V) = $Area \cdot D_m$ [m^3]

$WB = Y_{Ex1} \cdot 45.7 \cdot (Area \cdot 10^{-6})^{0.5}/(21.4+(Area \cdot 10^{-6})^{0.5})$; if $Ex < 0.003$ then $Y_{Ex2} = 1$ else $Y_{Ex2} = (Ex/0.003)^{0.25}$; if $Y_{Ex2} > 10$ then $Y_{Ex1} = 10$ else $Y_{Ex1} = Y_{Ex2}$ [wave base and boundary conditions; m]

Y_{cur} = if $Y_{Ex} > 1$ then $Y_{cur} = 1$ else $Y_{cur} = Y_{ex}$ [Y_{cur} dimensionless moderator for current influences on water exchange]

$Y_{ex} = (1+0.5 \cdot ((Ex/10)\text{-}1))$ [Y_{ex} dimensionless moderator for influences of exposure on water exchange]

$Y_{sal} = (1+1 \cdot (Sal/1\text{-}1))$ [dimensionless moderator for salinity influences on sedimentation]

$Y_{SPM} = 1+0.75 \cdot (SPM/50\text{-}1)$ [dimensionless moderator for SPM influences on sedimentation]

Y_{tide} = if $Y_{ex} > 1$ then 1 else Y_{ex} [dimensionless moderator for tidal effects on water exchange]

Notes: M = mass (Bq); F = flux (Bq/month); R = rate (1/month); C = concentration (Bq/m^3); DC = distribution coefficient (dim. less); T = age (months); V = volume (m3); de = decay; bur = burial; SW = surface water; DW = deep water; ET = ET-areas; A = A-areas; flux from SW to DW = FSWDW, etc.; concentration in SW = CSW, etc.; age of ET-sediments = TET, etc.; Table II.8 gives calculated values for many models constants for the default coastal area.

Table II.8. Data need to run the CoastMab-moodel for the Black Sea estuary.

Obligatory coastal-area specific driving variables
Coastal area (= Area)
Latitude (= Lat)
Max depth (= D_{max})
Mean depth (= D_m)
Mean annual precipitation (= Prec)
Salinity (= Sal)
Section area (= At)
Mean fallout to the catchment of Bug
Mean fallout to the catchment of Dnieper
Mean fallout to the catchment of the Black Sea

II.2.2. The University of Seville model
Raúl Periáñez, University o0f Seville, Spain

II.2.2.1. Introduction

A 2D depth-averaged model has been adopted at the University of Seville to simulate the flux of radionuclides in the Dnieper-Bug estuarine system. The Institute of Mathematical Machine and System Problems has a 3D baroclinic model. Of course, a 3D model is more appropriate than a 2D approach for this system due to the stratification existing in the water column. However, we could not expect to remake the excellent modelling work that they have carried out along several years. On the other hand, a box model is being using at the University of Uppsala. Consequently, it was decided to use an intemediate approach between the box and full 3D models. This may also enrich the discussion on coastal models by providing a different point of view. Nevertheless, the limitations of the approach must be kept in mind.

The model solves the 2D depth averaged hydrodynamic equations off-line using monthly averaged wind conditions and water discharge from the rivers. Thus 24 water current fields are obtained, corresponding to the period 1986–1987. These current fields are used to solve the advection/diffusion dispersion equation for radionuclides.

II.2.2.2. Hydrodynamics

The 2D depth-averaged hydrodynamic equations are used. Nevertheless, although the effect of vertical density gradients cannot be considered, horizontal density gradients are included in the equations since will also affect currents in the estuary. The hydrodynamic equations also include the standard non-linear, Coriolis, gravity and horizontal friction terms. The density of water is obtained from its salinity through a standard equation of state. Equations are:

$$\frac{\partial z}{\partial t}+\frac{\partial}{\partial x}(Hu)+\frac{\partial}{\partial y}(Hv)=0$$

$$\frac{\partial u}{\partial t}+u\frac{\partial u}{\partial x}+v\frac{\partial u}{\partial y}+g\frac{\partial z}{\partial x}+\frac{Hg}{2\rho_0}\frac{\partial \rho}{\partial x}-\Omega v+k\frac{u\sqrt{u^2+v^2}}{H}-\frac{\tau_x}{\rho_0 H}=A\left(\frac{\partial^2 u}{\partial x^2}+\frac{\partial^2 u}{\partial y^2}\right) \qquad \text{(II.20)}$$

$$\frac{\partial v}{\partial t}+u\frac{\partial v}{\partial x}+v\frac{\partial v}{\partial y}+g\frac{\partial z}{\partial y}+\frac{Hg}{2\rho_0}\frac{\partial \rho}{\partial x}+\Omega u+k\frac{v\sqrt{u^2+v^2}}{H}-\frac{\tau_x}{\rho_0 H}=A\left(\frac{\partial^2 v}{\partial x^2}+\frac{\partial^2 v}{\partial y^2}\right)$$

where u and v are the components of the water current along the x and y axis, z is the surface elevation over the mean water level, H is total water depth, k is the bed friction coefficient, A is horizontal viscosity, ρ is density of water and the wind stress components are:

$$\tau_x = C_D \rho_a |W| W_x$$
$$\tau_y = C_D \rho_a |W| W_y \qquad \text{(II.21)}$$

where C_D is a drag coefficient, ρa is air density and W is wind speed. The water density is obtained from the following standard equation of state:

$$\rho = \rho_0 (1 + \alpha S) \qquad \text{(II.22)}$$

where ρ_0 is a reference density taken as 998.9 kg/m^3 and S is water salinity. Coefficient α is defined as 7.45×10^{-4}. Water salinity is obtained from an advection/diffusion dispersion equation with appropriate boundary conditions at the river mouths and Kinbourn Strait.

The hydrodynamic equations are forced by the monthly averaged winds, river discharges and salinity at the Kinbourn Strait (salinity at the river mouths is fixed to zero). The bed friction coefficient has been fixed as k=0.025. However, the estuary is covered by ice during the winter months. In this case the friction coefficient is increased to 0.050 to account for the reduction in water velocity because of friction with the ice cover. It has been checked that a realistic order of magnitude for currents is obtained (in comparison with measurements provided with the scenario description) and that continuity is satisfied. Thus, currents into the estuary are of the order of 5 cm/s.

A map of the currents obtained in April 1986 is presented in Figure II.10 as an example. These are depth-averaged currents, thus the distribution cannot be compared with the surface currents provided by the 3D baroclinic model and included with the scenario description.

As an example, the computed salinity distribution for April 1987 is presented in Figure II.11 Salinity decreases quickly as going from Kinbourn Strait into the estuary, which is in qualitative agreement with the distribution computed by means of the 3D baroclinic model, provided in the scenario description.

The hydrodynamic model is run separately for each month in the period 1986–1987. Each model run is carried out until a steady situation is achieved, starting from rest conditions. It can be seen in Figure II.12 that a steady situation is reached in less than 100 hours of simulation.

The corresponding steady current and water surface elevation fields are stored in files that will be read by the dispersion code. 24 model runs are carried out and 24 files are generated. Horizontal resolution of the model is 1000 m (the same computational grid provided with the scenario is used) and time step in the hydrodynamic calculation is 20 s due to the CFL stability condition (a explicit finite difference scheme is used to solve the equations).

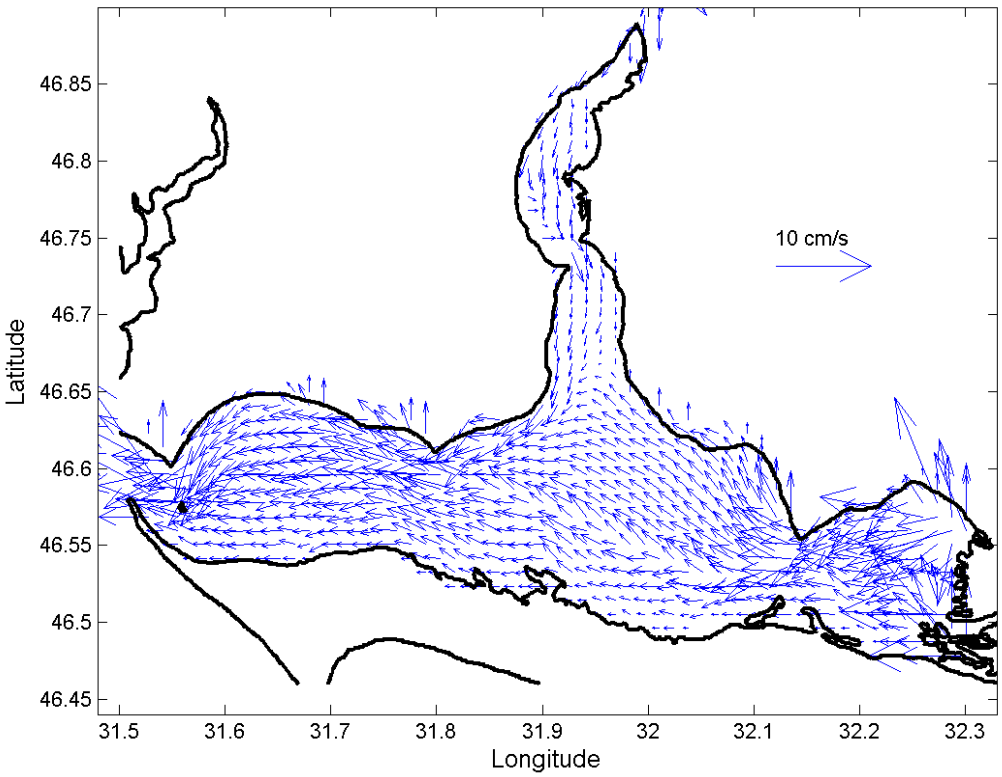

Fig. II.10. Computed depth-averaged currents for April 1986.

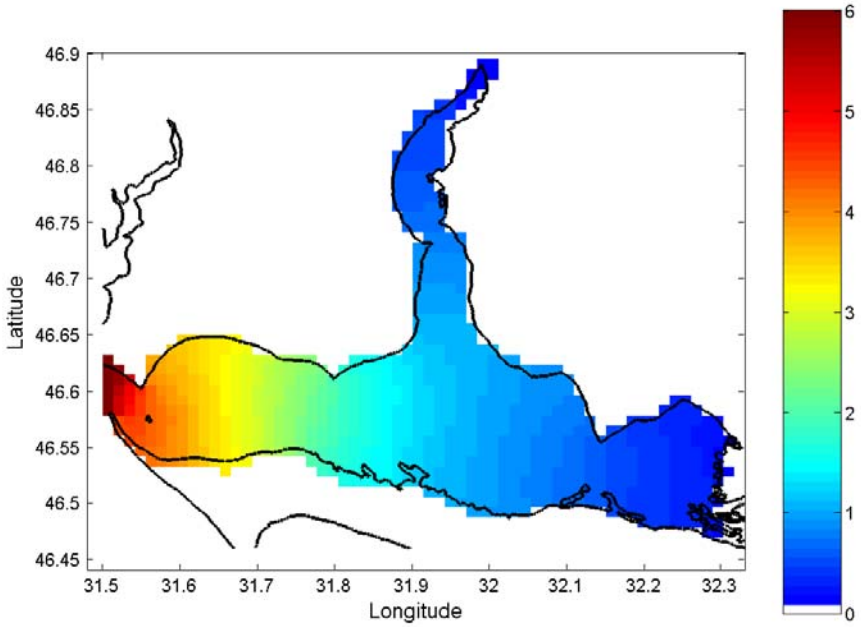

Fig. II.11. Computed salinity (g L^{-1}) for April 1987.

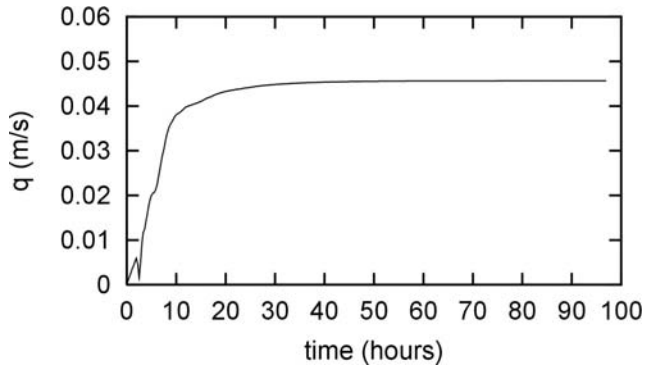

Fig. II.12. Time evolution of the computed depth averaged current in the central part of the estuary for the simulation corresponding to April 1986.

II.2.2.3. Dispersion

The dispersion model consists of an advection/diffusion equation with appropriate boundary conditions. Files containing current fields are read to compute the advection terms. Linear interpolation between these currents fields is used to have a smooth transition from one month to the following. The dispersion equation is:

$$\frac{\partial C_d}{\partial t} + \frac{1}{H}\left(\frac{\partial (C_d H)}{\partial x} + \frac{\partial (C_d H)}{\partial y}\right) = \frac{1}{H}\left(\frac{\partial}{\partial x}\left(HK\frac{\partial C_d}{\partial x}\right) + \frac{\partial}{\partial y}\left(HK\frac{\partial C_d}{\partial y}\right)\right) \quad \text{(II.23)}$$

where C_d is the concentration of dissolved radionuclides and K is the diffusion coefficient.

The same computational grid as in the hydrodynamic calculations is used. However, stability conditions are not so restrictive and time step could be increased to 720 s. Explicit second order accuracy finite difference schemes are used to solve the advection and diffusion terms in the dispersion equation. In particular, the MSOU (monotonic second order upstream) scheme is used for advection and a centered scheme is used for diffusion.

Radionuclide concentrations at the three open boundaries (Dnieper and Bug mouths and Kinbourn Strait) are fixed for each month from provided data. The dataset is not complete. Thus, linear interpolation is used when data is lacking for a time period. Also, the average concentration is used if a range of concentrations is provided or if there are results from different institutes. In the case of Cs, there are no data for Kinbourn Strait. Thus data corresponding to the Black Sea are used. Initial conditions must also be specified for radionuclide concentrations. These conditions consist of considering an uniform background concentration over all the estuary. It has been taken as 3 and 9 Bq/m^3 for Cs and Sr respectively, which are the minimum measured concentrations according to the provided dataset.

The diffusion coefficient has been selected according to the model grid size, following the classical Okubo's relation. It leads to a value equal to 0.58 m^2/s.

The model provides the temporal evolution of the average radionuclide concentration over the complete estuary on a daily basis. A map of the computed distribution of ^{90}Sr in December 1987 is presented in Figure II.13 as an example. Activity levels seem in agreement with those provided in the data set (150–300 Bq/m^3).

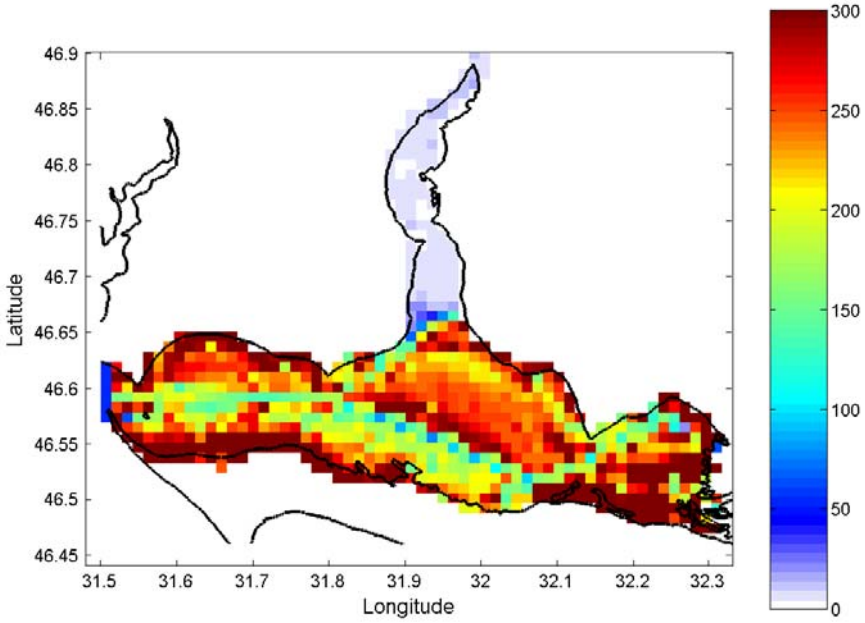

Fig. II.13. Computed ^{90}Sr concentrations (Bq m^{-3}) in December 1987.

II.2.2.4. Sensitivity analysis

Three different runs have been made with the University of Seville model in the case of the ^{137}Cs simulation. Results are presented in Figure II.14, where run A is a simulation in which deposition of radionuclides on the water surface is not included, run B is the nominal simulation with a surface deposition of 5000 Bq/m^2 occurring after the accident and run C includes the same surface deposition plus interactions of dissolved radionuclides with the bed sediments of the estuary. These interactions have been described by a kinetic model consisting of a single reversible reaction. Equations are essentially the same as in the Pripyat floodplain exercise and will not be repeated here.

As should be expected, mean concentrations are lower when the surface deposition is not included. The surface deposition of Chernobyl radionuclides produces an intense peak in the average concentration in April 1986. Mean ^{137}Cs concentration decreases faster when interactions with sediments are included (run C) since the bed sediment acts as a sink for dissolved radionuclides. Nevertheless, it is also known that bed sediments are a long-term source of previously released radionuclides when concentrations in the water column are small enough to allow the desorption reaction dominates over adsorption. Thus, after some 500 days mean concentration in the water column is lower in run B because of flushing of radionuclides to the sea, while in the case of run C the bed sediment is still acting as a delayed source of ^{137}Cs, and dissolved concentration is slightly higher than in run B.

The main differences in model output may arise from the description of the water-sediment interactions. Thus, a simple exercise has been proposed to compare model outputs when these processes are included. This exercise is described in the following section.

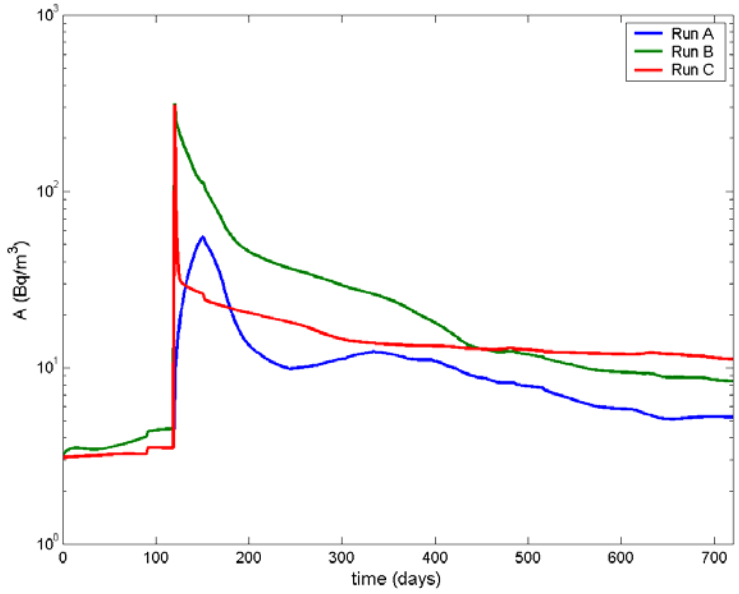

Fig. II.14. Time evolution of dissolved mean ^{137}Cs concentrations obtained with the University of Seville model for three different runs. A: no surface deposition, B: with surface deposition (nominal simulation), C: surface deposition and interactions with bed sediments.

II.2.2.5. Modelling application to non-conservative radionuclides

The objective of the present exercise consists of testing the models already applied in the Dnieper-Bug estuary when interactions of radionuclides with sediments are included. A set of parameters describing sediments and radionuclide characteristics are provided, and each modeller should adapt them, or directly use them, to the requirements of his own model. Nevertheless, the exercise is set as simple as possible. The selected radionuclide is ^{137}Cs.

The affinity of ^{137}Cs for the solid phase is described by his equilibrium distribution coefficient. The following value is proposed, taken from reference [II.24]:

$$\text{Cs: } 4\times10^{3} \text{ L/kg}$$

For simplicity, sediment properties are considered uniform over the estuary. These basic properties are:

- Particle density: 2600 kg/m^3
- Particle mean radius: 15 μm
- Sediment porosity: 0.5

Sediment composition: it is considered that over all the estuary sediments are 100 % muds.

If a given model requires some more parameters, their values should be selected according to the modeller own criteria.

Suspended matter particles are neglected at this stage since other processes as deposition and erosion of the bed, not easy to parametrize, should be included. At the moment, the objective of the exercise is simply to test the descriptions of the uptake/release reactions.

Initial conditions: zero concentrations over the estuary in water and bed sediments.

Radionuclide sources: It is considered a zero radionuclide concentration at the Black Sea and Bug River mouth. Contamination is introduced from the Dnieper River in two pulses of two months of duration each (February–March 1986 and 1987). Radionuclide concentration at the Dnieper mouth during these months will be assumed to be 100 Bq/m^3. During the remaining months of the two years of simulation a zero concentration will be assumed at the Dnieper mouth. This way, an initial contamination of the sediment will occur, followed by a cleaning process and a new contamination event. The first contamination will occur over totally clean sediments and the second one over already contaminated sediments. This way, the behaviour of models is tested in a wide range of conditions.

Simulation endpoint: As in the previous exercise, average radionuclide concentrations over the complete estuary in water (Bq/m^3) and sediment (Bq/kg) will be provided for each day.

Two models have participated in this exercise: COASTOX and the University of Seville model (USEV). Results may be seen in Figure II.15.

Both models give very similar results in the case of the dissolved phase. There are two peaks in concentrations resulting from the input of radionuclides from the Dnieper mouth and a fast cleaning process. In the case of bed sediments, however, differences between mean concentrations produced by both models reach a factor 5, although a much more persistent contamination of the estuary bed than of the water column is predicted by both models.

In spite of the simplicity of the exercise, it highlights the difficulties of simulating the interactions of radionuclides with the solid phases. It is not surprising that in real applications model outputs may differ by orders of magnitude. Consequently, this is a problem that should be carefully addressed in future model intercomparison exercises for coastal environments.

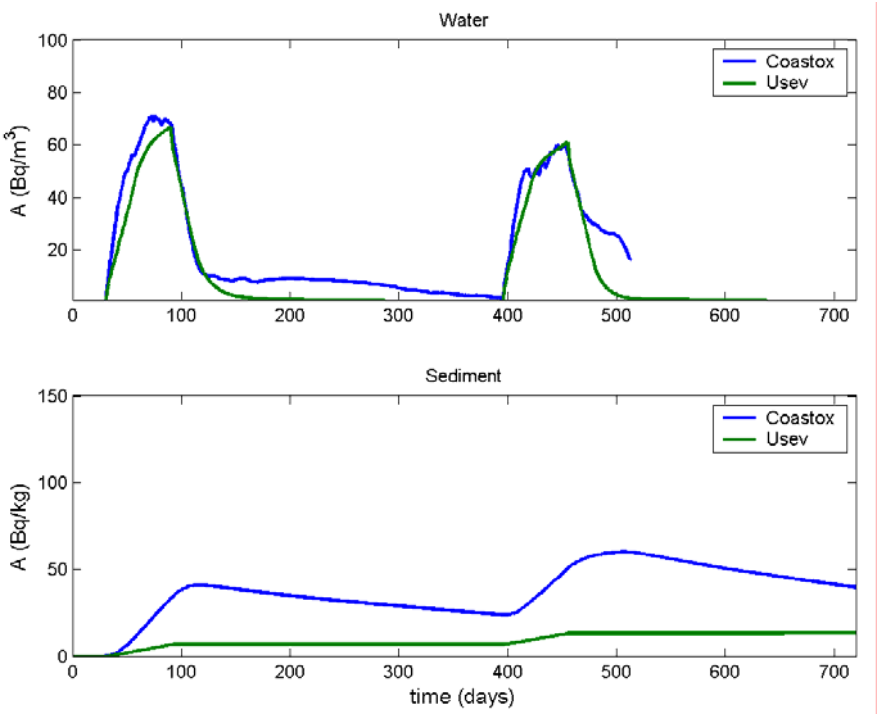

Fig. II.15. Average ^{137}Cs concentrations over the estuary for the dissolved phase and bed sediments predicted by COASTOX and USEV models.

II.2.3. The THREETOX Model
Mark Zheleznyak, Vladimir Maderich, Vladimir Koshebutsky, IMMSP, Ukraine

The THREETOX code is an advanced three-dimensional surface water modelling system for hydrodynamics, sediment and radionuclide transport in lakes, reservoirs, estuaries and coastal ocean [II.25–II.27]. It is most appropriate for short-term and local prediction radionuclide transport after release. The modelling system was applied to the water bodies of different scales: cooling pond of Chernobyl NPP [II.27], Dnieper-Bug, Ob' and Yenisey estuaries [II.26, II.28, II.29] and the Kara sea [II.29]. THREETOX includes hydrodynamics, ice, sediment and radionuclide transport sub-models.

Hydrodynamics sub-model: The hydrodynamics is simulated on the base of three-dimensional, time-dependent, free surface, primitive equation model. The model equations are written in Cartesian coordinates. The prognostic variables of the hydrodynamics code are the three components of the velocity fields, temperature, salinity and surface elevation. The water body is assumed to be hydrostatic and incompressible. The concept of eddy viscosity/diffusivity and model of turbulence are used to define the turbulent stresses and scalar fluxes. Heat fluxes at the sea surface are derived from parameterisations that employ observed atmospheric temperatures, humidity, cloudiness and wind.

Suspended sediment transport submodel: The particulate matter is represented by three different grain size fractions. Suspended sediment transport is described by the advection-diffusion equation, taking into account the settling velocity of the sediment. For cohesive sediment the erosion and deposition rates are modelled by using the formulae of Partheniades [II.30] and Krone [II.31]. For non-cohesive sediments the bottom boundary condition describes the resuspension or settling of sediments, which depends on the ratio between the actual and the near-bed equilibrium concentration of the sediments [II.32]. The effective bottom shear stresses induced by currents and wind waves are summed. The mass conservation equations for the bottom deposits describe evolution of bed level.

Radionuclides transport submodel: The sub-model of radionuclide transport describes the specific water-sediment sorption processes. It includes the advection-diffusion equations for dissolved and adsorbed by suspended sediment radioactivity in the water column, and the equations for concentration of the dissolved and adsorbed radioactivity in the bottom deposits. The exchanges between the different phases are described by diffusion, sorption, and sedimentation-resuspension processes. Adsorption and desorption of radionuclides between liquid and solid phases are described by the radionuclide exchange rates and by the distribution coefficients for suspended sediments and bottom, respectively.

Numerical method: Sigma co-ordinates are used to avoid difficulties in numerical solution of problem for realistic bottom topography. Splitting of the barotropic and baroclinic modes imposed in the code [II.33]. The governing equations together with the boundary conditions are solved by finite difference techniques. A horizontally and vertically staggered mesh is used for the computations.

II.2.3.1. Model forcing

THEETOX was customized in the Dnieper-Bug estuary using bathymetry from navigational maps. The horizontal grid size is one km, whereas model has 20 sigma-layers in vertical direction. The initial thickness of the upper bottom sediment layer was taken to be 2 cm. The monthly averaged concentrations of the suspended sediment in the Dnieper and Southern Bug

mouth were specified according to the State Water Cadastre. The daily discharges and temperature of Dnieper and Southern Bug were prescribed. The observed in Ochakiv atmospheric temperature, humidity, cloudiness and wind with 3hr interval were used. At the estuary mouth in the Kinbourn strait the measured daily level variations and temperature and salinity profiles were used as boundary conditions when flows were directed into the estuary. For outflow the radiation conditions were used for velocity and scalars.

II.2.3.2. ^{137}Cs and ^{90}Sr dispersion

The following coefficients of radionuclides' equilibrium distribution in the "solute-suspended sediments" (K_{ds}) and "solute-bottom sediments" (K_{db}) systems were used: K_{ds} =15 m^3kg^{-1}, K_{db} =3 m^3kg^{-1} for ^{137}Cs and $K_{ds} = K_{db}$= 0.3 $m^3kg,^{-1}$ in the case of ^{90}Sr. The monthly averaged concentrations of the radionuclides in the solute and attached to sediment in the Dnieper and Southern Bug mouth were prescribed using the data of [II.34–II.36]. The concentrations of the radionuclides in the Kinbourn Strait was prescribed from UHMI data and [II.36] data. The fallout of ^{137}Cs that took place 30 April 1986 was 5000 Bq m^{-2}.

II.2.4. The ENEA Model
Luigi Monte, ENEA, Italy

The ENEA model is based on quantitative evaluations and balance of radionuclide contents in the water system components (surface water, deep water, bottom sediment) accounting for the fluxes among these. The model structure is conceptually similar to the one adopted for the sub-model MARTE (Model for Assessing Radionuclide Transport and countermeasure Effects in complex catchment) [II.5] implemented in the Computerised Decision Support Systems MOIRA [II.37]. The water body is divided in three sectors from the river mouth to the sea. Each sector is sub-divided in three compartments: surface water, deep water and bottom sediment. A fourth compartment representing the sediment interface between bottom sediment and water is considered for ^{137}Cs to simulate the quick interaction processes of such a radionuclide with particulate matter. The first order differential equations of the model were obtained by calculating radionuclide budget in the system compartments from the balance between input and output radionuclide fluxes. These are supposed proportional to the amount of radionuclide in the respective "source" compartment. Eddy diffusion (horizontal, between sectors, and vertical between surface and deep waters) is simulated by two-way fluxes that are calculated as the difference between radionuclide concentrations in two contiguous sectors (or water compartments) divided by the distance of the sectors (or compartments) and multiplied by the horizontal (vertical) eddy diffusion coefficient [II.38]. We outline briefly the principles and the equations of the model.

The radionuclide absorption by suspended matter and by the sediment interface layer is modelled according to the well-know "k_d concept" (k_d = partition coefficient "particulate form/dissolved form") based on the hypothesis of a reversible quick equilibrium between the dissolved (C) and the adsorbed phases (C_{ad}) of radionuclide:

$$\frac{C_{ad}}{C} = k_d \tag{II.24}$$

The total amount, T_i (Bq), of radionuclide in deep water (dissolved + particulate form) and in sediment interface layer is:

$$T_i = C_i L_i h_i \Delta_i + C_i k_d w_{sm} L_i h_i \Delta_i + C_i k_d D_l \delta L_i \Delta_i \tag{II.25}$$

where L_i , h_i and Δ_i are, respectively, the width, the thickness and the length of sector i, w_{sm} is the suspended matter (kg m^{-3}) and D_l and δ are the thickness and the density of the sediment interface layer.

The previous equation can be written as follows:

$$T_i = C_i\left[1 + k_d w_{sm} + k_d D_l \delta / h_i\right] h_i L_i \Delta_i \tag{II.26}$$

If we put:

$$heff_i = h_i + h_\Delta \tag{II.27}$$

where:

$$h_\Delta = k_d w_{sm} h_i + k_d D_l \delta \tag{II.28}$$

we get:

$$T_i = C_i\, heff_i L_i \Delta_i \tag{II.29}$$

Similar equations govern the behaviour of radionuclide concentration C_s in surface water provided that:

$$h_\Delta = k_d w_{sm} h_i \tag{II.30}$$

where $w_{sm} k_d$ is the factor “particulate/dissolved” radionuclide (f.p.d.).

The time variation of radionuclide concentration obeys the following equations:

(a) Deep water:

$$\frac{\partial C_i}{\partial t} = -\frac{E_o}{Dist}\frac{h_i}{\Delta_i heff_i}\left[-Ct_{i-1} + 2Ct_i - Ct_{i+1}\right] + \frac{E_v}{h/2}\frac{1}{heff_i}\left[Ct_i^s - Ct_i\right]$$
$$-\frac{v_s C_i}{heff_i} + \frac{K_{sw} Dep_i}{heff_i} - \lambda C_i \tag{II.31}$$

where C_i and C_{ti} are, respectively, the dissolved and the total radionuclide concentrations in sector i of deep water, E_o and E_v are the horizontal and the vertical eddy diffusion coefficients, Dist is the distance between the barycentre of two contiguous sectors, h is the depth of the water column, Ctis is the total radionuclide concentration in sector i of surface water, v_s is the radionuclide sedimentation velocity, K_{sw} is the rate of resuspension of radionuclide from sediment and $\lambda$is the radioactive decay constant;

Table II.9. Values of model parameters.

Parameter	Dimension	^{137}Cs	^{90}Sr	Note
v_s	ms^{-1}	3.6×10^{-7}	1.2×10^{-8}	
K_{sw}	s^{-1}	2.9×10^{-8}	3.0×10^{-8}	
K_{ds}	s^{-1}	5.8×10^{-9}	1.0×10^{-10}	
E_v	m^2s^{-1}	$1.9\times10^{-7} - 1.9\times10^{-6}$	$1.9\times10^{-7} - 1.9\times10^{-6}$	Independent of radionuclide (range)
E_o	m^2s^{-1}	120	120	Diffusion sea-coastal water. Independent of radionuclide.
f.p.d.	dimensionless	1	≈ 0	Fresh water
f.p.d.	dimensionless	0.125	≈ 0	Sea water
$D_l\ \delta\ k_d$	m	0.6	≈ 0	Bottom sediment in contact with sea water

(b) Surface water:

$$\frac{\partial C_i^s}{\partial t} = -\frac{1}{\Delta_i L h_s}\left[\Phi_i Ct_i^s - \Phi_{i-1} Ct_{i-1}^s\right] + \frac{E_v}{h/2}\frac{1}{h_s}\left[Ct_i - Ct_i^s\right] - \lambda C_i^s \qquad \text{(II.32)}$$

where C_i^s is the dissolved radionuclide in sector i of surface water, h_s is the effective thickness of surface water, Φ_i is the surface water flux from sector i to the contiguous sector (it is supposed that the prevailing horizontal component of water movement is due to the fresh water flux from the river).

Obviously, if the sections of contiguous boxes are different the above equations sould be appropriately modified.

The following equation governs the deposit Dep (Bq m^{-2}) of radionuclide in sediment:

$$\frac{\partial Dep_i}{\partial t} = v_s C_i - K_{sw} Dep_i(x,t) - K_{ds} Dep_i(x,t) - \lambda Dep_i(x,t) \qquad \text{(II.33)}$$

where K_{ds} is the rate of migration of radionuclide to passive sediments.

The complete description of the model is reported [II.39].

II.3. Migration of tritium in the Loire River

II.3.1. CASTEAUR (IRSN, France)
P. Boyer, IRSN, France

II.3.1.1. General considerations

The code CASTEAUR v0.1 [II.40] is dedicated to operational assessments of the radionuclides transfers in rivers. It is an extension for average and long terms periods of the prototype version CASTEAUR v0.0 [II.41–II.43] that has been previously developed to be used in case of crisis situations, when the calculation domain concerns periods of some hours.

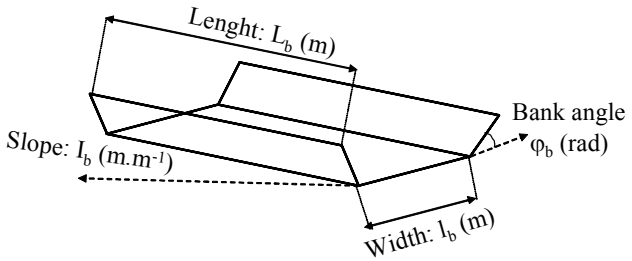

Fig. II.16. Hydrographical parameters.

The code is based on five modelling layers: an hydrographical model to represent the river, an hydraulic model to assess the water movements, a sedimentary model for the calculation of the matter dynamic, a trophic chain model to consider the links between the main biotic components (phytoplankton, zooplankton, macrobenthos, planktonivorous and omnivorous fishes) and a radioecological model based on the four previous ones.

As the Loire scenario aimed to assess the tritium concentration along the river, only the hydrographical model, the hydraulics model and the dissolved part of the radioecological model are involved. These models are described hereafter.

II.3.1.2. Hydrographical model

The hydrographical model proposes a simplified description of the river geometry. This description is based on a succession of reaches constituting a linear hydrographic network. The main criteria to identify these reaches are the confluences along the river. Then, a reach is mainly limited by an upstream and a downstream water inflow points and/or by an important variation among one of its characteristic hydrographical parameters that are its length *L(b)* (m), its average slope *I(b)* ($m.m^{-1}$) and its trapezium bathymetric section form (Figure II.16) defined by the width *l(b)* (m) and the angle of the bank, *φ(b)* (rad).

For the Loire scenario, 33 reaches have been defined. Their parameters are presented in the Table II.10.

II.3.1.3. Hydraulic models

The hydraulic model is a box dynamic model. With a temporal step, Δt (s) it gives the temporal evolutions of the water flow Q_b^t ($m^3.s^{-1}$), the average speed U_b^t ($m.s^{-1}$), and the water column volume wc_b^t (m^3) on each reach b characterized by their length or a same spatial step Δx (m). These variables are calculated with the Equations II.34 to II.36. Equation II.35 is the equation of continuity and the Equation II.36 is the Strickler relation corresponding to the simplification of the one dimensional equation of Barré de St Venant in case of permanent and homogeneous conditions.

$$wc(b,t) = L(b) \cdot A(b,t) \tag{II.34}$$

$$\frac{dwc(b,t)}{dt} = Q(b-1,t) + q(b,t) - Q(b,t) \tag{II.35}$$

$$Q(b,t) = V(b,t) \cdot A(b,t) = Str(b) \cdot R(b,t)^{\frac{2}{3}} \cdot \sqrt{I(b)} \tag{II.36}$$

where:

wc(b,t) is theolume of water column in the reach b at the time t (m^3);
q(b,t) is the specific water inflow in the reach b at the time t ($m^3.s^{-1}$);
A(b,t) is the wet section area of the reach b at the time t (m^2);
R(b,t) is the hydraulic radius of the reach b at the time t (m);
V(b,t) is the flow mean speed in the reach b at the time t ($m.s^{-1}$); and
Str(b) is the Strickler coefficient of the reach b ($m^{1/3}.s^{-1}$).

The input data, q(b,t), given by the scenario at the discharge points are taken into account (blue lines in Table II.10).

Considering the hydrographical model, SM_b^t and Rh_b^t are respectively given by the following relations:

$$A(b,t) = h(b,t) \cdot \frac{l(b) \cdot \sin(\varphi(b)) + h(b,t) \cdot \cos(\varphi(b))}{\sin(\varphi(b))} \quad \text{(II.37)}$$

$$R(b,t) = h(b,t) \cdot \frac{l(b) \cdot \sin(\varphi(b)) + h(b,t) \cdot \cos(\varphi(b))}{2 \cdot h(b,t) + l(b) \cdot \sin(\varphi(b))} \quad \text{(II.38)}$$

From these relations, the resolution of the Equations II.34 to I.36 gives the water depth, h_b^t (m), and consequently all the others hydraulics variables.

II.3.1.4. Dissolved part of the radioecological model

The dissolved part of the radioecological model of CASTEAUR v0.1 proposes also a box dynamic approach. With the same temporal step than this used for the hydraulic model, the model gives the temporal evolution of the total activities (Bq) in the different reaches characterized by their length or a same spatial step Δx. The equation is:

$$\frac{dr(b,t)}{dt} = Q(b-1,t) \cdot C(b-1,t) + S(b,t) - Q(b,t) \cdot C(b,t) - \lambda \cdot r(b,t) \quad \text{(II.39)}$$

where:

r(b,t) is the total activity of the radionuclide r in the reach b at the time t (Bq);
S(b,t) is the specific radionuclide inflow in the reach b at the time t ($Bq.s^{-1}$);
$C(b,t) = \frac{r(b,t)}{wc(b,t)}$ is the volumes activities ($Bq.m^{-3}$); and
S(b,t) are input data given in the scenario at the release points.

II.3.1.5. Customisation

Table II.10 presents the hydrographical and hydraulics parameters the hydrographical and hydraulics parameters used for the scenario Loire. Table II.11 gives the average water discharges considered for CASTEAUR v0.0.

II.3.1.6. Parameters of calculation

In the context of this blind test, one simulation has been realised with CASTEAUR v0.0 and one with CASTEAUR v0.1. The parameters of calculation are presented in Table II.12.

Table II.10. Hydrographical and hydraulics parameters.

ID_Reach	Name	Length *(km)*	Width *(m)*	Banks angle *(°)*	Slope *(10^{-4} m/m)*	Strickler coefficient *($m^{1/3}/s$)*
0	Belleville release	17.5	235	11.5	5.1	31.5
1	Briare	18.72	200	8.0	3.9	31.5
2	Dampierre release	12.5	320	6.9	5.3	31.5
3	Sully	23	290	7.5	5.3	31.5
4	Ouvrouer	20	360	10.3	5.8	31.5
5	Combleux	9.0	270	10.3	4.2	31.5
6	Orléans discharge	5.71	270	10.3	4.2	31.5
7	Confluence Loiret	9.5	300	9.7	3.4	31.5
8	Meung sur Loire	15	270	6.9	5.3	31.5
9	Saint Laurent des eaux	2.56	270	6.9	5.3	31.5
10	Saint Laurent release	11	270	6.9	5.3	31.5
11	Muides	15.5	330	9.0	3.2	31.5
12	Blois	14	350	16.0	4.6	31.5
13	Candé sur Beuvron	2.97	360	10.9	4.5	31.5
14	Onzain discharge	6.03	360	10.9	4.5	31.5
15	Candé sur Beuvron	3	360	10.9	4.5	31.5
16	Montlouis_1	5.6	300	9.7	3.6	31.5
17	Montlouis_2	18.1	300	9.7	3.6	31.5
18	Montlouis_3	14.1	230	8.0	3.7	31.5
19	Tours	11.59	215	5.7	3.8	31.5
20	Cher discharge	2.41	215	5.7	3.8	31.5
21	Langeais	4.17	282.5	8.0	3.9	31.5
22	Langeais discharge	10.33	350	8.0	3.9	31.5
23	Port Plat	8.31	410	9.2	4.2	31.5
24	Indre discharge	3.81	310	6.9	4.6	31.5
25	Chinon release	6.81	310	6.9	4.6	31.5
26	Confluence_Vienne	15.5	430	18.3	3.5	31.5
27	Saumur	11.5	510	12.6	1.8	31.5
28	Gennes	16	450	10.3	2.4	31.5
29	La Bohalle	8	580	8.0	1.0	31.5
30	Les Ponts de Cé	8.98	440	11.5	2.3	31.5
31	Maine discharge	10	340	5.7	1.1	31.5
32	Chalonnes sur Loire	11.36	395	10.3	2.3	31.5

Table II.11. Averaged water discharges considered for CASTEAURv0.0.

ID_Reach	Name	$q_{b\ \infty}^{ave}$ *($m^3.s^{-1}$)*
0	Belleville release	195.75
6	Orléans discharge	7.96
14	Onzain discharge	3.94
20	Cher discharge	54.4
22	Langeais discharge	15.45
24	Indre discharge	10.48
26	Confluence_Vienne	169.48
31	Maine discharge	152.12

Table II.12. Parameters of calculation.

Parameter	CASTEAUR v0.0 (ave)	CASTEAUR v0.1
Δt	20 s	1 day
Δx	1 km	0 m (*)

(*) $\Delta x = 0$ m indicates that the length of each reach is considered.

II.3.2. MASCARET – module Tracer (EDF R&D, France)

II.3.2.1. General description of MASCARET

MASCARET is a 1D hydrodynamic system for simulating hydrodynamic flows, water quality and sediment transport. So, there are the following including modules:

- the hydrodynamic module solves the 1D shallow-water equations on a looped and branched network. According to the flow characteristics, three hydraulic components are available: steady subcritical regime, unsteady subcritical regime and unsteady mixed flow regime. In case of unsteady subcritical flow, the hydrodynamic module uses an implicit finite difference computation method (Preissman scheme);
- the module 'Casier' simulates the flow in the floodplain by domain decomposition in basins where only the continuity equation is taken into account;
- the module 'Courlis' simulates the transport of cohesive sediments; and
- the module 'Tracer' simulates the dispersion of pollutants; this module can be coupled with water quality modules (in the case of interacting pollutants). The Tracer module is only coupled with the hydrodynamic module for subcritical flow regimes (steady and unsteady).

The module Tracer solves the 1D advection-diffusion equation, in its non-conservative form:

$$\frac{\partial C}{\partial t} + u\frac{\partial C}{\partial x} = \frac{1}{A}\cdot\frac{\partial}{\partial x}\left(A\cdot k\cdot\frac{\partial C}{\partial x}\right) + S \qquad \text{(II.40)}$$

where:

C is the tracer concentration (kg/m^3);
u is the flow velocity (m/s);
A is the river section (m^2);
S is the sources of tracer (kg/m^{3}s); and
K is the dispersion coefficient (m^2/s).

In a computation involving different tracers of concentration C_i, the source terms S_i for a tracer i can depend on the concentration of other tracers C_j. As a result, the module Tracer can be applied to water quality modelling, by computing the source terms S_i, representing the interactions between the different tracers.

The resolution is made by a method with fractional steps: a convection step (using the method of characteristics in weak convection) and a diffusion step (implicit scheme).

II.3.2.2. Application to the Loire River

In the application on the Loire River, the hydrodynamic module of MASCARET was used in subcritical unsteady mode, with a complete description of the river geometry (all the 368 profiles were taken into account to describe the river geometry) and a fine representation of the weirs.

The step for the discretisation in space is approximatively 200 m, so that the Loire River is described by 2656 points.

The time step for the computation is 300 s. We used a constant Strickler coefficient (Str = 30 m$^{1/3}$.s^{-1}) and a constant dispersion coefficient in the module Tracer (k = 100 m^2/s).

II.3.3. MOIRA – module Marte
(ENEA, Italy)

II.3.3.1. Model description

MARTE (Models for Assessing Radionuclide Transport and countermeasure Effects in complex catchments) is a structured set of codes implemented in MOIRA Decision Support System (MOdel-based computerised system for management support to Identify optimal Remedial strategies for restoring radionuclide contaminated Aquatic ecosystem and drainage areas) for applications to complex water river basins:

- HydroAV (Hydrological module – Algebraic calculation for variable Volume): MARTE sub-code simulating the temporal behaviour of the hydrological and morphologic parameters of a complex water body;
- Cat (Catchment module): MARTE sub-code simulating the migration of the pollutant from the catchment to the aquatic system;
- Migra (Simulation of contaminant Migration through abiotic components of aquatic systems): MARTE sub-code simulating the migration of a pollutant through the abiotic components of an aquatic system;
- Biot (Simulation of contaminant migration from the abiotic to the Biotic components of an aquatic system): MARTE sub-code simulating the migration of a pollutant from the abiotic components of an aquatic system to the fishes species.

For the present application modules HydrAV and Migra were used.

The river is assumed to be composed of a chain of interconnected “Elementary Boxes” (Ess). Therefore, the model supplies predictions averaged over a spatially defined part of the water system (the EB).

The water balance is calculated by the following simple equation:

$$Q_i = Q_0 + \sum_1^i \Delta Q_j \qquad \text{(II.41)}$$

where Q_i is the water flux from box i^{th}, Q_0 is the water flux from the river source and ΔQ_i is the increment of water flux in box j^{th} calculated as follows:

$$\Delta Q_i = ROFF_i - E_i + R_i - W_{di} \qquad \text{(II.42)}$$

$ROFF_i$ is the total runoff from the sub-catchment i^{th}, E_i and R_i are, respectively, the evaporation and the precipitation rates. W_{di} is the water withdrawal rate.

The average width (B) and depth (h) of each box are calculated as non-linear functions of the water fluxes :

$$\begin{aligned} B &= a Q_i^b \\ h &= c Q_i^d \end{aligned} \qquad \text{(II.43)}$$

where a, b, c and d are parameters.

Table II.13. List of symbols in Equation II.44.

Symbol	Definition	Units
C(x,t)	concentration of dissolved radionuclide in water	$Bq.m^{-3}$
h(x)	depth of the water body	m
B(x)	width of the water body	m
P(x,t)	water withdrawal rate per unit length of water course	$m^3.s^{-1}.m^{-1}$
t	time	s
x	distance of the observation point from the origin	m
λ	radioactive decay constant	s^{-1}
Q(x,t)	water flow	$m^3.s^{-1}$

Each ES is comprised of:

- the water column;
- an upper sediment layer strongly interacting with water ("interface layer);
- an intermediate sediment layer below the "interface layer" ("bottom sediment");
- a sink sediment layer below the "bottom sediment"; and
- the right and left sub-catchments of the ES.

The model accounts for the fluxes of radionuclide due to the following processes: sedimentation, radionuclide removal due to water withdrawal, radionuclide migration from water to sediment (diffusion component), radionuclide migration from sediment to water (resuspension), radionuclide migration from catchment, radionuclide transport through the ES chain. The parameters in the equation controlling the radionuclide exchange from water and sediment were set equal to 0 for the present applications to ^3H. Therefore, the time variation of radionuclide concentration obeys the following partial differential equations when Δx--> 0:

$$\frac{\partial C(x,t)}{\partial t} = -\frac{1}{B(x)h(x)}\frac{\partial}{\partial x}\left[C(x,t)Q(x,t)\right] - \frac{C(x,t)P(x,t)}{B(x)h(x)} - \lambda C(x,t) \qquad \text{(II.44)}$$

The subdivision of the water body in segments corresponds to the discretisation of variable x in the previous equation. A list of symbols is reported in Table II.13.

II.3.3.2. Model customisation

In view of the present application, the Loire River was subdivided in 20 segments (Table II.14). Each segment correspond to an EB in the MARTE code. The description of these segments is reported in the Table II.14.

Table II.14. List of the river segments.

Profile No.	Abscissa (m) of the profile	Name	Segment	Initial segment point	Abscissa (m) of the segment (Initial point)	Segment length (m)
1	532820	CtrBell_P8bC	SEGMENT 1	Belleville	532820	
10	537540	CtrBell_P28C				4790
11	538530	CtrBell_P0C	SEGMENT 2	Beaulieu	537610	
32	557050	pro95_B020Bis				21990
33	561150	pro95_B024	SEGMENT 3	Gien	559600	
64	575020	CtrDamp_PKA17				15430
65	579400	pro95_B042	SEGMENT 4	Ouzouer	575030	
86	611570	pro95_B073				37630
87	612910	pro95_B075	SEGMENT 5	**Saint Denis Hotel**	612660	
101	627100	Orl_pro+_b0892		*WEIR*		14480
102	627850	Orl_pro+_P3	SEGMENT 6	Orleans	627140	
117	633190	Orl_pro+_b0953				6390
118	633910	Orl_pro+_b0961	SEGMENT 7	**Orleans**	633530	
141	657090	pro95_B120		*TRIBUTARY*		25300
142	660500	pro95_B123	SEGMENT 8	Beaugency	658830	
164	672000	CtrStlaur_P15F				13460
165	672310	CtrStlaur_P16F	SEGMENT 9	Nouan	672290	
205	690660	Blois_P3				18810
206	691320	pro95_C025	SEGMENT 10	**Chaussee Saint Victor**	691100	
213	708170	pro95_C042		*WEIR*		18670
214	710370	pro95_C044	SEGMENT 11	**Onzain**	709770	
253	746960	pro95_D029		*TRIBUTARY*		37630
254	748120	pro95_D030	SEGMENT 12	Tours	747400	
264	767780	pro95_D050				20790
265	768730	pro95_D051	SEGMENT 13	**Cher**	768190	
270	773810	pro95_PK225		*TRIBUTARY*		6580
271	776040	pro95_PK221-7	SEGMENT 14	**Langeais**	774770	
283	790500	pro95_PK208		*TRIBUTARY*		15970
284	792050	pro95_E005	SEGMENT 15	LaChapelle	790740	
						2670
285	793410	pro95_PK205	SEGMENT 16	**Indre**	793410	
301	800150	CtrChin_EDF14		*TRIBUTARY*		6800
302	800210	pro95_E007	SEGMENT 17	Bertignolles	800210	
312	803580	CtrChin_EDF25				3820
313	804030	pro95_F001	SEGMENT 18	**Vienne**	804030	
334	853980	pro95_F19		*TRIBUTARY*		52110
335	856740	lapointingr_P001	SEGMENT 19	Angers	856140	
340	862550	lapointingr_P0051				7870
341	864190	lapointingr_P007	SEGMENT 20	**Maine**	864010	
368	885370	lapointingr_P0241		*TRIBUTARY*		21360
				Montjean	885350	
				Montjean	885370	
				TRIBUTARY		

II.3.3.3. Model applications

Case 1: Generic standard version (monthly averages of water fluxes)

HydroAV makes use of monthly averages of runoff data.

For this application, HydroAV makes use of generic functions [II.44] to estimate the morphological characteristics of the Loire River. Generic functions were used to determine average values of depth and width (of each river segment) as power functions of the water fluxes.

The present results were obtained by running a "stand-alone" version of the model.

Data input:

- Monthly averages of upstream water fluxes at Belleville and of the four main tributaries (hydraulic boundary conditions);
- $h=0.163*\Phi^{0.447}$ and $B=10*\Phi^{0.460}$, where h is the average depth (m), B the average width (m) and Φ is the monthly average water outflow ($m^3.s^{-1}$) of each river segment.

Model outputs are monthly averaged fluxes and hourly averaged concentrations.

Case 2: Site-specific standard version (monthly averages of water fluxes)

HydroAV works with monthly average data.

It makes use of site-specific functions to evaluate morphologic parameters of the Loire River. Available experimental data were not sufficient to fit average depths and widths to power functions of water fluxes. Therefore, the used power functions were selected to assure that water velocity, depths and widths were reasonably close to available empirical estimates.

Data input:

- Monthly averages of upstream water fluxes at Belleville and of the water fluxes from four main tributaries (hydraulic boundary conditions);
- $h=0.163*\Phi^{0.384}$ and $B=29.4*\Phi^{0.398}$.

Functions for evaluating h and B in model MARTE "site-specific standard version" were obtained by fitting the experimental water velocity to power functions of the water flux ($v=a\,b$). These functions assure that the predicted values of h and B are comparable with experimental data. The functions in MARTE "site-specific standard version" are more realistic for the specific conditions of the Loire River in comparison with the default functions used by MARTE "generic standard version".

Model outputs are monthly averaged fluxes and hourly averaged concentrations.

Case 3: Site-specific customised version (hourly averages of water fluxes)

Customised HydroAV works with hourly data.

As for the above site-specific standard version application, HydroAV makes use of site-specific functions to determine morphologic parameters of the Loire River.

Table II.15. Main features of the performed exercises.

Model applications	Morphometry	Water fluxes
Case 1: Generic standard	$h=0.163*\Phi^{0.447}$ and $B=10*\Phi^{0.460}$ generic default functions	Monthly averages
Case 2: Site-specific standard	$h=0.163*\Phi^{0.384}$ and $B=29.4*\Phi^{0.398}$ site-specific functions obtained by a calibration of water velocity	Monthly averages
Case 3: Site-specific customised	$h=0.163*\Phi^{0.384}$ and $B=29.4*\Phi^{0.398}$ site-specific functions obtained by a calibration of water velocity	Hourly averages

(h = average depth (m), B = average width (m), Φ = average water outflow (m^3s^{-1}) of each river segment)

Data input:

- Hourly values of water fluxes;
- $h=0.163*\Phi^{0.384}$ and $B=29.4*\Phi^{0.398}$.

Model outputs are hourly averaged fluxes and hourly averaged concentrations.

II.3.3.4. Summary of the simulations made

The description of the main characteristics of the exercises of model application are summarised in Table II.15.

II.3.4. RIVTOX (IMMSP, Ukraine)

II.3.4.1. General description

The river model RIVTOX integrated into HDM (Hydrological Dispersion Module) of RODOS includes three modules:

- an hydraulic model based on the diffusive wave approximation of Saint-Venant equation;
- a suspended sediment transport model; and
- a radionuclide transport model.

In the frame of the ongoing 6-FP EURANOS project, the version of the RIVTOX (RIVTOX-SV) is under development, in which the hydraulics model is based on full Saint-Venant equation, that provides possibilities to simulate flow in the rivers with weirs, gates, dams and other structure in the river channel.

Nowadays (November 2004), this module RIVTOX-SV exists in the stand-alone PC-based version, and will be integrated into the HP-UX based HDM-RODOS in nearest months.

Taking into account that Loire River hydraulics is under the strong influence of the set of the weirs, this new version of RIVTOX was used for the Loire Scenario simulations. Time step used in calculations is 1 hour.

The Loire hydraulics was simulated using the scenario data about the river cross-sections and weirs on the basis of the boundary conditions for year 1999. The numerical solution of full Saint-Venant equation in RIVTOX –SV is based on the Preissmann four-point implicit finite-difference scheme as in CHARIMA code [II.45].

The model of the Tritium transport is based on the numerical solution of the advection-diffusion equation:

$$\frac{\partial AC}{\partial t} + \frac{\partial QC}{\partial x} = \frac{\partial}{\partial x}\left(AE_x \frac{\partial C}{\partial x} \right). \qquad \text{(II.45)}$$

where:

A is the cross-sectional area;
Q is the water discharge;
E_x is the dispersion coefficient;
C is the concentration of transported pollutant (tritium); and
A and Q are calculated in the hydraulic module of RIVTOX-SV.

For the estimation of dispersion coefficient E_x, the approach suggested recently [II.46] is used:

$$Ex = \alpha_w \left(\frac{b}{h} \right)^{1.23} \left(\frac{U}{U^*} \right)^{1.25} \qquad \text{(II.46)}$$

For the parameter α_w, the recommended default value 0.64 has been used.

II.3.5. UNDBE (IGE, Ukraine)

II.3.5.1. General description of the model

The model UNDBE takes into account that the pollutant flows past in two stages. In the first step each portion of the water and pollutant only moves through the reservoir to the outflow. There is no dilution, no interaction with bottom and suspended sediments, and no chemical and physical transformations. With such assumptions it is possible to write:

$$\vec{C}_{out}(t,x) = \vec{C}_{inf}(t - \frac{A}{Q}x) = \vec{C}_{inf}(t - \frac{L}{v}) \qquad \text{(II.47)}$$

where:

$\vec{C}_{out}$ is the vector of concentrations in the outflow;
$\vec{C}_{inf}$ is the vector of concentrations in the inflow;
A is the cross-sectional area;
Q is the stream flow rate;
v is the average velocity of flowing (= Q/A);
L is the length of streamline; and
L/v is the time of transportation of water (and of the pollutant) through a reservoir.

In the second step, only at the end of transportation, each portion of the water and pollutant mix in a certain part (V/n) of compartment volume V and interacts there with suspended and bottom sediments as in a usual box model.

Therefore with allowance (Equation II.47) for volume V/n located near the outflow of the box, it can be written:

$$\frac{d(V\vec{C}^*)}{ndt} = Q_{inf}\vec{C}_{inf}(t-\frac{L}{V}) - Q\vec{C}^* + V\vec{R}^*(\vec{C}^*,\vec{P}^*) \quad \text{(II.48)}$$

where:

$\vec{C}^*$ is the vector of average concentrations in volume V/n;
Q_{inf} is the stream flow rate in the inflow;
Q is the stream flow rate in the outflow;
$\vec{R}^*(\vec{C}^*,\vec{P}^*)$ is the vector of rates of change of the averaged concentrations due to conversion processes; and
P* are the parameters of transformation of the contamination.

Such an approach takes account time of movement of water masses and mixing of contamination in some part of volume of the box at the moment of a termination of the transport, and all transformations of contamination during the transport are reduced to equivalent transformations in volume V/n.

These assumptions are incorporated into a model which includes a system of differential equations with retardation parameter T_R = L/v = W/Q, where W = volume of the box where water exchange occurs (Figure II.17).

The processes of sorption-desorption are modeled as follows:

$$\frac{dC^d}{dt} = a_{1,2}(K_d C - C^d) \quad \text{(II.49)}$$

where:

$a_{1,2} = \frac{f_{1,2}}{\tau_s} + \frac{f_{2,1}}{\tau_{ds}}$;
K_d is the distribution coefficient; and
τ_s , τ_{ds} are the time sorption and desorption respectively.

Parameters $f_{1,2}$ and $f_{2,1}$ determine the direction of the pollution movement:

$$f_{1,2} = \begin{cases} 1, & K_d C > C^d \\ 0, & K_d C < C^d \end{cases} \quad f_{2,1} = \begin{cases} 1, & K_d C < C^d \\ 0, & K_d C > C^d \end{cases} \quad \text{(II.50)}$$

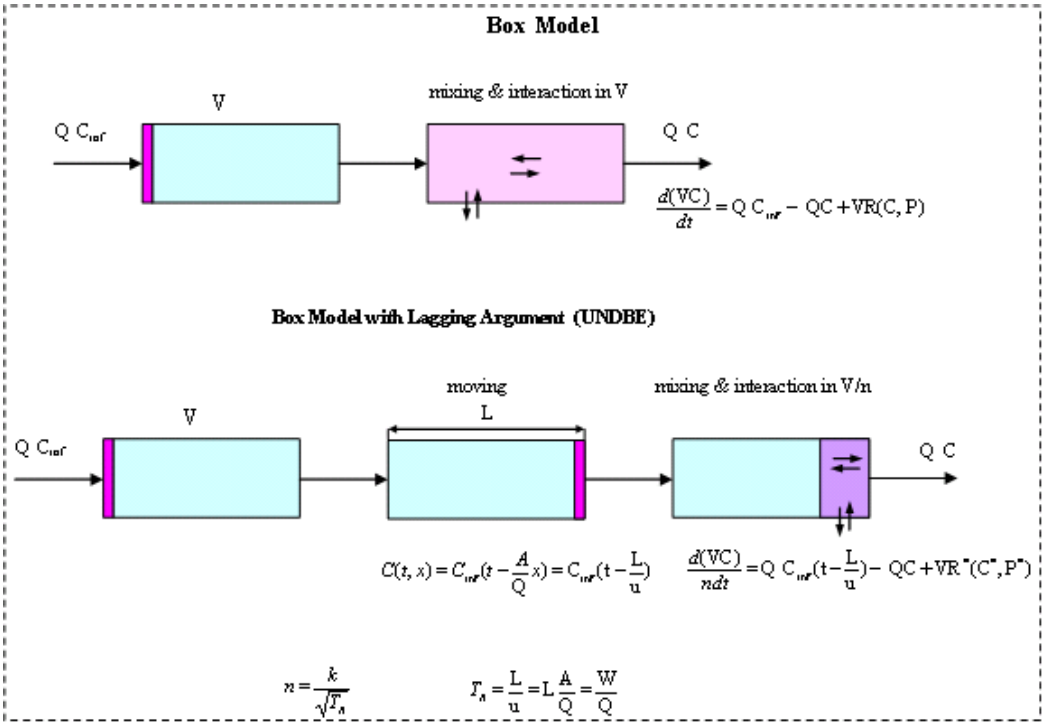

Fig. II.17. Assumptions of the box model and box model with lagging argument (UNDBE).

If the boxes are connected sequentially, for i[th] box the set of equations becomes:

$$\frac{d(V_i S_i)}{n dt} = Q_i \left[\tilde{S}_{i-1}(t - T_R) - S_i\right] + q_i^b - q_i^s + R_i^h \qquad \text{(II.51)}$$

$$\frac{d(V_i C_i)}{n dt} = Q_i \left[\tilde{C}_{i-1}(t - T_R) - C_i\right] - a_{1,2}(K_s C_i - C_i^s) - a_{1,3}(K_d C_i - C_i^b) - \lambda V_i C_i \qquad \text{(II.52)}$$

$$\frac{d(V_i S_i C_i^s)}{n_e dt} = Q_i \left[S_{i-1}^*(t - T_R) C_{i-1}^{s*}(t - T_R) - S_i C_i^s\right] + a_{1,2}(K_s C_i - C_i^s) - \lambda V_i S_i C_i^s + C_i^b q_i^b - C_i^s q_i^s \qquad \text{(II.53)}$$

$$\frac{dC_i^b}{dt} = \frac{1}{M_i^b}\left[-C_i^b(a_{1,3} + q_i^b + \lambda M_i^b) + C_i^s q_i^s + K_d a_{1,3} C_i\right] \qquad \text{(II.54)}$$

where:

q_i^b and q_i^s are the compartmentally integrated rates of resuspension and sedimentation;

K_d, K_s are the distribution coefficients in the water-bottom sediment and water-suspended sediments systems, respectively;

M^b_i is the mass of bottom deposits;

$\lambda = \ln 2 / T^*$ where T^* is the radionuclide half-life; and

$\tilde{S}_{i-1}$, $\tilde{C}_{i-1}$, $\tilde{C}^s_{i-1}$ are the concentrations in the inflow of the compartment from previous compartment and j tributaries. It is assumed that the tributaries are situated at the inflow of the box. If there are major tributaries significantly affecting water exchange, the partition of the water body in boxes should be realized such that the beginning of the box coincides with the location of the tributaries.

$$\tilde{S}_{i-1}(t-T_R)=\frac{Q_{i-1}(t-T_R)S_{i-1}(t-T_R)+\sum_j Q_j^t(t-T_R)S_j^t(t-T_R)}{Q_{i-1}(t-T_R)+\sum_j Q_j^t(t-T_R)} \quad \text{(II.55)}$$

$$\tilde{C}_{i-1}(t-T_R)=\frac{Q_{i-1}(t-T_R)C_{i-1}(t-T_R)+\sum_j Q_j^t(t-T_R)C_j^t(t-T_R)}{Q_{i-1}(t-T_R)+\sum_j Q_j^t(t-T_R)} \quad \text{(II.56)}$$

$$\tilde{C}_{i-1}^{s}(t-T_R)=\frac{Q_{i-1}(t-T_R)S_{i-1}(t-T_R)C_{i-1}^{s}(t-T_R)+\sum_j Q_j^t(t-T_R)S_j^t(t-T_R)C_j^{st}(t-T_R)}{Q_{i-1}(t-T_R)+\sum_j Q_j^t(t-T_R)} \quad \text{(II.57)}$$

where Q^t, S^t, C^t are the stream flow rate, sediment concentration and concentration of contamination in tributaries.

In the Equations II.51 to II.57, S_i, C_i, C_i^s, C_i^b are concentrations averaged, not over the total volume of the compartment, but only over the V/n part found at the outlet. Therefore for separation of a water body into boxes, it is necessary to arrange the inflow of boxes so that they coincide with the locations necessary for the analysis of the water body.

This model was used for predicting the concentrations ^{90}Sr in the cascade of r. Dnieper reservoirs after the Chernobyl catastrophe [II.47, II.48].

II.3.5.2. Customisation of the model UNDBE for River Loire

The channel of the River Loire, with a length of 350 km, was divided into 33 sequential boxes. The boundaries of boxes were located in the following places:

- beginning and end of a river segment;
- places where values of concentration are required;
- locations of weirs;
- locations of tributaries; and
- places where Nuclear Power Plants are located (points of inflow of Tritium).

A lack of interaction with suspended sediments was assumed for simulation of tritium transport. Therefore values of S_i, C_i^s, q_i^b and q_i^s in the equations II.51 to II.57 were given a value of zero.

The time step of the simulation was one hour. The stream flow rates within each hour were considered as constants.

For the definition of the volumes of the boxes, which were used in the equations II.51 to II.53, for each hour the curve of a free surface was calculated. The spatial step of the calculations along the channel was 10 m.

The calculations of levels of the water surface were undertaken in a one-dimensional stationary model:

$$\frac{dz}{dx} = \frac{Q^2}{c^2 h F^2}\left[1 - \frac{c^2 h}{gF} \cdot \frac{dF}{dx}\right] \qquad \text{(II.58)}$$

where:

Q is the stream flow rate;

$c = \frac{1}{M} h^{\frac{1}{6}}$ is the Chezy coefficient;

M is the roughness coefficient;

g is the gravity;

B is the width of a water flow;

F is the area of profile; and

h = F/B is the average depth.

For each part of the channel in the River Loire located between two weirs the calibration for several various values of Q was made.

The roughness coefficient was defined for each Q,so that for given level of the lower weir $z_d = f_d(Q)$, the level of water at the upper weir calculated in the Equation II.58, in which $z_u = f_u(Q)$, where $f_d(Q)$ and $f_u(Q)$ are given rules of a modification of levels from stream flow rate in places of the lower and upper weirs accordingly.

The approximation $M = f_m(Q)$ was used on several pairs of values (M : Q).

For majority of sites in the river channel the approximation looks like: $M = k_1 Q^{-k_2}$, where k_1 and k_2 constants. The obtained approximations have allowed the calculation the flow at the water levels for each hour during the time interval of the modelling.

The cross-section profiles appropriate to calculate levels, multiplied by a spatial step of the calculations along the channel were obtained in the total length of the boxes for determination of the volumes of the boxes.

The wetted perimeters of the river profiles appropriate to calculate levels, multiplied by a spatial step of the calculations along the channel were obtained in the total length of the boxes for evaluation of the area of the bottom of the boxes.

For definition of time of transportation in connection with the formula $T_R = L/v = W/Q$, it was taken into account that not whole volume of the box V participates in water exchange. In each box there is a volume, which is not displaced by the water masses arriving at the box.

During the first test example the volume of the box participating in water exchange, from a current stream flow rate in the box was defined as (average for all boxes):

$$W_i(t) = V_i(t)(1 - k_3 EXP(-k_4 Q_i(t)/Q_{0i})) \qquad \text{(II.59)}$$

where:

W_i is the volume of the box participating in water exchange;

V_i is the compartment volume;

k_3, k_4 are the constants;

Q_i is the stream flow rate; and

Q_{0i} is the minimal stream flow rate.

The magnitude of the volume of mixing V/n depends on the time of transporting of water masses in the box. The value of n was defined by the formula: $n = \frac{k_5}{\sqrt{T_R}}$ [II.49], where T_R is time of transportation of water through a reservoir in a day. For the River Loire k_5 was taken as equal to 3.9.

The following values of the parameters for exchange with the bottom sediments were used for simulation:

K_d = 150 l/kg, τ_s = 50 day, τ_{ds} = 50 day.

The mass of contaminated sediments was assumed to be constant and is described as:

$$M_i^b = \rho_s Z_* U_i \qquad \text{(II.60)}$$

where:

ρ_s is the density of sediment with allowance for porosity (1.6);
Z_* is the effective thickness of the contaminated sediment (0.6 cm); and
U_i is the area of the bottom of the box.

The outputs obtained with the model UNDBE in Angers and compared to measurements, are represented in Figure 4.12 in the main text. The figure demonstrates good agreement between the model output and the measurements, but for an evaluation of a more exact comparison it is necessary to know the numerical values and errors of the measurements.

The offered test examples comprise single, short-term releases of tritium, which gives rise to rapid increases of concentration, especially close to the NPP. The concentration can increase and decrease tenfold within a day. Therefore the average daily concentration cannot be representative. Such a situation requires only one hour steps in the modelling.

In the absence of any interaction between tritium between the water and suspended sediments and minimum levels of interaction between water and bottom sediments the basic difficulty consist of calibrating the hydrological part of the model including the definition of parameters associated with the roughness coefficient $M = f_m(Q)$ and $W_i(t)$ (Equation II.59).

The water levels measurements and flow rates data on the Loire River for different flow regimes (on different dates) and field water tracer studies were not used for adaptating the model.

The numerical box model with the lagging argument (UNDBE) is simple, less dependent on full-scale measurements and entails only a short time of computation. The short time required gives the opportunity to address the task of parameter identification – adapting the model for the scenario. This contributes to increase the accuracy of the model and provides the possibility of adapting it to a particular water body.

II.4. Radioactive contamination of the Techa River

II.4.1. Model CASTEAUR (IRSN, Cadarache, France)

Four box modelling modules of the code CASTEAURv0.1 are involved: hydrographical, hydraulic, sedimentary and radioecological for the water and the solids matters.

II.4.1.1. Hydrographical module

The hydrographical model describes the geometry of the river. Based on a succession of reaches, constituting a linear hydrographic network, the aim of the model is to give a linear grid in function of a space step Δx (m) precise by the user. At this end, a simplified trapezium bathymetric form is considered to describe the sections.

The variables are the hydrographical parameters at each space step i:

L_i: length ($\approx \Delta x$ *m*);
l_i: width (*m*);
φ_i: bank angle (*rad*); and
I_i: slope ($m.m^{-1}$).

The input data are a linear succession of reach characterized by:

L_b: length (*m*);
l_b: width (*m*);
φ_b: bank angle (*rad*); and
I_b: slope ($m.m^{-1}$).

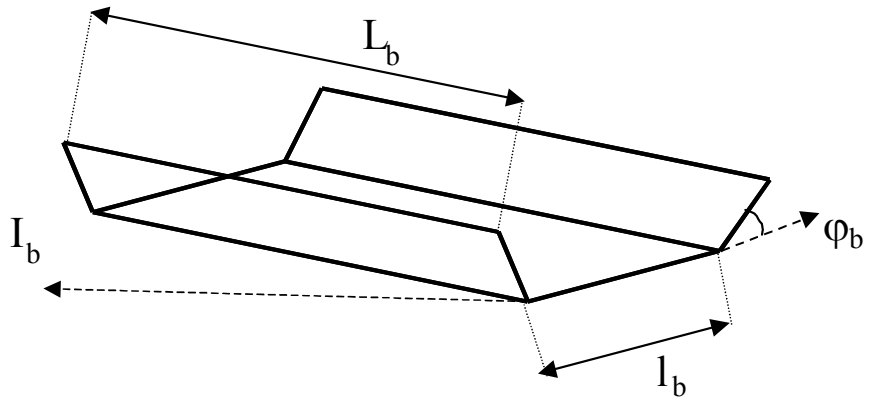

Fig. II.18. Hydrographical paramters.

II.4.1.2. Hydraulic module

The hydraulic module assesses the spatial and temporal evolutions of the water column.

Variables

The hydraulics variables are:

Q_i^j: water flow ($m^3.s^{-1}$);
$w_{i\ wc}^j$: water volume (m^3);
h_i^j: water depth (m^3);
SM_i^j: wet section (m^2);
PM_i^j: wet perimeter (m);
Rh_i^j: hydraulic radius (m); and
τ_i^j: bottom shear stress ($N.m^{-2}$).

Input data

The input data are:

q_i^j: specific water inflow ($m^3.s^{-1}$); and
Ks_i: Strickler coefficient ($m^{1/3}.s^{-1}$).

Modelling

The modelling is based on the two following equations allowing the determination of the water flow Q_i^j and of the water depths h_i^j:

$$\frac{d\, w_{i\ wc}^j}{dt} = Q_{i-1}^j + q_i^j - Q_i^j \qquad \text{(II.61)}$$

and

$$U_i^j = \frac{Q_i^j}{SM_i^j} = Ks_i \cdot Rh_i^{j\,\frac{2}{3}} \cdot \sqrt{I_i} \qquad \text{(II.62)}$$

The others parameters are deduced from h_i^j:

$$SM_i^j = h_b^t \cdot \frac{l_i \cdot \sin(\varphi_i) + h_i^j \cdot \cos(\varphi_i)}{\sin(\varphi i_i)} \;;\; PM_i^j = \frac{l_i \cdot \sin(\varphi_i) + 2 \cdot h_i^j}{\sin(\varphi i_i)} \;;\; Rh_i^j = \frac{SM_i^j}{PM_i^j} \;;$$

$$w_{i\ wc}^j = L_i \cdot SM_i^j \;;\; \tau_i^j = I_i \cdot \rho_w \cdot g \cdot Rh_i^j \qquad \text{(II.63)}$$

II.4.1.3. Sedimentary module

The the sedimentary model calculates the stocks and the fluxes of matters in the water column and the bottom sediment. The model can take into account several classes of matter and considers three bottom sediment layers: an interface, an active and a passive. The interface layer is a very fine layer constituted of recent deposit not compacted yet. It is supposed that whatever the matters, their behaviour in this layer is always non-cohesive. The active layer results from the compaction of the interface. It is called active because the interstitial water remains enough mobile to allow the dissolved radionuclide phases to be exchanged with the column by interstitial diffusion. The compaction of the active layer feeds the passive layer. In this third layer the consolidation becomes strong enough to reduce the mobility of interstitial water and the exchanges of dissolved radionuclide phases become negligible.

Variables

The variables of this modelling are:

$m_{i\ wc}^{j}$: mass of class m in the water column (*kg and* m^3);
$m_{i\ il}^{j}$ and $w_{i\ il}^{j}$: mass of class m and volume of water in the interface layer (*kg and* m^3);
$m_{i\ al}^{j}$ and $w_{i\ al}^{j}$: mass of class m and volume of water in the active layer (*kg and* m^3); and
$m_{i\ pl}^{j}$ and $w_{i\ pl}^{j}$: mass of class m and volume of water in the passive layer (*kg and* m^3);

Input data

The input data are the parameters of the class of matter and of the bottom sediment layers. Each class of matter is defined by:

ϕ_j : diameter (μm);
ρ_j : volume masses ($kg.m^{-3}$); and
$q^j_{i,m}$: specific import ($kg.s^{-1}$).

The diameter and the volume masses are used to give ws_m ($m.s^{-1}$), the settling velocity (Stokes formula), τce_m ($N.m^{-2}$), the critical erosion shear stress (Yalin method, see reference [II.50]) and e_m ($kg.m^{-2}.s^{-1}$), the erosion rate (empirical relation, $e_m = 1{,}4 \cdot 10^{-3} \cdot \tau ce_m^{\ 1.8}$).

The bottom sediment layers are characterized by:

$hmax_{il}$: maximal thickness of the interface layer (m);
ϕ_{il}: water content of the interface layer ($\%$);
$hmax_{al}$: maximal thickness of the active layer (m);
ϕ_{al}: water content of the active layer (%);
tas_{al}: coefficient of consolidation of the active layer (-);
ϕ_{pl}: water content of the passive layer (%); and
tas_{pl}: coefficient of consolidation of the passive layer (-).

Modelling

The fluxes involved in the sedimentary modelling are illustrated in Figure II.19.

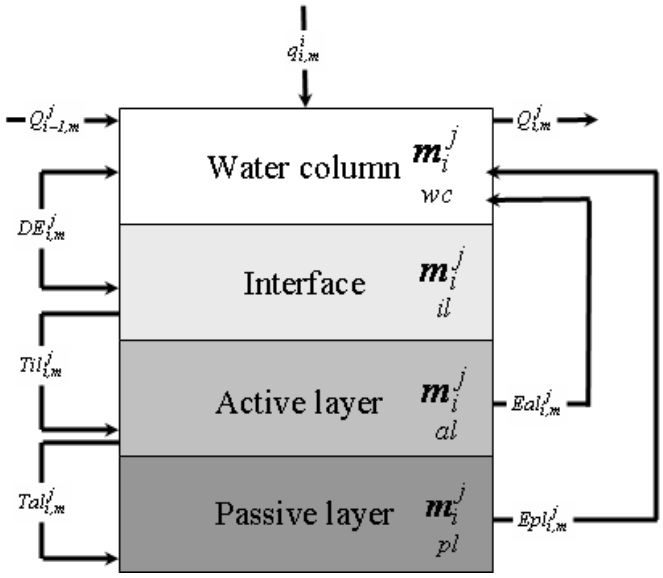

Fig. II.19. Structure of the sedimentary sub-model.

This view is associated to the following equation set:

Class of matter	Water
$\frac{d\, m^j_{i\ wc}}{dt} = Q^j_{i-1,m} + q^j_{i,m} - Q^j_{i,m} - DE^j_{i,m} + Eal^j_{i,m} + Epl^j_{i,m}$	$w^j_{i\ wc}$: given by the hydraulic model
$\frac{d\, m^j_{i\ il}}{dt} = DE^j_{i,m} - Til^j_{i,m}$	$w^j_{i\ il} = \frac{\Phi_{il} \cdot \sum_m m^j_{i\ il}}{\rho_w}$
$\frac{d\, m^j_{i\ al}}{dt} = Til^j_{i,m} - Tal^j_{i,m} - Eal^j_{i,m}$	$w^j_{i\ al} = \frac{\Phi_{al} \cdot \sum_m m^j_{i\ al}}{\rho_w}$
$\frac{d\, m^j_{i\ pl}}{dt} = Tal^j_{i,m} - Epl^j_{i,m}$	$w^j_{i\ pl} = \frac{\Phi_{pl} \cdot \sum_m m^j_{i\ pl}}{\rho_w}$

where:

$Q_{i\text{-}1,m}{}^j$ and $Q_{i,m}{}^j$ are the entering flux, coming from the upstream reach, and the outgoing flux.

$$Q^j_{i-1,m} = Q^j_{i-1} \cdot \frac{m^j_{i-1\ wc}}{wc^j_{i-1}} \qquad \text{(II.64)}$$

and

$$Q_{i,m}^{j} = Q_i^j \cdot \frac{m_i^j}{wc_i^j} \quad \text{(II.65)}$$

$q_{i,m}^{j}$ are the specific entering flux coming from outside the study domain. They are input data.

$DE_{i,m}^{j}$ is the balance, for the particle class *m*, of the erosion and deposition fluxes between the water column and the interface layer. Its formulation is given by [II.51]:

$$DE_{i,m}^{j} = \frac{Wc_m}{Rh_i^j} \cdot (m_{i\ wc}^{j} - m_{i\ wc}^{j\ *}) \quad \text{(II.66)}$$

$m_{i\ wc}^{j\ *}$ is the equilibrium mass of class m in the water column. It is given by:

$$m_{i\ wc}^{j\ *} = \frac{e_m}{Wc_m} \cdot (\frac{\tau_i^j}{\tau ce_m} - 1) \cdot wc_i^j \text{ if } \tau_i^j > \tau ce_m \quad \text{(II.67)}$$

and

$$m_{i\ wc}^{j\ *} = 0 \text{ if } \tau_i^j \le \tau ce_m \quad \text{(II.68)}$$

$Til_{b,m}^{j}$ and $Tal_{b,m}^{j}$ are the matter fluxes resulting from the compaction of the interface and active layers. When the thickness of a layer becomes larger than its maximal value, the matter in excess is transferred to the inferior layer. These transfers concern the melange. The fluxes by class are deduced from the contribution of each class to the melange.

$Eal_{b,m}^{j}$ and $Epl_{b,m}^{j}$ are the erosion fluxes of the active and passive layers. For each one, these fluxes are activated only if the superior layer has been totally eroded. These fluxes, modelled with the approach of Partheniades [II.30], are applied to the melange considering its average sedimentary properties pondered by the coefficients of consolidation. The transfers by class are already known, according to the contribution of each class to the melange.

II.4.1.4. Radioecological module

The radioecological model uses the results provided by the hydraulic and sedimentary models to compute spatio-temporal distributions of the radionuclides activities (Bq) under their dissolved and solid forms in the different compartments: water column, interface, active and passive layers. Considering the small thickness of the interface layer, an equilibrium hypothesis between this layer and the water column is assumed. So, these two compartments are joining, for the radioecological model, in a same one noted *wcil*.

Variables

The variables of the radioecoligical model are the activities in the different components.

$r_{b,w\ wc}^{j}$ and $r_{b,m\ wc}^{j}$:dissolved and particulate activities in the water column (*Bq*);

$r^{j}_{\substack{b,w \\ il}}$ and $r^{j}_{\substack{b,m \\ il}}$:dissolved and particulate activities in the interface (*Bq*);

$r^{j}_{\substack{b,w \\ wcil}}$ and $r^{j}_{\substack{b,m \\ wcil}}$: dissolved and particulate activities in the join compartment (*wc*+ *il*) (*Bq*);

$r^{j}_{\substack{b,w \\ al}}$ and $r^{j}_{\substack{b,m \\ al}}$:dissolved and particulate activities in the active layer (*Bq*); and

$r^{j}_{\substack{b,w \\ pl}}$ and $r^{j}_{\substack{b,m \\ pl}}$:dissolved and particulate activities in the passive layer (*Bq*).

Input data

The input data are:

λ_r: radioactive decay (s^{-1})
Kd_r: coefficient of equilibrium fractionation between dissolved and solid phases ($m^3.kg^{-1}$)
$q^j_{i,m,r}$: specific radionuclide import under m particulate phase (*Bq.s-1*)
$q^j_{i,w,r}$: specific radionuclide import under dissolved phase ($Bq.s^{-1}$)

Modelling

Two kinds of radionuclide fluxes are taken into account: (1) between reaches and components and (2) between solid and dissolved phases.

Fluxes between the reaches and the components

These fluxes which concern the dissolved and the solid phases are respectively presented in Figure II.20.

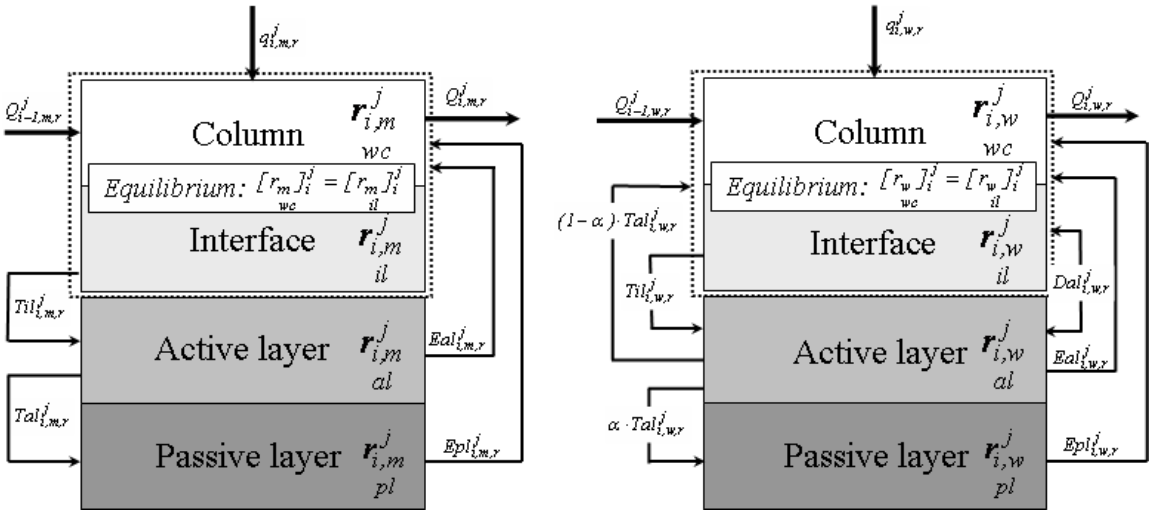

Solids fluxes **Dissolved fluxes**

Fig. II.20. Structure of the submodels of the dissolved and solid phases.

These concepts are associated to the following set of equation for the solid phases:

$$\frac{d\, r_{i,m}^{j}}{dt}_{wcil} = Q_{i-1,m,r}^{j} + q_{i,m,r}^{j} - Q_{i,m,r}^{j} - Til_{i,m,r}^{j} + Eal_{i,m,r}^{j} + Epl_{i,m,r}^{j} - \lambda_r \cdot r_{i,m}^{j}_{wcil} \quad \text{(II.69)}$$

$$\frac{d\, r_{i,m}^{j}}{dt}_{al} = -Eal_{i,m,r}^{j} - Tal_{i,m,r}^{j} + Til_{i,m,r}^{j} - \lambda_r \cdot r_{i,m}^{j}_{al} \quad \text{(II.70)}$$

$$\frac{d\, r_{i,m}^{j}}{dt}_{pl} = -Epl_{i,m,r}^{j} + Tal_{i,m,r}^{j} - \lambda_r \cdot r_{i,m}^{j}_{pl} \quad \text{(II.71)}$$

and to the following one for the dissolved phases:

$$\frac{d\, r_{i,w}^{j}}{dt}_{wcil} = Q_{i-1,w,r}^{j} + q_{i,w,r}^{j} - Q_{i,w,r}^{j} + Eal_{i,w,r}^{j} + Epl_{i,w,r}^{j} - Til_{i,w,r}^{j} + (1-\alpha)\cdot Tal_{i,w,r}^{j} + Dal_{i,w,r}^{j} - \lambda_r \cdot r_{i,w}^{j}_{wcil} \quad \text{(II.72)}$$

$$\frac{d\, r_{i,w}^{j}}{dt}_{al} = -Eal_{i,w,r}^{j} - Tal_{i,w,r}^{j} + Til_{i,w,r}^{j} + Dal_{i,w,r}^{j} - \lambda_r \cdot r_{i,w}^{j}_{al} \quad \text{(II.73)}$$

$$\frac{d\, r_{i,w}^{j}}{dt}_{pl} = -Epl_{i,w,r}^{j} + \alpha \cdot Tal_{i,w,r}^{j} - \lambda_r \cdot r_{i,w}^{j}_{pl} \quad \text{(II.74)}$$

The fluxes with a same notation than a hydraulic or a sedimentary one ($Q_{b,m,r}^{j}$, $q_{b,m,r}^{j}$, $Cil_{b,m,r}^{j}$, $Cal_{b,m,r}^{j}$, $Eal_{b,m,r}^{j}$, $Epl_{b,m,r}^{j}$, $Q_{b,w,r}^{j}$, $q_{b,w,r}^{j}$, $Cil_{b,w,r}^{j}$, $Cal_{b,w,r}^{j}$, $Eal_{b,w,r}^{j}$, $Epl_{b,w,r}^{j}$) correspond to the radioecological fluxes consecutively to these physicals fluxes. With the generic notations *cmp* for component and *F* for flux, they are directly given by:

$$F_{i,m,r}^{j} = F_{i,m}^{j} \cdot [\, r \,]_{i,m}^{j}_{cmp} = F_{i,m}^{j} \cdot \frac{r_{i,m}^{j}}{m_i^{j}}_{cmp} \quad \text{(II.75)}$$

and

$$F_{i,w,r}^{j} = \frac{\phi_{cmp} \cdot F_{b,m}^{j}}{\rho_w} \cdot \frac{r_{b,w}^{j}}{w_b^{j}}_{cmp} \quad \text{(II.76)}$$

Not the particular case of the compartment *wcil,* where the entering and the exiting fluxes are given by:

$$Q_{i,m,r}^{j} = Q_{i,m}^{j} \cdot \frac{r_{i,m}^{j}}{m_i^{j}}_{wc} \quad \text{(II.77)}$$

and

$$Q_{i,w,r}^{j} = Q_{i}^{j} \cdot \frac{r_{i,w}^{j}}{\underset{wc}{w_{i}^{j}}} \qquad \text{(II.78)}$$

$q_{i,m,r}{}^{j}$ and $q_{i,w,r}{}^{j}$ are the entering fluxes coming from outside the study domain. They are input data.

$Dal_{i,w,r}{}^{j}$ is the diffusing flux of the dissolved phase between the active layer and the water column. It is given by [II.52]:

$$Dal_{i,w,r}^{j} = K_{i}^{j} \cdot \left(\frac{r_{i,w}^{j}}{\underset{wcil}{w_{i}^{j}}} - \frac{r_{i,w}^{j}}{\underset{al}{w_{i}^{j}}}\right) = \frac{Kal_{i}^{j} \cdot Kwcil_{i}^{i}}{Kal_{i}^{j} + Kwcil_{i}^{j}} \cdot \left(\frac{r_{i,w}^{j}}{\underset{wcil}{w_{i}^{j}}} - \frac{r_{i,w}^{j}}{\underset{al}{w_{i}^{j}}}\right) \cdot L_{i} \cdot PM_{i}^{j} \qquad \text{(II.79)}$$

Kal_{i}^{j} and $Kwcil_{i}^{i}$ (m.s^{-1}) are the transfers coefficient respectively from the active layer and from the column. They are given by:

$$Kwcil_{i}^{j} = max\left(\frac{10^{-9}}{h_{i}^{j}}; 10^{-3} \cdot u*_{i}^{j}\right) \qquad \text{(II.80)}$$

and

$$Kal_{i}^{j} = \frac{10^{-9} \cdot pal_{i}^{j}}{hal_{i}^{j} \cdot (1 - ln(pal_{i}^{j\,2}))} \qquad \text{(II.81)}$$

In these expressions:

u^{*j}_{i} : friction velocity, $\quad u^{*j}_{i} = \sqrt{\frac{\tau_{i}^{j}}{\rho_{w}}}$

hal_{i}^{j} : depth of the active layer, $\quad hal_{i}^{j} = \frac{\underset{al}{w_{i}^{j}} + \sum_{m} \frac{m_{i}^{j}}{\underset{al}{\rho_{m}}}}{PM_{i}^{j} \cdot L_{i}}$

pal_{i}^{j} : porosity of the active layer, $\quad pal_{i}^{j} = \frac{\underset{al}{w_{i}^{j}}}{\underset{al}{w_{i}^{j}} + \sum_{m} \frac{m_{i}^{j}}{\rho_{m}}}$

$\underset{al}{w_{i}^{j}}$: water volume of the active layer, $\quad \underset{al}{w_{i}^{j}} = \frac{\phi al}{\rho_{w}} \cdot \sum_{m} m_{i}^{j}$

Fractionation between solid and dissolved phases

The fractionation between the solids and the dissolved phases is considered with an equilibrium hypothesis. In each component *cmp*, this partition is given by:

$$r^{j}_{i,w\ cmp} = \frac{w^{j}_{i\ cmp} \cdot r^{j}_{i\ cmp}}{w^{j}_{i\ cmp} + \sum_{m} Kd_{m,r} \cdot m^{j}_{i\ cmp}} \quad \text{(II.82)}$$

and

$$r^{j}_{i,m\ cmp} = Kd_{m,r} \cdot \frac{m^{j}_{i\ cmp}}{w^{j}_{i\ cmp}} \cdot r^{j}_{i,w\ cmp} \quad \text{(II.83)}$$

with:

$$r^{j}_{i\ cpm} = r^{j}_{i,w\ cmp} + \sum_{m} r^{j}_{i,m\ cmp}$$

$Kd_{m,r}$: coefficient of equilibrium fractionation between dissolved and solid phase m ($m^3.kg^{-1}$).

For each class $Kd_{m,r}$ are calculated by [II.53]:

$$\text{If } \xi_{m,r} \geq \delta_m \Rightarrow Kd_{m,r} = \frac{[rs]_m}{[r]_w} = Kd_r \quad \text{(II.84)}$$

$$\text{If } \xi_{m,r} < \delta_m \Rightarrow Kd_{m,r} = Kd_r \cdot (1 - (1 - \frac{\xi_{m,r}}{\delta_m})^3) \quad \text{(II.85)}$$

with:

$\xi_{m,r}$: thickness of the particles available for the adsorption ($\approx 1.7\ \mu m$),
$\delta_{m,r}$: radius of the particles (μm).

Partition of the activities between the water column and the interface

The activities in the compartment *wcil* correspond to:

$$w^{j}_{b,m\ wcil} = w^{j}_{b\ wc} + w^{j}_{b\ il} \;;\; m^{j}_{b,w\ wcil} = m^{j}_{b,w\ wc} + m^{j}_{b,w\ il} \;;\; r^{j}_{b,m\ wcil} = r^{j}_{b,m\ wc} + r^{j}_{b,m\ il} \;;\; r^{j}_{b,w\ wcil} = r^{j}_{b,w\ wc} + r^{j}_{b,w\ il} \;;\; r^{j}_{b\ wcil} = r^{j}_{b,w\ wcil} + r^{j}_{b,m\ wcil} \quad \text{(II.86)}$$

The dissolved and solid activities in the water column and the interface layer are:

$$r^{j}_{b,m\ wc} = m^{j}_{b\ wc} \cdot [r]^{j}_{b,m\ wcil} \;;\; r^{j}_{b,w\ wc} = w^{j}_{b\ wc} \cdot [r]^{j}_{b,w\ wcil} \;;\; r^{j}_{b,m\ il} = m^{j}_{b\ il} \cdot [r]^{j}_{b,m\ wcil} \;;\; r^{j}_{b,w\ il} = w^{j}_{b\ il} \cdot [r]^{j}_{b,w\ wcil} \quad \text{(II.87)}$$

II.4.1.5. Parameterization for the Techa scenario

This part describes the parameterization of the previous models for the application to the Techa River. This parameterization is based on the scenario proposed by Typhoon [II.54]. It can be noted that the application involves two calibrations: *Ks*, the strickler coefficient and Kd_r, the coefficient of equilibrium fractionation between the solid and liquid phases. All the others parameters are input data.

Hydrographic parameters

The calculation domain is 207 km long from the dam 11 to the river mouth. The domain is characterized by an average slope of 0.0006 m/m. The hydrographical data divide the domain into 18 reaches to represent, from 0 to 207 km an increase of the width by step of 1m, from 18 to 35 m. The bank angle is put at 45° all along the domain. Table II.16 and Figure II.21 present these data.

For the calculations, this domain is divided with a space step Δx = 1km.

Table II.16. Hydrographical data.

ID_Reach	Entering PK Slope	(km) (m/m)	Length Bank slope	(km) (°)	Width
0	0	11.5	18	0.0006	45
1	11.5	11.5	19	0.0006	45
2	23	11.5	20	0.0006	45
3	34.5	11.5	21	0.0006	45
4	46	11.5	22	0.0006	45
5	57.5	11.5	23	0.0006	45
6	69	11.5	24	0.0006	45
7	80.5	11.5	25	0.0006	45
8	92	11.5	26	0.0006	45
9	103.5	11.5	27	0.0006	45
10	115	11.5	28	0.0006	45
11	126.5	11.5	29	0.0006	45
12	138	11.5	30	0.0006	45
13	149.5	11.5	31	0.0006	45
14	161	11.5	32	0.0006	45
15	172.5	11.5	33	0.0006	45
16	184	11.5	34	0.0006	45
17	195.5	11.5	35	0.0006	45
18	207	11.5	36	0.0006	45

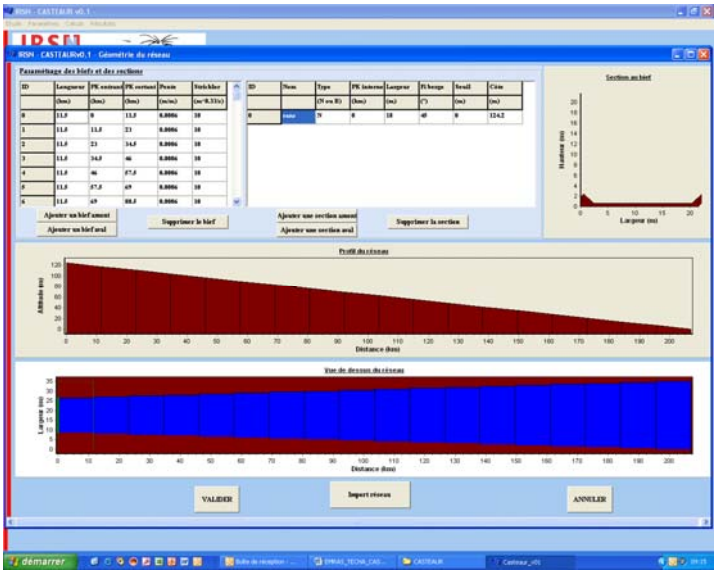

Fig. II.21. Hydrographical data window of CASTEAUR.

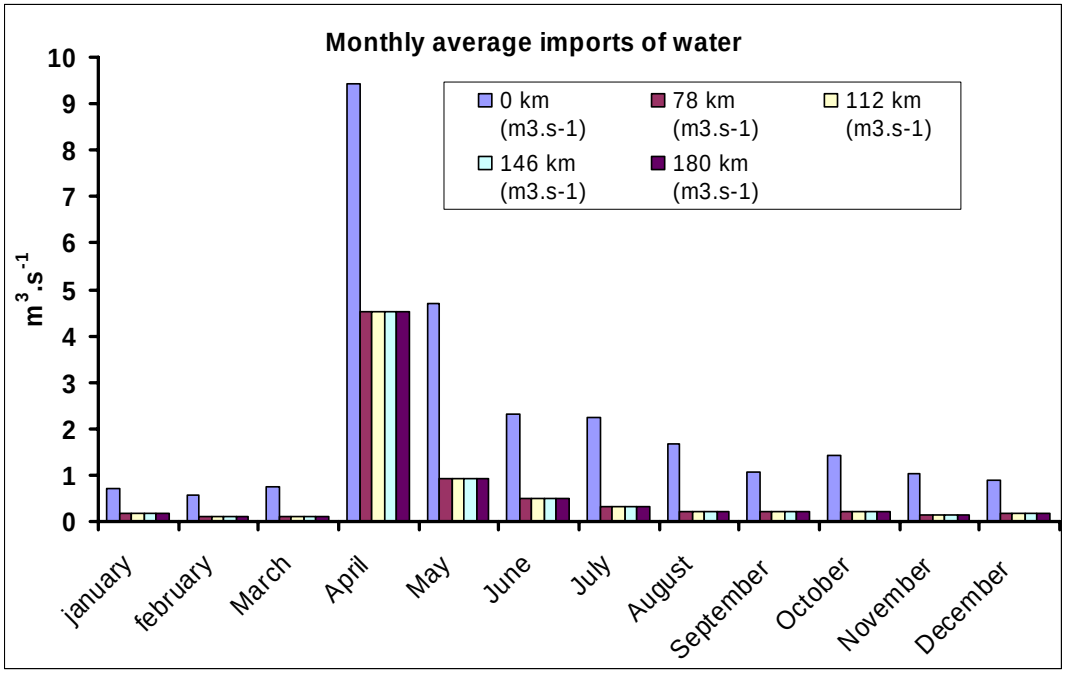

Fig. II.22. Water imports.

Hydraulics parameters

Water imports

At the entrance of the domain (*pk = 0km*), the imports of water are equalized to the average monthly values given at Muslyumovo (*pk = 44km*). Between 44 and 180 km, the waters discharges are defined by four contributions regularly distributed between 78 and 180 km. These contributions allow obtaining the monthly average water discharges given at 180 km in Table I.18 in Appendix I.

Calibration of the Strickler coefficient

The river depth is varying from 0.5 to 2 m. To obtain this range with the considered geometrical and the specific water inflow data, the calibration of the Strickler coefficient gives a value of 10 $m^{1/3}.s^{-1}$.

Sedimentary parameters

For the suspended matter, the scenario gives the monthly average turbidity at Pershinskoe and the granulometric distribution for the diameters 4, 8, 16, 32, 63, 125, 250, 500 and 1000 µm. Table II.17 presents the sedimentary parameters associated to each class of suspended matter.

Table II.17. Sedimentary parameters associated to each class of suspended matter.

D_m (µm)	ρ_m (kg.m^{-3})	w_m (cm.s^{-1})	Tce_m (N.m^{-2})	e_m (g.m^{-2}.s^{-1})
4	2650	0.0014	0.03	0.0021
8	2650	0.0057	0.04	0.0031
16	2650	0.0230	0.05	0.0050
32	2650	0.0900	0.06	0.0085
63	2650	0.3500	0.08	0.0150
125	2650	1.5000	0.12	0.0300
250	2650	6.0000	0.18	0.0620
500	2650	22.000	0.28	0.1400
1000	2650	90.000	0.48	0.3600

The parameters of the sedimentary layers are:

For interface layer: *hil = 50µm* *ϕil = 400%*
For active layer: *hal = 2 cm* *ϕal = 150%*
For passive layer: *ϕpl = 60%*

For this exercise, the erosive fluxes of the active and passive layers have been annihilated (*tasal and taspl* = ∞).

Imports of suspended matter

Each import of water is associated to a concentration for each class of suspended matter. These concentrations are deduced from the turbidity (Appendix I, Table I.19) and from the composition (Appendix I, Table I.21). The obtained values are presented in Figure II.23.

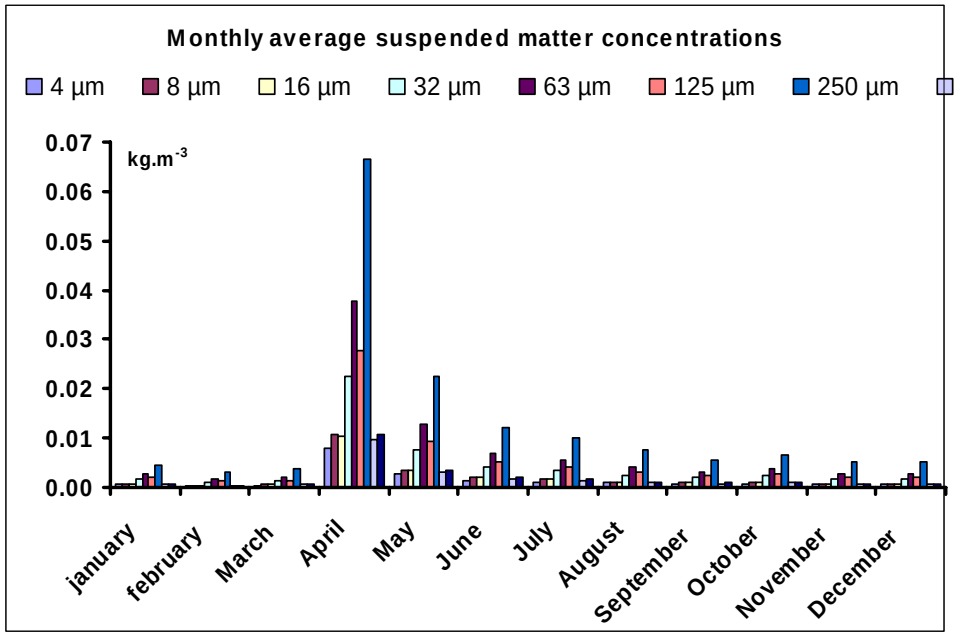

Fig. II.23. Monthly averages of suspended matter concentrations.

Radioecological parameters

The scenario considers three radionuclides: ^{90}Sr, ^{137}Cs $^{239,240}Pu$. Their parameters are λ_r, Kd_r and the imports. The decay constants are presented in Table II.18.

Imports of radionuclides

The scenario gives some details on the releases of radionuclides during the period from March 1950 to November 1951 and it gives the total annual values from 1976 to December 1996. On these bases, the imports are described considering three periods of release: 1) January 1950 to February 1950, 2) March 1950 to November 1951 and 3) November 1951 to December 1996. Whatever the period, all the imports are situated at the entrance of the domain ($pk = 0\ km$).

— **From January 1950 to February 1950:** No releases are considered during this period.

— **From March 1950 to November 1951:** During this period a daily discharge of 1.5·1014 Bq/day is given by the scenario. The radionuclides contributions allow determining the specific imports by radionuclides (see Table II.19).

— **From November 1951 to December 1996:** During this period, the releases are determined averaging the annual releases given by scenario from 1976 to 1994 (see Table II.20).

— **Kd calibration:** The Kd_r are adjusted to obtain the best agreement between the calculation and the measurements (see Table II.21).

— **Calculation parameters:** The parameters for the calculation are resumed in Table II.22.

For the correspondence between date and days, a constant period of 30 days has been considered for each month. For the sediment, the results are given for the active layer which corresponds to the first 2cm associated to the measurements in the scenario.

The empirical data of the scenario correspond to spatial distribution in the water column and in the two first centimetres of the bottom sediment. The date associated to these distributions is not precise (just the year, 1996). As the CASTEAUR calculations give the results with a temporal resolution of 10 days, the comparisons are given for the periods associated to the best agreement during 1996.

Table II.18. Radionuclide decay half-life.

Radionuclides	Half life
^{90}Sr	29 years
^{137}Cs	30 years
$^{239,240}Pu$	6563 years

Table II.19. Estimated radionuclide discharges from March 1950 to November 1951.

Radionuclides	Contribution	Bq/s
^{90}Sr	12%	2.08×10^{8}
^{137}Cs	12.2%	2.12×10^{8}
$^{239,240}Pu$	< 1%	1.74×10^{7}

Table II.20. Estimated values of radionuclide discharges from December 1951 to December 1996.

Radionuclides	Bq/s
^{90}Sr	$7.9 \cdot 10^{4}$
^{137}Cs	$2.4 \cdot 10^{3}$
$^{239,240}Pu$	3.5

Table II.21. Adjusted values of K_d.

Radionuclides	Kd ($m^3.kg^{-1}$)
^{90}Sr	0.3
^{137}Cs	15
$^{239,240}Pu$	10

Table II.22. Values of the parameters used for calculations.

Period	January 1950 to December 1996
Duration	16560 days
Time step	10 days
Space step	1 km

II.4.2. Model TRANSFER-2 (Atomenergoproject, Moscow, Russia)
Nosov A.V., Atomenergoproject, Moscow, Russia

For calculating the radionuclides concentrations in water in the Techa River in the case of stationary discharges from the nuclear facility a stationary two component model TRANSFER-2 for transport of radioactive material in the one-dimensional flow was used. The model is based on the turbulent diffusion equation and accounts for the interaction of radioactive substances between the water mass (solution, suspended material) and bottom sediments. The model is based on several simplifying assumptions:

(1) The exchange of radioactive material between water and bottom sediments is proportional to the radionuclide concentration in the liquid and solid phases;
(2) Sorption and desorption of radionuclides between the solution and solid phase is considered to be instantaneous, equilibrium and follows the linear isotherm with a constant distribution coefficient;
(3) Exchange between the bottom and water mass occurs within the equally accessible upper layer of bottom sediments with depth *h*;
(4) It is assumed that the channel does not get silted;
(5) In water, radioactive material is transported by the water flow and dispersed due to longitudinal turbulent dispersion. Radioactive material is distributed uniformly by river depth and account is taken only of the longitudinal component of convective dispersion
(6) The morphometric characteristics of the channel are invariable over the whole section of the river. The total water discharge of the lateral tributaries is negligible as compared to that of the main channel. Variations in the water discharge along the length of the river are due to changes in the flow velocity by the linear law.

The system of equations describing the radionuclides transport in the river downstream of the source of discharges is written as:

$$\begin{cases} \dfrac{\partial C_1}{\partial t} = \dfrac{1}{A}\dfrac{\partial}{\partial x}\left(A \cdot D_L \dfrac{\partial C_1}{\partial x} - QC_1 \right) - C_1\lambda - \dfrac{C_1\alpha_{T1}U}{H} - \dfrac{\beta}{H}(C_1\alpha_{p1} - C_2\alpha_{p2}) + \dfrac{C_2\alpha_{T2}\vartheta}{H} - \dfrac{C_1\alpha_{p1}\xi}{H} + F_t; \\ \dfrac{\partial C_2}{\partial t} = -C_2\lambda - \dfrac{C_2\alpha_{T2}\vartheta}{h} - \dfrac{\beta}{h}(C_2\alpha_{p2} - C_1\alpha_{p1}) + \dfrac{C_1\alpha_{T1}U}{h} - \dfrac{\gamma C_2\alpha_{p2}}{h}, \end{cases} \quad \text{(II.88)}$$

where:

C_1 is the total radionuclide concentration in water mass (Bq/m^3);
C_2 is the total radionuclide concentration in bottom sediments (Bq/m^3);
x is the longitudinal coordinate with the stream (m);
D_L is the longitudinal coefficient of turbulent dispersion along the axis *x* (m^2 / day);
ν is the mean current velocity (m/day);
λ is the radionuclide decay constant (1/day);
U is the mean deposition rate for suspended particles of considered size (m/day);
H is the mean depth of the river over the studied river stretch (m);
h is the depth of the exchangeable layer (m);
A is the transverse cross-section of the river channel (m);
ϑ is the radionuclide mass transfer coefficient in case of resuspension (wash-out) of contaminated bottom sediments (m/day);
F_t is the distributed sources of activity;

β is the radionuclide mass transfer coefficient between water mass and bottom sediments due to diffusion (m/day);

γ is the mass transfer coefficient for radionuclides occurring in the porous water between the effective layer of the bottom sediments and bottom (m/day);

ζ is the coefficient of exchange of dissolved radionuclides between the main flow and underflow (for water reservoirs filtration coefficient) (m/day);

α_{T1} is the part of the i-th radionuclide adsorbed by suspended particles, non-dimensional;

α_{T3} is the part of the i-th radionuclide adsorbed by the solid phase of the effective layer of the bottom sediments, non-dimensional; and

α_{p1} and α_{p3} are the part of the i-th radionuclide occurring in dissolved form in water and the effective layer of bottom sediments, respectively, non-dimensional.

As required by the formulated problem, let us express the discharge along the river length as a linear function:

$$Q(x) = A \cdot V(x) = A(ax + b), \tag{II.89}$$

where: A =BH – the river channel cross-section = const.

In view of Equation II.89 the system of equations (II.88) with the stationary supply of radionuclides and in the absence of sources of radionuclides takes the form:

$$\begin{cases} \frac{d}{dx}\left(D_L \frac{dC_1}{dx}\right) - \frac{d}{dx}(V(x)C_1) - C_1\lambda - \frac{C_1\alpha_{T1}U}{H} - \frac{\beta}{H}(C_1\alpha_{p1} - C_2\alpha_{p2}) + \frac{C_2\alpha_{T2}\vartheta}{H} - \frac{C_1\alpha_{p1}\xi}{H} = 0; \\ -C_2\lambda - \frac{C_2\alpha_{T2}\vartheta}{h} - \frac{\beta}{h}(C_2\alpha_{p2} - C_1\alpha_{p1}) + \frac{C_1\alpha_{T1}U}{h} - \frac{\gamma C_2\alpha_{p2}}{h} = 0, \end{cases} \tag{II.90}$$

With the invariable longitudinal dispersion coefficient, the system in Equation II-90 can be written as:

$$\begin{cases} D_L\frac{d^2C_1}{dx^2} - V(x)\frac{dC_1}{dx} - C_1\frac{dV(x)}{dx} - C_1\lambda - \frac{C_1\alpha_{T1}U}{H} - \frac{\beta}{H}(C_1\alpha_{p1} - C_2\alpha_{p2}) + \frac{C_2\alpha_{T2}\vartheta}{H} - \frac{C_1\alpha_{p1}\xi}{H} = 0; \\ -C_2\lambda - \frac{C_2\alpha_{T2}\vartheta}{h} - \frac{\beta}{h}(C_2\alpha_{p2} - C_1\alpha_{p1}) + \frac{C_1\alpha_{T1}U}{h} - \frac{\gamma C_2\alpha_{p2}}{h} = 0, \end{cases} \tag{II.91}$$

In view of Equation II.89 the system takes the form:

$$\begin{cases} D_L\frac{d^2C_1}{dx^2} - V(x)\frac{dC_1}{dx} - C_1a - C_1\lambda - \frac{C_1\alpha_{T1}U}{H} - \frac{\beta}{H}(C_1\alpha_{p1} - C_2\alpha_{p2}) + \frac{C_2\alpha_{T2}\vartheta}{H} - \frac{C_1\alpha_{p1}\xi}{H} = 0; \\ -C_2\lambda - \frac{C_2\alpha_{T2}\vartheta}{h} - \frac{\beta}{h}(C_2\alpha_{p2} - C_1\alpha_{p1}) + \frac{C_1\alpha_{T1}U}{h} - \frac{\gamma C_2\alpha_{p2}}{h} = 0, \end{cases} \tag{II.92}$$

or, in the general form:

$$\begin{cases} D_L\frac{d^2C_1}{dx^2} - V(x)\frac{dC_1}{dx} - \lambda_1 \cdot C_1 + \lambda_{12}C_2 = 0; \\ \lambda_{21}C_1 - \lambda_2C_2 = 0, \end{cases} \tag{II.93}$$

where λ_1, λ_2, λ_{12} и λ_{21} are the transport constants determining the processes of interaction in the system the water mass–river bottom, with allowance for the decay (day^{-1}). The equations for determining λ_1, λ_2, λ_{12} and λ_{21} are written as:

$$\lambda_1 = \lambda + \frac{U\alpha_{T1}}{H} + \frac{\beta\alpha_{p1}}{H} + \frac{\xi\alpha_{p1}}{H} + a \quad ; \tag{II.94}$$

$$\lambda_2 = \lambda + \frac{\alpha_{T2}\vartheta}{h} + \frac{\beta\alpha_{p2}}{h} + \frac{\gamma\alpha_{p2}}{h} \quad ; \tag{II.95}$$

$$\lambda_{12} = \frac{\beta\alpha_{p2}}{H} + \frac{\vartheta\alpha_{T2}}{H}; \tag{II.96}$$

$$\lambda_{21} = \frac{\beta\alpha_{p1}}{h} + \frac{U\alpha_{T1}}{h} \quad ; \tag{II.97}$$

The values α_{T1}, $\alpha_{T2,}$ α_{P1} and α_{P2} determining the proportion of radionuclides adsorbed on suspended particles and in solution in Equations II.90 to II.93 are found from the following relations:

$$\alpha_{p1} = \frac{1}{1 + S_1 k_{d1}} \quad ; \tag{II.98}$$

$$\alpha_{p3} = \frac{1}{1 + m_2 k_{d2}} \quad ; \tag{II.99}$$

$$\alpha_{T1} = \frac{S_1 k_{d1}}{1 + S_1 k_{d1}} \quad ; \tag{II.100}$$

$$\alpha_{T3} = \frac{m_2 k_{d2}}{1 + m_2 k_{d2}} \quad , \tag{II.101}$$

where:

k_{d1} is the distribution coefficient for the i–th radionuclide in the system the water-suspended material (m^3/kg);
k_{d2} si the distribution coefficient of the i–th radionuclide between the porous water and the solid phase of the effective layer of bottom sediments (m^3/kg);
S1 is the water turbidity (kg/m^3); and
m_2 is the volumetric weight of the effective layer of bottom sediments (kg/m^3).

The differential equation accounting for the stationary discharge finally takes the form:

$$D_L \frac{d^2 C_1}{dx^2} - V(x)\frac{dC_1}{dx} - kC_1 = 0 \tag{II.102}$$

where: k is the coefficient accounting for the mechanisms of interaction between the water mass and river bottom and the decay (day^{-1}). In the stationary conditions it is determined as:

$$k = (\lambda_1 - \frac{\lambda_{12}\lambda_{21}}{\lambda_2}) \tag{II.103}$$

In the cases when the longitudinal dispersion can be neglected as compared to the convective transport the equation becomes even more simple and is written as:

$$-V(x)\frac{dC_1}{dx} - kC_1 = 0 \tag{II.104}$$

the boundary conditions (Equation II.104) are as follows:

$$x = 0, \quad C_1 = C_0 \tag{II.105}$$

The solution of Equation II.104 accounting for the variations in the concentrations along the river with the initial conditions (Equation II.105) takes the form:

$$C_1(x) = \frac{C_0(a+bx)^{(-\frac{k}{b})}}{a^{(-\frac{k}{b})}} \tag{II.106}$$

Table II.23 includes input parameters used in calculations.

Table II.23. Input parameters for the Techa River Model.

Parameter	Value
^{90}Sr distribution coefficient between water and suspended matter, m^3/kg	0.03
^{90}Sr distribution coefficient between porous water and the solid phase of bottom sediments, m^3/kg	0.01
^{137}Cs distribution coefficient between water and suspended matter, m^3/kg	10.0
^{137}Cs distribution coefficient between porous water and the solid phase of bottom sediments, m^3/kg	5.0
^{239,240}Pu distribution coefficient between water and suspended matter, m^3/kg	15.0
^{239,240}Pu distribution coefficient between porous water and the solid phase of bottom sediments, m^3/kg	7.5
Depth, m	1.0
River channel width, m	25.0
Volumetric mass (sand-clay) of bottom sediments , kg/m^3	1000
^{90}Sr decay constant, year^{-1}	0.024
^{137}Cs decay constant, year^{-1}	0.023
^{239}Pu decay constant, year^{-1}	0.000029
Mean depth of the exchangeable layer of bottom sediments, m	0.05
Water turbidity, kg/m^3	0.03
Sedimentation rate for suspended particles of characteristic size (0,05mm), m/day	86.4
Mass exchange rate, m/day	0.00164
Resuspension rate, m/day	0.0026
Coefficient of radionuclides mass transfer between the effective layer of bottom sediments and the bottom, m/day	0.00164
River water discharge at zero point, m^3/s	2.23
Water discharge, the river mouth, m^3/s	6.35
Flow velocity , m/day V(x) = 7706,88+0,074515x	

Calculations were performed for water and bottom sediment contamination with ^{90}Sr, ^{137}Cs and $^{239,240}Pu$ along the Techa under normal operational condition. In doing so, an assumption was made that there are no external sources of ^{90}Sr and ^{137}Cs to the river, i.e. the concentrations of the radionuclides in the Techa are attributed only to the contamination of bottom sediments and transport of ^{90}Sr with the Techa waters merging downstream of the Muslyumovo and for ^{137}Cs – the Techa water of the upper parts. The initial concentrations in the bottom sediments were estimated under the assumption of the equilibrium between the radionuclides occurring in bottom sediments and in water. Results of modeling suggest that the estimates are in good agreement with the measurements (Figure 5.6), the errors not exceeding 50%. The distribution coefficients are selected assuming the equilibrium between the radionuclides occurring in water and in bottom sediments. The exchange with the underflow was set to be zero, with the assumption that as a result of long-term discharges of ^{90}Sr the underflow concentrations of the radionuclide are not lower than those in the channel flow.

It can be concluded that calculation results for different radionuclides are dependent, to a great extent, on ζ – the coefficient of radionuclides exchange between the main flow and the underflow and on the value of the coefficient *a* representing the linear increase in the velocity (discharge), given the invariable river cross-section along the length of the river. Considering that over the time of the "Mayak" operations the river underflow was contaminated with radionuclides to a different extent, it can be assumed that for some radionuclides (^{90}Sr and partly ^{137}Cs) this flow serves as a source of radioactivity, like the Asanov swamps. For others ($^{239,240}Pu$) the underflow is a sink to which the radionuclides keep entering.

II.4.3. Model CASSANDRA
(Krylov A.L., Institute of safety development of atomic energy, Moscow, Russia)

The integrated information-modeling system CASSANDRA based on using geoinformation technologies is designed to predict and estimate the consequences of radioactive contamination of rivers and water bodies.

The system is composed of:

- a geographical information system *Komponovka* (based on the package Mapinfo);
- a model predicting radionuclide behavior in water bodies with a weak flow and models of long-term transport of radionuclides in river channel integrated within the computer model *Basin*; and
- a model predicting internal and external doses (aquatic pathways of exposures) for different population groups, estimates of radiation risk for developing appropriate recommendations *Inter*.

Komponvka is the core of the system. It is used for entering, storing, processing and representation of spatially distributed information. The computer models *Basin* are designed for predicting the contamination of water bodies.

Within the computer model *Basin* several different eco-mathematical models have been integrated. A model is selected for prediction of contamination depending on the type of water body, what type of radionuclides it has been contaminated with, time of prediction and some other conditions.

The system is arranged in such a way that results of calculations can be replaced by experimental data (if available). For example, a measured radionuclide concentration in bottom sediments can be used instead of the concentration estimated by the model.

The radionuclide transport along the river channel (included in the computer model *Basin*) is predicted using the model accounting for

- radiation decay;
- advective transport of radionuclides;
- variance;
- exchange processes between radionuclides occurring in water mass and adsorbed on suspended particles and occurring in bottom sediments;
- removal of radionuclides from a water body through evaporation, inputs to underflow, transport of radionuclides from different sources; and
- migration of radionuclides down the bottom sediments.

The principal assumptions made in the model are the following:

- the radionuclide concentration and all river characteristics have been averaged over the river lateral cross-section. In other words, the mixing in the river channel perpendicular to the channel is instantaneous and uniform;
- the river averaging scale is taken to be much greater than the river width;
- migration of radionuclides on suspension particles of different sizes is described by processes occurring with mono-dispersed suspension particles of characteristic size with equivalent sorption properties;
- the processes of radionuclides sorption and desorption by suspended particles and bottom sediments are instantaneous, reversible and described by a linear isotherm with a constant distribution coefficient K*d*;
- dynamic factors (currents) have no impact on the radionuclide mass exchange diffusion coefficient;
- the leading role in the processes of interaction of bottom sediments is played by the effective layer of bottom sediments, the thickness of which is estimated or determined experimentally;
- the activity of biomass activity is negligible as compared with the levels of radionuclides in bottom sediments.

The key equations of the model are written as:

$$\frac{\partial(A*C_w(x,t))}{\partial t}+\frac{\partial}{\partial x}(Q*C_w-E*A*\frac{\partial C_w}{\partial x})=-\lambda*A*C_w-A*C_w*\frac{u}{H}*\frac{K_{d1}*S_1}{1+K_{d1}*S_1}+$$
$$+\frac{(u*\frac{S_1}{m}-W_c)}{H}*A*C_b*\frac{K_{d2}*m}{1+K_{d2}*m}+\frac{A*\beta}{H}*(\frac{C_b}{1+K_{d2}*m}-\frac{C_w}{1+K_{d1}*S_1})-q_n*\frac{C_w}{1+K_{d1}*S_1}-$$
$$-\frac{K_{П}*q_u*C_w}{1+K_{d1}*S_1}+F \qquad \text{(II.107)}$$

$$\frac{\partial C_b(x,t)}{\partial t} = -\lambda * C_b + Cw * \frac{u}{h} * \frac{K_{d1} * S_1}{1 + K_{d1} * S_1} -$$

$$-\frac{(u * \frac{S_1}{m})}{h} * C_b * \frac{K_{d2} * m}{1 + K_{d2} * m} - \frac{\beta}{h} * (\frac{C_b}{1 + K_{d2} * m} - \frac{C_w}{1 + K_{d1} * S_1}) \quad \text{(II.108)}$$

$$\frac{\partial C_{bz}(x,z,t)}{\partial t} + W_c * \frac{\partial C_{bz}}{\partial z} = D\frac{\partial^2 C_{bz}}{\partial z^2} - \lambda * C_{bz} \quad \text{(II.109)}$$

$$C_b(x,t) = C_{bz}(x,z,t)\big|_{z=0} \quad \text{(II.110)}$$

The boundary condition at the lower boundary (within the bottom sediment layer) will take the form:

$$\frac{\partial C_b}{\partial z} = 0 \quad \text{(II.111)}$$

where:

C_w and C_{bz} are concentrations in water and bottom sediments respectively (Bq/ m^3);
λ is the decay constant (1/s);
H is the mean depth (m);
S_1 is the water turbidity corresponding to the mean transporting capacity of the flow in the time interval of prediction (kg/ m^3);
K_{d1}, K_{d2} are the distribution coefficients water-suspension and water-bottom sediments (m^3/kg);
m is the volumetric mass of bottom sediment skeleton (kg/m^3);
β is the coefficient of diffusion mass exchange (m/s);
Q is the discharge of running water (m^3/s);
W_c is the mean rate of sedimentation (m/s);
h is the depth of effective layer of bottom sediments (m);
$q_И$ is the water loss for evaporation (m^3/s);
$K_П$ is the distribution coefficient between water and vapor above the water surface for a given radionuclide (б/р). For tritium K = 1 , for other radionuclides K = 0; $q_П$ is other water losses (m^3/s);
D is the diffusion coefficient down the bottom sediment profile (m^2/s);
t is the time (s);
x is the coordinate along the channel (m);
z is the coordinate down the bottom sediment profile (m);
A is channel cross-section area (m^2);
E is the longitudinal dispersion coefficient (m^2/s); can be estimated from the hydrological characteristics of the flow; and
F is the source of radionuclides (Bq/(m*s)).

The solution is sought numerically. CASSANDRA allows simplification of the CASSANDRA system of differential equations. What makes the CASSANDRA system different from TRANSFER-2 is the following:

- the CASSANDRA system is more general and unlike TRANSFER-2 allows modeling a changeable water discharge and river cross-section (river width);
- the CASSANDRA system of equations includes the longitudinal cross-section and the radionuclide concentration in water is averaged over the cross-section, while the TRANSFER-2 system accounts for lateral diffusion and concentration across the width of the river;
- the CASSANDRA system includes the equation for diffusion down the bottom sediment profile, permitting the vertical profile of bottom sediments to be considered. It is worth mentioning that consideration of diffusion down the bottom sediments is part of the specific problems (secondary contamination etc), since it requires information about radionuclide levels down the vertical profile of bottom sediments. Note that results of modeling water and bottom sediment contamination levels in this case do not differ significantly from simpler calculating schemes.

Given simpler calculation schemes, i.e. neglecting the longitudinal and lateral diffusion in the water flow over a given river stretch and the vertical heterogeneity of bottom sediments, and assuming that the flow width and water discharge are constant, the CASSANDRA equations become identical to those of the model TRANSFER-2.

The model CASSANDRA was used for modeling on the river section downstream of the village Muslyumovo, assuming that there were no external sources of radioactivity to the river and the radionuclide levels in the Techa water were attributed exclusively to the contamination of bottom sediments and their transport from the upstream sections. The experimentally measured concentrations of radionuclides in water near Muslyumovo were considered to be preset values. The concentration in bottom sediments near Muslyumovo was taken to be prescribed for Sr, while for Pu and Cs the levels were recalculated from the concentrations in water. It is worth noting that there were some differences in calculations using the analytical model TRANSFER-2 and the numerical model forming part of the CASSANDRA system. With CASSANDRA, some of the model parameters were considered to be variable along the river channel, in particular, the water discharge, the channel width, the distribution coefficients for Cs and Pu (selected from the database of typical values of the CASSANDRA system and assuming the equilibrium between radionuclides in water and bottom sediments on different parts of the river.)

Table II.24 contains input parameters and results of calculations. Note that the measured concentrations of caesium and plutonium in bottom sediments near Muslyumovo and Brodokalmak are abnormally high and, given the equilibrium, do not match the concentrations of the same radionuclides in water. This suggests that the values were obtained in the points with locally increased contamination of bottom sediments.

Comparison of the modeling results by TRANSFER-2 and CASSANDRA with the experimental data indicates that the largest discrepancy were observed for the specific activity of strontium in bottom sediments. The differences can be due to different reasons such as unaccounted mechanisms of channel interaction with heavily contaminated floodplain or errors associated with radiochemical recovery of radionuclide from bottom sediments, or some other reasons. The discrepancies with respect to the ^{137}Cs specific activity in bottom sediments appeared to be somewhat higher when using TRANSFER-2 as compared to the CASSANDRA calculations. This suggests that using identical distribution coefficients for caesium through the length of the Techa, as is the case in the analytical model TRANSFER-2, may not be always the right thing to do. As to strontium, the same distribution coefficients throughout the river are not worth using either.

Table II.24. Parameters and calculation results by the model CASSANDRA.

Paramter	Muslyumovo 44 km	78 km	143 km	mouth 205 km
Water discharge (m^3/s)	2.23	2.23	2.23	4.765
Mean depth (m)	1	1	1	1
Width (m)	21	21	21	32
Turbidity (g/m^3)	39	39	39	39
Bottom sediment skeleton volumetric mass (kg/m^3)	1000	1000	1000	1000
Mean sedimentation velocity (mm/s)	1	1	1	1
Transport to underflow (ml/(s* m^2))	2*	2*	2*	2*
Pu				
Water-suspended particles distribution coefficient (m^3/kg)	15	15	15	11.2
Porous water-b.s. distribution coefficient (m^3/kg)	7.5	7.5	7.5	5.6
Concentration (by model) in water (Bq/m^3)	0.25	0.1398	0.1022	0.0577
Experimentally obtained concentration in water (Bq/m^3)	2.5	0.13	0.092	0.055
Concentration (by model) in b.s.. (Bq/kg)	2.5	1.3192	0.9689	0.45
Experimentally obtained concentration in b.s. (Bq/kg)	*2.5 / 40*	*16.6*	1.04	0.43
^{137}Cs				
Water-suspended particles distribution coefficient (m^3/kg)	27		6.1	3.215
Porous water-b.s. distribution coefficient (m^3/kg)	13		3.05	1.61
Concentration (by model) in water (Bq/m^3)	430	276	132.39	33.7
Experimentally obtained concentration in water (Bq/m^3)	430		120	70
Concentration (by model) in b.s.. (Bq/kg)	5655	3100	665.84	96.354
Experimentally obtained concentration in b.s. Bq/kg	*5655 / 49000*		590	200
^{90}Sr				
Water-suspended particles distribution coefficient (m^3/kg)	0.03		0.03	0.03
Porous water-b.s. distribution coefficient (m^3/kg)	0.01		0.01	0.01
Concentration (by model) in water (Bq/m^3)	18000	17973	17234	8692.3
Experimentally obtained concentration in water (Bq/m^3)	18000		11000	8000
Concentration (by model) in b.s. (Bq/kg)	670	573	549.91	277.38
Experimentally obtained concentration in b.s. (Bq/kg)	*670*		150	200

Note. * For ^{90}Sr the process was not considered

Similarity and difference of the analytical model and CASSANDRA

The features the analytical model and CASSANDRA have in common include:

(1) they both account for the same processes;
(2) they both are based on the same equations; and
(3) they both build on the following assumptions:
   (a) The exchange of radioactive material between water and bottom sediments is proportional to radionuclides concentrations in the liquid and solid phases.
   (b) Sorption-desorption of radionuclides between the solution and solid phase is taken to be instantaneous, equilibrium and corresponding to the linear isotherm with the constant distribution coefficient.
   (c) The exchange between the bottom and water mass occurs within the equally accessible upper layer of bottom sediment of depth *h*.
   (d) Radioactive material is transported by water flow and dispersed due to the longitudinal turbulent dispersion. Radioactive material is distributed equally across the river cross section and it is only the longitudinal component of the convective dispersion that is taken into account.

The differences between them are as follows:

— The analytical model is added with the assumption that the morphometric characteristics of the channel are constant over the entire river stretch under study. The total discharge of lateral tributaries is taken to be negligible as compared with the discharge of the main channel. The changes in the water discharge along the river are due to the changes in the current velocity n accordance with the linear law. On the other hand, CASSANDRA allows for side tributaries, changes in the morphometric characteristics of the channel, the distribution coefficients and other parameters along the river, as well as time variations.
— CASSANDRA, unlike the analytical model, allows for the sources of radionuclides along the river channel and not only the flow of radionuclides from the upper parts of the river. There can be several sources taken into account. This model thereby accounts for the radionuclides wash-off from contaminated catchment area.
— CASSANDRA provides a numerical solution for the system of Equation II.107 in time. It therefore needs input information about the flow of radionuclides to the river and on this basis calculates the radionuclides distribution along the river. In case of a discharge to the river unvarying in time a steady state distribution occurs. The analytical model, on the other hand, makes possible solving the reverse problem – what should be the magnitude of the steady state flow of radionuclides from the upper parts of the river to ensure that the distribution be like this.
— The analytical model further assumes that no siltation of the bottom occurs. CASSANDRA accounts for siltation, but calculations for the Techa do not include this process.
— CASSANDRA seeks the solution numerically, while the analytical model, analytically.

Key parameters

The key parameters are

(1) water discharge (its variations along the river channel and in time, if considered);
(2) flow of radionuclides to the river (where, when and how much);
(3) characteristics of suspended particles (turbidity, size distribution) and sedimentation rate;
(4) distribution coefficients in the system water-suspended particles, water-bottom sediments; and
(5) parameters of the exchange with underflow.

Effective depth of the bottom sediment layer

The modeling results are also influenced by the river depth and other parameters, though to a lesser extent.

II.4.4. Model GIDRO-W
(Kryshev A.I., Sanina K.D., SPA "Typhoon", Obninsk, Russia)

For calculating of plutonium transport in the Techa River from Muslyumovo point to the river mouth the model of piston displacement has been used (one-dimension model of radionuclide migration). In this model lateral variance of pollutant was neglected. The system of equations for concentrations of plutonium in water C_1 (Bq/m^3) and bottom sediments C_2 (Bq/m^3) downstream the river has the form:

$$\begin{cases} -V\dfrac{dC_1}{dx} - \lambda_1 \cdot C_1 + \lambda_{12} C_2 = 0; \\ \lambda_{21} C_1 - \lambda_2 C_2 = 0, \end{cases} \tag{II.112}$$

with the boundary conditions:

$$C_1(0) = C_0 = T / Q\,. \tag{II.113}$$

where:

T is the flow of plutonium to the river at Muslyumovo (Bq/day); and
Q is the river discharge at Muslyumovo, (m^3/day).

The solution of equation takes the form:

$$C_1(x) = C_0 \cdot \exp\left(\frac{-k \cdot x}{V}\right) \tag{II.114}$$

where:

C(x) is the dependence of the radionuclide concentration in water on distance downstream the river (Bq/m^3);
x is the longitudinal coordinate along the flow (m);
k is the coefficient accounting for the mechanisms of interaction between water mass and river bottom and decay (day^{-1});
V is the river mean current velocity (m/day); and
C_0 is the initial concentration of the radionuclide in water (Bq/m^3).

$$C_0 = \frac{T}{Q} \tag{II.115}$$

$$k = \lambda_1 - \frac{\lambda_{12} \cdot \lambda_{21}}{\lambda_2}; \tag{II.116}$$

where:

λ_1, λ_2, λ_{12}, λ_{21} are the transport constants governing the processes of interaction in the system "water mass-river bottom" with allowance for radioactive decay (1/day).

$$\lambda_1 = \lambda + \frac{Q}{V} + \frac{U \cdot \alpha_{T1}}{H} + \frac{\beta \cdot \alpha_{P1}}{H} \tag{II.117}$$

$$\lambda_2 = \lambda + \frac{\alpha_{T2} \cdot \vartheta}{h} + \frac{\beta \cdot \alpha_{P2}}{h} \quad \text{(II.118)}$$

$$\lambda_{12} = \frac{\beta \cdot \alpha_{P2}}{H} + \frac{\vartheta \cdot \alpha_{T2}}{H} \quad \text{(II.119)}$$

$$\lambda_{21} = \frac{\beta \cdot \alpha_{P1}}{h} - \frac{U \cdot \alpha_{T1}}{h} \quad \text{(II.120)}$$

$$\alpha_{P1} = \frac{1}{1 + S \cdot K_d} \quad \text{(II.121)}$$

$$\alpha_{T1} = 1 - \alpha_{P1} \quad \text{(II.122)}$$

where:

λ is the radioactive decay constant (1/day);
U is the mean sedimentation velocity for suspended particles of considered size (m/day);
H is the mean depth of the river at the considered section (m);
ϑ is the coefficient of radionuclide mass transport with resuspension of contaminated bottom sediments (m/day);
β is the coefficient of diffusion mass transport between water and bottom sediments (m/day);
α_{T1} is the part of radionuclides adsorbed by suspended particles;
α_{T2} is the part of radionuclides adsorbed by the solid phase of the effective layer of bottom sediments;
α_{P1} and α_{P2} are the parts of radionuclides occurring in the solved form in water and in the effective layer of bottom sediments, respectively;
h is the mean depth of bottom sediment layer (m);
K_d is the water-suspended matter distribution coefficient for the radionuclide (m^3/kg);
S is the water turbidity in the river, g/m^3.

Values of the model parameters are presented in Table II.25.

The radionuclide concentration in water was calculated from the village Muslyumovo (44 km from water reservoir 11) to the estuary of the river (207 km) with the interval of 3 km. The mean annual transport of ^{239}Pu through the Techa cross-section near Muslyumovo is accounted to be $(8 \pm 4) \cdot 10^7$ Bq/year.

The proposed model for plutonium transport in the river system was validated with available observational data. The validation was carried out for two model parameters whose estimates were characterized by the greatest uncertainty: the sedimentation velocity U of suspended matter and the coefficient of radionuclide distribution in the system water-suspended matter K_d. Good agreement between the calculated values and the measured decrease in the activity concentration of the radionuclide in water with distance downstream was achieved with the parameters taken to be U=0.1 m/day, K_d=500.

Table II.25. Values of model parameters used for calculations.

Parameter	Symbol	Numerical value	Dimension
Annual discharge of radionuclides to the river	T	$(8\pm4)*10^7$	Bq/year
River discharge in June	Q	6.88	m^3/s
Water turbidity in June	S	66.1	g/m^3
Mean river width	W	21	M
Mean river depth	H	1.5	M
Radionuclide half-life	$T_{1/2}$	$2.41*10^4$	Year
Acceleration of gravity	G	9.81	m/s^2
River slope angle	S	0.0006	Dimensionless
Depth of effective bottom sediment layer	H	0.05	M
Sedimentation velocity for suspended matter of characteristic size	U	0.1	m/day
Resuspension velocity	ϑ	$1.2*10^{-2}$	m/day
Coefficient of radionuclide distribution between water and suspended matter	K_d	500	m^3/kg
Rate of diffusion mass transport of radionuclides between water mass and river bottom	B	$1.6*10^{-3}$	m/day
Part of radionuclides absorbed by the solid phase of the effective layer of bottom sediments	α_{T2}	1	Dimensionless
Part of radionuclide occurring in the effective layer of bottom sediments	α_{P2}	0	Dimensionless

II.4.5. Model RIVTOX
(Dzyuba N.N., Zheleznyak M.I., IMMSP, Kiev, Ukraine)

II.4.5.1. Model of river hydraulics

The model of river hydraulics for simulation cross-sectional averaged flow velocity and water elevation in a network of river canals is based on the full set of the Saint-Venant equations and include continuity equation (mass conservation law) and momentum equation:

$$\frac{\partial A}{\partial t}+\frac{\partial Q}{\partial x}=q_l \qquad \text{(II.123)}$$

$$\frac{\partial Q}{\partial t}+\frac{\partial}{\partial x}\left(\frac{Q^2}{A}\right)+gA\left(\frac{\partial h}{\partial x}+S_f\right)=0 \qquad \text{(II.124)}$$

The glossary of terms used in the models is presented at the Table II.26.

Table II.26. The glossary of terms used in the hydraulics submodel.

Symbol	Dimension	Parameter
Q	m^3/s	water discharge
A	m^2	water sectional area
h	m	water depth
q_l	m/s^2	water discharge of lateral inflow, distributed along stream
g	m^2/s	gravitational acceleration
S_f		Stream friction slope
t	s	time variable
x	m	spatial coordinate

The friction slope S_f is calculated using one of the empirical resistance laws, such as Chezy's or Manning's, for example:

$$S_f = \frac{Q|Q|}{K^2} \tag{II.125}$$

where K is a stream metering characteristics.

The usual approach in river hydraulics is to use empirical Chezy's friction coefficient C_{Cz}.

$$K = C_{Cz} A\sqrt{R} \tag{II.126}$$

The hydraulic radius of the flow R is defined as A/P, where P is "wetted perimeter" of the stream. For a wide river channel P value is close to a river width b ($P \approx b$) and then $R \approx h$.

On the basis of the Mannings's empirical "friction parameter" n (average value is $0,02 \div 0,03$ for the plain rivers) C_{Cz} is determined as:

$$C_{Cz} = \frac{1}{n} R^{\frac{1}{6}} \tag{II.127}$$

II.4.5.2. Sediment transport submodel

The suspended sediment transport in river channels is described by the 1-D advection-diffusion equation that includes a sink-source term describing sedimentation and resuspension rates:

$$\frac{\partial(AS)}{\partial t} + \frac{\partial(QS)}{\partial x} - \frac{\partial}{\partial x}\left(E_S \frac{\partial(AS)}{\partial x}\right) = \Phi_b \tag{II.128}$$

where Φ_b is a vertical sediment flux at the bottom, describing sedimentation or resuspension processes in the dependence on the flow dynamical parameters and size of bottom sediments.

$$\Phi_b = \frac{A}{h} \cdot \left(q_{res} - q_{sed}\right). \tag{II.129}$$

The fluxes are calculated as a difference between actual and equilibrium suspended sediment concentration multiplied on fall velocity of sediment grains:

$$\begin{aligned} q_{res} &= \beta w_0 \cdot F\left(S_* - S\right) \\ q_{sed} &= w_0 \cdot F\left(S - S_*\right) \end{aligned}, \tag{II.130}$$

where F(x) is a function defined as:

$$F(x) = \frac{x + |x|}{2} \equiv \begin{cases} x, & x > 0 \\ 0, & x < 0 \end{cases} \tag{II.131}$$

The coefficient of the erodibility β characterizes the bottom protection from erosion due to cohesion and natural armoring of the upper layer of river bed, vegetation. This empirical coefficient as usually has values of magnitude 0.1–0.01.

The equilibrium suspended sediment concentration (flow capacity) S_** can be calculated by different approaches. The first empirical formula used in RIVTOX was taken from Bijker's method.

The equilibrium discharge of the suspended sediments p=QS$_*$ is calculated as a function of the bed load p_b:

$$p = 1.83 p_b (I_1 \ln \frac{h}{z_0} + I_2) \tag{II.132}$$

where I_1 and I_2 are the functions of the undimensional fall velocity $w_* = w_0 /(kU_*)$ and bottom roughness $r_* = r / h$

$$I_1 = 0.216 \frac{r_*^{w_*-1}}{(1-r_*)^{w_*}} \int_{r_*}^{1} \left[\frac{1-z'}{z'} \right]^{w_*} dz', \tag{II.133}$$

$$I_2 = 0.216 \frac{r_*^{w_*-1}}{(1-r_*)^{w_*}} \int_{r_*}^{1} \left[\frac{1-z'}{z'} \right]^{w_*} \ln z' dz' \tag{II.134}$$

where:

z'=z/h, r=30
r_0 typical size of the bottom inhomogeneity;
k is the von Karman parameter (k=0.4); U_* is the bottom shear stress velocity:

$$U_* = \sqrt{T_c / \rho_w} = \sqrt{ghS_f} \tag{II.135}$$

The bottom sediment equilibrium flow is described as follows:

$$\vec{p}_b = 5D \frac{\vec{T}_c}{\sqrt{\vec{T}_{cw}}} \left(\frac{\mu}{\rho} \right)^{0.5} \exp\left(-0.27 \frac{\rho D}{|\vec{T}_{cw}|} \right) \tag{II.136}$$

where:

$\vec{T}_c$ is the current driven bottom shear stress;
$\vec{T}_c$ is the bottom shear stress driven by joint action of the currents and waves;
D is the averaged size of sediments; and
μ is the parameter of the bottom ripples.

Table II.27. Glossary of terms used in sediment transport submodel.

Symbol	Dimension	Parameter
S	kg/m^3	Suspended sediment concentration
S_*	kg/m^3	Suspended sediment equilibrium concentration
Φ_b	kg/m·sec	total vertical flux of sediments at water-river bed interface per unit of river branch length
q_{res}	kg/m^2·sec	Resuspension (erosion) rate per unit area of the bottom (upward directed flux)
q_{sed}	kg/m^2·sec	Sedimentation rate per unit area of the bottom (dawnward directed flux)
β		Erodibility empirical coefficient
w_0	m^2/sec	Sediment fall velocity
Φ_l	kg/m·sec	Suspended sediment flux from lateral inflow per unit of river branch length
S_l	kg/m^3	suspended sediment concentration in the lateral water inflow
E_S	m^2/sec	longitudinal dispersion coefficient for sediments
E_x	m^2/sec	longitudinal dispersion coefficient for soluble tracer
α_E		parameter of the longitudinal dispersion for Elder's formula
U	m/sec	cross-sectionally averaged flow velocity
U_*	m/sec	bottom shear stress velocity
K		von Karman parameter
$\vec{T}_c$	kg/(m sec^2)	current driven bottom shear stress
D	M	averaged size of sediments,
Z^*	M	thickness of the bottom sediment upper layer
ρ_S	Kg/m^3	density of the suspended sediments (default value 2600)
ρ_S	Kg/m^3	water density (default value 1000)
ε		porosity of the bottom sediments

II.4.5.3. Submodel of radionuclide transport

This submodel of radionuclide transport describes the advection-diffusion transport of the cross-sectionally averaged concentrations of radionuclides in the solution C, the concentration of radionuclides on the suspended sediments C^s and the concentration C^b in the top layer of the bottom depositions. The adsorption/desorption and the diffusive contamination transport in the systems "solution – suspended sediments" and "solution – bottom deposition" is treated via the Kd approach for the equilibrium state, additionally taking into account the exchange rates $a_{i,j}$ between solution and particles for the more realistic simulation of the kinetic processes.

The present version of this model uses different values of the sorption and desorption rates $a_{1,2}$ and $a_{2,1}$ for the system "water-suspended sediment" and $a_{1,3}$ and $a_{3,1}$ for the system "water-bottom deposits" because this fits better with the real physical-chemical behaviour of radionuclides in the water systems. Furthermore, the use of the different exchange rates gives a better fit in the simulations

$$
\begin{aligned}
&\frac{\partial \mathrm{C}}{\partial t}+\frac{Q}{A}\frac{\partial \mathrm{C}}{\partial x}-\frac{1}{A}\frac{\partial}{\partial x}\left(AE_C\frac{\partial \mathrm{C}}{\partial x}\right)=f^{C}\left(S,\,C,\,C^S,\,C^b,\,Z^*,\,\vec{p}^{\,C}\right)+f^{C_l}\left(C,\,C_l\right)\\
&\frac{\partial \mathrm{C}^{\mathrm{S}}}{\partial t}+\frac{Q}{A}\frac{\partial \mathrm{C}^{\mathrm{S}}}{\partial x}-\frac{1}{A}\frac{\partial}{\partial x}\left(AE_C\frac{\partial \mathrm{C}^{\mathrm{S}}}{\partial x}\right)=f^{C^S}\left(S,\,C,\,C^S,\,C^b,\,Z^*,\,\vec{p}^{\,C^S}\right)+f^{C_l^S}\left(C,\,C^S,\,C_l,\,C_l^S\right)\\
&\frac{\partial \mathrm{C}^{\mathrm{b}}}{\partial t}=f^{C^b}\left(S,\,C,\,C^S,\,C^b,\,Z^*,\,\vec{p}^{\,C^b}\right)\\
&\frac{\partial Z^*}{\partial t}=f^{C^b}\left(S,\,\vec{p}^{\,Z^*}\right)
\end{aligned}
\quad , \qquad \text{(II.137)}
$$

where:

$$
\begin{aligned}
f^{C}&=-\lambda C-a_{1,2}\left(K_{dS}SC-C^S\right)-a_{1,3}\left(K_{db}C-C^b\right)\frac{\rho_S\left(1-\varepsilon\right)Z^*}{h}\\
f^{C_l}&=\frac{Q}{A}\left(C_l-C\right)\\
f^{C^S}&=-\lambda C^S+a_{1,2}\left(K_{dS}C-C^S\right)+\frac{q_{sed}\left(C^b-C^S\right)}{hS}\\
f^{C_l}&=\frac{QS_l\left(C_l^S-C^S\right)}{AS}\\
f^{C^b}&=a_{1,3}\left(K_{db}C-C^b\right)-\frac{q_{res}\left(C^b-C^S\right)}{\rho_S\left(1-\varepsilon\right)Z^*}-\lambda C^b
\end{aligned}
\quad , \qquad \text{(II.138)}
$$

Table II.28. Glossary of terms used in Section II.4.5.3.

Symbol	Dimension	Parameter
C	Bq/m^3	radionuclide concentration in solution
C^S	Bq/kg	radionuclide concentration on suspended sediments
C^b	Bq/kg	radionuclide concentration in bottom depositions
C_l	Bq/m^3	radionuclide concentration in solution of lateral inflow
C_l^S	Bq/kg	radionuclide concentration on suspended sediments in lateral inflow
E_C	m^2/sec	radionuclide longitudinal dispersion coefficient
λ	sec^{-1}	decay coefficient
$a_{1,2}$	sec^{-1}	sorption rate in “water-suspended sediments” system
$a_{2,1}$	sec^{-1}	desorption rate in “water-suspended sediments” system
$a_{1,3}$	sec^{-1}	sorption rate in “water-bottom deposition” system
$a_{3,1}$	sec^{-1}	desorption rate in “water-bottom deposition” system
K_{dS}	m^3/kg	distribution coefficient in “water-suspended sediments” system
K_{db}	m^3/kg	distribution coefficient in “water-bottom deposition” system

II.5. Modelling ^{226}Ra self-cleaning in the Huelva Estuary

Models applied in this exercise have already been described in the previous sections, thus only the new aspects of each model in relation to their application to a tidal estuary will be commented here.

II.5.1. MASCARET

MASCARET is a 1-D model that solves hydrodynamics and dispersion of pollutants on-line. The hydrodynamic module solves the shallow water equations on a looped and branched network. Equations are solved using implicit finite differences. The estuary geometry was described by means of 42 profiles extracted from the provided bathymetry. The model contains 250 sections with 50 m length in Odiel and Tinto and 150 m in the common channel. The Canal del Burro was not implemented in the model.

The monthly water flows were imposed at both the Odiel and Tinto rivers and water elevation was defined at the entrance of the estuary from the provided data for tides. Both tidal constituents were used.

The 1D advection-diffusion equation in its conservative form is solved together with hydrodynamics. A constant diffusion coefficient equal to 10 m^2 s^{-1} is used. Time step for calculations is 60 s.

Initial conditions were obtained from the file provided with the scenario description, although the two-dimensional structure of the data had to be converted into a one-dimensional structure suitable for MASCARET.

A sediment concentration was calculated in the form:

$$SED = \frac{\rho_s e}{H} \tag{II.139}$$

where ρ_s is the sediment bulk density (fixed as 700 kg m^{-3} , average value of measured densities), e is the sediment mixing depth (10 cm) and H is average water depth calculated as A/B, where A and B are, respectively, the river cross section and width. This enabled to use the radioecological model that was initially developed for describing the exchanges of radionuclides between water and suspended matter.

Two different models have been used to describe the interactions between the dissolved phase and the bed sediment. The first is based upon the application of an equilibrium distribution coefficient (the average value of the ^{226}Ra k_d measured in the estuary, provided in the scenario description, has been used, i.e. k_d=9000 l kg^{-1}). The second model is a kinetic model consisting of two reversible consecutive reactions (a fast process describing an exchange between radionuclides in solution and some non-specific sites on particle surfaces and a slower process representing a migration to more specific sites in particles). The model is represented in Figure II.24. Four kinetic rates are required, whose values are provided in the scenario description.

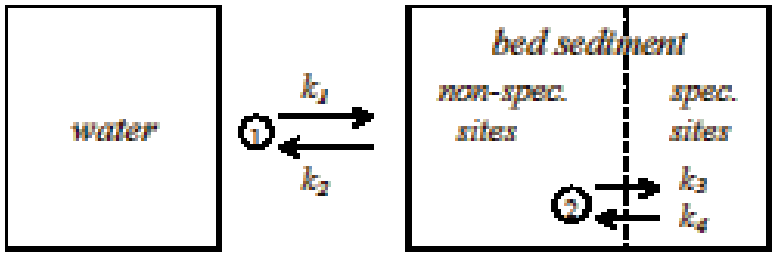

Fig. II.24. Kinetic model consisting of two reversible consecutive reactions.

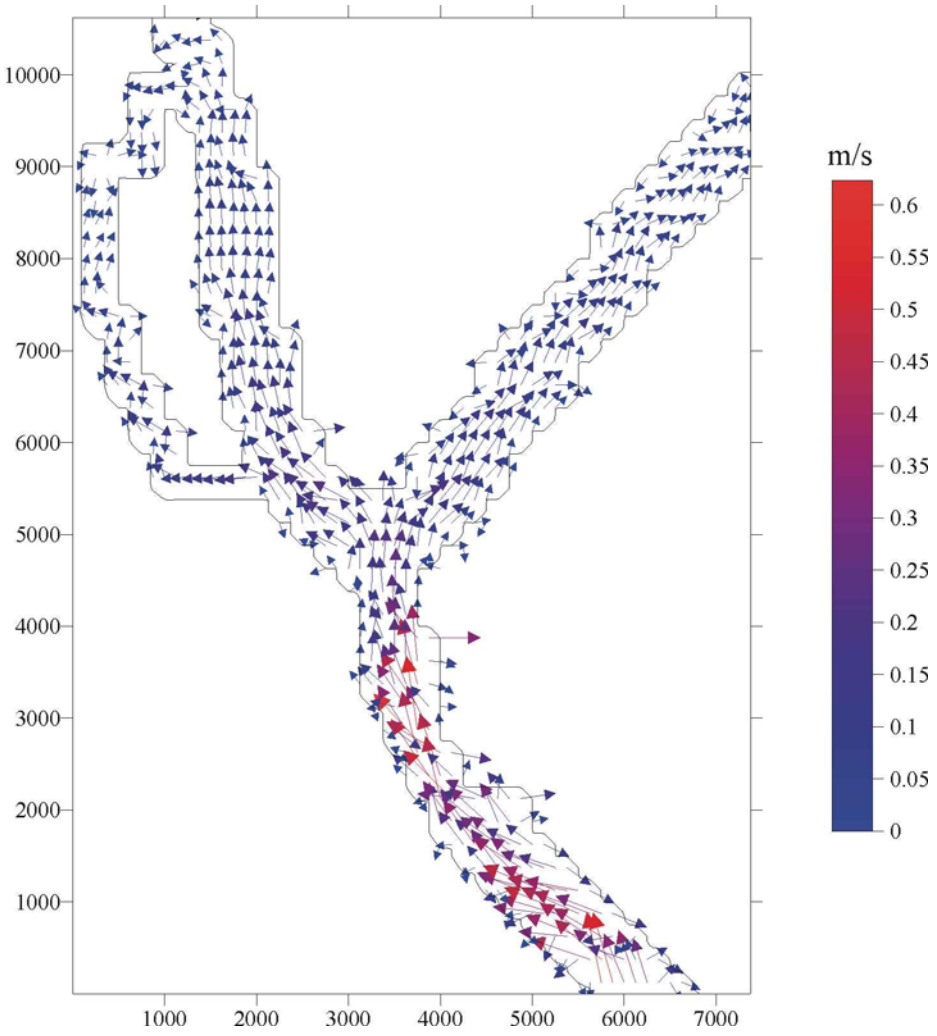

Fig. II.25. Currents calcualted by COASTOX during the flood tide. The colorbar indicate the magnitude of the current in m s^{-1}.

II.5.2. COASTOX

COASTOX has been applied in the version that has already been used in the Pripyat River floodplain simulations. 2-D depth-averaged shallow water equations and advection-diffusion equations are solved on-line using finite differences. The simulation of the flow hydrodynamics was provided on the basis of the tide data and river discharge data presented in the scenario description. To diminish the computational time (calculation time step scale of minutes) the simulation was provided for periods 10–12 days for some values of the river discharges and then this hydrodynamics was replicated for other periods with the similar magnitude of the rivers discharges. An example of currents calculated by this model may be seen in Figure II.25.

Interactions between the dissolved and solid phases were described by using a kinetic model consisting of a single reversible reaction. Desorption is described by a kinetic coefficient k_2 and adsoption is calculated from the distribution coefficient and k_2. The average k_d measured in the estuary has been used.

II.5.3. USEV

The model applied by the University of Seville is a 2-D depth-averaged model, essentially the same as applies to the Pripyat River floodplain exercise. The grid cell size is $\Delta x=\Delta y=125$ m and time step is fixed as =6 s for the hydrodynamics.

The hydrodynamic and the dispersion models are coupled off-line, and tidal analysis is used to determine tidal constants. Tidal analysis consists of determining, by a standard fitting algorithm, the amplitude and phase (tidal constants) for each constituent included in the model and for each grid cell. These tidal constants have to be calculated for both components of the flow, u and v, and for water elevation z. Tidal constants, for each tide constituent, are calculated by the same hydrodynamic code and are stored in files that will be read by the dispersion model. Once tidal constants are known, computation of flow and water elevation at any cell and time just involves the evaluation and addition of a few cosine terms. This is very fast, and simultaneously, the dispersion model is not limited by the CFL stability condition [II.55]. The net residual current has to be evaluated by the hydrodynamic model and added to the current obtained from tidal analysis since a net transport cannot be obtained from the pure harmonic currents provided by the tidal analysis. It has to be clearly pointed out that tidal analysis is carried out running the hydrodynamic model for each constituent separately. This technique is usually applied in rapid response Lagrangian models, although has also been used in finite difference dispersion models. It has the clear advantage of joining the strengths of the off-line mode (higher computation speed due to less restrictive stability conditions and to the fact that hydrodynamic calculations have not to be carried out for each time step) with a temporal resolution that is high enough to solve tidal processes.

The two main tidal constituents, M_2 and S_2, are included in calculations. Since stability conditions are not as restrictive in the advection-diffusion equation as in the hydrodynamic equations, the time step in the dispersion model was increased to 30 s. In spite of this small time step, long-term simulations (tens of years) can be efficiently carried out (a few minutes of computation per simulated year on a PC) due to the use of tidal analysis.

The interactions between dissolved radionuclides and sediments are described by the same kinetic model consisting of two consecutive reversible reactions as MASCARET. Values for the different kinetic rates have been taken from the scenario description.

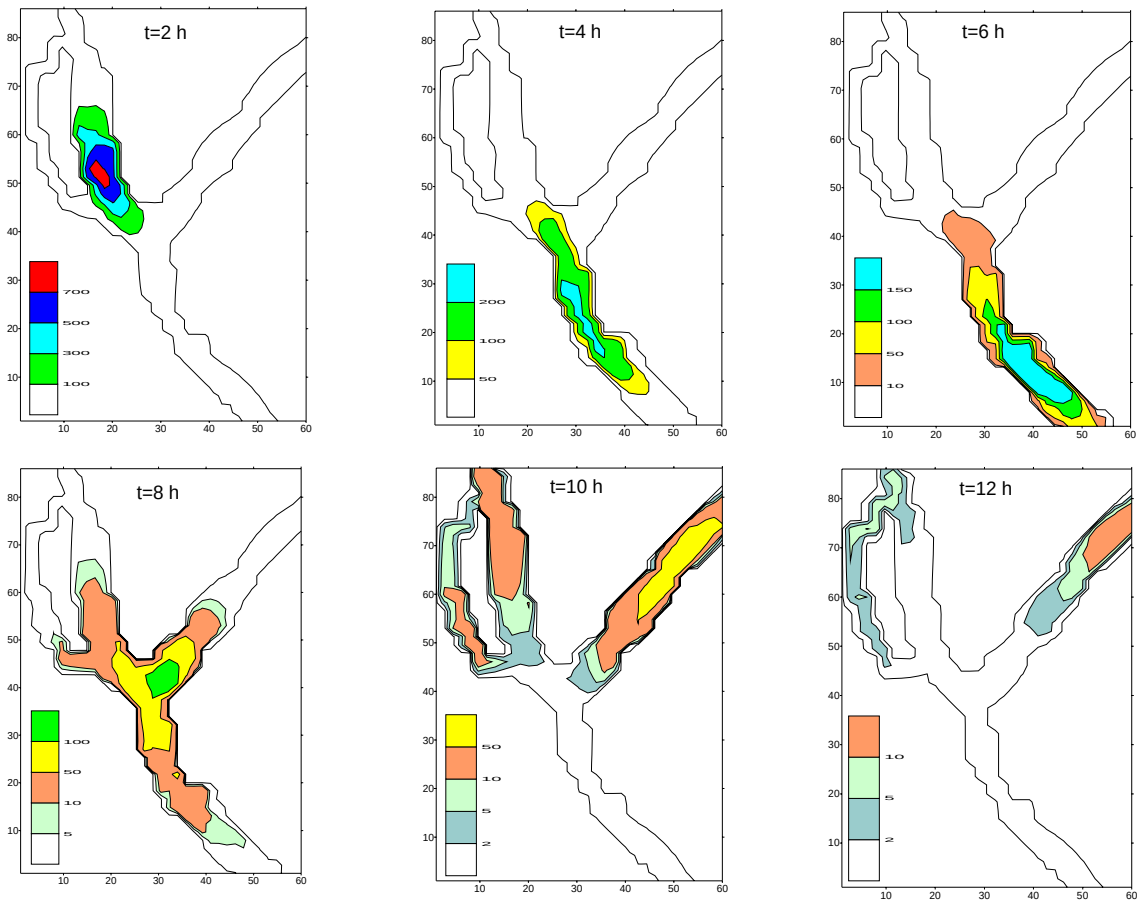

Fig. II.26. Evolution, over a tidal cycle, of dissolved ^{226}Ra concentrations after an activity input of arbitrary magnitude carried out into the Odiel River during high water.

As an example, we can see in Figure II.26 the time evolution of a radioactive pulse released during high water into the Odiel River, at the point where discharges from the fertilizer complex took place in the past. It can be seen that the pulse moves dowstream during the ebb tide. After the flood starts (some 6 hours after the release), radionuclides enter the Tinto River, Canal del Burro and the Odiel River again. Thus, the discharged radionuclides reach the complete estuary.

II.5.4. ENEA

As described before, the ENEA model is a box model in which the estuary is divided into three segments. Each segment includes the following compartments: surface water, deep water and bottom sediment. A fourth compartment representing the sediment interface between bottom sediment and water is considered to simulate the quick interaction processes of radionuclide with particulate matter. The detailed description of the model is reported in the Section II.2.4..

A list of parameter values used by the model may be seen in Table II.29.

Table II.29. Values of the parameters in model ENEA.

Parameter	Value	Units
Vertical mixing coefficient (surface-deep waters) (E_v)	3.9×10^{-6}	m^2s^{-1}
Horizontal diffusion coefficient (E_o)	10^4	m^2s^{-1}
Mixing coefficient sea water-coastal waters	10	m^2s^{-1}
Incremental depth (h_Δ)	6	m
Migration velocity to sediment (v_s)	1×10^{-6}	$m\ s^{-1}$
Migration rate from sediments (k_{sw})	1.4×10^{-8}	s^{-1}
Migration rate to deep sediment (K_{ds})	≈ 0	s^{-1}
Radioactive decay constant (λ)	1.37×10^{-11}	s^{-1}

The model is aimed at evaluating the radionuclide concentrations in the abiotic components of the water body averaged over 1 month, approximately. Consequently, the effects due to the tidal cycle are accounted for as an average exchange rate of radionuclides between the sea and the estuary. It is hypothesed that the flux of pollutant from the sea can be evaluated by the following formula, on the analogy of Fick's law:

$$F = E_s \frac{C_{sw}}{L} S \qquad \text{(II.140)}$$

where:

F is the radionuclide flux from the sea to coastal water (Bq s^{-1});
E_s is the mixing coefficient "sea water-estuary water" ($m^2\ s^{-1}$);
C_{sw} is the concentration of radionuclides in sea water (Bq m^{-3});
L is the length of the box (m); and
S is the area of the sea-estuary interface (m^2).

The fluxes of water are calculated from the monthly averages of water discharges from the rivers Odiel and Tinto and the simulation time step was 1 day. The values of the parameters controlling the dispersion of the radionuclides through the water assure that the water mixing is achieved in intervals of time that are very short compared with the run time of the model (10 years). It is also supposed that 50% of radionuclide in water column is in dissolved form.

REFERENCES

[II.1] KONOPLEV, A.V., BULGAKOV, A.A., POPOV, V.E., BOBOVNIKOVA, T.I., Behaviour of long-lived Chernobyl radionuclides in a water-soil system, Analyst 117, 1041–1047 (1992).

[II.2] KONOPLEV, A.V., BULGAKOV, A.A., POPOV, V.E., POPOV, O.F., SCHERBAK, A.V., SCHVEIKIN, Y.V., HOFFMAN, F.O., Model testing using Chernobyl data: wash-off of ^{90}Sr and ^{137}Cs from two experimental plots established in the vicinity of Chernobyl reactor, Health Physics 70, 8–12 (1996).

[II.3] PERIÁÑEZ, R., Testing the behaviour of different kinetic models for uptake-release of radionuclides between water and sediments when implemented on a marine dispersion model, Journal of Environmental Radioactivity 71, 243–259 (2004).

[II.4] BARROS, H., Estudio de la cinética de intercambio de radionúclidos y metales pesados, en relación con la modelización de su dispersión en ambientes acuáticos naturales. PhD Thesis, University of Seville (in Spanish) (2005).

[II.5] MONTE, L., A generic model for assessing the effects of countermeasures to reduce the radionuclide contamination levels in abiotic components of fresh water systems and complex catchments, Environmental Modelling and Software, 16, 669–690 (2001).

[II.6] MONTE, L., BRITTAIN, J.E., HÅKANSON, L., HELING, R., SMITH, J.T., ZHELEZNYAK, M., Review and assessment of models used to predict the fate of radionuclides in lakes, Journal of Environmental Radioactivity, 69, 177–205 (2003).

[II.7] ZHELEZNYAK, M., ET AL., Mathematical modeling of radionuclide dispersion in the Pripyat-Dnieper aquatic system after the Chernobyl accident, The Science of the Total Environment, v.112, p.89–114 (1992).

[II.8] ZHELEZNYAK, M., SHEPELEVA, T., SIZONENKO, V., MEZHUEVA, I., Simulation of countermeasures to diminish radionuclide fluxes from Chernobyl zone via aquatic pathways, Radiation Protection Dosimetry, 1997, v.73, No.1–4, pp.181–186 (1997).

[II.9] ZHELEZNYAK, M., Multiple scale analyses of radioactive contamination for rivers and reservoirs after the Chernobyl accident, Multiple Scale Analyses and Coupled Physical Systems, Proc. Saint-Venant Symposium, 28–29 August 1997, Presses de l'ecole nationale des ponts et chaussees, Paris, pp. 45–52 (1997).

[II.10] ZHELEZNYAK, M., HELING, R., RASKOB, W., Hydrological Dispersion Module of the Decision Support System RODOS,Proc. Conf. ECORAD-2001, 3–6 September 2001, Aix-de Provance, France (2002).

[II.11] KIVVA, S.L., ZHELEZNYAK, M.J., Numerical modelling of the 2-D open flow with the moving boundaries: simulation of the watershed runoff and tsunami wave runup, Computational Technologies, Novosibirsk, v.6, No. 2, p. 343–350 (In Russian) (2001).

[II.12] VAN DER PERK, M., JETTEN, V., KARSSENBERG, D., WALLING, E., LAPTEV, G., VOITSEKHOVICH, O., SVETLICHNYI, A., SLAVIK, O., LINNIK, V., KOROBOVA, E., KIVVA, S., ZHELEZNYAK, M., Assessment of spatial redistribution of Chernobyl – derived radiocaesium within catchments using GIS-embedded models, The Role of Erosion and Sediment Transport in Nutrient and Contaminant Transfer, IAHS Publ. No. 263, pp.277–284 (2000).

[II.13] KRONE, R.B., Flume studies of the transport of sediment in estuarial shoaling processes, Hydraulic Engineering Laboratory and Sanitary Engineering Research Laboratory, University of California at Berkeley, California (1962).

[II.14] PARTHENIADES, E., A study of erosion and deposition of cohesive soils in salt water, Thesis presented to the University of California at Berkeley, California (1962).
[II.15] VAN RIJN, L.C., Sediment Transport, Part I: Bed Load Transport, J. Hydr. Engrg., ASCE, 110(10), 1431–1456 (1983).
[II.16] VAN RIJN, L.C., Sediment Transport, Part II: Suspended Load Transport, J. Hydr. Engrg., ASCE, 110(11), 1613–1641 (1984b).
[II.17] MEHTA, A.J., DYER, K.R., Cohesive sediment transport in estuarine and coastal waters, in The sea: John Willey and Sons, New York, v.9, 815–839 (1990).
[II.18] HÅKANSON, L., Modelling radiocesium in lakes and coastal areas, new approaches for ecosystem modelers, Kluwer Academic Publishers, Dordrecht/Boston/London, pp. 215 (2000).
[II.19] HÅKANSON, L., A new general model predicting radionuclide concentrations and fluxes in coastal areas from readily accessible driving variables, Journal of Environmental Radioactivity 78, 217–245 (2005).
[II.20] PILESJÖ, P., PERSSON, J., HÅKANSON, L., Digital bathymetric information for calculations of coast morphometrical parameters and surface water retention time, Swedish Environmental Protection Agency, Report 3916, 76 p (in Swedish with English summary) (1991).
[II.21] PERSSON, J., HÅKANSON, L., WALLIN, H., A geographical information system for coastal water planning based on chart information, Copenhagen, Denmark; Nordic Council of Ministers TernaNord; p. 667 (1994).
[II.22] HÅKANSON, L., GYLLENHAMMAR, A., BROLIN, A., A dynamic compartment model to predict sedimentation and suspended particulate matter in coastal areas, Ecological Modelling, 175, 353–384 (2004).
[II.23] HÅKANSON, L., KARLSSON, M., A dynamic model to predict phosphorus fluxes, concentrations and eutrophication effects in Baltic coastal areas, In: Karlsson, M. Editor: Predictive Modelling a tool for aquatic environmental management, Uppsala University; Thesis, Dept. Earth Sciences; 108 p. (2004).
[II.24] INTERNATIONAL ATOMIC ENERGY AGENCY, Sediment distribution coefficients and concentration factors for biota in the marine environment, Technical Reports Series 422, IAEA, Vienna (2004).
[II.25] MARGVELASHVILY, N, MADERICH, V., ZHELEZNYAK, M., THREETOX: A computer code to simulate three dimensional dispersion of radionuclides in stratified water bodies, Radiation Protection Dosimetry 73, 177–180 (1997).
[II.26] KOZIY, L., MADERICH, V., MARGVELASHVILI, N., ZHELEZNYAK, M., Three-dimensional model of radionuclide dispersion in the estuaries and shelf seas, J. Environmental Modeling and Software, 13 (5–6), 413–420 (1998).
[II.27] MARGVELASHVILI, N., MADERICH,. V., YUSCHENKO, S., ZHELEZNYAK, M., 3D modelling of the mud and radionuclide transport in Chernobyl cooling pond and Dnieper-Bug Estuary, Fine Sediments Dynamics in the Marine Environment Proceedings of INTERCOH-2000, J.C. Winterwerp and C. Kranenburg (Eds.), Elsevier, p. 595–610 (2002).
[II.28] MARGVELASHVILI, N., MADERICH, V., ZHELEZNYAK, M., Simulation of radionuclide fluxes from the Dnieper-Bug Estuary into the Black Sea, J. Environmental Radioactivity, 43, 157–171 (1999).
[II.29] KOZIY, L., MADERICH V., MARGVELASHVILI, N., ZHELEZNYAK, M., Numerical modelling of seasonal dynamics and radionuclide transport in the Kara Sea, Oceanic fronts and Related Phenomena, Konstantin Fedorov Int. Memorial Symp., IOC Workshop Rep. Series, N 159, UNESCO'2000, p. 296–301 (2000).

[II.30] PARTHENIADES, E., Erosion and deposition of cohesive soil, J. Hydr. Div.ASCE. 91, 105–139 (1965).
[II.31] KRONE, R.B., Flume studies of the transport of sediment in estuarial processes, Final Report, Hydraulic Engineering Laboratory and Sanitary Engeeniring Research Laboratory, University of California, Berkeley, 120 p. (1962).
[II.32] VAN RIJN, L.C., Sediment transport, Part II: Suspended load transport, J. Hyd. Engr., 110, 1613–1641 (1984).
[II.33] BLUMBERG, A.F., MELLOR, G.L., Diagnostic and Prognostic Numerical Circulation Studies of the South Atlantic Bight, Journal Geophys. Res., 88, 4579–4592 (1983).
[II.34] POLIKARPOV, G.G., TIMOSCHUK, V.I., KULEBAKINA, L.G., Concentration of ^{90}Sr in the aquatic environment of Lower Dnieper toward the Black Sea, Dopovidi (Proceedings) of National Academy of Sciences of Ukraine, ser. B, N3, p.75–76 (1988).
[II.35] POLIKARPOV, G.G., LIVINGSTON, H.D., KULEBAKINA, L.G., BUESSELER, K.O., STOKOZOV, N.A., CASSO, S.A., Inflow of Chernobyl ^{90}Sr to the Black Sea from the Dniepr river, J. Estuarine, Coastal and Shelf Science, V. 34, 315–320 (1992).
[II.36] KATRICH, I.YU., NIKITIN, A.I., MEDINETS, V.I., LEPESHKIN, V.I., KABANOV, A.I., SEMKO, N.N., BAZHANOV, V.N., Dynamics of the radioactive contamination caused by CNPP accident on observed data 1986–1990, In: Borzilov, V.A., Kryshev, I.I., Ecological and hydrophysical consequences of the nuclear accidents, Hydrometerological Publ., Moscow, p. 57–61 (in Russian) (1992).
[II.37] APPELGREN, A., BERGSTRÖM, U., BRITTAIN, J., GALLEGO DIAZ, E., HÅKANSON, L., HELING, R., MONTE, L., An outline of a model-based expert system to identify optimal remedial strategies for restoring contaminated aquatic ecosystems: the project MOIRA, ENEA, RT/AMB/96/17, Roma, Italy (1996).
[II.38] MONTE, L., FRATARCANGELI, S., QUAGGIA, S., POMPEI, F., A predictive model for the behaviour of dissolved radioactive substances in stratified lakes, Journal of Environmental Radioactivity 13, 297–308 (1991).
[II.39] MONTE, L., HÅKANSON, L., PERIANEZ, R., LAPTEV, G., ZHELEZNYAK, M., MADERICH, V., ANGELI, G., KOSHEBUTSKY, V., Experiences from a case study of multi-model application to assess the behaviour of pollutants in the Dnieper-Bug Estuary, Ecological Modelling, 195, 247–263 (2006).
[II.40] BOYER, P., BEAUGELIN-SEILLER, K., TERNAT, F., ANSELMET, F., AMIELH, M., A dynamic box model to predict the radionuclide behaviour in rivers for medium and long-term periods, Radioprotection, Suppl. 1, Vol. 40, S307–S313 (2005).
[II.41] BOYER, P., BEAUGELIN-SEILLER, K., CASTEAUR: a tool for operational assessments of radioactive nuclides transfers in river ecosystems, Radioprotection – Colloques, vol. 37, C1, 1127–1131 (2002).
[II.42] BEAUGELIN-SEILLER, K., BOYER, P., GARNIER-LAPLACE, J., ADAM, C., CASTEAUR: a simple tool to assess the transfer of radionuclides in waterways, Health Physics, 84(3), 539–542 (2002).
[II.43] DUCHESNE, S., BOYER, P., BEAUGELIN-SEILLER, K., Sensitivity and uncertainty analysis of a model computing radionuclides transfers in fluvial ecosystems (CASTEAUR): application to ^{137}Cs accumulation in chubs, Ecological modelling, vol. 166, 257–276 (2003).

[II.44] INTERNATIONAL ATOMIC ENERGY AGENCY, Generic Models for Use in Assessing the Impact of Discharge of Radioactive Substances to the Environment, Safety Reports Series No.19, IAEA, Vienna, (2001).

[II.45] HOLLY, F.M., YANG, J.C., SCHWARZ, P., SCHAEFER, J., HSU, S.H., EINHELLIG, R., CHARIMA: Numerical simulation on unsteady water and sediment movement in multiply connected networcs of mobile-bed channels, IIHR Report No. 343, Institute of Hydraulic Research, University of Iowa, Iowa City, 327 p (1990).

[II.46] WON SEO, I. SUNG CHEONG, T., Predicting longitudinal dispersion coefficient in natural streams, J. Hydraulic Eng., Vol. 124, No. 1, pp.25–32 (1998).

[II.47] SIZONENKO, V.P., Increasing accuracy of the box model, In: Hydroinformatics '98 – Proceedings of the Third International Conference on Hydroinformatics / Copenhagen / Denmark / 24–26 August 1998, V. Babovic AND L.C. Larson (ed.), vol. 1, A.A.Balkema, Rotterdam, pp. 225–230 (1998).

[II.48] SIZONENKO, V.P., The evaluation of influences of modes of operation the Kiev HPP on Sr-90 concentration in the outflow of the Kiev Reservoir, In: The Problems of General Energy, Kiev, vol. 2, pp. 58–63 (in Russian) (2000).

[II.49] DENISOVA, A.I., TIMCHENKO, V.M., NAHSHINA, E.P., NOVIKOV, B.I., RJABOV, A.K., BASS, J.I., Hydrology and hydrochemistry of Dnieper and it of reservoirs, Naukova Dumka, Kiev, 216 p. (in Russian) (1989).

[II.50] LI, M.Z., AMOS, C.L., SEDTRANS96: the upgraded and better calibrated sediment-transport model for continental shelves, Computers and Geosciences 27(6) 619–645 (2001).

[II.51] EL GANAOUI, O., SCHAAF, E., BOYER, P., AMIELH, M., ANSELMET, F., GRENZ, C., The deposition and erosion of cohesive sediments determined by a multi-class model, Estuarine, Coastal and Shelf Science, 60, 457–475 (2004).

[II.52] BOYER, P., TERNAT, F., CASTEAUR v0.1 – Modèles abiotiques, Report IRSNSDEI/SECRE, n°2005-01 (2005).

[II.53] ABRIL, J.M., FRAGA, E., Some physical and chemical features of the variability of kd distribution coefficients for radionuclides, Journal of Environmental Radioactivity 30(3), 253–270 (1996).

[II.54] KRYSHEV, I.I., KRYSHEV, A.I., Scenario on model validation Radioactive Contamination of the Techa River, South Urals, Russia, Draft 3.3, EMRAS, Working Group 4, SPA Typhoon, Obninsk (2006).

[II.55] PERIAÑEZ, R., ABSI, A., VILLA, M., MORERO, H.P., MANJON, G., Self-cleaning in an estuarine area formerly affected by ^{226}Ra anthropogenic enhancements: numerical solutions, Science of the Total Environment, 339, 207–218 (2005).

ADDITIONAL PUBLICATIONS USED IN THE PREPARATION OF THIS REPORT

AMOS, C.L., GRANT, J., DABORN, G.R., BLACK, K., Sea carousel – a benthic, annular flume, Estuarine, Coastal and Shelf Science, 34, 6, 557–577 (1992).

BIOMOVS, Dynamics within lake ecosystems. Scenario A5, B. Technical Report 12, National Institute of Radiation Protection, Sweden (1991).

DE CORT, M., DUBOIS, G., FRIDMAN, S.D., GERMENCHUK, M.G., ET AL., Atlas of Caesium deposition on Europe after the Chernobyl accident. EUR 16733 Luxemburg, Office for Official Publication of the European Communities, ISBN 92-828-3140-X (1998).

DYER, K.R., Estuarine oceanography, In: Parker, S. P. (Ed.) McGraw-Hill Encyclopedia of Environmental Science, McGraw-Hill Book Company, New York (1980).

EISMA, D., Suspended Matter in the Aquatic Environment, Springer Verlag, Berlin (1993).

GODUNOV, S.K., A Finite Difference Method for the computation of Discontinuous Solutions of Fluid Dynamics, Mat. Sb. 47, 357–393 (1959).

HARTEN, A., High resolution schemes for hyperbolic conservation laws, Journ. Comp. Physics, Vol. 49, 357–393 (1983).

HARTEN, A., OSHER, S., Uniformly high-order accurate nonoscillatory schemes, SIAM Journ. Num. Analysis, Vol. 24(2), 279–309 (1987).

INTERNATIONAL ATOMIC ENERGY AGENCY, Modelling of the transfer of radiocaesium from deposition to lake ecosystems, Report of the VAMP Aquatic Working Group, IAEA-TECDOC-1143, IAEA, Vienna (2000).

KANIVETS, V.V., VOITSEKHOVICH, O.V., SIMOV, Radioactive contamination of the Black and Azov seas, In: Voitsekhovich O.V. ed. Radioecology of water objects of the Chernobyl NPP accident impact area, Chernobylinterinform, Kiev, 127–151 (1997). (in Russian).

KONOPLEV, A.V., BULGAKOV, A.A., POPOV, V.E., POPOV, O.F., SCHERBAK, A.V., SHVEIKIN, YU.V., HOFFMAN, F.O., Model testing using Chernobyl data: I. Wash-off of ^{90}Sr and ^{137}Cs from two experimental plots established in the vicinity of Chernobyl reactor, Health Physics 70(1):8–12 (1996).

KONOPLEV, A.V., BULGAKOV, A.A., HOFFMAN, F.O., KANYÁR, B., LYASHENKO, G., NAIR, S.K., POPOV, A., RASKOB, W., THIESSEN, K.M., WATKINS, B., ZHELEZNYAK, M., Validation of models of radionuclide wash-off from contaminated watersheds using Chernobyl data, J. Environ. Radioactivity 42(2-3):131–141 (1999).

KOSTYANITSYN, M.N., Hydrology of the Dnieper and Southern Bug Estuary, M. Gidrometeoizdat, 336 p (1964) (in Russian).

KRYSHEV, I.I., SAZYKINA, T.G., Dose assessment and radioecological consequences to aquatic organisms in the areas of Russia exposed to radioactive contamination, In: Protection of the Natural Environment, Proceedings of the International Symposium on Ionising Radiation, 20–24 May 1996, Stockholm, Vol. 1, pp. 147–152 (1996).

KRYSHEV, I.I., SAZYKINA, T.G., Radioecological consequences of the radiation accident for aquatic environment, In: Proc. Int. Conf. "A radioactivity after nuclear explosions and accidents", 24–26 April 2000, Moscow, Gidrometeoizdat, St.-Petersburg, Vol. 2. pp. 533–538 (2000) (in Russian).

KRYSHEV, I.I., KRYSHEV, A.I., Scenario on Model Validation Radioactive Contamination of the Techa River, South Urals, Russia (Draft 3), SPA "Typhoon", Obninsk (2005).

KRYSHEV, I.I., KRYSHEV, A.I., NOSOV, S.V., BADALYAN, K.D., Modelling of plutonium transfer into the Techa River, Proceedings of the International Conference RADLEG-RADINFO-2005, Moscow (2005).

KRYSHEV A.I., NOSOV, A.V., Radioecological model for ^{90}Sr and ^{137}Cs transport in the river system Iset – Tobol – Irtysh. Izvestia vuzov, Yadernaya Energetika (Transactions of High School, Nuclear Energy), No. 3, 16–25 (2005) (in Russian).

LUCK, M., GOUTAL, N., Système MASCARET: Note de principe de l'outil Tracer (transport de traceurs) et des modules de qualité d'eau O2, Biomass, Eutro, Micropol et Thermic, Rapport EDF-LNHE HP-75/03/047/A (2003).

MEHTA, A.J., ET AL., Cohesive sediment transport, In: Process description, J. Hydraul. Eng. Div. ASCE 115(8), 1076–1093 (1989).

MOLCHANOVA, I.V., KARAVAIEVA, E.N., POZOLOTINA, V.N., The regularities of the behavior of radionuclides in the floodplain landscapes of the Techa River in the Urals, Ecology 3, 43–49 (1994).

MONTE, L., BOYER, P., BRITTAIN, J.E., HÅKANSON, L., LEPICARD, S. SMITH, J.T., Review and assessment of models for predicting the migration of radionuclides through rivers, Journal of Environmental Radioactivity 79, 273–296 (2005).

OSHER, S., CHAKRAVARTHY, S., High resolution schemes and the entropy condition, SIAM Journ. Num. Analysis, Vol. 21(5), 955–984 (1984).

OUGHTON, D.H., FIFIELD, L.K., DAY, J.P., ET AL., Plutonium from Mayak: Measurement of isotope ratios and activities using accelerator mass spectrometry, Environmental Science and Technology, 34, 1938–1945 (2000).

PARTHENIADES, E., Erosion and deposition of cohesive soils, J. Hydraul. Div. ASCE 91, 105–139 (1965).

PARTHENIADES, E., Unified view of wash load and bed material load, J. Hydraul. Div. ASCE 103(HY9), 1037–1057 (1971).

PERIAÑEZ, R., ABRIL, J.M., GARCÍA-LEÓN, M., Modelling the dispersion of non conservative radionuclides in tidal waters, Part 1: conceptual and mathematical model, Journal of Environmental Radioactivity 31, 127–141 (1996).

PERIAÑEZ, R., Modelling the suspended matter dynamics in a marine environment using a three dimensional s coordinate models: application to the eastern Irish Sea, Applied Mathematical Modelling 26, 583–601 (2002).

ROE, P.L., Approximate Riemann solvers, parameter vectors, and difference schemes., J. Computational Physics, Vol. 43, 357–372 (1981).

SKIPPERUD, L., SALBU, B., OUGHTON, D.H., ET AL., Plutonium contamination in soils and sediments at Mayak PA, Russia, Health Physics, 89, 3, 255–266 (2005).

SPA "TYPHOON", The Radiation Situation in the Territory of Russia and Contiguous States in 2004, Yearbook, Moscow, Rosgidromet (2005).

SWEBY, P.K., High resolution schemes using flux limiters for hyperbolic conservation laws, SIAM Journ. Num. Analysis, Vol. 21(5), 995–1011 (1984).

TORO, E., Riemann problems and the WAF method for solving the two-dimensional shallow water equations, Philosophical Trans. Royal Soc., London, U.K., A338, 43–68 (1992).

TRAPEZNIKOV, A.V., POZOLOTINA, V.N.,YUSHKOV, P.I., ET AL., Study of the radioecological situation in the rivers Techa and Iset' contaminated with the discharges of the Mayak plant, Problems of radioecology and adjacent disciplines, 2, 20–66 (1999).

UNCLES, R.J., STEPHENS, J.A., Distribution of suspended sediment at high water in a macrotidal estuary, J. Geophys. Res., 94(C10), 14395–14405 (1989).

VOITSEKHOVICH, O., PRISTER, B., NASVIT, O., LOS, I., BERKOVSKY, V., Present concept on current water protection and remediation activities for the areas contaminated by the 1986 Chernobyl accident, Health Physics 71(1):19–28 (1996).

VOJTSEKHOVICH, O., NASVIT, O., LOS', I., BERKOVSKIJ, V., Assessment of water protection operations to minimize the risk from using water from the Dnieper water system at various stages after the accident at the Chernobyl nuclear power plant, In: Environmental Impact of Radioactive Releases, Proceedings of an international symposium, Vienna, Austria, 8–12 May 1995, IAEA-SM-339/140, International Atomic Energy Agency, Vienna, pp. 549–557 (1995).

VOROBIOVA, M.I., DEGTEVA, M.O., BURMISTROV, D.S., SAFRONOVA, N.G., KOZHEUROV, V.P., ANSPAUGH, L.R., NAPIER, B.A., Review of historical monitoring data of Techa River contamination, Health Physics 76(6):605-617 (1999).

WINKELMANN, I., ROMANOV, G.N., GOLOSHAPOV, P., GESEWSKY, P., MUNDIGL, S., BUCHRODER, H., THOMAS, M., BRUMMER, C., BURKART, W., Measurements of radioactivity in environmental samples from the Southern Urals, Radiat. Environ. Biophys. 37, 57–61 (1998).

YEE, H.C., Semi-implicit and fully implicit shock-capturing methods for nonequilib-rium flows, AIAA Journal, Vol. 27(3), 299–307 (1989).

ZHAO, D.H., SHEN, H.W., TABIOS, G.Q., LAI, J.S., Approximate Riemann solvers in FVM for 2D hydraulic shock wave modelling., J. Hydr.Eng. Vol. 122(12), 692–702 (1996).

ZHELEZNYAK, M., DONTCHITS, G., DZJUBA, N., GIGINYAK, V., LYASHENKO, G., MARINETS, A., TKALICH, P., RIVTOX – One dimensional model for the simulation of the transport of radionuclides in a network of river channels, RODOS Report WG4-TN(97)05, Forschungszentrum Karlsruhe, 48 p. (2000).

ZHYKINSKY, V.N., The Dnieper and Bug Estuary Ecosystem, Kyiv, Naukova Dumka, 239 p (1989) (in Russian).

LIST OF PARTICIPANTS

Amano, H.	Japan Atomic Energy Research Institute, Japan
Angeli, G.	Ente per le Nuove tecnologie e l'Ambiente, Italy
Barros, H.	University of Seville, Spain
Boyer, P.	Institut de Radioprotection et de Sûreté Nucléaire, France
Brittain, J.E.	University of Oslo, Norway
Dzyuba, N.	Institute of Mathematical Machines and System Problems, Ukraine
Galeriu, D.	National Institute for Physics and Nuclear Engineering "Horia Hulubei", Romania
Goutal, N.	Electricité de France, France
Håkanson, L.	Uppsala University,Sweden
Heling, R.	Nuclear Research and Consultancy Group, The Netherlands
Hofman, D.	Studsvik RadWaste AB, Sweden
Inaba, J.	Institute for Environmental Sciences, Japan
Kivva, S.	Institute of Mathematical Machines and System Problems, Ukraine
Konoplev, A.	Institute of Experimental Meteorology, SPA "Typhoon", Russian Federation
Koshebutskyy, V.	Institute of Mathematical Machines and System Problems, Ukraine
Krylov, A.	Institute of Safety Development Atomic Energy, Russian Federation
Kryshev, A.	Institute of Experimental Meteorology, SPA "Typhoon", Russian Federation
Kryshev, I.	Institute of Experimental Meteorology, SPA "Typhoon", Russia Federation
Laptev, G.	Ukrainian Institute for Hydrometeorology, Ukraine
Luck, M.	Electricité de France, France
Maderich, V.	Institute of Mathematical Machines and System Problems, Ukraine
Melintescu, A.	National Institute for Physics and Nuclear Engineering "Horia Hulubei", Romania
Monte, L.	Ente per le Nuove tecnologie e l'Ambiente, Italy
Neves, F.	University of Evora, Portugal

Nosov, A.	Atomenergoproject, Russian Federation
Olyslaegers, G.	Studiecentrum voor Kernenergie (SCK/CEN), Belgium
Periáñez, R.	University of Seville, Spain
Sanina, K.	Institute of Experimental Meteorology, SPA "Typhoon", Russian Federation
Sazykina, T.	Institute of Experimental Meteorology, SPA "Typhoon", Russia Federation
Siclet, F.	Electricité de France, France
Sizonenko, V.P.	Institute of General Energy, Ukraine
Slávik, O.	VÚJE Trnava, Inc., Slovak Republic
Suh, K.-S.	Korea Atomic Energy Research Institute, Republic of Korea
Sweeck, L.	Studiecentrum voor Kernenergie (SCK/CEN), Belgium
Telleria, D.	International Atomic Energy Agency
Treebushny, D.	Institute of Mathematical Machines and System Problems, Ukraine
Zheleznyak, M.	Institute of Mathematical Machines and System Problems, Ukraine
Zibold, G.	University of Applied Sciences, Germany